

**HEARING IN ZEBRAFISH: FROM
MECHANOTRANSDUCTION TO SYNAPTIC TRANSMISSION**

By

Weike Mo

A DISSERTATION

Presented to the Department of Cell and Developmental Biology
Oregon Health & Science University School of Medicine

in partial fulfillment of the requirements for the degree of
Doctor of Philosophy

March 2013

School of Medicine
Oregon Health & Science University

CERTIFICATE OF APPROVAL

This is to certify that the PhD dissertation of

WEIKE MO

has been approved

Mentor/Advisor, Teresa Nicolson, PhD

Committee Chair, Peter Barr-Gillespie, PhD

Member, Alex Nechiporuk, PhD

Member, Gail Mandel, PhD

Member, Henrique von Gersdorff, PhD

Member, Laurence Trussell, PhD

Table of Contents

List of Figures	vi
Acknowledgement	ix
Abstract	x
Chapter 1. Introduction	1
1. Zebrafish as a model organism for hearing research	1
1.1. Auditory and vestibular organs in zebrafish	1
1.2. Genetic screen in zebrafish	5
2. Functional assessment of auditory and vestibular function	8
2.1. Measuring hearing and balance in mammals	8
2.2. Measuring hearing and balance in zebrafish	9
3. Mechanoelectrical Transduction in hair cells	12
3.1. Hair bundle structure	12
3.2. MET channels	13
3.3. Tip links and mechanosensation	16
4. The tip link and MET complex	18
4.1. Molecular components of the tip link	18
4.2. Cytoplasmic domains of the tip-link components	20
4.3. Proteins that interact with the cytoplasmic domains of CDH23 and PCDH15	22
4.4. MET channel candidates	25
5. Synaptic transmission in hair cells	27
5.1. Properties of synaptic transmission in hair cells	27

5.2.	Structure of ribbon synapses	28
5.3.	Molecular composition of ribbon synapses	30
6.	NSF and synaptic transmission.....	37
6.1.	Exocytotic complex in conventional synapses	37
6.2.	Structure and function of NSF	38
6.3.	Exocytotic complex at hair-cell ribbon synapses.....	40
6.4.	Exocytotic complex and neurological diseases.....	42
Chapter 2.	Quantification of vestibular-induced eye movements in zebrafish larvae	44
1.	Summary	45
2.	Materials and methods	46
2.1.	Animals.....	46
2.2.	Microscopic system	48
2.3.	Experimental condition.....	49
2.4.	Data acquisition	50
2.5.	Image processing	52
2.6.	Quantification of rotation of the eye.....	53
3.	Results.....	56
3.1.	Quantifying vestibular-induced eye movements in zebrafish larvae	56
3.2.	Earth horizontal versus earth vertical rotations	62
3.3.	Zebrafish larvae develop vestibular-induced eye movements at 3dpf.....	63
3.4.	Anterior otolith is required for vestibular-induced eye movements in zebrafish larvae	66
4.	Discussion	67

Chapter 3. Nsf function in hair-cell ribbon synapses: lesson from a point mutation	72
1. Summary	73
2. Materials and methods	74
3. Results.....	77
3.1. An nsf point mutation identified in milky way.....	77
3.2. Behavioral analysis: hearing and balance defects in nsfI209N/st53 mutants	79
3.3. Synaptic transmission is impaired in nsfI209N/st53 mutants.....	88
3.4. No defects of myelination found in nsfI209N/st53 mutants.....	90
3.5. Hair-cell ribbon synapses in nsfI209N/st53 mutants show subtle changes.	91
3.6. Expression of neuronal SNAREs in zebrafish hair cells	95
3.7. Enhanced transcription of nsf in nsfI209N mutants	98
4. Discussion.....	99
4.1. Mutation I209N in zebrafish Nsf protein.....	100
4.2. NSF and SNAREs in hair-cell ribbon synapses.....	102
Chapter 4. Nsf in preventing Degeneration of Hair-Cell Synapses	104
1. Summary	105
2. Materials and methods	106
3. Results.....	110
3.1. Innervation in zebrafish nsf and nsfb mutants	110
3.2. Degeneration of hair-cell afferent synapses in nsf mutants	114
3.3. Neurodegeneration in the CNS of nsf mutants	118
3.4. Apoptosis in nsf mutants.....	124
3.5. Pre- and postsynaptic function of Nsf.....	126

3.6.	Loss of Nsf affects BDNF function	130
4.	Discussion.....	136
4.1.	Differing roles of Nsf and Nsfb in zebrafish	137
4.2.	Nsf and neurodegeneration	139
4.3.	Myelination and neurodegeneration	140
4.4.	Nsf function in hair cells.....	141
4.5.	Factors acting downstream of NSF-mediated vesicle fusion.....	142
Chapter 5. Fishing for the hair-cell mechanotransduction complex.....		144
1.	Summary	144
2.	Materials and methods	145
3.	Screen TRP channel candidates for mechanotransduction	149
3.1.	Expression of TRP channels in zebrafish hair cells.....	149
3.2.	Trpm7 in zebrafish hair cells	152
4.	Yeast two-hybrid screen of interactors of Pcdh15a	155
4.1.	Expression of pcdh15a splice variants in zebrafish	155
4.2.	Generation of Pcdh15a bait.....	157
4.3.	Split-Ubiquitin Membrane Yeast Two-Hybrid using Pcdh15a	161
4.4.	Expression of tmc genes in zebrafish.....	165
5.	Discussion.....	166
5.1.	TRP channels as candidates for MET channel	167
5.2.	TMC channels as candidates for mechanoreceptors of hearing.....	169
Chapter 6. Summary and Conclusions		172
6.1.	Behavioral analysis of zebrafish larvae	172
6.2.	Nsf function in hair cells.....	174

6.3.	Mechanotransduction in hair cells	176
Appendices	179
1.	Gravity changes in VOR measurement.....	179
2.	Detailed protocol of VOR measurement.....	183
2.1.	Data acquisition.....	183
2.2.	Using Matlab to analyze videos	184
3.	Whole mount immunohistochemical detection of proteins in embryonic zebrafish	186
References	188
List of Publications	221

List of Figures

Figure 1. Structure of the mammalian (A) and zebrafish (B) inner ears.	2
Figure 2. Organization of hair cells in zebrafish larvae.	4
Figure 3. Neural circuitry of the startle reflex and vestibuloocular reflex (VOR).	11
Figure 4. Illustrations of the hair bundle, mechanotransduction machinery, and action of MET channels.	15
Figure 5. Models of connections between tip-links and MET channels.....	17
Figure 6. Diagram of molecules involved in mechanotransduction.	20
Figure 7. Diagram of a hair cell innervated by afferent nerves (green) and an efferent nerve (blue).	28
Figure 8. Diagrammatic representation of mature synapses in the rodent CNS, hair cells, and photoreceptor cells.	32
Figure 9. The SNARE cycle in vesicle fusion.	33
Figure 10. Mammalian SNAREs for trafficking in different pathways.....	34
Figure 11. Structure and mode of action for the NSF protein.	36
Figure 12. The equipment and diagram of the experimental set up used to evoke eye movements in zebrafish larvae.....	47
Figure 13. Defining the eye regions in fish larvae.....	51
Figure 14. Features for quantifying eye movements under infrared illumination.	54
Figure 15. Representative eye movements in response to platform movements.....	56
Figure 16. Vestibular-induced eye movements in wild-type and mutant larvae.	58
Figure 17. Presence of the optokinetic reflex, but not vestibular-induced eye movements in <i>cdh231619ag</i> mutants (5 dpf).	62

Figure 18. Vestibular-induced eye movements occur during rotation at 0.25 Hz around an earth horizontal axis, but not around an earth vertical axis.	64
Figure 19. Development of the vestibular-induced response in zebrafish larvae.	65
Figure 20. Vestibular-induced eye movements were absent in larvae lacking anterior/utricle otoliths.	66
Figure 21. Molecular cloning of milky way.	78
Figure 22. Vestibular and auditory defects in nsfI209N mutants (5 dpf).	80
Figure 23. Spontaneous activity in nsfI209N/st53mutants is normal.	82
Figure 24. Delayed action potentials at pLLG in nsfI209N/st53 mutants.	83
Figure 25. Structure of the posterior lateral line nerve (PLLn) in WT, nsfI209N/st53, and nsfst53 larvae at 5 dpf.	84
Figure 26. Antibody labelling of Vglut3, CSP, Ribeye b, and MAGUK in nsf mutants..	86
Figure 27. Antibody labeling of SNARE proteins in 5 dpf zebrafish neuromasts.	92
Figure 28. Increased nsf transcripts but not proteins in nsfI209N mutants.	97
Figure 29. Expression of nsf and nsfb in zebrafish, and defective innervation of hair cells in nsf mutants.	111
Figure 30. Expression of Nsf in the CNS and lateral line organ (5 dpf).....	112
Figure 31. Degeneration of hair-cell synapses in nsfst53 mutants during development.	114
Figure 32. Reduction of glutamatergic synapses in the CNS of nsfst53 mutants (5 dpf).....	116
Figure 33. Glutamatergic synapses in the cerebellum.	119
Figure 34. Apoptosis in nsfst53 mutants (5 dpf).	120
Figure 35. Nsf function is required in both pre- and postsynaptic cells to stabilize afferent innervation of hair cells.	122
Figure 36. Quantification of GFP fluorescence in Tg(-6myo6b:nsf-GFP)vo1 and Tg(-6myo6b:nsf-GFP)vo2 lines.	125

Figure 37. Rescue of afferent innervation by double transgenic expression of Nsf-GFP in nsfst53 mutants.	128
Figure 38. Expression of genes important for synaptic stability is reduced in nsfst53 mutants.	130
Figure 39. Expression of BDNF in wild-type hair cells and the pLLG, and accumulation of BDNF protein in the lateral line nerve of nsfst53 mutants.....	132
Figure 40. Partial rescue of synaptic contacts in nsfst53 mutants by BDNF injection at 2dpf.	134
Figure 41. Decreased labeling of acetylated Tubulin and Myelin Basic Protein in nsfst53 mutants.	138
Figure 42. Myelin Basic Protein expresses is present in peripheral nerves, but not in the CNS.	141
Figure 43. Expression of trpm7 in zebrafish neuromasts.	151
Figure 44. FM4-64 uptake in trpm7 mutants.....	153
Figure 45. Structure and expression of intracellular domains of Pcdh15a.	156
Figure 46. The principle and flow chart of membrane yeast two-hybrid screen.	158
Figure 47. Validate expression of tagged Pcdh15a in yeast.	159
Figure 48. Confirmation of interaction proteins of Pcdh15a.	164
Figure 49. Expression of tmc genes in zebrafish adult tissues.	165
Figure 50. Schematic of gEff change during a rotation cycle.....	182

Acknowledgments

I would like to thank my advisor Dr. Teresa Nicolson for her constant guidance and support that helped me to finish my dissertation and develop my professional career. I am also very grateful to my committee members, chair Dr. Peter Barr-Gillespie, Dr. Gail Mandel, Dr. Alex Nechiporuk, and Dr. Henrique von Gersdorff for their invaluable suggestions and encouragement in the past years.

I am thankful to the current and past members of the Nicolson lab for their kindness, tolerance, and feedback on my work, and for the non-scientific time we spent together. I want to first thank Gabe Finch for managing a great lab and help with experiments. I am thankful to Sireesha Govadas, Juli Zeppieri, Norm Eden, and Lisa Hayashi for technical assistance and maintaining the fish. I want to give many thanks to Fangyi Chen for our great collaboration on the VOR project. Thank you to Lavinia Sheets, Joe Trapani, and Katie Kindt who mentored me in the many ways. It was a great pleasure to work with all of you. I am also grateful to Timothy Erickson and Cecilia Phillips for all your help on experiments and scientific writing. Thank you to Rachel Clemens-Grisham and Zev Einhorn for being great peer graduate students and our great discussion time. I would like also thank members in the Nechiporuk lab for discussions and our fish club.

I am grateful to my parents and parents-in-law for their encouragement and efforts to take care my little Estella Yinya Mo when I was preparing my dissertation. And finally, I have my biggest thanks to Huilan Yao for being supportive and the joyful time we have spent together.

Abstract

The zebrafish is a model organism for hearing and balance research. Although lots of zebrafish mutants have been generated, experimental assessment of auditory and vestibular defects in many of these mutants has not been fully established. Our pioneering work has established a new methodology of measuring the vestibuloocular reflex to quantify vestibular defects in 5 day-old zebrafish larvae. Our study has shown robust eye movements with respect to changes in gravity in zebrafish larvae. We have determined herein the basis of sensitivity of the larval eye movements with respect to the vestibular stimulus, developmental stage, and sensory receptors of the inner ear. Our results provide evidence for a functional vestibulo-oculomotor circuit in 72 hours post-fertilization zebrafish larvae that relies upon sensory input from the anterior/utricle otolith organs.

An important function of auditory/vestibular hair-cells is to transmit sensory information to downstream neurons. Hair cells use ribbon synapses, which are known to have several unique synaptic proteins for sustained, high-speed synaptic transmission. Neuronal SNAREs are key regulators for synaptic vesicle fusion in most neurons. NSF is an ATPase that is thought to dissociate SNARE complexes after vesicle fusion. Both are required for synaptic transmission in the central nervous system. However, the existence of neuronal SNAREs at ribbon synapses is controversial. Neurotoxin cleavage or genetic mutation of neuronal SNAREs does not affect synaptic transmission in mouse inner hair cells. Here, we reported a novel point mutation I209N in the *nsf* gene. The *nsf*^{I209N} mutation likely affects synaptic transmission in hair cells, which appears to delay the

arrival of action potentials at the posterior lateral line ganglion. The *nsf*^{J209N} mutation does not change the structure of ribbon synapses, with the exception of decreased expression of cysteine string protein. In contrast, the *nsf* null mutation leads to a decrease of several synaptic markers, and causes degeneration of afferent innervation of hair cells. Both pre- and postsynaptic Nsf activity is required for maintenance of ribbon synapses. In addition, we have found Vamp2 and Vamp8 present in hair cells, but not other neuronal SNAREs. Our results suggest that Nsf is required for normal function and maintenance of ribbon synapses in zebrafish hair cells, and Nsf activity may be involved in non-conventional SNARE-mediated synaptic transmission.

Hair cells convert mechanic information into electrochemical signals, a process called mechano-electrical transduction. Searching for potential candidates for mechanosensory channels, we have examined the expression of TRP channels in hair cells. Although Trpm7 is a candidate, mechanotransduction remains unchanged in *trpm7* mutants. It is thought that mechanosensory channels could be directly or indirectly associated with PCDH15 in rat outer hair cells. Therefore, we have used the zebrafish Pcdh15a protein as bait for a membrane-specific yeast two-hybrid screen using zebrafish inner ear cDNA library. Several proteins were identified in the unbiased screen, including Transmembrane channel like 2a (Tmc2a). Tmc2a is particularly interesting because it was recently shown to be required for mechanotransduction in mouse hair cells. Future efforts will focus on the function and specificity of the interaction between Tmc2a and Pcdh15a in zebrafish.

Chapter 1. Introduction

1. Zebrafish as a model organism for hearing research

A number of model organisms have been introduced for biomedical research. Among those, lower vertebrates and invertebrates are often used as genetic models to identify genes that are required for specific biological processes because of their low cost of maintenance and quick growth. Although invertebrates are able to detect sound and body position, they lack the inner ear organ and the sensory receptor hair cells for hearing and balance sensation. Zebrafish (*Danio rerio*), in contrast, possess sensory hair cells and typical vertebrate inner ear, although they do not have the outer and middle ear like mammals. Additionally, zebrafish have proven to be a good genetic model in large-scale mutagenesis screens (Ackermann and Paw, 2003). Together, these properties have made zebrafish an ideal genetic model for hearing research. Through forward genetic screens, zebrafish mutants have revealed conserved molecules and mechanisms for ear development and function in vertebrates (reviewed by Nicolson, 2005).

1.1. Auditory and vestibular organs in zebrafish

In auditory system, hair cells detect sound with a wide range of frequencies and intensities. In the vestibular system, hair cells in the utricle, saccule, and semicircular canals detect gravity changes, linear acceleration, and angular acceleration, keeping the body properly oriented in space (Figure 1A).

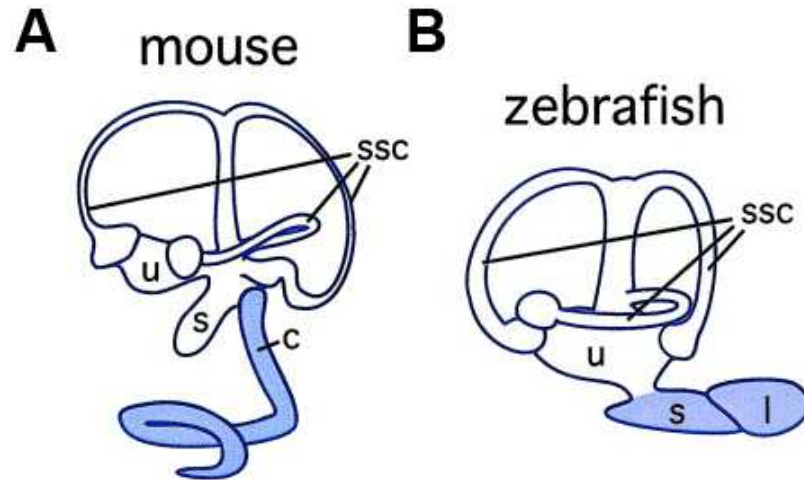


Figure 1. Structure of the mammalian (A) and zebrafish (B) inner ears. (anterior to the left). Blue areas outline the auditory organs. Abbreviations: c, cochlea, l, lagena; s, saccule; u, utricle; ssc, semicircular canal. (modified from Riley & Phillips, 2003).

Because the mammalian inner ear is embedded in temporal bones, the study of hair cells is more difficult than other sensory neurons, e.g. the rod and cone cells in visual system (reviewed by Goodrich, 2005). The zebrafish inner ear has a similar function to the mammalian inner ear, and is more easily accessible than its mammalian counterpart. In adult zebrafish, the vestibular organ includes the semicircular canals and utricles, while the saccule and lagena are used for auditory function (Figure 1B). Larval zebrafish also have a vestibular reflex to maintain an upright position as early as 72 hours post-fertilization (hpf) (Mo et al., 2010c), and they develop a hearing startle reflex or response at 5 days post-fertilization (dpf) (Zeddies and Fay, 2005). The larval inner ear features three patches of cristae (anterior crista, medial crista, and posterior crista), which will be

hair cells in the semicircular canal system in adults, and two groups of macular hair cells: the anterior macula that will develop into sensory cells in the utricle and the posterior macula that will develop into the saccule hair cells. Above each macular epithelium, there is a calcium carbonate crystal called an otolith (Figure 2B, C). Like adults, the larval utricular otolith is also required for vestibular function and survival (Riley and Moorman, 2000), while the larval saccular otolith is suggested to have a function in hearing (Popper and Fay, 1993; Riley and Moorman, 2000).

In addition to the ear, fish and amphibians have a lateral-line system to sense water flow and body movements, which also employ hair cells as sensory receptors. Hair cells in the lateral-line system are grouped within neuromasts on the surface of the fish body, and are responsible for a variety of behaviors such as rheotaxis and escaping from predators (Bleckmann and Zelick, 2009; Suli et al., 2012)(Figure 2A, D, E). The lateral-line system is divided into two branches, an anterior branch that mainly resides on the head, and a posterior branch that extends from the trunk to the tail. Studies of zebrafish hair cells have been focused on the lateral-line organ, especially the posterior lateral-line component, in part because it is simple in structure and readily accessible at the surface (reviewed by Ghysen and Dambly-Chaudière, 2007; Froehlicher et al., 2009). In this thesis, most of experiments in Chapter 2 and 3 are conducted with lateral-line neuromasts and the images are top-down views (Figure 2E) of the first posterior lateral-line neuromast (L1).

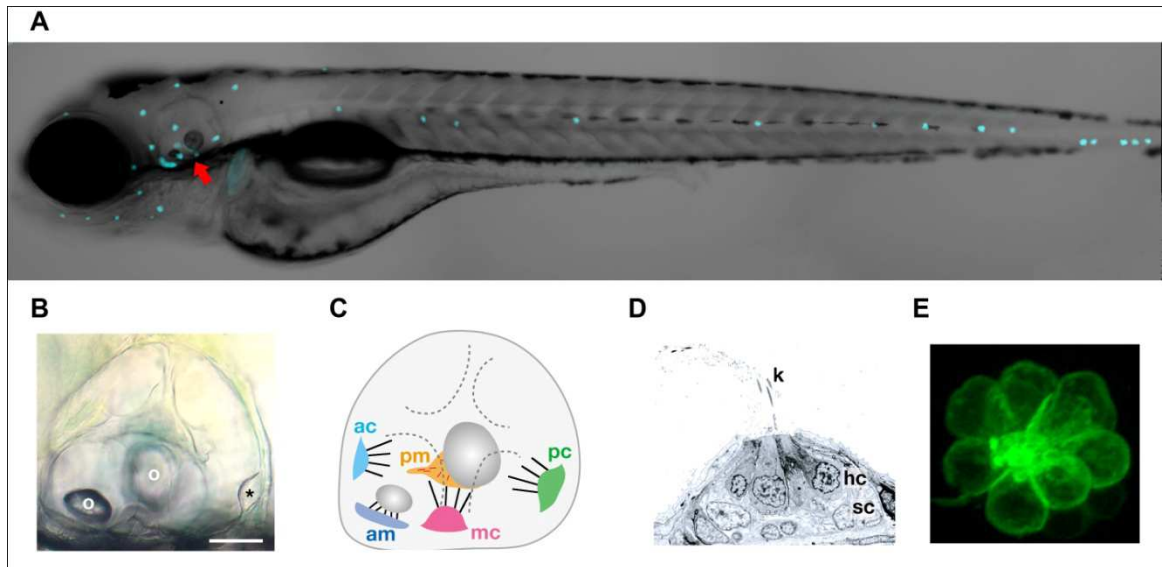


Figure 2. Organization of hair cells in zebrafish larvae. (A) Hair cells in the lateral line and inner ear as labeled by a fluorescent protein driven by the *myo6b* promoter in a 5 dpf zebrafish larva. The inner ear, pointed out by the arrow, is enlarged in (B) and illustrated in (C). Other dots on the trunk and head are superficial hair cells of the lateral line organ. (B) Lateral view of the zebrafish inner ear at 5dpf. (C) Illustration of the larval ear. Colored are the five patches of sensory hair cells. Two otoliths are associated with anterior and posterior maculae respectively. Epithelia that differentiate into semicircular canals are dotted. (D) Transmission EM micrograph of a lateral line neuromast (lateral view). (E) A top-down view of a neuromast labeled by mGFP in *Tg(brn3c:mGFP)* larvae. asterisk, posterior neuroepithelium; ac, anterior crista; am, anterior macula; hc, hair cells; k, kinocilia; mc, medial crista; o, otolith; pc, posterior crista; pm, posterior macula; sc, supporting cells. Modified from (Nicolson, 2005).

1.2. Genetic screen in zebrafish

One of the best feature of zebrafish as a model organism is its unusual capacity for genetic manipulation (Kimmel, 1989). Identification of mutants based on their phenotype allows researchers to define and dissect molecular pathways without existing knowledge. Application of forward genetic screens, which identify genes associated to a specific phenotype unbiasedly, has advanced comprehensive understanding of early development processes of both *Caenorhabditis elegans* and *Drosophila melanogaster* (Brenner, 1974; Nüsslein-Volhard and Wieschaus, 1980). To further extend our knowledge to vertebrates, zebrafish were introduced as a genetic model for studying embryonic development. Zebrafish have quite a few merits that make them an attractive model. First, adult zebrafish can be maintained at low cost with high density. Second, it is easy to obtain a large number of embryos with rapid and synchronized development. Finally, the externally fertilized embryo is transparent, which makes experimental manipulation and observation relatively easy (reviewed by Haffter and Nüsslein-Volhard, 1996).

The genetic approach is of special interest for hearing research because molecular and biochemical analysis of hearing perception has proven to be difficult (Chalfie, 2009). Similar to other mechanosensory systems, the mechanosensory hair cells are relatively scarce. Therefore there is limited material for molecular and biochemical analysis. However, genetic screening is not affected by quantity of protein. From genetic screens in worms and flies, we have gained comprehensive knowledge about our sensory processes, such as sight, smell, and taste on the molecular level. However, most of the structures and molecules of the complex auditory system are unique in vertebrates.

Genetic and molecular analyses of touch in *C.elegans* and *Drosophila*, and subsequent genetic screens for hearing mutants in *Drosophila* have uncovered several proteins important for mechanotransduction, but few of them seem to be essential for hearing in mammals (Kernan et al., 1994; Eberl et al., 1997; Chalfie, 2009). Zebrafish, which shares similar anatomy of the inner ear with higher vertebrates, is therefore a better genetic model to dissect the molecular basis of hair-cell function. Consequently, it has been shown that most zebrafish genes that affect auditory and vestibular function identified in genetic screens are conserved in higher vertebrates (Whitfield, 2002; Nicolson, 2005).

Simple behavioral assays such as the startle reflex and swimming were used to identify zebrafish mutants that affect auditory and vestibular function. Deaf larvae have no auditory startle reflex, an escape behavior in response to sound. Typical signs of vestibular dysfunction in larvae include abnormal body position at rest and swimming in circles (Nicolson et al., 1998). Screens of zebrafish larvae with hearing or balance defects using these criteria identified a number of known and novel deafness genes (Starr et al., 2004; Nicolson, 2005; Obholzer et al., 2008; Gleason et al., 2009; Trapani et al., 2009; Einhorn et al., 2012). Zebrafish mutants with deficits in auditory and vestibular function may or may not have visible anatomical defects (Whitfield et al., 1996; Nicolson et al., 1998; Nicolson, 2005). However, mutants that have developmental defects of the inner ear and/or lateral-line organ often display abnormal swimming behavior as well, if they are viable to 5 days (Granato et al., 1996; Whitfield et al., 1996; Nicolson et al., 1998). In this thesis, two zebrafish mutants identified from forward genetic screens will be presented: *rock solo* mutants, which have impaired development of otoliths (Chapter 2),

and *milky way* mutants, which have vestibular defects but not developmental defects (Chapter 3).

Genetic screens of hearing defects in adult zebrafish have been unsatisfactory. Simple behavioral assays on adults were used to identify mutants with hearing defects. Roughly 1% of over 6500 individual adults following N-ethyl-N-nitrosourea mutagenesis, had defects in responding to a 400 Hz sinusoidal tone burst. Abnormal swim bladders were seen in many of them (26 of 64 mutants), while the rest of them (38/64) had tilted vertebrae dislocating the Weberian ossicles. The swim bladder and Weberian organ interconnected by the vertebrae serve as the conductive system to amplify sound; hence the results of the screen indicates an important role of the auditory conductive system in adult hearing. Further analysis of random wild-type adults without ENU treatment revealed a similar rate (1%) of incidence of conductive defects, suggesting hearing loss in adults may be largely independent of genetic factors (Bang et al., 2002). This is likely because auditory and vestibular function is required for predatory behavior. Zebrafish larvae with severe defects in hearing or balance fail to inflate their swimbladders and usually survive until day 8. With extra feeding and care, a small portion of zebrafish larvae with mild hearing or balance defects can survive to the adult stage (Nicolson et al., 1998). The extra effort involved in raising adults, along with the low incidence of adult phenotypes indicates that large-scale screening is best accomplished at the larval stage.

2. Functional assessment of auditory and vestibular function

2.1. Measuring hearing and balance in mammals

Quick and reliable measurements, including physiological and behavioral analyses, are used as assessments of hearing function in animal models. Physiological measurement of the threshold of the auditory brainstem response (ABR) is the quickest and easiest way of assessing auditory function of mouse mutants. Behavioral analysis, e.g. the conditioned suppression method, measures the complete circuitry from auditory perception to behavior, and hence provides a more comprehensive picture of the auditory system than the ABR recording. Detailed comparisons of behavioral and ABR measures have shown that ABR measurements are more sensitive at low frequencies, while behavioral measurements are better at high frequencies (Heffner and Heffner, 2003). In contrast to ABR measurements, behavioral analysis is a more complete psychophysical determination of auditory function (Willott, 2006).

Behavior and physiological measurements are also available for vestibular function. Vestibular-evoked potentials that can be elicited by loud sound and linear and angular accelerations are developed as physiological measurements of vestibular function (Knox et al., 1993), but the complexity of the experiment prevents its utilization as a general tool for balance assessment. A few behavioral analyses have been used to measure vestibular defects in rodent models, including the rotarod test, circling behavior, contact righting reflex testing, and swim test (Löscher, 2010; Akil and Lustig, 2012). Another representative type of behavior that has been used to monitor vestibular function in model

organisms, as well as clinical tests, is vestibulo-ocular reflex (VOR). To measure VOR, a video-oculography is used to track vestibular-induced eye movements during linear or angular acceleration of head, which allows a comprehensive understanding of both peripheral sensation and central processing of vestibular information (reviewed by Wuyts et al., 2007).

2.2. Measuring hearing and balance in zebrafish

As zebrafish becomes a popular model for development and functional studies of the auditory and vestibular system, quantitative measurement of hearing and balance defects becomes critical. Not only can quantitative measurement give a picture of what is wrong in fish mutants, but it may also be used to screen for mutants with specific impairment. Genetic studies have identified zebrafish mutants with hearing and/or balance defects in larval stage (Nicolson, 2005), but genetic factors are not major causes of hearing defects in adult fish (Bang et al., 2002). Therefore, it is important to consider applying all measurements in zebrafish larvae. In comparison with mouse studies, these tools are very limited.

Like with mouse models, measurement of the ABR has also been used in a developmental study of auditory function in juvenile zebrafish from 10 to 45 mm in body size (Higgs et al., 2002, 2003). Other physiological measurements, such as saccular potentials, have been measured in adult fish (Sisneros, 2007), but few of them have been applied to fish larvae. Successful measurements of the ABR in 5 dpf *Xenopus* larvae have proven the feasibility of using it as a tool for zebrafish larvae (Katbamna et al., 2006).

Using optical monitoring and tracking systems, two behavioral responses have been used to quickly and reliably measure hearing and balance defects for larval zebrafish. The auditory startle reflex (ASR), an escape behavior that can be elicited by acoustic stimuli, was used to quantify hearing function in larval zebrafish. It is also referred as the acoustic evoked behavior response (AEBR) (Zeddies and Fay, 2005; Einhorn et al., 2012). Only three neurons are involved in eliciting startle reflex (Figure 3A): inputs from sensory neurons are transferred to CaP motor neurons by intermediate Mauthner cells (Korn and Faber, 2005). Because the function of Mauthner cells and CaP motor neurons downstream of auditory sensory neurons can be easily assessed using the touch startle reflex (Issa et al., 2011) (Figure 3A), ASR is a sensitive and specific measurement of auditory function in zebrafish larvae. It has been shown that larvae have ASRs to pure tone stimuli from 5 dpf and these responses retain the same threshold and frequency bandwidth until 26 dpf (Zeddies and Fay, 2005). A different set-up using a commercially available video tracking system has been used to monitor escape behavior from tapping, and found no hearing deficit in *trpa1* mutants (Prober et al., 2008). Because tapping of the Petri dish generates a mix of touch, pressure and hearing responses, a mini-shaker (Einhorn et al., 2012) or speaker (Buck et al., 2012) is used to monitor a pure tone elicited ASR. Using these improved devices, partial loss of hearing was observed in zebrafish *stardust* mutants (Einhorn et al., 2012) and larvae treated with ototoxins (Buck et al., 2012).

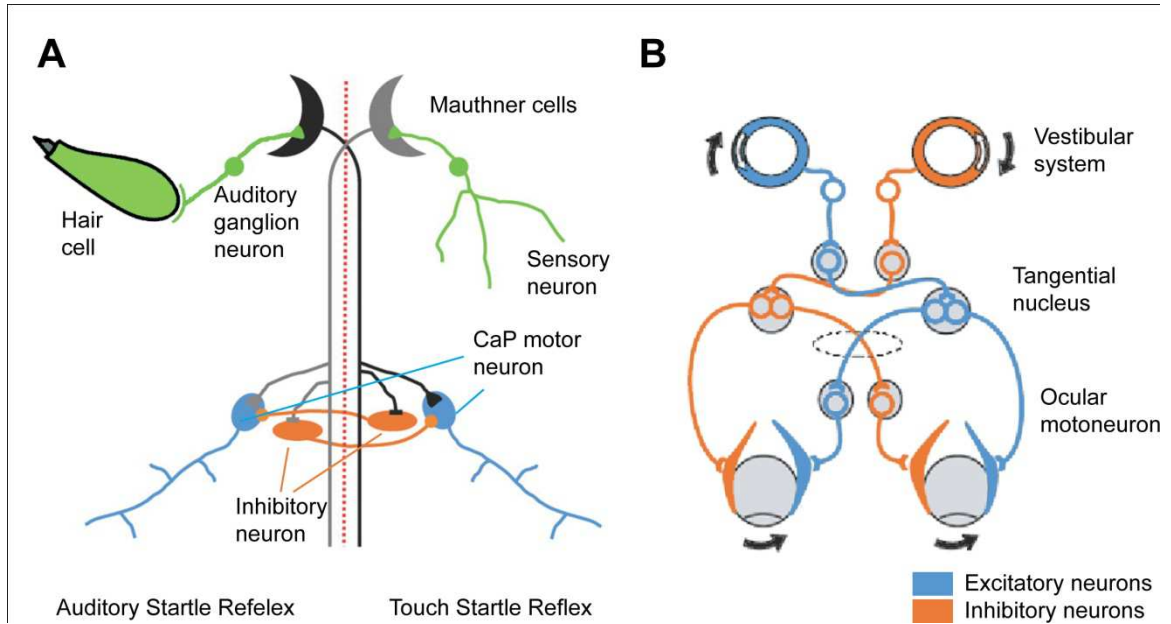


Figure 3. Neural circuitry of the startle reflex and vestibuloocular reflex (VOR). (A) Simplified circuitries of the auditory and touch startle responses. Both circuitries are bilaterally symmetric, but for simplicity, only one side of the circuitry is shown for each. Mauthner cells (black and gray) are innervated by sensory neurons (green). Axons from Mauthner cells cross the midline to innervate contralateral CaP motor neurons (blue) and interneurons that also inhibit the contralateral CaP motor neurons (orange). Modified from (Issa et al., 2011). (B) VOR circuitry in zebrafish. Accelerations are sensed by the vestibular system. Vestibular nerves then propagate information to the tangential nucleus and then ocular motor neurons. Excitatory motor neurons (blue) receive information from one side of the vestibular system; and inhibitory motor neurons (orange) on the other side of both eyes get information for the contralateral vestibular system.

Another behavioral response that has been used to assess balance function in zebrafish larvae is the vestibule-ocular reflex (VOR), which is used by animals to stabilize gaze in response to head movements (Figure 3B). Because the semicircular canals are not developed until approximately 1 month of age in zebrafish (Lambert et al., 2008), head or body tilts about the dorsal-ventral axis do not elicit angular VOR responses until 35 dpf (Beck et al., 2004). However, the larval feeding and escape behavior suggests a functional vestibular system is in place at as early as 4 days of age. In the current study (Chapter 2), we have analyzed the VOR response in larval zebrafish from 60 to 120 hpf. We found that fish larvae develop compensatory eye rotations when they are rotated about the earth-horizontal axis as early as 3 dpf. A follow-up study has confirmed our finding and suggested that the tangential nucleus is responsible for this gravito-inertial VOR (Bianco et al., 2012). The VOR measurement has been proven to be a valuable tool for quantitative measurement of balance function in several mutants (Obholzer et al., 2008; Trapani et al., 2009; Mo et al., 2010c).

3. Mechanoelectrical Transduction in hair cells

3.1. Hair bundle structure

Hair cells rely upon hair bundles for mechanoelectrical transduction (MET). Hair bundles are structures located at the apical surface of hair cells and are composed of a series of rows of actin-rich hair-like stereocilia and a single microtubule-based kinocilium (Figure 4A). Stereocilia are variable in size and shape in different species and hair cell types. A kinocilium is present in hair cells during development, but in most cases degenerate in

mature auditory hair cells. The general configuration of the kinocilium located adjacent to the tallest row of staircase-like stereocilia is found in all hair cells. Among the kinocilium and stereocilia, there are extracellular filaments that interconnect them, such as top connectors and lateral links. In mature mouse inner hair cells (IHCs), only tip-links, top connectors, and ankle links are detectable between stereocilia (Figure 4A). Lateral links are different in different hair cells and different developmental stages (reviewed by Richardson et al., 2011).

3.2. MET channels

Mechanosensation is not specific to hair cells but is a feature of all cells. Many physiological processes, such as osmotic pressure, blood pressure, touch sensation, and hearing, are regulated by MET channels. As their functions suggest, MET channels are a class of proteins with distinct molecular constitutions and properties that make them mechanosensitive. Some of these MET channels are better understood than others, for example, the bacterial MET channel that regulates osmotic pressure, and the MET channel in touch receptors in *C. elegans* have been studied at the molecular level (reviewed by Haswell et al., 2011). Biochemical and biophysical studies have revealed the structure and some basic mechanisms of bacterial MET channels with large (MscL) and small (MscS) conductance (Haswell et al., 2011), yet we do not know the molecular identity of the MET channel in hair cells. Many challenges stand in the way of the identification of the MET channel in hair cells. First, limited numbers of channels per hair cell and hair cells per animal restrict the amount of starting material for purification;

second, a stable *in vitro* culture of hair cells is not available; finally, access to, and manipulation of inner ear hair cells is difficult.

Despite not knowing the molecular components of the hair-cell MET channel, progress has been made in the past a few decades in understanding its properties. Hereinafter the term ‘MET channel’ will refer specifically to the hearing receptor channel if not specified otherwise. Electrophysiological recordings have shown that the MET channel is a non-selective cation channel with a large conductance, e.g. about 250 pS in rat IHCs (Beurg et al., 2006). At the resting membrane potential, the MET channel has a open probability of 10%, suggesting a tension of approximately 5-20 pN is applied to MET channels at rest (Jaramillo and Hudspeth, 1993). Displacement of hair bundles along the excitatory axis by 4-11 nm causes transduction channels to open in microseconds (Ricci et al., 2002; Waguespack et al., 2007). Further displacements of hair bundles to a hundred nanometers can generate currents larger than 1 nA (For more properties of MET channels, see review Fettiplace, 2009).

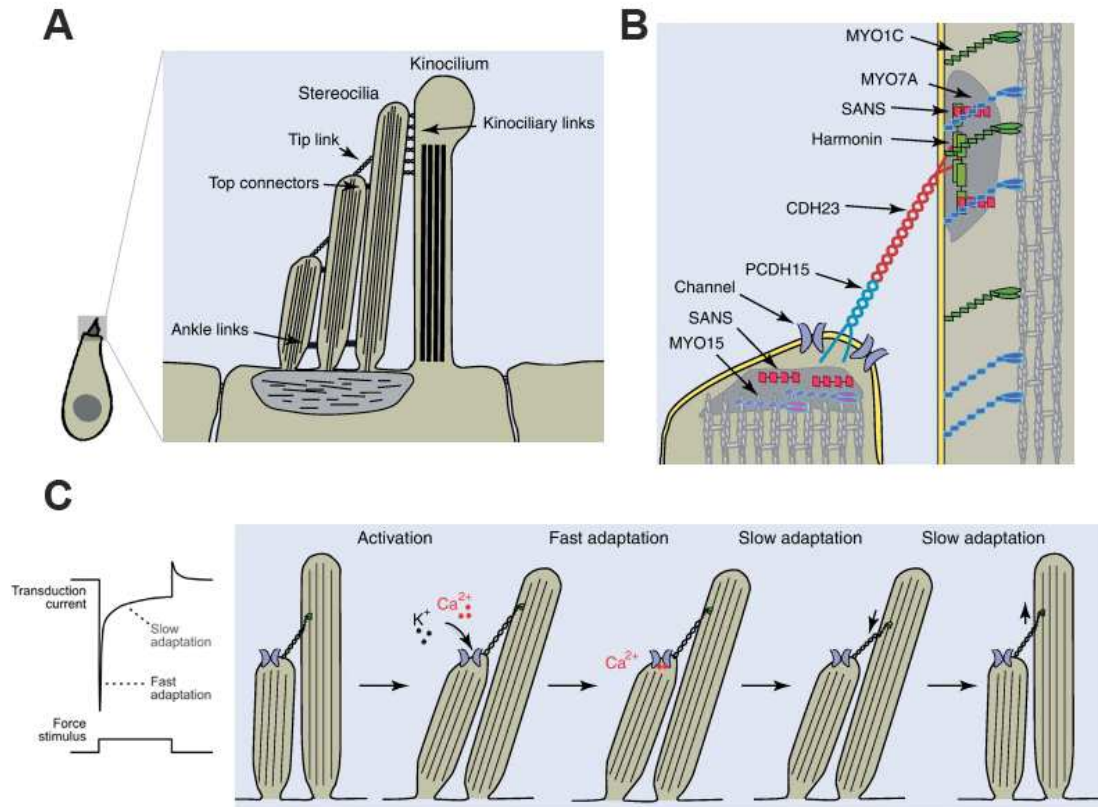


Figure 4. Illustrations of the hair bundle, mechanotransduction machinery, and action of MET channels. (A) Diagram of the hair cell's apical hair bundle shown in cross section. Linkages that connect the stereocilia and the kinocilium are shown. (B) Localization of a subset of known molecules of the mechanotransduction machinery. (C) On the left, a typical mechanosensory current elicited in response to the mechanical stimulus shown below. On the right, illustration of current model of opening and closing of MET channels in response to the mechanical stimulus. MET channels are activated by deflection of the hair bundle toward the longest stereocilia. Stretching of the tip-link is thought to be the gating force. Fast and slow adaptation occur in tandem after a mechanical stimulus is applied to the hair bundle. Modified from (Kazmierczak and Müller, 2012)

Following activation, MET channels undergo adaptation, seen as a decay of sensory currents in response to sustained mechanic stimuli (Figure 4C). Two phases of adaptation have been observed: fast adaptation in a few milliseconds or less, and a subsequent prolonged slower adaptation (Assad et al., 1989; Crawford et al., 1989). Direct Ca^{2+} binding or a biophysical change in the gating spring is thought to be important for fast adaptation, because the kinetics are too fast to be mediated by secondary messengers. A molecular motor is likely involved in driving slow adaptation. Because the extent of adaptation in different types of hair cells is variable, different cell types may use different mechanisms (for detailed discussion see reviews by Peng et al., 2011; Kazmierczak and Müller, 2012).

3.3. Tip links and mechanosensation

Tip links have been proposed to tether the MET channel to hair bundles since their discovery (Pickles et al., 1984). Deflection of hair bundles toward the kinocilia or the tallest stereocilia opens MET channels and depolarizes hair cells, while deflection in the opposite direction closes MET channels and hyperpolarizes hair cells (Shotwell et al., 1981). The orientation of tip links can be the source of directional sensitivity of MET channels (Pickles et al., 1984). MET currents are abolished when tip links are removed by reagents such as calcium chelators (Assad et al., 1991; Zhao et al., 1996) and proteases such as elastase (Preyer et al., 1995). Recovery of MET currents after drug treatment correlates with the reappearance of tip links (Zhao et al., 1996). Recent studies using high speed calcium imaging has found Ca^{2+} enters near the lower end of tip links (Beurg et al., 2009).

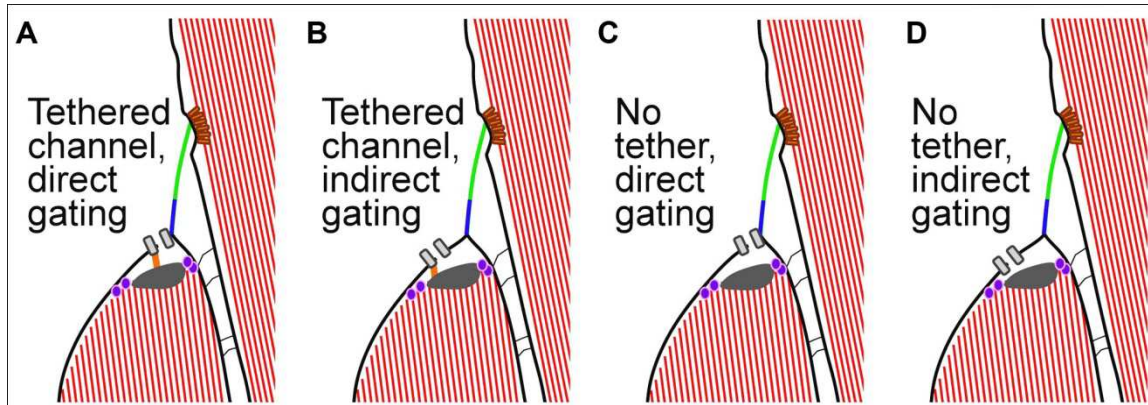


Figure 5. Models of connections between tip-links and MET channels. The upper tip-link protein (Green) is likely CDH23; while the lower tip-link protein (Blue) is likely PCDH15. (A) The MET channel is tethered to the cytoskeleton and gated by PCDH15 directly. (B) The MET channel is tethered to the cytoskeleton, but it does not bind with PCDH15 directly. (C) The MET channel is not tethered to the cytoskeleton, but it binds PCDH15 directly. (D) The MET channel is neither tethered to the cytoskeleton nor gated by PCDH15 directly. Modified from (Powers et al., 2012)

Tip links may connect to hair-cell MET channels directly or indirectly. Four different models are possible based on current experimental evidence (Figure 5). In each model, the tip link has a direct or indirect connection to the MET channel. Experimental measurement of the relationship between the transducer current, the force applied to the hair bundle, and the deflection of the hair bundle has given rise to a gating-spring model of the gating of the MET channel (Howard and Hudspeth, 1988). In this model, displacement of the hair bundle stretches an elastic spring with a stiffness of about 1 mN/m to open the MET channel. It may be reasonable to consider the tip link as the

spring; however, structural and modeling evidence suggests that tip links are too stiff to be the gating spring (Sotomayor et al., 2010). Another possible molecular component of the gating spring is the ankyrin repeats found on the C-terminal tail of ion channels, but they are also not as flexible as the gating spring, as suggested by molecular modeling (Howard and Bechstedt, 2004). Although it is still too early to make any conclusions, the gating spring may be a protein complex that experiences a conformational change, causing the MET channel to open. Alternatively, if tip links are not directly associated with MET channels, nonproteinaceous elements such as lipid membranes or lipid raft structures may also serve as an elastic component of the MET complex.

4. The tip link and MET complex

4.1. Molecular components of the tip link

Because of its clear role in mechanotransduction, extensive efforts have been invested to look for the molecular components of the tip link. Recent evidence has shown that protocadherin 15 (PCDH15) and cadherin 23 (CDH23) together form the lower and upper part of the tip link, respectively (Kazmierczak et al., 2007)(Figure 4B). Hair cells with mutations in either gene often have no tip links, morphological defects of their hair bundles, and hearing and balance defects in zebrafish, mice and humans (Alagramam et al., 2001, 2011; Di Palma et al., 2001; Söllner et al., 2004; Seiler et al., 2005). Antibody labeling of both proteins also detected PCDH15 and CDH23 at tip links (Siemens et al., 2004; Söllner et al., 2004; Ahmed et al., 2006). Further biochemical studies suggest that interactions between the extracellular cadherin (EC) domains of CDH23 and PCDH15

can be replicated *in vitro*. Immunogold labeling of the two proteins indicates a localization of CDH23 at the upper side and PCDH15 at the lower side of the tip link (Kazmierczak et al., 2007). However, some studies have found CDH23 in developing hair bundles but not in mature hair cells, questioning whether CDH23 is a true component of the tip link (Lagziel et al., 2005; Michel et al., 2005). This controversy is further supported by the observation that tip links are found in mouse mutants lacking CDH23 protein (Rzadzinska and Steel, 2009). Perhaps different isoforms of CDH23 or even other proteins are used for the tip link in CDH23 mutants.

Interactions between the tip-link proteins PCDH15 and CDH23 are likely through unconventional *trans*-interactions. In classic cadherins, e.g. C-cadherin (Figure 6A), there are 5 EC domains on each side of the interactive dimer. Usually, large numbers of cadherin molecules line up at intermediate junctions through binding of their first EC (EC1) domains (Niessen et al., 2011). There are many more N-terminal EC domains in CDH23 and PCDH15 than C-cadherins (Figure 6A). And in contrast, CDH23 and PCDH15 form homodimers before they interact each other to form heterotetramers (Kazmierczak et al., 2007). Crystal structures of the first two EC repeats of CDH23 have shown that, although they have typical EC folds, they form *cis*-homodimers *in vitro* (Elledge et al., 2010; Sotomayor et al., 2010). By combining molecular simulation, biochemical and crystallographic evidences, David Corey lab has shown that an antiparallel heterodimer is formed between the first two EC domains of PCDH15 and CDH23 (Sotomayor et al., 2012). In presence of Ca^{2+} , the interaction is thought to be strong enough to mediate mechanotransduction for hair cells.

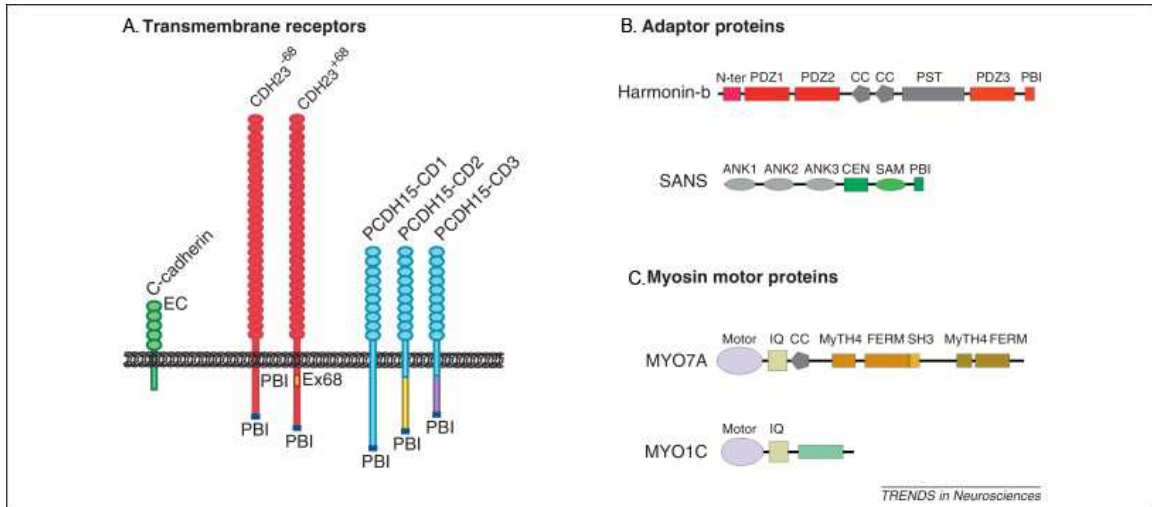


Figure 6. Diagram of molecules involved in mechanotransduction. The domain structure of transmembrane receptors (A), adaptor proteins (B), myosin motors (C) are drawn. Ank, ankyrin-like repeat; cc, coiled-coil domain; CEN, central sans domain; EC, extracellular cadherin repeat; FERM, protein 4.1, ezrin, radixin, moesin domain; IQ, calmodulin binding IQ domain; MyTH4, myosin tail homology 4 domain; N-ter, N-terminal domain of harmonin; PBI, PDZ binding interface; PDZ, PSD95/SAP90, Discs large, zonula occludens-1 domain; PST, proline-, serine-, threonine-rich domain; SAM, sterile alpha-motif domain; SH3, src-homology 3 domain. From (Kazmierczak and Müller, 2012)

4.2. Cytoplasmic domains of the tip-link components

Because they comprise the tip link, the cytoplasmic domains of both CDH23 and PCDH15 may interact with critical components of the MET complex. Since PCDH15 is

located at the lower tip-link (Kazmierczak et al., 2007), where Ca^{2+} enters when MET channels are open (Beurg et al., 2009), it is likely that the cytoplasmic domain of PCDH15 directly connects to the MET complex and CDH23's intracellular domain may be important for other aspects of MET, such as adaptation. In fact, both cytosolic domains have little homology to any other proteins, suggesting that they have a specific role in hair cells.

Two splice variants have been found in the cytoplasmic portion of CDH23 protein (Figure 6A). The shorter isoform without an exon 68 (CDH23-68), which encodes a 35 amino acid peptide, is expressed in many tissues including the inner ear (Siemens et al., 2002; Rzadzinska et al., 2005). The longer splice variant (CDH23+68) is found in hair cells but not the retina in mammals (Siemens et al., 2002); in zebrafish, the long splice variant is found in both the inner ear and the retina (Glover et al., 2012). A recent study also reports that a mammalian specific cysteine, Cys(3240), in CDH23+68 can react with glutathione in cultured cell lines (Yonezawa et al., 2008). The significance of Cys (3240) of CDH23 in mechanotransduction is arguable, as it is not conserved in lower vertebrates. More studies are required to determine which isoform of CDH23 could be the tip-link component.

Three major isoforms are found in the cytoplasmic domain of PCDH15, namely CD1, CD2 and CD3 (Figure 6A). All of them are expressed in hair cells and localized to the hair bundle (Ahmed et al., 2006). CD3 is predominantly at the tip-link location, but CD1 and CD2 are more broadly distributed in the hair bundle. However, genetic knock-out of CD1 or CD3 results in normal development of hair bundles and mechanotransduction

(Webb et al., 2011). CD2 defective mice do not have kinociliary links, and develop abnormal polarity of hair bundles. In zebrafish, only CD1 and CD3, but not CD2, are found in the genome and expressed in lateral-line hair cells (Chapter 5). Together, these results suggest the possibility of overlapping functions among different isoforms of PCDH15.

4.3. Proteins that interact with the cytoplasmic domains of CDH23 and PCDH15

Because of the important role of CDH23 and PCDH15 in mechanotransduction, much attention has been paid to finding proteins that interact with their cytoplasmic domains. Both PCDH15 and CDH23 proteins belong to a family called Usher syndrome type 1 (USH1) proteins, named from the eponymous syndrome with severe hearing and vision loss. This family also includes several other proteins including MYO7A (USH1B), harmonin (USH1C), and SANS (USH1G) (Figure 6A, B, and C). Some of the compound heterozygotes of mutations in proteins within the USH1 family also cause non-syndromic deafness in human beings, which suggests that USH1 proteins act in the same pathway (Schultz et al., 2011). *In vitro* biochemical studies of USH1 proteins have determined complex interactions among several of them, including harmonin, which can interact with all other USH1 proteins (Adato et al., 2005). Many USH1 proteins have also proven to be important for development of hair bundles and/or regulation of MET channels (reviewed by Richardson et al., 2011).

Multivalent interactions between harmonin and the cytoplasmic domain of CDH23 are important (Rzadzinska et al., 2005; Pan et al., 2009; Wu et al., 2012). The subcellular distribution of harmonin is similar to CDH23: both proteins localize throughout the hair

bundle in developing hair cells, but later in development, they are concentrated at the upper tip-link site (Grillet et al., 2009)(Figure 4B). In *deaf circler* mice, a spontaneous mutation in harmonin causes its mislocalization to the tip of stereocilia, which does not affect the formation of tip-links, but slows the activation and adaptation of MET channels (Grillet et al., 2009; Michalski et al., 2009). This suggests that harmonin may be a regulator of the slow adaptation motor. Moreover, harmonin uses its PDZ domains to bring two other USH1 proteins, MYO7A and SANS, to the CDH23 complex at the upper tip-link site (Boëda et al., 2002; Reiners et al., 2005b; Bahloul et al., 2010; Yan et al., 2010; Grati and Kachar, 2011)(Figure 4B, 6B). Mutations in both MYO7A and SANS affect the MET currents: smaller amplitudes in SANS mutants, and slower activation and faster adaptation in MYO7A mutants. Both mutants have morphological defects in their hair bundles (Self et al., 1998; Ernest et al., 2000; Kros et al., 2002; Caberlotto et al., 2011). In addition, MYO7A appears to control the resting tension of hair bundles (Kros et al., 2002).

Another important protein interacting with CDH23 is MYO1C (Siemens et al., 2004)(Figure 6C). Many studies have shown that MYO1C is localized ubiquitously in the hair bundle in rodents and affects adaptation when inactivated (Holt et al., 2002; Stauffer et al., 2005; Phillips et al., 2006). Because both MYO1C and MYO7A have been shown to interact with CDH23 and to affect adaptation of MET currents, these findings suggest that the CDH23 complex at the upper tip-link site is important for regulating adaptation of MET channels. Further studies will be needed to elucidate the real adaptation motor and how the upper tip-link site regulates adaptation.

To extend our knowledge of the CDH23 complex beyond the USH1 protein network, several efforts to look for interaction partners of CDH23 using unbiased yeast two-hybrid screens have been undertaken. In a screen using the cytoplasmic domain of CDH23+68 as bait, Xu and colleagues identified MAGI-1 as a potential scaffold protein localized in stereocilia (Xu et al., 2008). Meanwhile, they have also found PIST, a protein that appears to regulate vesicle trafficking (Xu et al., 2010). Another vesicle protein EHD4 was found in another screen to interact with CDH23 (Sengupta et al., 2009). Since CDH23 has been shown to localize at presynaptic regions in hair cells (Reiners et al., 2003; Lagziel et al., 2009; Zallocchi et al., 2012a, 2012b), these interaction proteins may be related to the potential function of CDH23 at ribbon synapses.

Less is known about the protein complex associated with the cytoplasmic domain of PCDH15 at the lower tip-link site. USH1 proteins MYO7A (Senften et al., 2006) and harmonin (Adato et al., 2005; Reiners et al., 2005a) were found to interact with PCDH15 *in vitro*. However, they are unlikely in the same protein complex in hair cells, because MYO7A and harmonin do not specifically localize to the lower tip-link site (Senften et al., 2006; Michalski et al., 2009). HCN1, which is expressed in hair cells, has been found to interact with PCDH15-CD3 in a Ca^{2+} dependent manner (Ramakrishnan et al., 2009, 2012b). However, HCN channels are mainly localized to the basolateral membrane and not in stereocilia (Horwitz et al., 2011). They can be activated by hyperpolarization (Horwitz et al., 2011), but not mechanic deflection of hair bundles (Horwitz et al., 2010). Whether HCN1 binds to PCDH15-CD3 *in vivo* and the physiological function of the interaction has yet to be determined.

There are also some proteins expressed at the lower tip-link site, but they have not been found to interact with PCDH15, such as MYO15, Whirlin, and SANS (Delprat et al., 2005; Mburu et al., 2006; Caberlotto et al., 2011). MYO15, when mutated, causes shortening of stereocilia and abnormal fast adaptation of MET currents (Stepanyan and Frolenkov, 2009). Mutations in MYO15 also lead to Usher-like symptoms in rats (Held et al., 2011). Whether there are direct or indirect connections between these proteins and PCDH15 is worthwhile to explore.

Because PCDH15 is proposed to connect with the MET channel complex directly or indirectly, finding its interacting partners is critical for understanding the mechanotransduction process in hair cells. So far, there is no compelling evidence of *bona fide* interactors with the cytoplasmic domain of PCDH15 *in vivo*. To find potential partners of PCDH15, I have conducted a membrane-based yeast two-hybrid screen using the full length of zebrafish PCDH15a as bait and zebrafish inner ear cDNA library as prey. A summary of the interactions is presented in Chapter 5.

4.4. MET channel candidates

From what is known about hair-cell mechanotransduction, there are certain criteria for candidates of MET channels. First, MET channels should be expressed in hair cells from the time of mechanotransduction onset and localized to the lower tip-link site, where the influx of Ca^{2+} has been observed (Beurg et al., 2009). Additionally, they should fulfill many distinct biophysical properties that have already been defined, e.g., nonselectivity to cations and permeability to aminoglycosides (reviewed by Peng et al., 2011). Last but not least, MET channels are members of either a protein family, or have multiple variants

or different posttranslational modifications, because the single-channel conductance and kinetics are largely variable even within the same species (Ricci et al., 2003). Based on our current knowledge, MET channels are most likely to operate as heterotetramers (reviewed by Fettiplace, 2009).

Although a few candidates have been proposed, no channels that fully satisfy the criteria for the hair-cell MET channel have been identified (reviewed by Vollrath et al., 2007). Among the most interesting candidates are transient receptor potential (TRP) channels. TRP channels are usually nonselective channels operating as tetramers with high single-channel conductance and Ca^{2+} permeability (Owsianik et al., 2006). NOMPC/TRPN1 was identified by genetic screens for mechanosensory genes in *Drosophila* that directly contribute to the MET currents (Kernan et al., 1994; Walker et al., 2000; Effertz et al., 2012). NOMPC appears to affect hearing in zebrafish as well (Sidi et al., 2003), but it cannot be the principle MET channel because it is not localized to stereocilia (Shin et al., 2005) and not found in mammals. TRPA1 has been proposed to be another candidate because of its expression in hair cells (Corey et al., 2004), but it also does not fit the criteria for the MET channel in either zebrafish (Prober et al., 2008) or mammals (Kwan et al., 2006). In our current work (Chapter 5), we have characterized the expression of several TRP channels in zebrafish hair cells, and a mutant is available for *trpm7*. Our imaging data of mechanically-dependent fluorescent dye labeling in hair cells indicate that mutation of *trpm7* does not affect mechanotransduction.

Another family of proteins, the TMCs (Transmembrane Channel-like), have recently become candidates for MET channels. Mutations in TMC1 were first identified to cause

hearing loss in both humans (Kurima et al., 2002) and mice (Vreugde et al., 2002; Manji et al., 2012). Subsequent studies have determined that both TMC1 and TMC2 are expressed in hair cells and required for mechanotransduction (Kawashima et al., 2011), although a previous study of TMC1 suggested that mutations affect maturation of hair cells (Marcotti et al., 2006). In our non-biased yeast-two hybrid screen (Chapter 5), we identified zebrafish *Tmc2a* as an interaction partner of *Pcdh15a*. We also detected *tmc1*, *tmc2a*, *tmc2b* mRNA expression in hair cells of the zebrafish inner ear. These results are promising, but further studies are required to determine how TMC1 and TMC2 affect MET currents of hair cells and whether TMC proteins are components of the MET channel complex.

5. Synaptic transmission in hair cells

5.1. Properties of synaptic transmission in hair cells

Ribbon synapses with specialized synaptic transmission characteristics are required for hair cells to faithfully transfer electrochemical information to downstream neurons (Figure 7). As displacements of hair bundles trigger mechanotransduction, mechanical stimuli are precisely transduced into graded electrical signals. In response, ribbon synapses couple vesicle fusion to changes in membrane potentials (Juusola et al., 1996). Vesicle fusion at ribbon synapses is different than the all-or-none vesicle fusion at conventional synapses in the central nervous system (CNS). In order to distinguish sounds with intervals less than 1 ms (Narayan et al., 1998), auditory hair cells have to maintain very fast and synchronized neurotransmitter release. Hair cells show sustained

vesicle releases in response to ever-present sound signals. This tonic release property is thought to rely on a large number of vesicles attached to the ribbon synapse (reviewed by von Gersdorff, 2001; Schmitz, 2009).

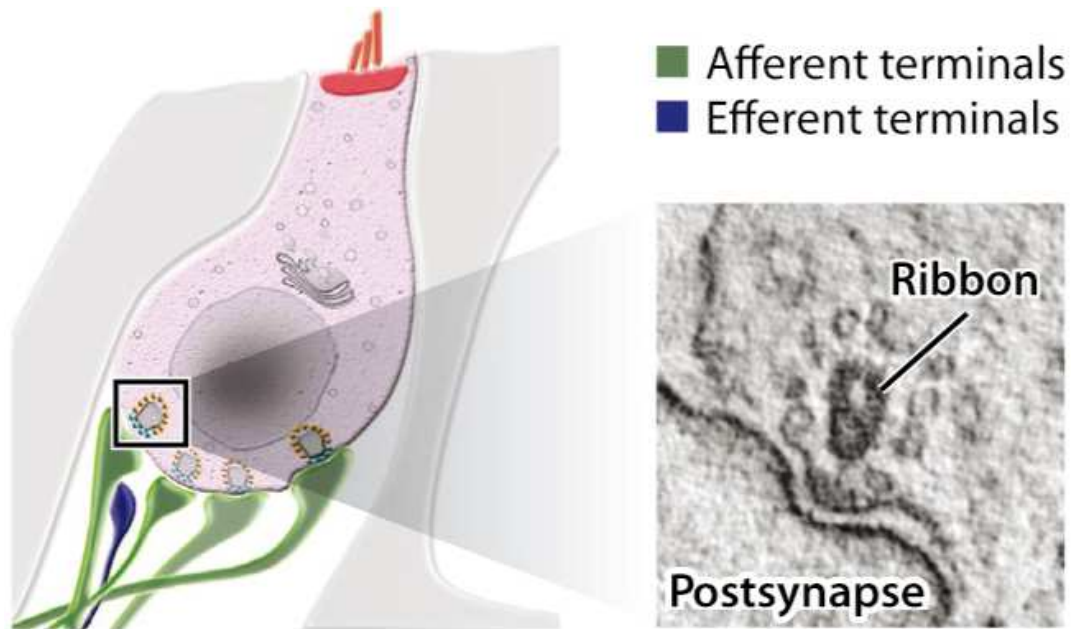


Figure 7. Diagram of a hair cell innervated by afferent nerves (green) and an efferent nerve (blue). At the presynaptic site, the hair cell has ribbon synapses. An EM picture of mammalian IHC's ribbon synapse is shown on the right with an electron dense ribbon body surrounded by synaptic vesicles. Modified from (Safieddine et al., 2012).

5.2. Structure of ribbon synapses

Ribbon synapses are named by the special electron dense structures called synaptic ribbons at the presynaptic active zone (Figure 7). In addition to being in hair cells, similar synaptic structures have been found in other sensory neurons in the retina and pineal

glands, suggesting that ribbon synapses are important to transmit sensory stimuli. In hair cells, synaptic ribbons are usually round or ellipsoid shape, in comparison with the rod or ribbon-like shape found in the retina. Most (>95%) ribbons are found attached to the membrane at active zones in a one-to-one pattern (Zenisek et al., 2004). The size and number of ribbon synapses is highly variable in different species, developmental stages, and tonotopic positions. In zebrafish neuromasts, each hair cell contains around 3 synaptic ribbons of about 100 nm in diameter (Sheets et al., 2011). Sacculus hair cells in frogs usually have about 20 large (>400 nm) ribbons (Roberts et al., 1990; Lenzi et al., 1999). In many other species, such as turtle (Schnee et al., 2005), gerbil (Slepecky et al., 2000), and cat (Lieberman et al., 1990), hair cells with different characteristic frequencies have diverse numbers and sizes of synaptic bodies. Ribbon synapses can also vary over development. In comparison to many small ribbons in mouse inner hair cells before hearing onset, fewer and larger ribbons are attached to the active zone after onset of hearing (Sobkowicz et al., 1982; Nemzou et al., 2006; Sendin et al., 2007).

Another feature of ribbon synapses is a halo of synaptic vesicles that physically link to the electron dense ribbon body by thin filaments of unknown composition (Lenzi et al., 1999) (Figure 7). In fact, hair cells have three pools of synaptic vesicles: vesicles docked to the plasma membrane, vesicles associated with ribbon bodies, and free floating vesicles. Three-dimensional reconstructions using electron tomography have estimated about 32 docked vesicles and around 376 tethered vesicles per ribbon body in frog sacculus hair cells (Lenzi et al., 1999). Another study using ultrathin EM sections has estimated 16–30 docked vesicles per ribbon in mouse IHCs (Khimich et al., 2005). The portion of tethered vesicles is relatively small considering the 10,000–30,000 cytoplasmic

vesicles near each active zone (Lenzi et al., 1999). Moreover, the number of both docked and floating vesicles in ribbon synapses is much greater than the numbers in conventional hippocampal synapses, in which 8 to 10 of about 200 vesicles are docked (Schikorski and Stevens, 1997). The large number of vesicles is thought to be important for fast and precise tonic release at ribbon synapses (reviewed by Nouvian et al.; and Schmitz, 2009).

5.3. Molecular composition of ribbon synapses

Recent unbiased surveys of protein components of ribbon synapses in the cochlea and retina have directly shown the similarity between ribbon synapses (Uthaiiah and Hudspeth, 2010). Although both ribbon synapses share most of their protein components with conventional synapses, they are unique in several components such as complexins and synaptotagmins (reviewed by Zanazzi and Matthews, 2009). Understanding how the molecular apparatus is built and functions at synaptic ribbons will be crucial for determining which components of synaptic transmission differ or are conserved in these sensory neurons.

RIBEYE is the most abundant and unique protein component of ribbon synapses (Figure 8). RIBEYE is estimated to make up to 67% of the total mass of the electron-dense ribbon body (Zenisek et al., 2004) and makes up 30% of the total protein content of the ribbon complex that associated with the ribbon body in the retina (Kantardzhieva et al., 2012). A putative role of RIBEYE in ribbon synapses is to build a scaffold to recruit other proteins (Schmitz et al., 2000). In fact, multiple self-interaction domains inside the RIBEYE protein make it an ideal structural element for the ribbon body. Exogenous RIBEYE proteins in cultured cells can aggregate by themselves and recruit surrounding

vesicles and membrane compartments (Magupalli et al., 2008). Overexpression of RIBEYE in hair cells creates extra-large ribbons and floating RIBEYE aggregates (Sheets et al., 2011). In contrast, genetic ablation of RIBEYE in zebrafish leads to smaller ribbons or total abolishment of ribbon bodies (Wan et al., 2005; Sheets et al., 2011; Lv et al., 2012). RIBEYE has been shown to interact with several proteins such as Bassoon (tom Dieck et al., 2005), Munc119 (Alpadi et al., 2008), BRAG1 (Katsumata et al., 2009), and GCAP2 (Venkatesan et al., 2010), which also participate in regulating synaptic transmission. Besides its structural role, RIBEYE is thought to have enzymatic activity that could be crucial for binding of other protein partners to the ribbons (Schmitz et al., 2000; Venkatesan et al., 2010; Schwarz et al., 2011). Recent studies using antibodies specifically against RIBEYE have pulled out a large number of important players in conventional synapses, suggesting that RIBEYE is the key for the structure and function of ribbon synapses (Uthaiiah and Hudspeth, 2010; Kantardzhieva et al., 2012).

Besides RIBEYE, synaptic transmission in hair cells requires several proteins that are less common at conventional synapses (Figure 8). Among them, the best characterized are the L-type Ca^{2+} channels (Ca_v1 family), vesicular glutamate transporter 3 (Vglut3), and otoferlin. Auditory hair-cell ribbon synapses predominantly require $\text{Ca}_v1.3$ Ca^{2+} channels ($\text{Ca}_v1.4$ in retina) to mediate synaptic transmission, rather than the $\text{Ca}_v2.1$ or $\text{Ca}_v2.2$ Ca^{2+} channels used at conventional synapses (Brandt et al., 2003, 2005; Michna et al., 2003; Sidi et al., 2004). Several lines of evidence suggest that clustered Ca^{2+} channels within nanodomains in the active zone of ribbon synapses are important for the synchronized release of neurotransmitters (Roberts et al., 1990; Tucker and Fettiplace, 1995; Rodriguez-Contreras and Yamoah, 2001; Brandt et al., 2005).

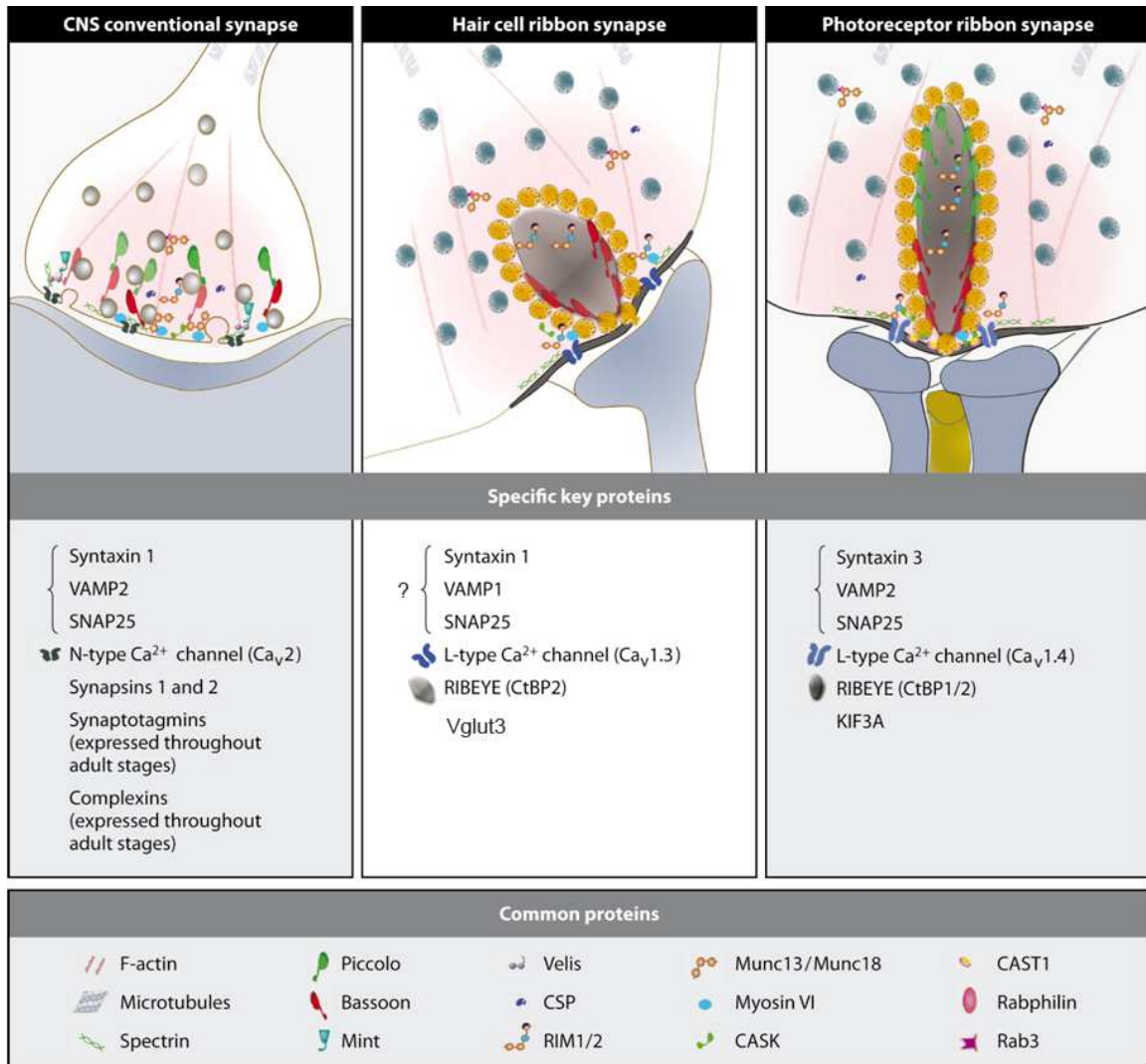


Figure 8. Diagrammatic representation of mature synapses in the rodent CNS, hair cells, and photoreceptor cells. Certain unique proteins are present in each type of synapse, while many proteins are shared by all of them. Modified from (Safieddine et al., 2012).

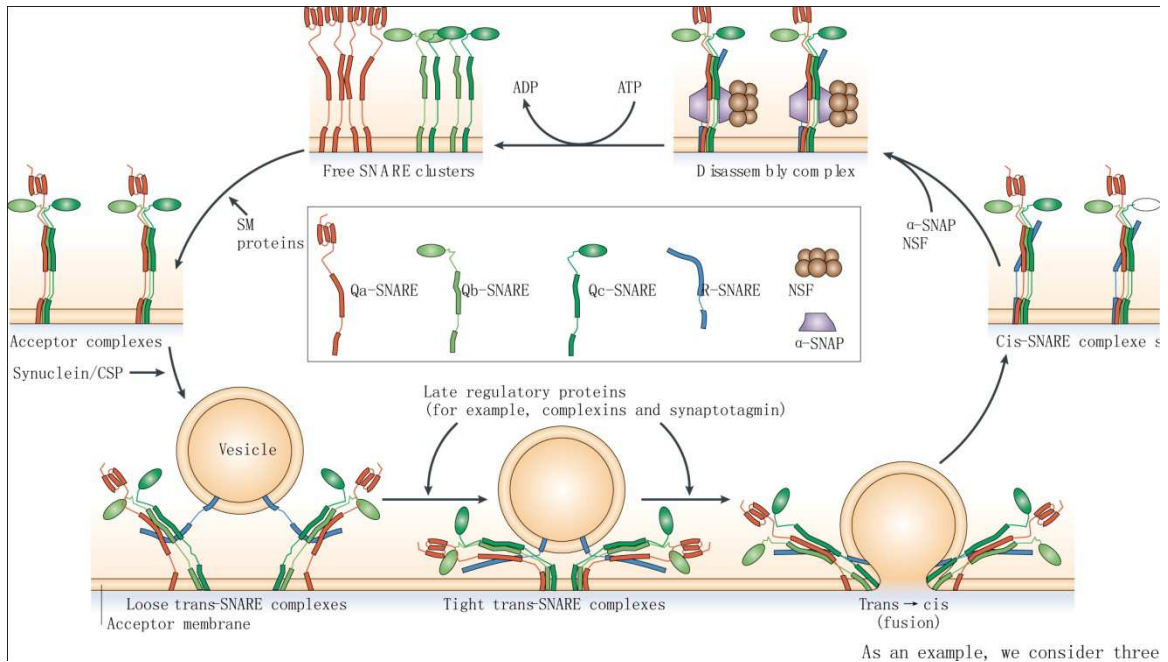


Figure 9. The SNARE cycle in vesicle fusion. As shown in the upper left hand side, first, free standing Q-SNAREs are on the presynaptic membrane with their N-termini toward the cytoplasm. SM (Sec1/Munc18-related) proteins are required for them to form acceptor complexes, which then interact with R-SNAREs on the vesicle membrane. This process is promoted by Synuclein and CSP proteins. Interacting Q- and R SNAREs go through serial stages from loose trans- to tight trans- then to cis-SNAREs. The transition from trans- to cis-SNAREs opens the fusion pore on the vesicle. After vesicle fusion, SNAP and NSF proteins dissociate cis-SNARE complexes to release free SNAREs, which is ATP dependent. Modified from (Jahn and Scheller, 2006).

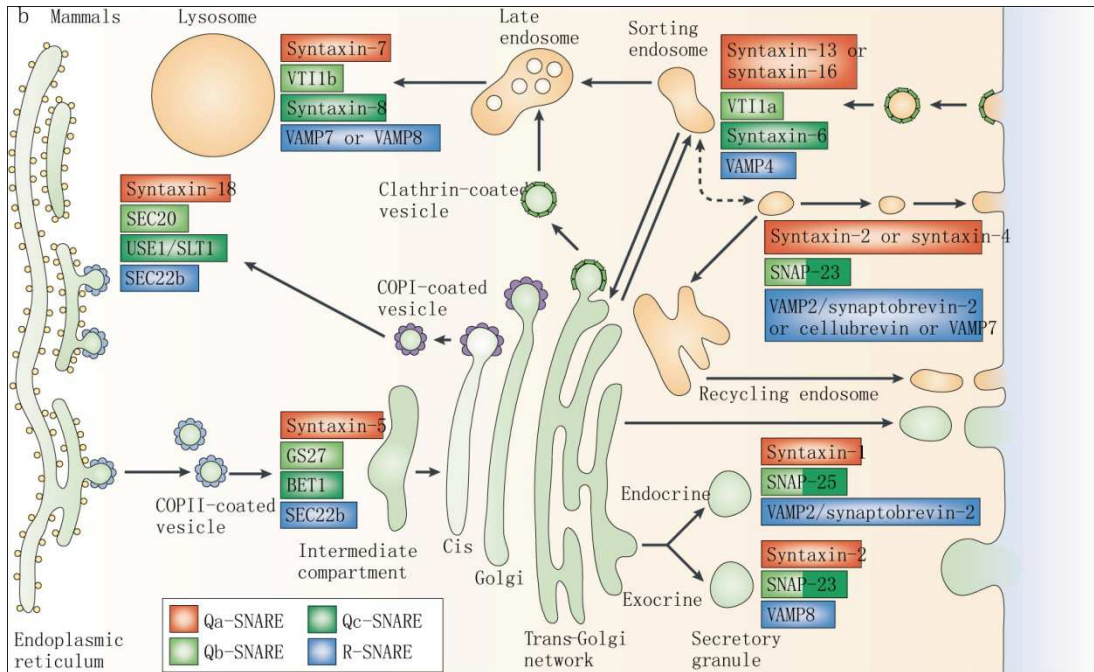


Figure 10. Mammalian SNAREs for trafficking in different pathways. Many pathways involving vesicle fusion do not yet have specific SNAREs identified. From (Jahn and Scheller, 2006).

The vesicular glutamate transporter fills synaptic vesicles with glutamate. Vglut1 and -2 proteins appear to have mutually exclusive distributions and functions in the central nervous system (Freneau et al., 2004), while mutations of Vglut3 specifically affect hair cells (Obholzer et al., 2008; Ruel et al., 2008; Seal et al., 2008). Considering that the transporter activity of Vglut3 is slightly different than Vglut1 and -2 (Gras et al., 2002), it would be interesting to test if Vglut1 or -2 can fully rescue Vglut3 defects in hair cells.

Otoferlin was first identified as a human nonsyndromic deafness gene, and is thought to be the Ca^{2+} sensor for synaptic transmission in auditory hair cells (Roux et al., 2006;

Dulon et al., 2009). However, its function is not equivalent to Synaptotagmin1, the Ca^{2+} sensor for conventional synapses (Reisinger et al., 2011). It is likely that Synaptotagmin IV and Otoferlin play different roles in Ca^{2+} -dependent vesicle fusion at ribbon synapses (Beurg et al., 2010; Johnson et al., 2010). Despite compelling data, the true Ca^{2+} sensor for ribbon synapses and how it is related to the kinetics of synaptic transmissions remains elusive.

Many studies suggest that ribbon synapses either lack or use different (though homologous) key proteins from those that are indispensable in conventional synapses (reviewed by Safieddine et al., 2012). The list of the synaptic proteins that are different in hair cells includes synapsins (Mandell et al., 1990), complexins (Reim et al., 2005; Zanazzi and Matthews, 2010), and synaptotagmins (Johnson et al., 2010). Although Munc13—a protein that completely eliminates primed synaptic vesicles in hippocampal neurons when mutated—is expressed in ribbon synapses, its defects do not affect synaptic transmission in mouse photoreceptor ribbon synapses (Cooper et al., 2012). Using proteins that are different from conventional synapses may be important for the specific duties that ribbon synapses face, but more detailed studies are needed.

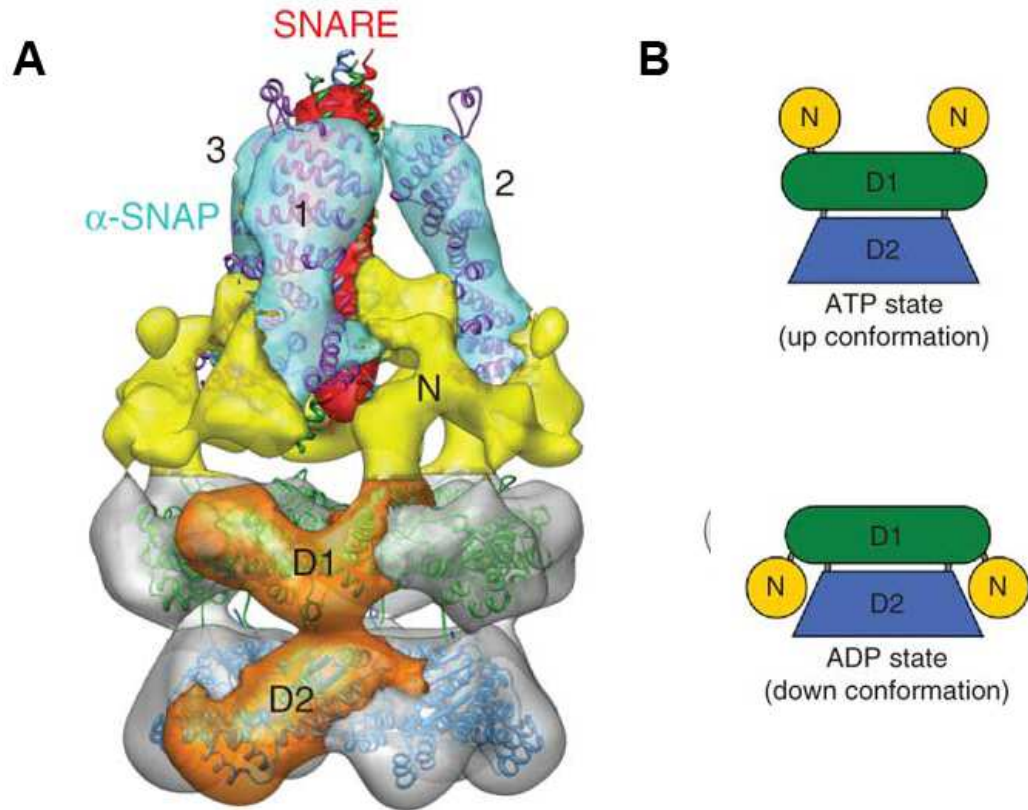


Figure 11. Structure and mode of action for the NSF protein. (A) 3D structure of the NSF-SNAP-SNARE 20S particle reconstructed using negative stain EM. Crystal structures of α -SNAP (PDB:1QQE; 1, 2, and 3 colored in light blue), and SNARE complex (PDB:1SFC; colored in red) are overlaid with the EM structure. Colored in yellow are EM structures of N-domains of NSF. The cryo-EM structures of the D2 (blue) and D1 (green) domains of NSF are also shown. (B) Diagram of NSF bound to either ATP (top) or ADP (bottom). Note the conformational change in the N domain of NSF from the up to the down position. Modified from (Chang et al., 2012).

6. NSF and synaptic transmission

6.1. Exocytotic complex in conventional synapses

In the established synaptic model, the soluble NSF attachment protein receptors (SNARE) protein complex is the central machinery for membrane fusion (Jahn and Scheller, 2006).

The SNARE hypothesis posits that two sets of SNAREs sitting on the opposing to-be-fused membranes interact to form complexes, which are then dissociated by N-ethylmaleimide-sensitive factor (NSF) after fusion. The role of NSF is to guarantee a pool of free SNARE proteins that are ready for membrane fusion. The cycling of SNAREs is key to high efficient synaptic fusion (Jahn and Scheller, 2006)(Figure 9). In Chapter 3, I will present my work on NSF and its potential SNARE substrates in zebrafish hair cells.

To effectively mediate vesicle fusion, one of each of four types of SNARE proteins is required: Qa-, Qb-, Qc- and R-SNAREs (Figure 9). They are classified based on the conserved glutamate (Q) and arginine (R) residues in the central motifs contributing to the fusion step (Fasshauer et al., 1998). The four SNARE subtypes are conserved in yeast, plants and mammals, suggesting a universal mechanism of binding (Bock et al., 2001).

Another system categorizes SNAREs into vesicular- or v-SNAREs, which are on vesicle membranes, and target- or t-SNAREs, which are on the target membranes. Although it is difficult to define v- and t-SNAREs in the scenario of vesicle-vesicle fusion, this nomenclature is commonly used to describe exocytosis.

Different sets of SNAREs are used for various intracellular processes (Figure 10). In eukaryotic cells, over 60 SNARE proteins are expressed. Many of them are specialized

for certain types of membrane fusion and require specific interaction partners (Hong, 2005). This provides a complex yet robust regulatory network of membrane fusions in the cell. For the synaptic vesicle fusion process, neuronal SNAREs are used: SNAP-25 (Qbc-SNARE) and Syntaxin1 (Qa-SNARE) as Q-SNAREs, and VAMP (Synaptobrevin)-1 or -2 as R-SNAREs.

The fusion cycle of synaptic vesicles is regulated by a few key proteins (Figure 9). In order to have Qa-, Qb-, Qc-SNAREs form a Qabc-complex on the trans-membrane, Munc18 is recruited (Voets et al., 2001; Weimer et al., 2003). Then the assembly of R-SNAREs with Qabc-complex is promoted by a few chaperones including CSPs and Synucleins (Burré et al., 2010; Sharma et al., 2011). Both protein families have neuroprotective roles (Fernández-Chacón et al., 2004; Chandra et al., 2005; Gretchen-Harrison et al., 2010; Burgoyne and Morgan, 2011). The catalytic step of synaptic vesicle fusion is Ca^{2+} dependent and regulated by Synaptotagmin-1 and Complexins (reviewed by Chapman, 2008; Südhof, 2012). After synaptic fusion, SNARE complexes have to be dissociated and recycled, for which two important chaperones are NSF and α -SNAP (reviewed by Südhof and Rizo, 2011; Zhao et al., 2012).

6.2. Structure and function of NSF

N-ethylmaleimide-sensitive factor (NSF) is a key protein to catalyze dissociation of SNARE complexes. It was the first protein identified to specifically regulate vesicle trafficking (Wilson et al., 1989). The function of NSF is well characterized: it is an ATPase that disassociates the SNARE complex upon ATP hydrolysis, which frees SNARE proteins from the exocytotic complex. It belongs to the protein family of ATPase

associated with various cellular activities (AAA+). Shared by all members of the AAA+ family is the AAA domain that binds ATP. In NSF, two AAA domains are at the C-terminus: NSF-D1 (206-477) and NSF-D2 (478-744). NSF-D1 is the ATPase domain that catalyzes SNARE disassembly, while the NSF-D2 is the self-interaction domain that helps NSF to form a homo-hexamer. The N-terminal domain (NSF-N, 1-205) is supposed to bind to the soluble NSF attachment protein (α SNAP) and the SNARE complex (reviewed by Zhao et al., 2012) (Figure 11A). The NSF- α -SNAP-SNARE complex has been purified as a 20S functional particle for membrane fusion (Wilson et al., 1992). A recent 3D structure of the 20S particle has demonstrated that the ATP driven conformational change of NSF-N is important for its catalytic function (Chang et al., 2012; Moeller et al., 2012) (Figure 11B).

As a key regulator of vesicle fusion, NSF activity is also regulated by enzymatic modifications. During synaptic transmission, influx of Ca^{2+} can promote phosphorylation of NSF by the PKC pathway, which dissociates the NSF-hexamer, thereby inhibiting neurotransmitter release (Matveeva et al., 2001). Phosphorylation of NSF by tyrosine kinases prevents its binding to α -SNAP, which also decreases synaptic release. Conversely, dephosphorylation by tyrosine phosphatase PTP-MEG2 increases vesicle fusion (Huynh et al., 2004). Similar regulation of phosphorylation of NSF by PTP1B is important in regulating exocytosis in human sperm (Zarelli et al., 2009). Other modifications such as oxidation (Matsushita et al., 2005) and nitrosylation (Matsushita et al., 2003) of NSF also affect exocytosis.

The canonical function of NSF is largely based on its interaction with the SNAP-SNARE complex and its corresponding enzymatic activity. However, identification of additional binding partners points to other roles for NSF (reviewed by Zhao et al., 2007). Besides the well characterized binding of NSF with AMPA receptors to regulate synaptic transmission (Nishimune et al., 1998; Osten et al., 1998; Song et al., 1998), NSF interacting proteins also include GABA receptors (Goto et al., 2005; Pontier et al., 2006), and dopamine receptors (Heydorn et al., 2004; Zou et al., 2005). In cell lines, NSF also binds with β 2 adrenergic receptors (Cong et al., 2001) and β -arrestins (McDonald et al., 1999; Huang et al., 2010), which suggests a role for NSF in regulating recycling of GPCRs. These results suggest that NSF is critical for regulating the trafficking of various receptors between different membrane compartments.

6.3. Exocytotic complex at hair-cell ribbon synapses

Similar to any other membrane fusion process, it is well accepted that synaptic exocytosis at ribbon synapses is also driven by SNARE complexes (Schmitz, 2009; Zanazzi and Matthews, 2009; Ramakrishnan et al., 2012a; Safieddine et al., 2012) (Figure 8).

Virtually all neuronal SNAREs have been reported to also localize to retinal ribbon synapses except Syntaxin-1 (reviewed by Zanazzi and Matthews, 2009). Syntaxin-3, instead of Syntaxin-1, is responsible for synaptic exocytosis at retinal ribbon synapses (Morgans et al., 1996; Sherry et al., 2006; Curtis et al., 2008, 2010). Transcripts and proteins of SNAP25 and Syntaxin-1 are in the inner and outer hair cells in rat and guinea pig (Safieddine and Wenthold, 1999; Eybalin et al., 2002). VAMP 1 and 2 proteins are also found in guinea pig hair cells (Safieddine and Wenthold, 1999; Layton et al., 2005).

Immunoprecipitation from chicken cochlea using antibodies against RIBEYE has identified all neuronal SNAREs as well (Uthaiiah and Hudspeth, 2010).

Despite existing data to support their expression in hair cells, a recent study by the Moser lab suggests that neuronal SNARE proteins are not required for synaptic transmission at hair-cell ribbon synapses. They did not detect VAMP-1 and -2, SNAP-25, and Syntaxin-1 in mouse IHCs by immunohistochemistry. In the same study, however, transcripts of VAMP-2 and SNAP-25 were reliably detected in IHCs using RT-PCR (Nouvian et al., 2011). A possible explanation is that immunohistochemistry can be less sensitive or is a less reliable technique. The Moser group found that botulinum neurotoxins (BoNT) that cleave SNAP-25, syntaxin-1–3, and synaptobrevin-1–3 cannot block exocytosis in IHCs. Genetic knockout of VAMP-1, or VAMP-2 and -3, or SNAP25 in mouse IHCs does not affect synaptic transmission either (Nouvian et al., 2011). Growing axons during neurogenesis (Verderio et al., 1999) or synaptic vesicles with high pH (Matteoli et al., 1996) have also been found insensitive to BoNT cleavage. Although it is unclear why some synapses are less sensitive to botulinum neurotoxins, it is possible that the special components of hair-cell ribbon synapses are insensitive to BoNT.

Based on our current knowledge, it is unclear whether hair cells use neuronal SNAREs, or unconventional SNAREs, or no SNAREs for their synaptic transmission. In this thesis I describe the detection of NSF, VAMP-2, and VAMP-8 proteins in zebrafish hair cells using immunohistochemistry (Chapter 3, 4). Although no direct evidence of the role of these proteins in regulating synaptic transmission has been obtained, forward genetic

screens for auditory/vestibular mutants in zebrafish uncovered a mutation in *nsf* (Chapter 3).

6.4. Exocytotic complex and neurological diseases

Dysfunction of neuronal SNAREs is often associated with severe neurological defects. Homologous VAMP2 and SNAP25 knockout mice are embryonic lethal with no evoked synaptic transmission, but nerve growth is not affected in mutants (Schoch et al., 2001; Molnár et al., 2002; Washbourne et al., 2002). A dominant mutation in SNAP25 causes ataxia with impaired vesicle trafficking (Jeans et al., 2007). VAMP1 null mutants are immobile and die early after birth with severe neurological defects (Nystuen et al., 2007). Loss of neuronal specific VAMP in *Drosophila* leads to neurodegeneration (Haberman et al., 2012). Ablation of Syntaxin1 causes more severe growth defects than VAMP1 mutants in that most embryos die *in utero* (McRory et al., 2008).

Mutations in proteins regulating SNARE complexes are also responsible for a variety of neurological diseases. The best known protein is α -Synuclein, which when mutated forms aggregates commonly known as Lewy Bodies, found in Parkinson's disease (PD) (Spillantini et al., 1997; van de Berg et al., 2012). The first mutation identified for PD was a missense dominant mutation found in α -Synuclein gene (Gasser, 2001); duplication or triplication of the gene locus also causes PD (Singleton et al., 2003; Chartier-Harlin et al., 2004). α -Synuclein, together with CSP- α protein, has also been shown to promote assembly of SNAREs (Burré et al., 2010; Sharma et al., 2011, 2012). As expected, CSP- α impairment also causes neurodegeneration (Fernández-Chacón et al., 2004; Schmitz et al., 2006; García-Junco-Clemente et al., 2010; Nosková et al., 2011; Sharma et al., 2012). As

another key regulator in dissociating SNARE complexes, dysfunction of NSF has been shown to impair neuromuscular junction development in *Drosophila* (Laviolette et al., 2005; Stewart et al., 2005) and formation of myelin sheaths in zebrafish (Woods et al., 2006). Here I present data describing a neuronal development and degeneration phenotype in zebrafish NSF mutants and my confirmation that NSF is essential for maintenance of CNS and peripheral innervation (Chapter 4).

Chapter 2. Quantification of vestibular-induced eye movements in zebrafish larvae

Reprinted from Mo W, Chen F, Nechiporuk A, Nicolson T.

Quantification of vestibular-induced eye movements in zebrafish larvae.

BMC Neurosci. 2010 Sep 3;11:110. Copyright: © 2010 Mo, Chen, Nechiporuk, Nicolson.

(Experiments of Figure 13 and Figure 14 were done by Dr. Fangyi Chen)

1. Summary

Vestibular reflexes coordinate movements or sensory input with changes in body or head position. Vestibular-evoked responses that involve the extraocular muscles include the vestibulo-ocular reflex (VOR), a compensatory eye movement to stabilize retinal images. Although an angular VOR attributable to semicircular canal stimulation was reported to be absent in free-swimming zebrafish larvae, recent studies reveal that vestibular-induced eye movements can be evoked in zebrafish larvae by both static tilts and dynamic rotations that tilt the head with respect to gravity. We have determined herein the basis of sensitivity of the larval eye movements with respect to vestibular stimulus, developmental stage, and sensory receptors of the inner ear. For our experiments, video recordings of larvae rotated sinusoidally at 0.25 Hz under infrared illumination were analyzed to quantitate eye movements. We observed a robust response that appeared as early as 72 hours post fertilization (hpf), which increased in amplitude at later stages. Unlike rotation about an earth horizontal axis, rotation about an earth vertical axis at 0.25 Hz did not evoke eye movements. Moreover, vestibular-induced responses were absent in mutant *cadherin 23* (*cdh23*) larvae and larvae lacking anterior otoliths. Our results provide evidence for a functional vestibulo-oculomotor circuit in 72 hpf zebrafish larvae that relies upon sensory input from anterior/utricle otolith organs.

2. Materials and methods

2.1. Animals

Animals used in this study were wild-type zebrafish larvae in the Tübingen or long fin background, and mutants identified in the present study (*rock solo*^{AN66}) or previous studies (*cdh23*^{1619ag} and *synj1*^{Q296X}) (Granato et al., 1996; Söllner et al., 2004; Trapani et al., 2009). The *rock solo* mutant (recessive lesion) was identified from an ethylnitrosourea mutagenesis screen using a Tübingen background. Fish embryos and larvae were kept at 30°C in E3 embryo medium (Westerfield, 1995). If necessary, 20 µl pronase was added into the medium to help larvae hatch out of the chorion at 2 dpf, followed by a change of E3 medium. All of the behavioral tests were carried out at room temperature (22-25°C).

We performed our experiments with 3-5 day old zebrafish larvae. For mounting, 2% low melting agarose in E3 media was kept at 42°C in a heating block. To immobilize fish larvae, a drop of low melting agarose was put on a cover slip and a larva was transferred into the agarose liquid by a glass pipette with minimal E3 media. Then the larva was adjusted to a dorsal-up position using fine forceps before the agarose solidified. The cover slip was placed on a metal rack for 5 minutes to allow the agarose to become firm. In order to free the eyes, a 0.5 - 1 µl region was excavated around the fish head using fine forceps, and then the exposed area was filled with E3 media. The E3 media allowed the eyes to move freely. The cover slip was then put onto the specimen platform, on which the larva was positioned head down, perpendicular to the platform plane (Figure 12).

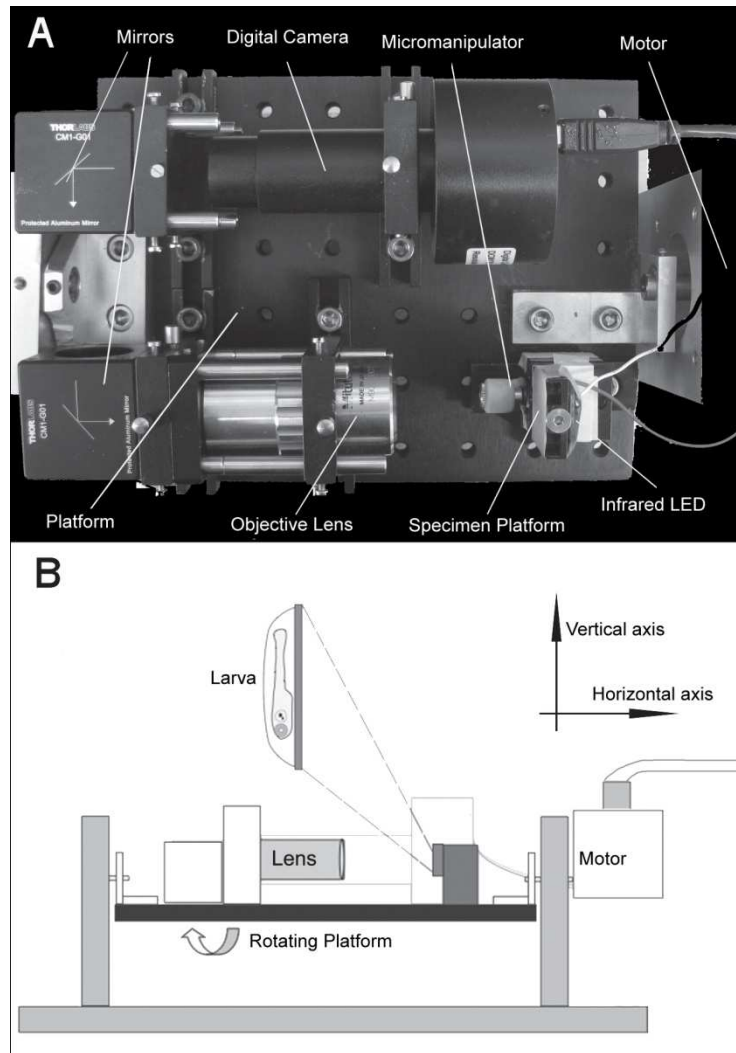


Figure 12. The equipment and diagram of the experimental set up used to evoke eye movements in zebrafish larvae. (A) An overview of the device constructed to stimulate and record vestibular-induced eye movements in larvae. (B) An illustration of the set up. Larvae were mounted on the specimen platform in a head-down position perpendicular to the platform. The platform was rotated around the axis shown by the curved arrow. The coordinate indicates the axes of two type of rotations used in this study.

2.2. Microscopic system

A customized microscopic system was constructed to monitor the eye movements during rotation. As shown in Figure 12A, this system was composed of a Mitutoyo 5X long working distance lens and a digital eyepiece (DCM300; Hangzhou Scopetek Opto-Electric, Zhejiang, China). Two 45° mirrors were placed between the objective and the digital eyepiece to guide the light. The U-shaped setup makes efficient usage of the rotation plate space and balances the motor load. All components were mounted on an aluminum platform, which could be rotated by a motor system with the supporting structure. Since all of the parts were fixed on the platform, no relative motion existed between the specimen and the eyepiece during the rotation process. This guaranteed a consistent viewing area during the experiment, which avoided blurring due to the relative motion between the camera and the fish. The same area under constant illumination also warranted relatively constant image brightness on each frame during a single trial.

A servo motor (Model# BE231DJ-NPSN, Parker Hannifin, Cleveland, OH, USA) and servo controller (Model# GV6K-U3E, Parker Hannifin) were used to rotate the platform, which held the microscopic system. A motor gear head (Model # 23SP100, Parker Hannifin) with a gear ratio of 1:100 was attached to the servo motor to reduce the speed and increase the torque. This servo motor system can control the angular position of the platform with a precision of less than 0.2 degree. An Ethernet cable connects the controller and a computer, allowing the computer to program the motor rotation profile and read the motor position.

All experiments were conducted in the dark with a cover box, if not otherwise specified. Larvae were mounted on a transparent specimen plate, which was supported by a 3D micromanipulator. Each fish was trans-illuminated by an infrared LED with emission wavelength around 820 nm. A dark background with infrared illumination was used to avoid stimulating the visually-evoked responses. The LED was approximately 10 mm away from the specimen plate. That distance, as well as the small size of the LED and a wide emitting angle, produced a relatively homogeneous illumination.

The digital eyepiece recorded a video with a resolution of 1024 x 768 pixels at a speed of about 7.8 frames per second. This speed produced more than 20 frames at each rotation cycle with a period of four seconds. The infrared filter inside the digital eyepiece was removed to increase the infrared sensitivity.

2.3. Experimental condition

Zebrafish larvae were mounted in a head-down position on the specimen platform, perpendicular to the rotation platform plane (Figure 12). During the experiment, the motor moved the platform in a sinusoidal profile with amplitude of $\pm 45^\circ$. In a single cycle, the head of the fish changed from 45° downward to 45° upward, altering the relative position of otoliths to their associated sensory hair cells. The forces acting on otoliths were much larger (several hundred fold) than the forces generated by angular rotations in previous studies (Beck et al., 2004)(see detailed analysis in Appendices 1). This type of rotation provided maximal stimulation to the otoliths and obvious eye movements were seen in the experimental conditions.

We tested zebrafish larvae in various orientations on the specimen platform. Since the magnitudes of forces applied to otoliths were similar in different directions, the larvae displayed eye movements in either head-up or head-down orientations. The eye movements in a head-down position produced the clearest changes of eye shape, which we then used for quantification.

2.4. Data acquisition

After the larvae were mounted and positioned, the video recording was performed with *ScopePhoto*, the software that accompanied the digital eyepiece. Before stimulation, the recorded frames were used to check the illumination. Ten seconds after the video started, the motor was turned on by the controller software *Motion planner* (Parker Hannifin). After a one-minute recording, which included about 13 cycle rotations, the video was saved as a Windows Media Video (WMV) format file for analysis.

During the rotation, the motor controller was also used to control the infrared LED to synchronize the video with the rotation. In each rotation cycle, the controller sent out a 100 ms pulse to the infrared LED when the angle of the motor was at about $+28^\circ$ in the clockwise direction. The illumination was turned off during the 100 ms pulse. This resulted in a dark frame in the video in every rotation cycle. This dark frame was detected by the image processing program and was used to synchronize the eye movements with the rotation angle changes (Movie 1: (Mo et al., 2010a)).

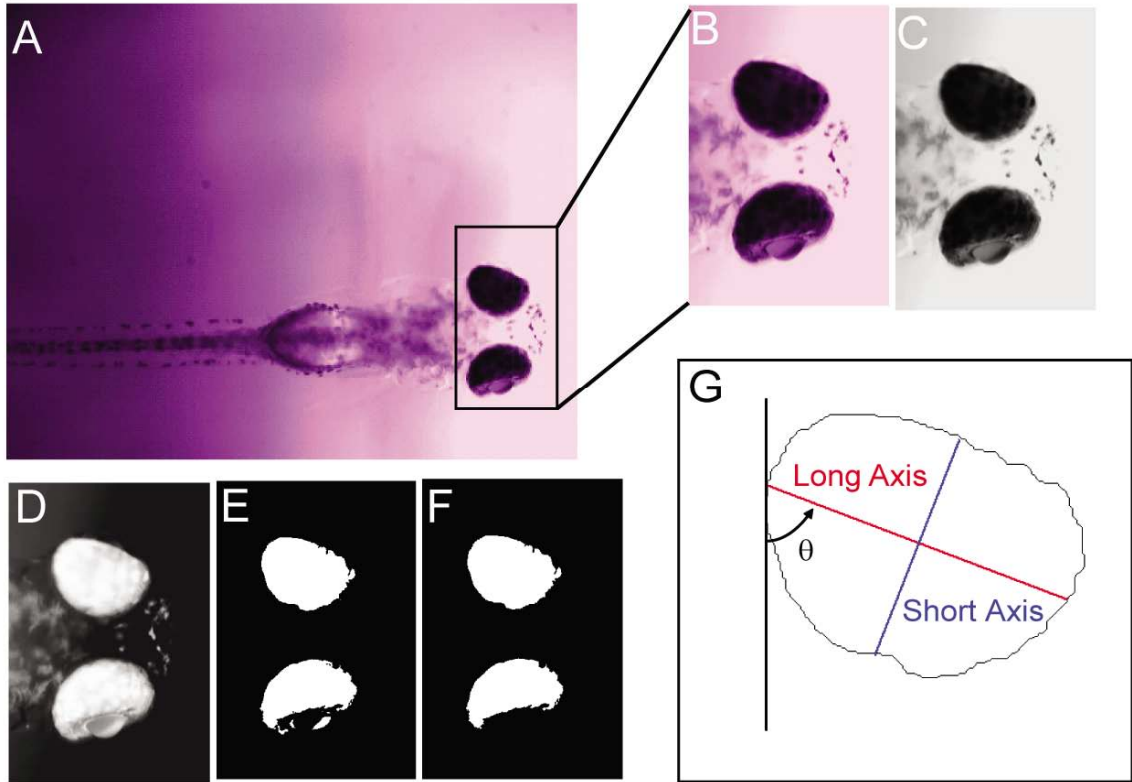


Figure 13. Defining the eye regions in fish larvae. Six steps (A-G) were programmed in MATLAB to quantify eye movements/eye changes in the videos. A head region image (B) was first outlined and extracted from the original image frame (A). The head region was converted into a grayscale image (C) with inverted color (D). Then, the inverted grayscale image was converted into a black-white image (E) using an arbitrary threshold. This black-white image was simplified by removing extra punctae around the retina to define the eye more clearly (F). The final step was to calculate the parameters used to quantify changes during eye movements. (G) Features calculated from the extracted eye region. θ designates the rotation angle. The red line indicates the long axis, and the blue line the short axis of the eye.

2.5. Image processing

The recorded video (Movie 1:(Mo et al., 2010a)) was processed in MATLAB (Mathworks, Natick, MA, USA) off-line. Figure 13A shows an image frame from a recorded video. The first step was to define the area of the fish head. As shown in Figure 13B, an imaging region containing the fish head was selected manually from the first frame of the video. Since there was no relative motion between the digital eyepiece and the fish, this region was the same for every frame. After defining the head area, a small image portion was cut from each frame. This process substantially reduced the amount of data to process. The colored image was then converted into the grayscale image shown in Figure 13C.

The second step was to define the eyes from the head image, and a grayscale threshold was then applied to invert the grayscale image (Figure 13C) into a black-and-white image (Figure 13D). The threshold was chosen using Otsu's method (Gonzalez et al., 2004). This was implemented in MATLAB with the function *graythresh*. Alternatively, manual adjustment of the threshold was sometimes used due to the image intensity change resulting from the motion of the E3 media around the fish head. A scale factor was then applied to the threshold. With a scaled threshold, the area containing the eye was defined for analysis (Figure 13E). An area threshold was then applied to the black-and-white image to remove the small dark island formed by the lens (Figure 13F). The two eyes were then separated in order to calculate the parameters for quantifying the rotations. A similar process was introduced in Beck et al., 2004. In contrast to Beck et al., we confined the eye area to the iris, which is darker than the rest of the eye. This definition

of the eye area facilitated the detection of the eye rotation along the anterior-posterior axis, as will be discussed in the next section.

2.6. Quantification of rotation of the eye

After defining the eye region, features were extracted and calculated from the eye to quantify the eye rotation and then to evaluate the reflex. During the experiments, eye rotations on two planes were observable: rotation about the dorsal-ventral axis and rotation about the anterior-posterior axis (Movie 1: (Mo et al., 2010a)). The former is on the image plane and the eye angle can be used to quantify it. To measure this angle, the extracted eye region was approximated by an ellipse, and the angle of the long axis was used to represent that of the eye, shown as θ in Figure 13G (outline of upper eye in panel 13F). The eye angle, together with the mass center of the eye, determined the long axis of the eye (red line in Figure 13G). Both the angle and the mass center coordinate were an output of a MATLAB function *regionprop*. The short axis (blue line in Figure 13G) was drawn perpendicular to the long axis. The length of the long axis and short axis were also determined by the function *regionprop*.

Because the eye rotation around the anterior-posterior axis was not in the image plane, direct measurement of this rotation was not practical. The videos showed that the anterior-posterior rotation resulted in a change in the shape of the eye (Movie 1: (Mo et al., 2010a)). By measuring the shape change of the eye in each image frame, we could quantify the rotation by examining changes in total area or ratio of the long and short axes.

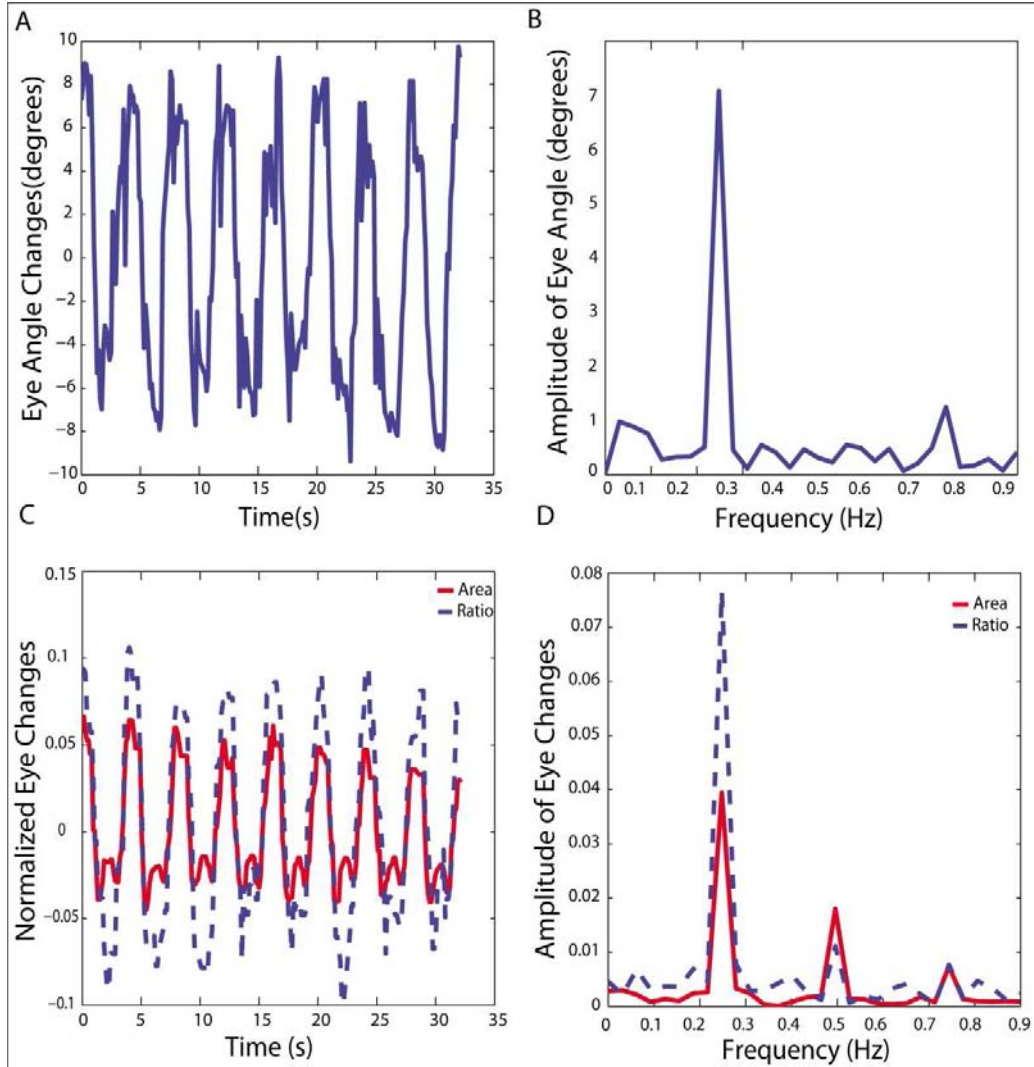


Figure 14. Features for quantifying eye movements under infrared illumination. (A)

Plot of changes in eye angle of a single eye over time. (B) Amplitude spectra of the continuous waveform in (A) as a function of frequency. A peak at 0.25 Hz corresponded to the rotation period of 4 seconds as shown in (A). In this case, the largest value of angle change observed was 7 degrees. (C) Normalized eye movements derived from changes in the total area (red line) or the long and short axis ratio (blue dashed line) of a single eye. (D) Amplitude spectrum of (C). Note that the eye ratio change yielded higher peaks at 0.25 Hz than changes in total eye area in both time domain (C) and spectral (D) plots.

In Figure 14, the results of 8-cycle tests are shown. Figure 13G shows an eye profile and the long axis and short axis of the eye. The eye angle, which is the angle between the long axis and the vertical direction of the image frame, is marked as θ . Figure 14A depicts the change of the angle of an eye during an experiment. Fast-Fourier-Transform (FFT) was applied to the waveform in Figure 14A to calculate the spectrum of the time domain signal, as shown in Figure 14B. The peak change or amplitude at the stimulus frequency was used to quantify the response. Our videos revealed that detecting angle changes in response to a vestibular stimulus was not always feasible, so we turned to the other two features of the eyes: total area versus the ratio of the length of the short axis over that of the long axis. The videos indicated that these two features are closely related. While the eye rotates about the anterior-posterior axis, the iris becomes visually thinner. This results in reduction of the area, which is mostly due to the reduction of the short axis length. Figure 14C (time domain plot) and 14D (spectra) compare the total area and eye axis ratio changes that occurred during the test. To reduce the influence of specimen variation due to eye shape or original position of the eyes, both the ratio and the area were normalized by its mean value during the test. The normalized value was calculated by $\tilde{X} = \frac{X - \text{mean}(X)}{\text{mean}(X)}$, where X is either the ratio or the area. As shown in both the time domain plots in Figure 14C and their spectra in Figure 14D, the amplitude of the eye axis ratio change was higher than the total area change. Also, the ratio change was less sensitive to the intensity variation, which influenced both the long axis and short axis in a similar manner. We therefore used ratio changes to determine the amplitude of the vestibular-induced eye movements. One drawback of the ratio method is that the ratio saturates when the rotation angle becomes more than ± 10 -20 degrees. However, this

limitation did not affect our ability to detect differences among various stages of development or genotypes as seen below.

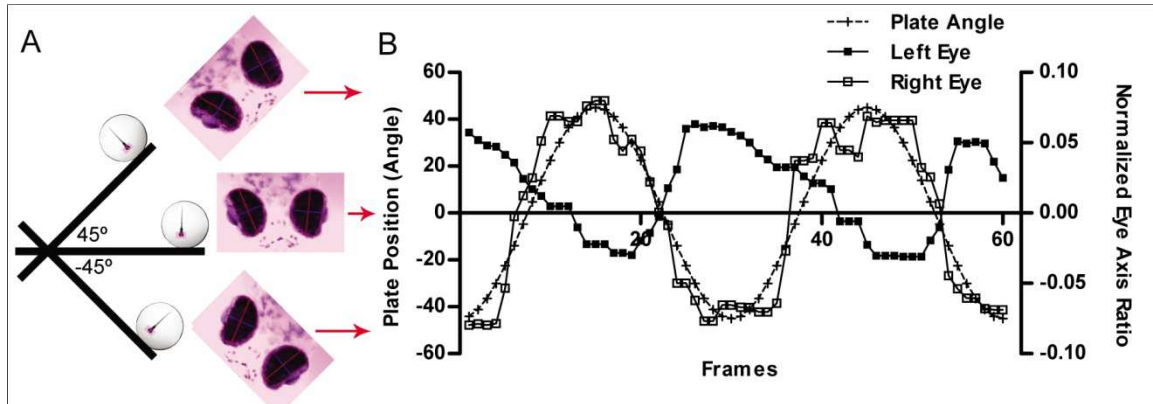


Figure 15. Representative eye movements in response to platform movements (5 dpf). (A) Illustration of the relationship between platform position, larval direction and eye movements. (B) The ratio of long and short axis of both eyes changed sinusoidally. The counter movements of the two eyes followed the platform movements (dashed line). Red arrows between (A) and (B) shows the corresponding position of the larva with respect to platform angle.

3. Results

3.1. Quantifying vestibular-induced eye movements in zebrafish larvae

To observe eye movements, we rotated larvae on the platform ± 45 degrees at 0.25 Hz. We found that upon stimulation with sinusoidal movements at 0.25 Hz, wild-type larvae at 5 dpf moved their eyes sinusoidally if positioned vertically, with the head pointing

downward (Figure 15A,B). Larvae also responded if mounted in the opposite direction with the head pointing up, but illumination of the larval head was not optimal in this position (data not shown). In our experiments, larvae were positioned off-axis by 3.2 cm, and movements of the platform lead to a combination of head tilt, and centripetal and tangential acceleration of the specimen. Figure 15B shows the average ratio changes of the long and short axes of both eyes of a representative specimen. In general, the average ratio changes in wild-type larvae displayed a robust response to changes of platform position. We performed our experiments in the dark with infrared illumination to eliminate visual cues. Accordingly, the eye movements we observed in the dark were vestibular-induced rather than visual responses.

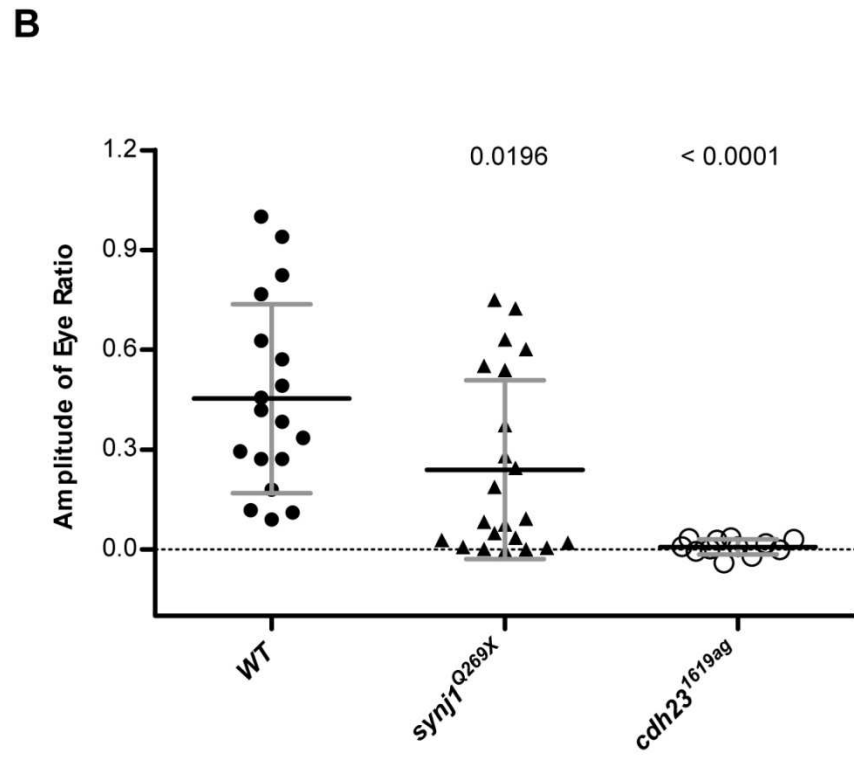
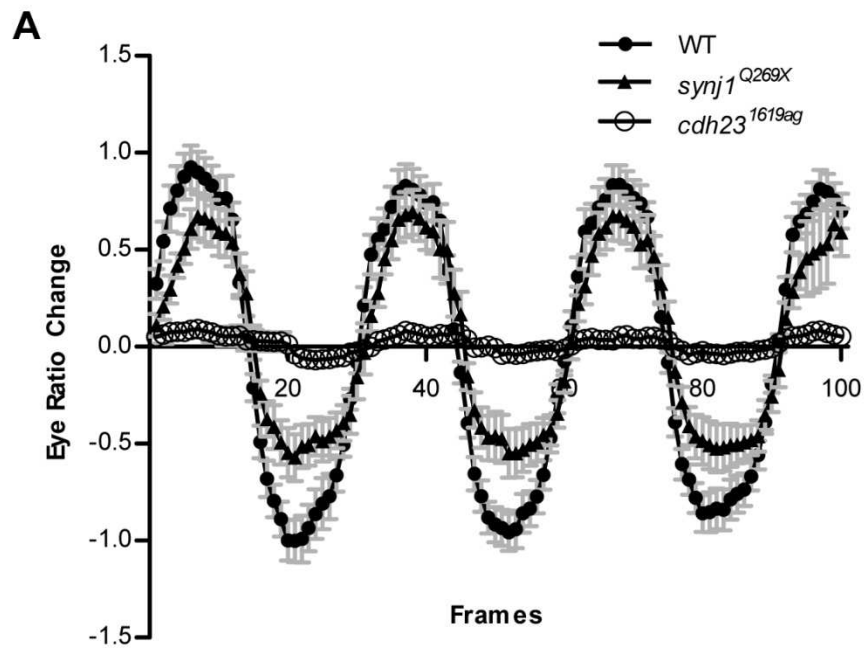


Figure 16. Vestibular-induced eye movements in wild-type and mutant larvae (5 dpf). (A) Averaged eye movements of *cdh23*^{1619ag}, *synj1*^{Q296X} and wild-type. Mean ± S.E. are depicted. (B) Amplitude of eye movements of *cdh23*^{1619ag}, *synj1*^{Q296X} and wild-type. The data points shown are the peak amplitude values at the rotational frequency calculated by subtracting the background, which is the average value of other frequencies. Each data point is derived from a single eye (n > 6 fish for each genotype). P values shown in (B) were determined by unpaired two-tailed t-tests of data collected from wild-type versus mutant larvae.

To confirm that eye movements were driven by the vestibular system, we measured the response of auditory/vestibular mutants. Eye movements were measured in *cdh23*^{1619ag} mutants, which lack hair-cell microphonics (Nicolson et al., 1998; Söllner et al., 2004), and *synптоjanin 1* (*synj1*^{Q296X}) mutants, which are completely blind yet have partially impaired vestibular function (Epps et al., 2004; Trapani et al., 2009). The *synj1*^{Q296X} mutants showed reduced average eye-ratio changes as previously reported, and the *cdh23*^{1619ag} mutants did not have any detectable eye movements during rotation in the dark (Figure 16A). To quantify the sinusoidal eye movements, the amplitude of ratio changes of each eye at the rotation frequency was calculated and normalized to the highest value seen with the wild-type larvae in all following figures. In our experiments, all wild-type larvae showed eye movements in the videos; however several had low amplitude values. On occasion, infrared illumination can vary such that the program miscalculates the retina region, resulting in depressions or concave regions within the peak regions and hence reduced calculated amplitude values. However, one can still detect overall differences between wild-type and mutant larvae. As shown in Figure 16B, mutants carrying the *synj1*^{Q296X} allele had a significantly lower mean amplitude of response (0.24 ± 0.27 s.d.; n = 11 larvae) than wild-type larvae (0.45 ± 0.28 ; n = 9 larvae), and mutants homozygous for the *cdh23*^{1619ag} allele had nearly zero amplitude values (0.01 ± 0.02 ; n = 6 larvae). Loss or reduction of eye movements in mutants with vestibular defects provided further evidence that we were observing a vestibular response to acceleration of the specimen.

Because the *synj1*^{Q296X} mutants completely lack OKR responses (Epps et al., 2004), partially reduced eye movements in our experimental conditions indicate that their eye

movements depend on vestibular function rather than vision. We noted that the difference between the OKR observed previously (Brockerhoff et al., 1995; Easter and Nicola, 1997; Beck et al., 2004) and the vestibular-evoked response reported here is the nature of eye movements. With respect to OKR responses, zebrafish larvae move their eyes in saccades around the dorsal-ventral axis of their body (Beck et al., 2004), whereas with vestibular-evoked responses, their eyes rotate around the anterior-posterior axis of the body (Movie 1:(Mo et al., 2010a)). In a parallel experiment, the *cdh23*^{1619ag} mutants showed vigorous eye movements in bright light (Movie2: (Mo et al., 2010b)) with typical gaze shifts for visually-evoked responses (Figure 17A). Quantification showed that these eye movements in bright light were driven by platform movements (Figure 17B; 0.39 ± 0.24 for bright light; -0.12 ± 0.16 for dark conditions, n = 6 larvae). This result suggested that *cdh23*^{1619ag} mutants have visual responses but lack vestibular responses. Together, our results confirmed that vestibular-induced eye movements are robust in larvae and can be quantified for comparative studies.

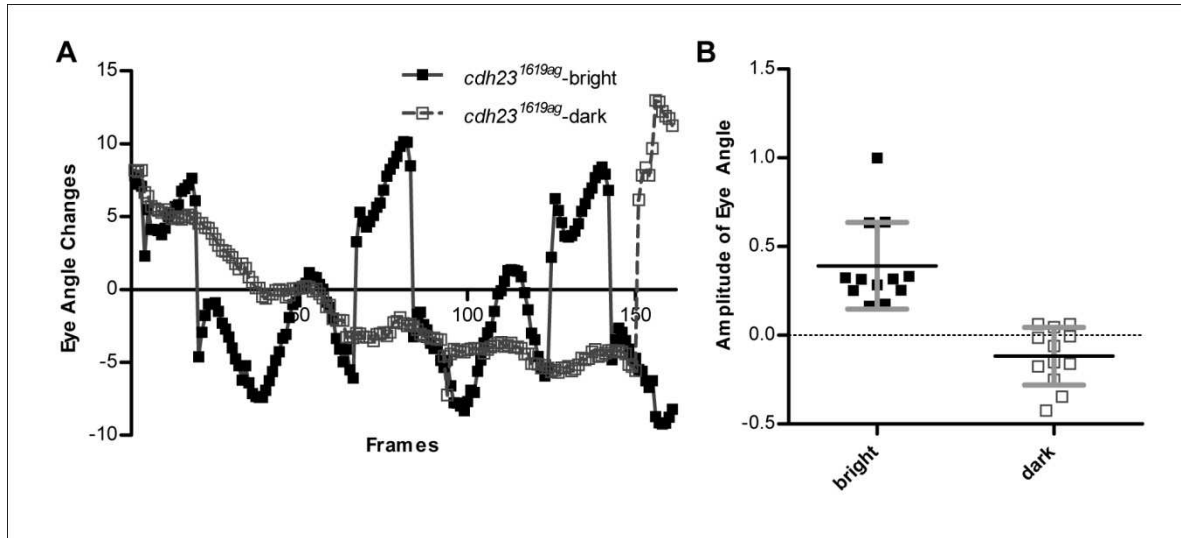


Figure 17. Presence of the optokinetic reflex, but not vestibular-induced eye movements in *cdh23*^{1619ag} mutants (5 dpf). (A) Representative changes of eye angle from a single *cdh23*^{1619ag} mutant larva in both dark and bright conditions. With bright illumination, the mutant larva showed changes in eye position in response to platform movements, whereas in the dark, the eye of this mutant larva spontaneously twitched once during the 150th frame. (B) Amplitude of eye movements of *cdh23*^{1619ag} mutants in bright and dark conditions. The same larvae were tested under both conditions (n = 6).

3.2. Earth horizontal versus earth vertical rotations

Vestibular-induced eye movements can be evoked by both angular and linear accelerations. The absence of an angular VOR in fish younger than 35 days is most likely due to the morphogenesis and maturation required for the semicircular canals to become fully functional (Beck et al., 2004). To determine the driving force of the eye movements

seen in our experiments, we performed our experiments with the platform in different orientations. To mimic the stimulation used in the experiments by Beck et al., we changed the orientation of our device by 90° . We found that wild-type larvae did not respond to rotation around the earth vertical axis at 0.25 Hz (Figure 18; mean amplitude 0.01 ± 0.05 , $n = 5$). Such a stimulus produces centripetal and tangential acceleration, but no changes with respect to head tilt. These same larvae had a robust response if rotated afterwards about the earth horizontal axis (Figure 18; 0.41 ± 0.35 , $n = 5$ larvae). This result suggests that the change in linear acceleration evoked by head tilt was the driving force of the eye movements.

3.3. Zebrafish larvae develop vestibular-induced eye movements at 3dpf

To determine the developmental stage at which zebrafish larvae develop a response to changes in linear acceleration, we measured eye movements of larvae from 60 hpf to 120 hpf. No eye movements were observed in 60 hpf old larvae (Figure 19). The eye movements in response to platform rotation were first detected in 72 hpf fish larvae, and larger eye movements were detected in older fish larvae at 120 hpf (Figure 19). In the videos, the older fish larvae appear to move their eyes more robustly and to a larger degree than younger larvae (data not shown). With respect to the number of fish larvae that have eye movements, we found that at the 72 hpf stage, 90% of the larvae had robust eye movements ($n = 11$).

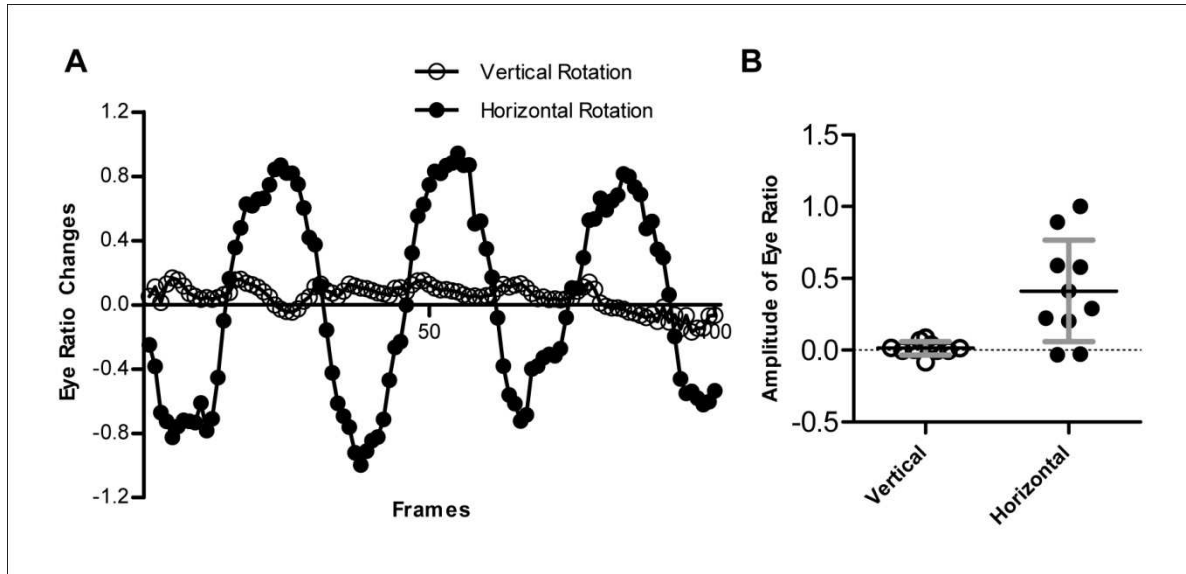


Figure 18. Vestibular-induced eye movements occur during rotation at 0.25 Hz around an earth horizontal axis, but not around an earth vertical axis. (A)

Representative eye movements of a 5 dpf wild-type larva rotated around an earth vertical axis (empty circles) or an earth horizontal axis (filled circles). (B) Amplitudes of eye movements in the two axes. The same larvae were tested under both conditions (n = 5).

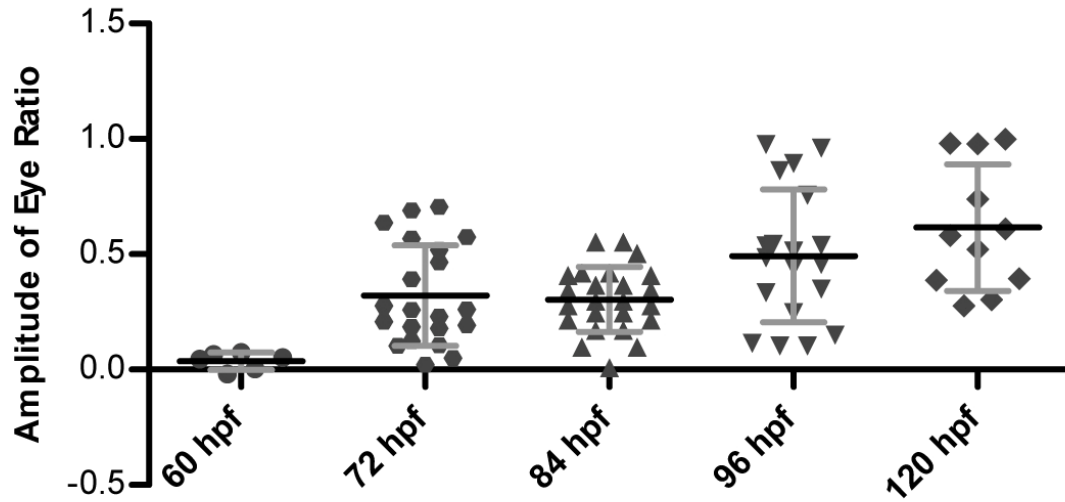


Figure 19. Development of the vestibular-induced response in zebrafish larvae.

Amplitudes of eye movements of larvae at various developmental stages are shown. The reflex is detectable at 72 hpf and becomes more robust over time. The mean amplitudes (\pm s.d.) are as follows: 60 hpf, 0.04 ± 0.04 $n = 3$; 72 hpf, 0.32 ± 0.22 $n = 11$; 84 hpf, 0.30 ± 0.14 $n = 12$; 96 hpf, 0.49 ± 0.29 $n = 10$; 120 hpf, 0.62 ± 0.27 $n = 6$.

(Figure 20 A, B). Mutant *rock solo* larvae survive for more than a week and appear healthy during the stages used for our experiments. We tested eye movements under infrared illumination in homozygous *rock solo* mutants and found that they did not have any detectable responses to rotation about the earth horizontal axis. (Figure 20C; wild-type mean amplitude 0.32 ± 0.28 , $n = 6$; *rock solo* mutant 0.009 ± 0.03 , $n = 8$). In contrast, *rock solo* mutants responded to acoustic stimuli (tapping on the Petri dish) and light touch, suggesting that they have functional sensory hair cells and do not have defects in their motor system (data not shown). This result provides strong evidence that the anterior/utricle otolith in zebrafish larvae is required for vestibular-induced eye movements in response to changes in linear acceleration due to head tilt with respect to gravity.

4. Discussion

Our experiments demonstrate that zebrafish larvae have robust eye movements in response to rotation around an earth horizontal axis. At larval stages, both vestibular and visual input may contribute to eye movements. Two lines of evidence support the notion that we are measuring vestibular function rather than visual function. Firstly, motion of the eyes occurred in the dark using infrared illumination. Secondly, vestibular mutants did not respond or had attenuated responses to rotation on the platform. The 1619ag mutation in *cdh23* used in this study causes a premature truncation of the extracellular domain of Cdh23. Larvae homozygous for this allele have severe balance defects and lack microphonics, suggesting that mechanotransduction is absent in hair cells (Nicolson et al., 1998; Söllner et al., 2004). Mutant *cdh23*^{1619ag} larvae did not respond to the

stimulus under infrared illumination, indicating that hair-cell function was required for movement of the eyes in our experiments. In contrast to experiments in the dark, *cdh23*^{1619ag} larvae exhibited an OKR in response to rotation in bright light, eliminating the possibility that OKRs occurred under infrared illumination. Mutant *synj1* larvae present the opposite phenotype of *cdh23*^{1619ag} larvae in that *synj1* mutants exhibit partial vestibular function, but vision is lost (Epps et al., 2004; Trapani et al., 2009). We observed that the OKR was absent in *synj1*^{Q296X} mutants (data not shown), indicating that the remaining vestibular-evoked responses were driven by the partially functional vestibular system, and not the visual system. With respect to developmental onset, vestibular-induced eye movements were detectable by 72 hpf. At this stage, zebrafish begin to exhibit OKR responses (Easter and Nicola, 1997; Beck et al., 2004) and the auditory/vestibular nerve appears to be fully functional (Tanimoto et al., 2009). Our data indicate that the vestibulo-oculomotor projections are operational at this early stage as well.

Testing *rock solo* mutants allowed us to identify which hair cells mediate vestibular-induced eye movements in zebrafish larvae. In every case, the anterior otolith was absent in *rock solo* mutants, whereas the posterior otolith was always present. Mutant *rock solo* larvae failed to respond to earth horizontal rotation of the body, indicating that the anterior utricular macula is required for the response in larvae. In teleosts, the utricular otolith has been previously implicated in vestibular function (Riley and Moorman, 2000; Moorman et al., 2002) whereas the posterior saccular otolith is thought to be primarily for hearing (Popper and Fay, 1993). Larval zebrafish begin to maintain balance, keeping their dorsal side up, as early as 3 dpf (Riley and Moorman, 2000). Following a startle

involving sound, touch, or vision, they can coordinate their motor system to produce a forward movement, with an upright posture. Experiments in adult frogs have also shown that the utricular otolith is important for sensing linear acceleration and gravity (Rohregger and Dieringer, 2002). Our experiments with *rock solo* mutants support the notion that the anterior otolith acts as a detector of linear acceleration in developing larvae.

The rotation around the earth horizontal axis using our set up presents a complex stimulus to the larval vestibular system. The stimulus includes linear acceleration, components of centripetal and tangential acceleration, as well as changes in linear acceleration due to head tilt with respect to gravity. The vestibular system typically uses combined semicircular canal and otolith information to distinguish between translational and roll tilt movements (Angelaki et al., 2004). Both types of inputs should be able to evoke compensatory eye movements (Angelaki et al., 1999). However, we did not observe any eye movements in fish larvae during rotations about an earth-vertical axis. One reason is that the vertical-axis rotation we delivered would primarily stimulate semicircular canals, which are not fully developed in our preparation (Beck et al., 2004). Hypothetically, a much stronger stimulus may activate the ampullary hair cells, but such a stimulus would not be physiological. The maximal angular acceleration used by Beck et al. ($>180^\circ/S^2$) was much larger than the stimulus used here (approximately 30 fold), yet they did not detect an angular VOR in zebrafish larvae. A second reason for a lack of response is that the centripetal and tangential accelerations due to the off-axis location of the preparation produced only negligible otolith stimulation (See Appendices 1). In contrast, during earth horizontal-axis rotation, there was a large change in linear acceleration that provided a

sufficient stimulus to the otoliths. Again, the same stimulus was not sufficient to stimulate ampullary hair cells, which we assume were normal in homozygous *rock solo* mutants. Thus, we infer that the vestibular-induced eye movements we observed in larvae were due to otolith stimulation evoked by the change in head tilt of the specimen. This hypothesis is supported by our experiments with *rock solo* mutants.

The eye movements we observed in larvae included changes in eye position about the dorsal-ventral axis. These movements represent compensatory VOR responses. Other movements include skewed vertical eye movements (about the anterior-posterior axis) and are most likely related to the ocular tilt reaction (OTR) present in lateral-eyed animals such as fish or rabbits (reviewed by Brodsky et al., 2006). In such animals, the OTR is thought to be an otolithic righting reflex. Our measurement of the changes in ratio of eye area likely included both VOR and OTR movements. Despite the complexity of the eye movement, the vestibular-evoked changes in eye position are sufficiently robust, permitting comparison of responses among mutants and experimental parameters.

In conclusion, our results indicate that zebrafish larvae exhibit robust eye movements in response to changes in head tilt with respect to gravity. Our data also confirms that zebrafish larvae rely on the anterior/utricle otolith for maintaining an upright position and coordinating movements with respect to gravity. Measuring the robustness of vestibular-induced eye movements will be invaluable for genetic or pharmacological studies of vestibular function in larvae. In addition, the ability to test vestibular function at earlier stages is especially useful for early lethal phenotypes or accessing gene knockdown with morpholinos as their effectiveness normally decreases over time.

Chapter 3. Nsf function in hair-cell ribbon synapses: lesson from a point mutation

**Prepared for submission to the Journal of the Association for Research
in Otolaryngology**

Authors

Weike Mo, Josef Trapani, Lavinia Sheets and Teresa Nicolson

Oregon Hearing Research Center and Vollum Institute

3181 SW Sam Jackson Park Road,

Oregon Health and Science University, Portland, OR USA 97239

**(Experiments of Figure 23 and Figure 24 were done by Dr. Josef Trapani; Dr.
Lavinia Sheets contributed Panel A of Figure 27.)**

1. Summary

Synaptic transmission depends on the N-ethylmaleimide-sensitive factor (NSF) and soluble NSF attachment protein receptors (SNAREs) expressed in neurons. Exocytosis of synaptic vesicles in neurons is blocked when neuronal SNAREs or NSF are pharmacologically or genetically abolished. The ribbon synapses of auditory and vestibular hair cells are known for their ability to sustain high-speed synaptic transmission. The unique structure of ribbon synapses differs from conventional synapses, as does the molecular machinery used for synaptic exocytosis. Whether neuronal SNAREs, the key complex of exocytosis, are expressed in hair cells is controversial. Both genetic and pharmacological manipulations of neuronal SNAREs do not affect synaptic transmission in mouse inner hair cells. It is therefore unclear whether synaptic transmission in hair cells depends on NSF and SNAREs. Here, we describe a point mutation of zebrafish *nsf* (*nsf*^{I209N}) that affects balance and hearing. Similar to *synптоjanin* mutants with defective synaptic vesicle recycling, we observed that *nsf*^{I209N} mutation causes a shift in phase locking, resulting in a delay of action potentials in afferent neurons. Unlike the null *nsf* mutation, *nsf*^{I209N} does not have a dramatic effect on the morphology of ribbon synapses in hair cells and postsynaptic afferent innervations, with the exception that cysteine string protein (CSP) is slightly decreased in *nsf*^{I209N} hair cells. We also found that *nsf* mRNA but not protein is increased in *nsf*^{I209N} mutants. Collectively, our results suggest that NSF is required for normal balance and hearing, and is essential for accurate synaptic transmission at ribbon synapses in zebrafish hair cells.

2. Materials and methods

Fish Strains. Wild-type, mutant, and transgenic strains were maintained in a Tübingen or Top Long Fin background as described (Westerfield, 1995). Larvae were raised at 28.5 °C in the dark in E3 buffer and kept in the dark as often as possible during behavioral tests. The *nsf*^{st153} allele was obtained from the Zebrafish International Resource Center; the *nsf*^{f209N} allele was identified in the large-scale genetic screen (Nicolson et al., 1998).

Positional Cloning of nsf^{f209N}. The mutation was genetically mapped using segregation analysis with PCR-based simple sequence length polymorphisms (SSLPs) (Nusslein-Volhard and Dham, 2002). To determine the mutation in *nsf* gene, exons from the *nsf* region of mutant and wild-type sibling embryos were amplified and sequenced. Primers to amplify exon 8 (F: GGT CGG CCT GTT GGT TGG AAA CAG TCA AGT; R: CAT CTG CTC CAC AAT GTC TGG AGGAAA) were used for genotyping.

qPCR. mRNA was extracted from 5 dpf zebrafish larvae using RNeasy kit (Qiagen). mRNA samples from different resources were then adjusted to equal concentration before reverse transcription. EcoDry Premix was used to reverse transcribe 5µg RNA to cDNA (Clontech Laboratories, Inc.). 0.2µl cDNA and 10µl SYBR green mixtures were used for each reaction in a 384-well plate on an Applied Biosystems 7900 HT real-time PCR machine. Expression levels of genes were calculated from a cDNA standard curve and then normalized to *actin* RNA level. Sequences used for qPCR are: *sypa* (F:TAC CCA TCT GTA GGC CGT CT; R:CTG CGT TTA CTG GTG GGT TT), *nsf* (F:CGT GGT

TGA TGA CAT TGA GC; R: CGA CCA TGA GGT GGA GTC TT), *nsfb* (F: CAT GTC CGA CTC TTT CAG CA; R: CCT TTC ACC TGT TTG CCA AT).

Measure the auditory evoked behavioral response. Measure of the auditory evoked behavioral response (AEBR) and recording of the behavior was adopted from previous publication with minor changes (Einhorn et al., 2012). Briefly, 5 dpf zebrafish larvae in 96-well microplate were stimulated by a mini-shaker (type 4810, Bruel & Kjaer) in the dark and recorded using a Zebrabox monitoring system (ViewPoint Life Sciences). The sound pressure level (SPL) was pre-determined using a hydrophone (WP-23502-P16, Knowles Electronics) and an oscilloscope (TDS 1002B, Tektronix) before AEBR tests. 100ms stimuli at certain frequencies and SPLs were separated by 5 minutes resting periods. For each larva, to quantify AEBR, 5 trials were performed at each SPL and averaged to calculate the percentage of responses. Movements at resting stages were used to calculate spontaneous movements: wild-type = 6.9%, *nsf*^{d209N} = 5.7%.

Immunofluorescence labeling and imaging. Antibodies and their staining protocols used in this research were described previously (Mo and Nicolson, 2011). Briefly, after 5 dpf zebrafish larvae fixed in PBS buffer supplied by 4% PFA/4% Sucrose/0.01% Tween-20 overnight at 4°C, they were then permeablized with acetone for 7 minutes at -20°C, and blocked in PBS containing 2% fish gelatin/1% BSA/1% goat serum/1% DMSO (FGBS). After blocking, they were incubated with primary antibodies in FGBS overnight at 4°C, and followed by incubation with secondary antibodies in FGBS overnight at 4°C. Zeiss Axiovert ImagerM.1 microscope with an LSM700 confocal scanhead, Axiocam MrM

camera, oil-immersion lens Zeiss Plan Apochromat 63X/1.4NA objective (Zeiss) was used to take Z-stacks through hair cells.

As described earlier, the same quantification steps were taken to measure fluorescent intensity of antibody labeling (Mo and Nicolson, 2011). To measure the size and distribution of Ribeye b labeling, the maximum projections of Z planes of the entire neuromast were taken. Fluorescent signals containing ≥ 20 pixels with three-fold intensity above background were counted as ribbon synapses.

Electrophysiology and Lateral-line Afferent Recordings. Our recording setup and method for action potentials has been done according to what previously described (Trapani and Nicolson, 2010). In brief, larvae were anesthetized by injecting α -bungarotoxin into the heart. Glass pipettes were pulled (P-97, Sutter Instruments) for both waterjet stimulation (with resistances from 1 to 5 M Ω) and extracellular recording (with resistances from 5 to 15 M Ω). An EPC 10 amplifier and Patchmaster software (Heka Electronic) was used to record signals. Extracellular action potentials at the soma of lateral line neurons were recorded with seal resistances ranging from 20 to 80 M Ω . To record action currents, the electrode (MPC-385, Sutter Instruments) was positioned into the posterior lateral-line ganglion. Then, waterjet was moved from neuromast to neuromast to find a neuromast that innervates the neuron near the recording electrode.

3. Results

3.1. An *nsf* point mutation identified in *milky way*

milky way was isolated in a large scale screen to identify zebrafish larvae with hearing or balance defects (Nicolson et al., 1998 and unpublished results). *milky way* mutants have a have an intact escape response to a crude acoustic stimulus such as tapping, and they display obvious balance defects (Figure 21D). In addition to its behavioral defects, *milky way* mutant larvae have enlarged melanocytes and non-inflated swim bladders. Meiotic mapping using SSLP markers on 302 mutants from eight pairs of heterozygous fish located the mutation to a 400 kb critical region containing five genes (Figure 21A). Sequencing of cDNA from three genes in the region identified a point mutation in *nsf* (N-ethylmaleimide-sensitive factor a), a gene encoding an ATPase that catalyzes dissociation of SNAREs (soluble NSF attachment protein receptors) after membrane fusion. The point mutation at codon 209, 626T → A, predicts a change from an isoleucine to an asparagine residue (I209N, *nsf*^{I209N}, Figure 21B). This particular isoleucine residue is conserved across eukaryotic species from yeast to human, indicating its importance to Nsf function (Figure 21B). To further verify that the point mutation is not a single nucleotide polymorphism, 32 samples of genomic DNA from different genetic backgrounds (Tubingen, AB, WIK, SJD) were sequenced. No nucleotide change in the *nsf* gene was found (data not shown).

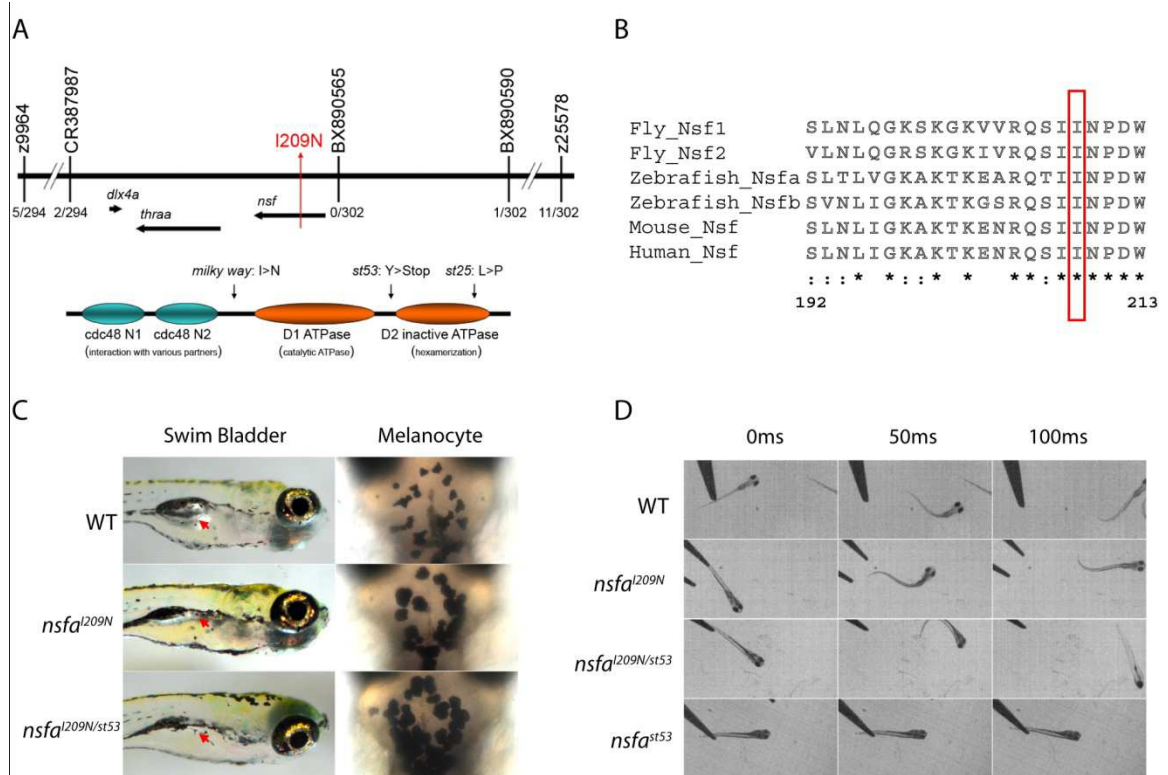


Figure 21. Molecular cloning of *milky way*. (A) A total of 302 fish larvae were used for PCR amplification of SSCP markers z9964, z25578, BX890590, BX890565, and CR387987. Markers on contig BX890590 and CR387987 found 1 and 2 recombinants respectively, which narrowed the critical region to about 400KB. A point mutation I209N was found in *nsf* gene (*nsf*^{I209N}). Two other mutations (*nsf*^{st53} and *nsf*^{st25}) found previously are also shown. (B) Alignment of protein sequences of NSF from fly, zebrafish, mouse and human. The isoleucine (I) at 209 outlined in red box is conserved across species, which was mutated into asparagine (N) in *milky way* mutants. (C) *nsf*^{I209N} homozygotes and *nsf*^{I209N/st53} compound heterozygotes had no swim bladders (arrows) and expanded pigment cells (arrowheads). (D) Image frames from videos of larvae at 5 dpf. *nsf*^{st53} homozygotes displayed motility defects, but *nsf*^{I209N} homozygote and *nsf*^{I209N/st53} transheterozygote larvae only had balance defects (swam or laid on their sides).

To confirm the nsf^{d209N} mutation, we crossed nsf^{d209N} heterozygotes to nsf^{st53} heterozygotes to obtain transheterozygous mutants. nsf^{st53} is a null allele previously found to cause paralytic behavior and enlarged melanocytes (Woods et al., 2006; Kurrasch et al., 2009; Mo and Nicolson, 2011). As we predicted, $nsf^{d209N/st53}$ compound mutants had enlarged melanocytes and the swim bladder was not inflated (Figure 21C). In contrast to the paralysis seen in nsf^{st53} homozygous mutants, the compound mutants responded to touch, but also had a balance defect similar to nsf^{d209N} homozygous mutants (Figure 21D). Therefore, we conclude that the mutation nsf^{d209N} is hypomorphic and is the causal mutation in *milky way* mutants. We had done most of experiments in both $nsf^{d209N/st53}$ and nsf^{d209N} mutants. No significant differences were found between the two mutants. Because many of our results were compared with nsf^{st53} homozygotes, results from $nsf^{d209N/st53}$ compound heterozygotes are shown in this chapter to keep the genetic background of two mutant lines consistent, with the exception of Nsf expression data shown in Figure 28.

3.2. Behavioral analysis: hearing and balance defects in $nsf^{d209N/st53}$ mutants

Like weaker mutants identified in our large scale screens (Nicolson et al., 1998; Trapani et al., 2009; Einhorn et al., 2012), $nsf^{d209N/st53}$ mutants respond to the sound of tapping on the side of the dish, but they fail to orient their body to gravity when they swim (Figure 21D). To determine the extent of vestibular dysfunction and whether an auditory deficit in $nsf^{d209N/st53}$ mutants is, we utilized two types of behavior to quantify their hearing and balance more rigorously.

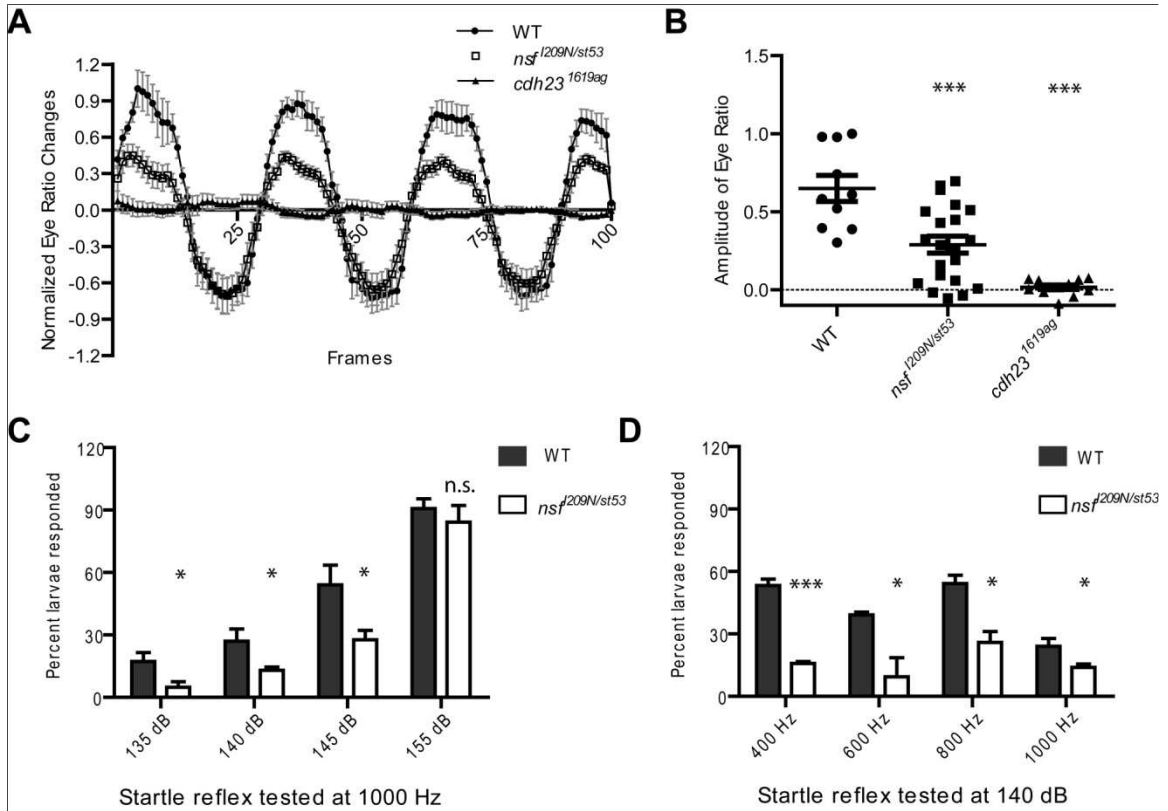


Figure 22. Vestibular and auditory defects in *nsf*^{Δ209N} mutants (5 dpf). (A) Averaged eye movements (VOR responses) of *cdh*^{231619a}, *nsf*^{Δ209N/st53} and WT larvae in respond to body rotation. (B) Amplitude of eye movements of *cdh23*^{1619ag}, *nsf*^{Δ209N/st53} and WT larvae. Each data point represents the peak of power spectrum of calculated from movements of a single eye in panel A. The average value of every power spectrum was subtracted as background. (C) Quantification of percentage of escaping behaviour in 5 dpf larvae exposed to 1kHz stimuli in different sound pressure levels. (D) Percentage of 5 dpf larvae that have escaping behaviour at different frequencies in 140 dB sound pressure level. Mean ± S.E. are shown. P values are determined by two-tail unpaired t-test. *p<0.05, **p<0.01, ***p<0.001. For each genotype, n > 6 were used for vestibular tests; n>60 were used for acoustic response.

To examine vestibular function in *nsf*^{I209N/st53} mutants, we measured vestibular-induced eye movements at 5 days postfertilization (dpf) zebrafish larvae as was done previously (Trapani et al., 2009; Mo et al., 2010c). Movements of the eye in response to body rotation under dark conditions were significantly reduced, but phase-locked to the stimulus in mutants (Figure 22A). Although the responses were variable, the mean amplitude of the eye movements in *nsf*^{I209N/st53} mutants was reduced by approximately half in comparison to the WT mean (Figure 22B). Compared with *cdh23* mutants that have completely abolished vestibular function, *nsf*^{I209N/st53} mutants had a significantly larger amplitude (Figure 22B), indicating a partial loss of vestibular function in *nsf*^{I209N/st53} mutants.

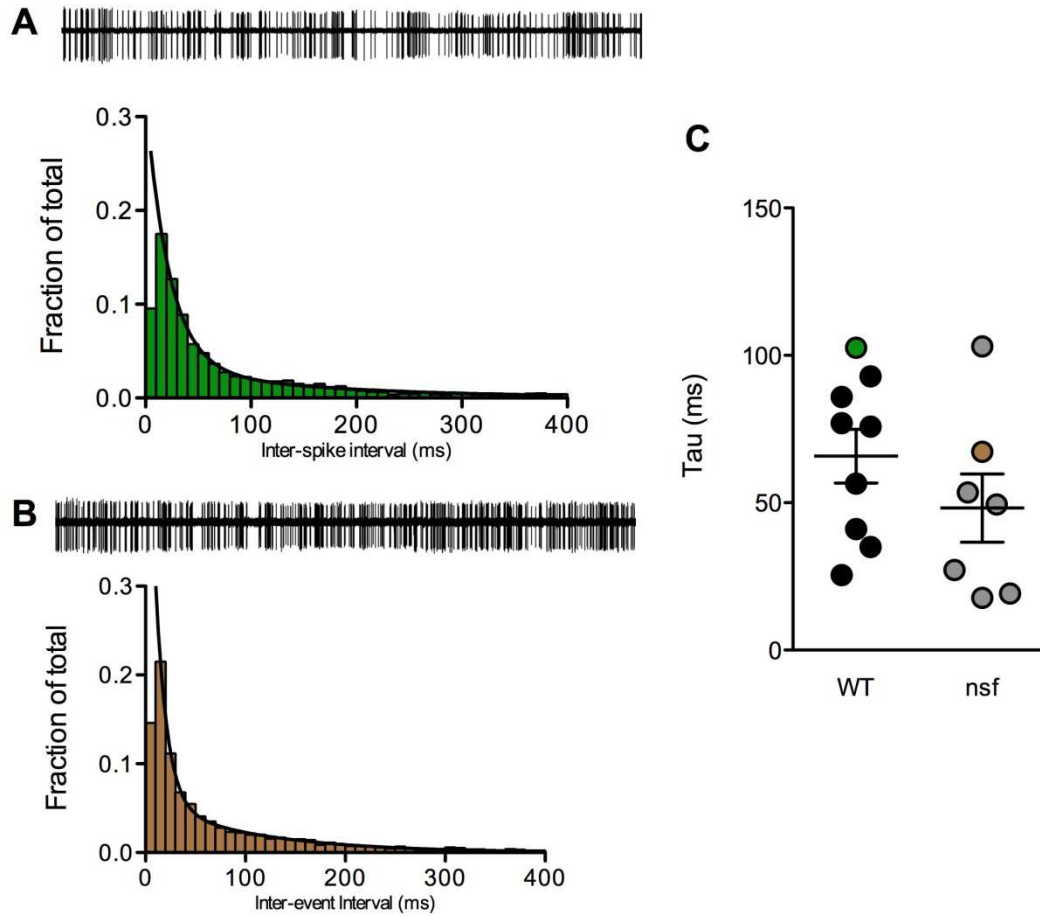


Figure 23. Spontaneous activity in *nsf*^{d209N/st53} mutants is normal. (A) Single 60-second trace of spontaneous spikes recorded from lateral-line neuron of a 5 dpf WT larva (upper) and corresponding inter-spike interval (ISI) histogram with 10 ms bins (lower). (B) Spontaneous spikes and ISI histogram of *nsf*^{d209N/st53} mutants. (C) Time constants (Tau) of spontaneous activities recorded from WT and *nsf*^{d209N/st53} mutant larvae. They are calculated by fitting arrival times of spontaneous spikes to single-phase exponential decay equations. The Tau of each larva is plotted.

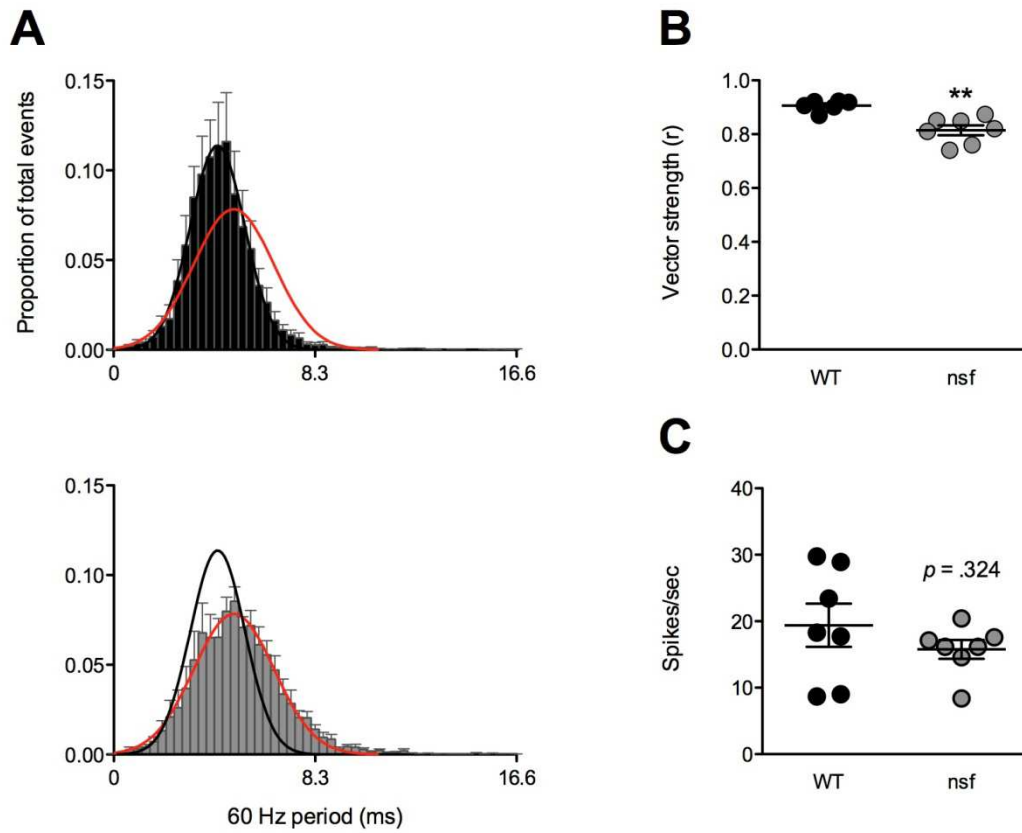


Figure 24. Delayed action potentials at pLLG in *nsf*^{I209N/st53} mutants. (A)

Representative histograms of spikes with 60 Hz stimulus recorded at the soma of pLLG from WT (black) and *nsf*^{I209N/st53} mutants (gray). The x-axis shows the time (ms) of single cycle of 60 Hz stimulus; and y-axis is the relative number of spikes. The curves for WT (black line) and mutants (red line) are fit to Gaussian distributions. (B) Vector strength values, which are the relative mean arrival times of spikes, of WT and *nsf*^{I209N/st53} mutants. ** $p < 0.01$. (C) The spike rate of WT and *nsf*^{I209N/st53} mutants is shown. No significant difference between WT and mutants.

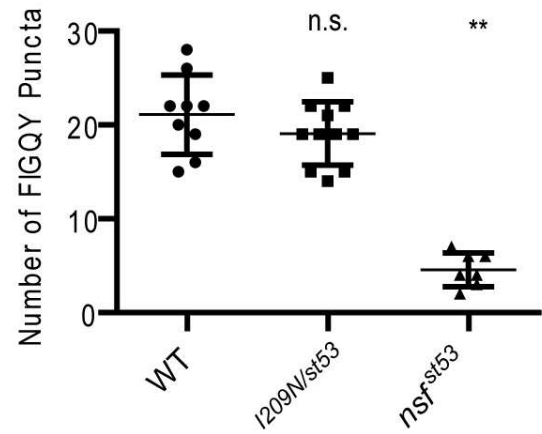
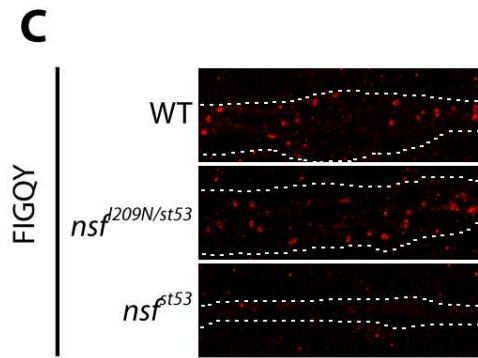
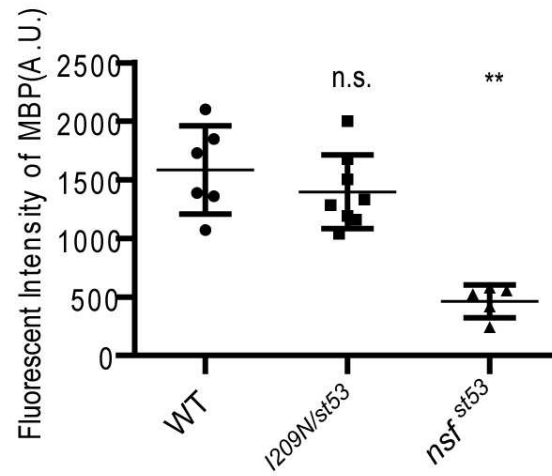
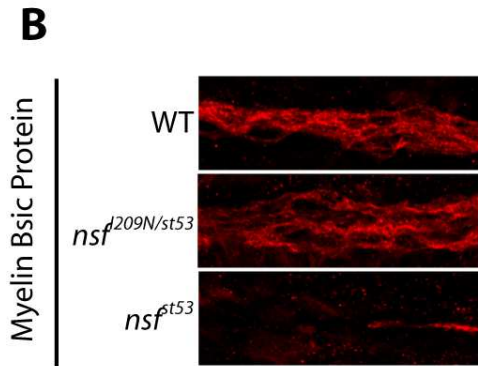
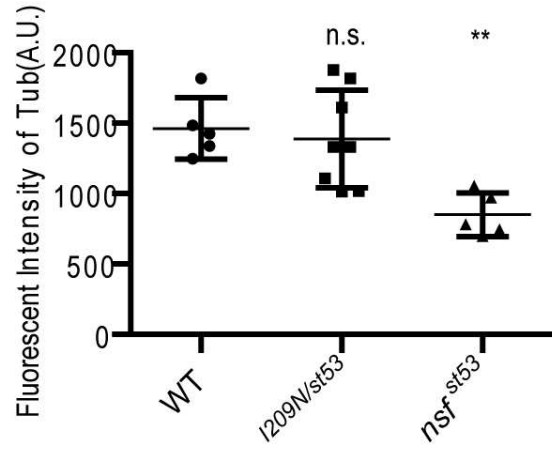
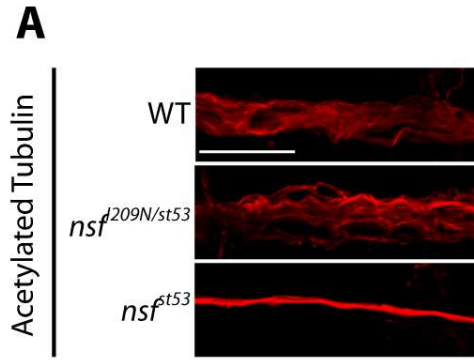


Figure 25. Structure of the posterior lateral line nerve (PLLn) in WT, *nsf*^{d209N/st53}, and *nsf*^{st53} larvae at 5 dpf. Images (left column) and quantification (right column) of Acetylated Tubulin (AcTub, A), Myelin Basic Protein (MBP, B), and FIGQY (C) antibody labeling in WT, *nsf*^{d209N/st53}, and *nsf*^{st53}. MBP and AcTub staining in the PLLn is reduced in *nsf*^{st53} mutants compared to WT, but there is no change in *nsf*^{d209N/st53} mutants. Quantification of AcTub (A) labelling in WT (1295±89), *nsf*^{d209N/st53} (1326±215), and *nsf*^{st53} (851±69); fluorescent intensity of MBP labelling (B) is also quantified in WT (1583±154), *nsf*^{d209N/st53} (1398±111), and *nsf*^{st53} (463±62). FIGQY signals (C) are clustered along PLLn in WT and *nsf*^{d209N/st53} mutants, but are not detectable in *nsf*^{st53} mutants. The average number of FIGQY puncta are quantified in WT (21.1±1.4), *nsf*^{d209N/st53} (19.1±1.0), and *nsf*^{st53} (4.6±0.7) larvae. Images are maximal projections of 5 z-stack images (1 µm each) from the initial segment of the PLLn before the first lateral line neuromast. Quantification data are shown as mean ± S.E.; P values are determined by ANOVA tests to compare with WT group. n.s.=nonsignificant, **p<0.01. Each dot in the quantitative plot represents an individual fish larva. Scale bar equals 20 µm.

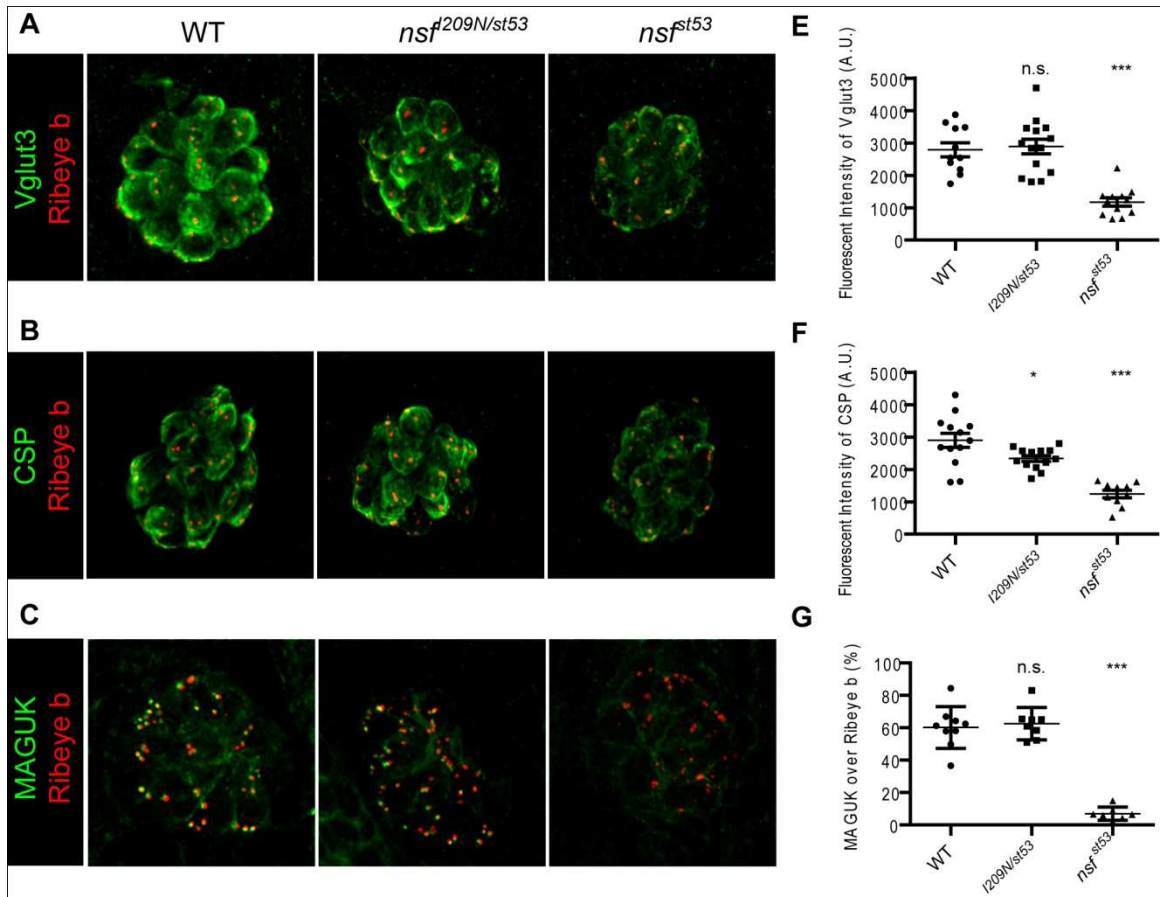


Figure 26. Antibody labelling of Vglut3, CSP, Ribeye b, and MAGUK in *nsf* mutants. (A-C) For each antibody stain, fluorescent confocal z-projections (8 sections at 1 μm) of posterior lateral line neuromast 1 (L1) are shown (5 dpf). Ribeye b antibody labelling is used to mark the presynaptic ribbons located at the basal end of hair cells. (A) Hair cell synaptic vesicles are labelled by Vesicular Glutamate Transporter 3 (Vglut3) antibody stain, which is concentrated in the basolateral region of hair cells. (B) Antibody for CSP protein also stains the basolateral region. (C) A pan-MAGUK antibody that recognizes a common peptide of the PSD (post-synaptic density) protein family labels the postsynaptic density of afferent terminals. (E-G) Quantification of images in panel A-C. The fluorescent intensity (A.U.) of Vglut3 (E) was quantified in WT (2788 ± 216), *nsf*^{d209N/st53} (2887 ± 223), and *nsf*^{st53} (1175 ± 127) larvae. CSP fluorescent intensity per neuromast in WT (2893 ± 218), *nsf*^{d209N/st53} (2334 ± 910), and *nsf*^{st53} larvae (1237 ± 117) is quantified in panel (F). Numbers of MAGUK and Ribeye b puncta are unchanged between WT and *nsf*^{d209N/st53} mutants (data not shown). Percentage of fluorescent pixels that MAGUK colocalize with Ribeye b are quantified in WT (60.2 ± 4.3), *nsf*^{d209N/st53} mutants (62.6 ± 3.5), and *nsf*^{st53} mutants (6.97 ± 1.5). Quantification data are shown as mean \pm S.E.; P values are determined by ANOVA tests to compare with WT group. *p<0.05, **p<0.01, ***p<0.001.

To understand the contribution of *nsf* in the auditory system, the auditory evoked behavioral response (AEBR) was measured. AEBR is a simple measurement of the escape behavior in response to acoustic stimuli, and is also known as the acoustic startle reflex (ASR) (Zeddies and Fay, 2005; Cervi et al., 2012; Einhorn et al., 2012). Although *nsf*^{I209N/st53} mutants can respond to a crude acoustic stimulus, they may have mild hearing loss, as was shown to be the case for *rabconnectin 3α* mutants (Einhorn et al., 2012). In order to assess potential hearing loss in *nsf*^{I209N/st53} mutants, we first quantified the AEBR at four different sound pressure levels (SPL) ranging from 135 to 155 dB at 1000Hz. We observed that 5 dpf zebrafish larvae displayed an escape response at 135 dB and higher. In comparison to WT larvae, fewer *nsf*^{I209N/st53} mutants displayed an escape response when SPLs were less than 155dB. At 155 dB SPL, the percentage of *nsf*^{I209N/st53} mutant larvae responding to sound did not significantly differ from their WT siblings (Figure 22C). To determine whether the *nsf*^{I209N} mutation can affect hearing perception in different sound frequencies, we then measured the AEBR at 140dB at four different frequencies. They had reduced AEBR at all frequencies tested (Figure 22D). The reduced AEBR suggested a partial loss of hearing in *nsf*^{I209N/st53} mutants.

3.3. Synaptic transmission is impaired in *nsf*^{I209N/st53} mutants

An important function of hair cells is to accurately transmit information about sound and head movements. For this purpose, ribbon synapses in hair cells are thought to facilitate fast and continuous release of synaptic vesicles (Nouvian et al., 2006). It is well-known that NSF plays a role in synaptic vesicle fusion (Haas, 1998). The I209N change is at the beginning of the D1 domain of Nsf protein (Figure 21A), a critical region of Nsf that

undergoes a conformational change during catalysis (Chang et al., 2012). The substitution of asparagine for isoleucine dramatically increases the hydrophilic nature of this residue, presumably causing a reduction of Nsf activity. Therefore, we hypothesize that defects in synaptic transmission are causal to the hearing and balance defects in *nsf*^{I209N/st53} mutants.

To examine if the *nsf*^{I209N} mutation perturbs synaptic transmission from hair cells to afferent neurons, we examined spiking in lateral-line afferent neurons in response to fluid jet stimulation of lateral-line hair cells. For both WT and *nsf*^{I209N/st53} mutants, we first measured the spontaneous activity, which is unevoked action potentials in afferent neurons due to a basal release of glutamate from the ribbon synapse (Trapani and Nicolson, 2011). Both WT and *nsf*^{I209N/st53} larvae have a temporal pattern of spontaneous firing that fit a single exponential distribution (Figure 23A, B). We did not observe a difference in number or kinetics of spontaneous spikes between WT and *nsf*^{I209N/st53} neurons (Figure 23C). We then recorded evoked action potentials from afferent neurons using a 60 Hz sinusoidal stimulus. Shown in Figure 24A, the timing of each spike is plotted relative to the start of the 60 Hz cycle. The distribution of the timing of spikes was fitted with a Gaussian curve (Black and Red solid lines in Figure 24A). Compared with the WT distribution, we saw a delayed and more dispersed distribution of spiking activity in *nsf*^{I209N/st53} mutants (Figure 24A). The precision of timing can also be quantitatively measured by vector strength, which was significantly reduced in *nsf*^{I209N/st53} larvae (Figure 24B). A similar delay of action potentials has been observed in *synj1*^{Q296X} mutants, which also have a similar behavioral phenotype (Trapani et al., 2009). However, in contrast to *synj1*^{Q296X} mutants, we did not see a decrease in spike rate in *nsf*^{I209N/st53} mutants (Figure 24C). Our results indicate phase locking is significantly reduced in

nsf^{d209N/st53} mutants, suggesting that synaptic transmission is delayed at hair cell synapses and/or propagation of action potentials is slower in the posterior lateral line nerve (PLLn).

3.4. No defects of myelination found in *nsf*^{d209N/st53} mutants

Our electrophysiological data suggests two possible causes of delayed action potentials: (1) defects in vesicle exocytosis and/or (2) slowed action potential propagation. Studies of *nsf*^{st53} zebrafish, the *nsf* null mutant with a stop codon before the D2 domain (Figure 21A), have shown that Nsf is essential for myelination and maintenance of the PLLn (Woods et al., 2006; Mo and Nicolson, 2011). Since the myelin sheath and clustering of sodium channels at Nodes of Ranvier are well-known requirements for fast propagation of action potentials in vertebrates, their defects could cause a delay of spikes in *nsf*^{d209N/st53} mutants. To see if defects to the myelin sheath or Nodes of Ranvier are present in *nsf*^{d209N/st53} larvae, we examined protein markers of the PLLn.

We used antibodies against Acetylated Tubulin (AceTu) and myelin basic protein (MBP) to label the lateral line nerve and its myelin sheath respectively. As shown previously, MBP is an important marker to label the sheath (Brösamle and Halpern, 2002). Other studies have also used MBP expression to assess myelination of PLLn in zebrafish larvae (Fan et al.; Lyons et al., 2005; Mo and Nicolson, 2011). The expression levels and patterns of both AceTu and MBP were dramatically changed in 5 dpf *nsf*^{st53} mutants, but in *nsf*^{d209N/st53} mutants their levels were similar to WT levels (Figure 25A, B). The function of myelin sheath surrounding nerve fibers is to electrically insulate axons between nodes of Ranvier, and hence facilitate propagation of action potentials along axons. Although it has been shown that *nsf*^{st53} mutation in zebrafish affects both

myelination and nodes of Ranvier (Woods et al., 2006), mutations in other zebrafish genes have been found to disrupt the mature node of Ranvier without disrupting the formation of myelin sheath (Voas et al., 2007). We used FIGQY antibody, which recognizes conserved peptides present at nodes of Ranvier (Rasband et al., 1999; Woods et al., 2006). In comparison to *nsf^{st53}* mutants, which have drastically reduced clustering of FIGQY labeling, both WT and *nsf^{I209N/st53}* larvae showed comparable numbers of FIGQY clusters (Figure 25C). Collectively, our results suggest that the *nsf^{I209N}* point mutation in zebrafish does not affect myelination and clustering of the nodes of Ranvier in PLLn.

3.5. Hair-cell ribbon synapses in *nsf^{I209N/st53}* mutants show subtle changes.

As NSF has been implicated in protein trafficking and the localization of receptors, a reduction in synaptic transmission in *nsf* mutants may be caused by indirect changes in the structure or molecular composition of synapses. To determine if the components of hair-cell synapses are altered in *nsf^{I209N/st53}* larvae, we first quantified a marker of synaptic vesicles using a Vglut3 antibody (Obholzer et al., 2008). Although Vglut3 labeling is dramatically reduced in *nsf* null mutants, its intensity in WT and *nsf^{I209N/st53}* mutants is comparable (Figure 26A). This result suggests that *nsf^{I209N/st53}* mutants maintain normal number of synaptic vesicles.

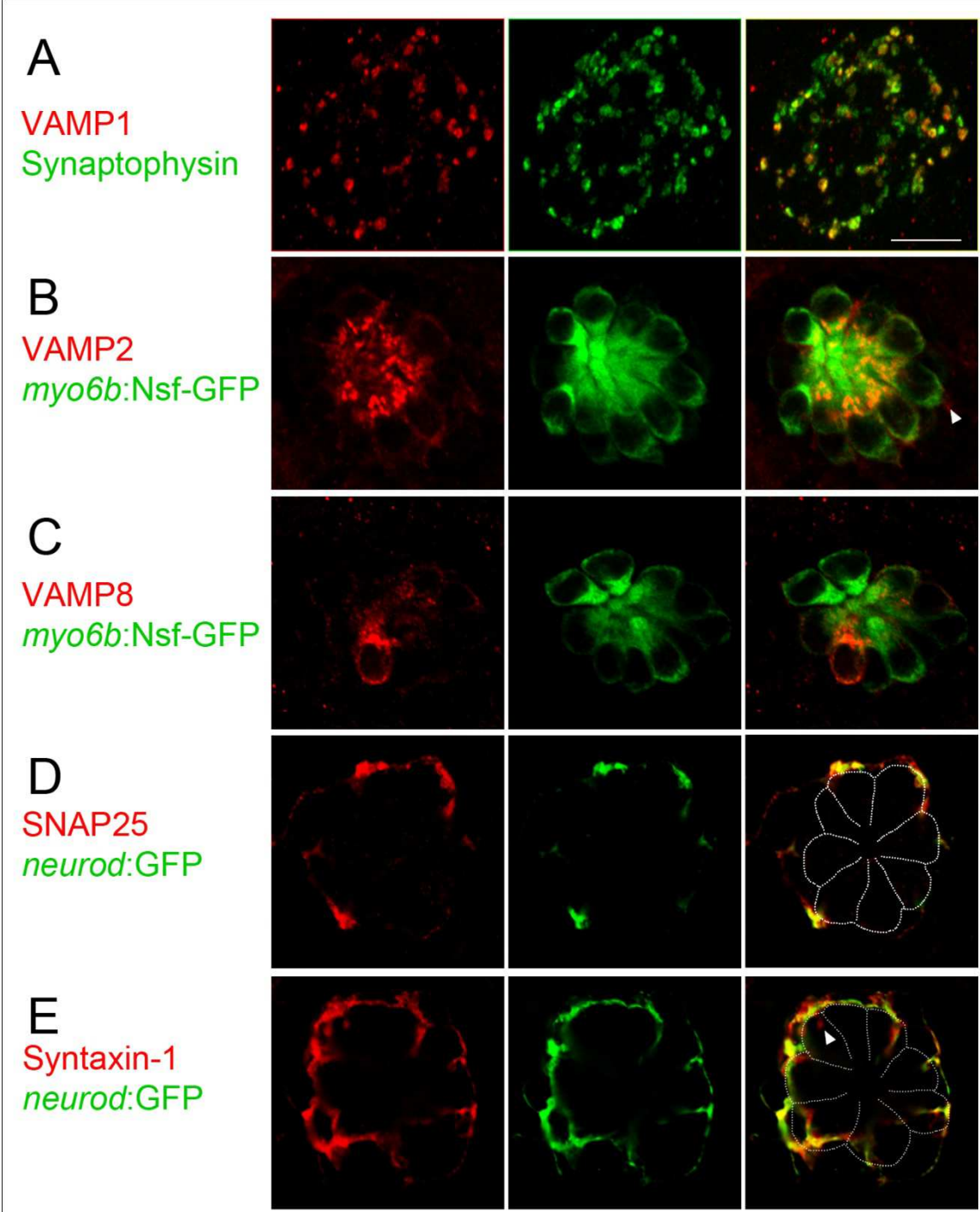


Figure 27. Antibody labeling of SNARE proteins in 5 dpf zebrafish neuromasts.

Confocal z-projection (A) and single confocal images (B-C) of 5 dpf L1 neuromasts are shown. (A) Vesicle-associated membrane protein 1 (VAMP-1) colocalizes with Synaptophysin, a marker for efferent synaptic synapses. (B, C) VAMP-2 and -8 are expressed in hair cells, which are labelled by *myo6b* promoter driven Nsf-GFP. VAMP-2 also likely presents in afferent nerves (arrow head). (D, E) SNAP25 and Syntaxin-1 are both in afferent nerve fibers, which are labelled by *neurod* promoter driven GFP. Hair cells are outlined by dashed lines. Syntaxin-1 may also be expressed in efferent nerves (arrow head). Scale bar is 10 μm .

As Nsf functions to dissociate SNARE complexes after synaptic transmission, its malfunction may also lead to changes in trafficking and subcellular localization of SNARE or associated proteins, such as cysteine string protein (CSP) (Ohyama et al., 2007; Stowers and Isacoff, 2007). CSP proteins are important chaperones that facilitate synaptic transmission by promoting assembly of SNARE complexes (Sharma et al., 2011; Rozas et al., 2012). As CSP is also found in ribbon synapses (Eybalin et al., 2002; von Kriegstein and Schmitz, 2003), we analyzed its distribution using antibody against CSP protein in both WT and mutant larvae. Compared with WT, CSP remained localized to the basolateral regions in *nsf*^{I209N/st53} hair cells, but its expression was significantly decreased, and a further reduction of CSP was observed in *nsf* null mutants (Figure 26B). Considering the important role of CSP in regulating synaptic vesicles, misregulation of CSP indicates an effect of the *nsf* mutation on synaptic transmission in hair cells.

As Nsf has been shown to affect maintenance of synapses (Mo and Nicolson, 2011), we examined the structural integrity of hair-cell ribbon synapses. We used anti-Ribeye b antibody to label presynaptic ribbon bodies and anti-MAGUK antibody to label postsynaptic densities (Sheets et al., 2011). Since the number and size of ribbon synapses is important for synaptic transmission in hair cells (Zou et al., 2005; Liberman et al., 2011; and unpublished observations from Sheets, L), we quantified puncta of both Ribeye b and MAGUK staining. We observed that there was no change of the average size and number of pre- and postsynaptic puncta in *nsf*^{I209N/st53} larvae (data not shown). To determine if the synaptic structure was affected in either *nsf* mutants, we looked at the co-localization of MAGUK and Ribeye b by calculating the percentage of MAGUK fluorescence overlapping with Ribeye b signal. Postsynaptic MAGUK co-localization

with presynaptic Ribeye b was the same in both mutants and WT siblings (Figure 26C). In addition, we did not find any cell death within neuromasts and pLLG neurons as well. Together, only slightly reduced CSP expression was seen in *nsf*^{d209N/st53} mutants, which may explain why the behavioral and electrophysiological defects are subtle. This data also suggests that the *nsf*^{d209N} mutation does not affect development of the ribbon synapse.

3.6. Expression of neuronal SNAREs in zebrafish hair cells

Our existing results suggest that *nsf*^{d209N} mutation affects hair-cell synaptic transmission but not structure. In contrast, Nouvian and colleagues recently showed that synaptic transmission in hair cells was independent of neuronal SNAREs (Nouvian et al., 2011). In neurons, neuronal SNARE complexes are dissociated by NSF after the fusion of synaptic vesicles. It is unclear whether NSF mediates the dissociation of different SNARE complexes for synaptic transmission in hair cells, or if neuronal SNAREs are required in zebrafish hair cells. We therefore used antibodies against neuronal SNAREs, Syntaxin-1, VAMP-1 and -2, and SNAP25, all of which are not found in mouse IHCs, to label zebrafish hair cells (Nouvian et al., 2011). With these antibodies, we observe that VAMP-1 is colocalized with Synaptophysin, a marker for efferent synapses (Nemzou N et al., 2006) (Figure 27A). VAMP2 was the only neuronal SNARE we observed exclusively in zebrafish hair cells. It was localized within the basolateral compartment, but was also highly expressed on the apical end of hair cells (Figure 27B). Both SNAP25 and Syntaxin-1 proteins were in afferent nerve fibers underneath hair cells, but were not found in hair cells (Figure 27 D, E). Although not many SNARE genes are characterized in zebrafish, another SNARE gene, *vamp8*, was found to express specifically in hair cells

of the inner ear and lateral line systems (Thisse et al., 2004). Antibody staining of VAMP8 revealed a similar expression pattern to VAMP2, but it displayed heterogeneous expression in zebrafish hair cells (Figure 27C). Another possible SNARE protein expressed in hair cells is Syntaxin-3, which has been confirmed to act as a key player of SNARE complexes in photoreceptor cells (Morgans et al., 1996; Curtis et al., 2008, 2010). Although we saw expression of Syntaxin-3 in the retina, no expression of Syntaxin-3 in neuromasts or inner ear hair cells was found (data not shown). Our results confirmed that hair cells in zebrafish lack several essential neuronal SNAREs that mediate synaptic transmission in neurons. However, we did find two VAMP proteins in hair cells, subcellularly localized to both apical and basal compartments. In combination with our observation that hair cells likely require Nsf for synaptic transmission, it further suggests that hair-cell ribbon-synapses use unconventional SNAREs.

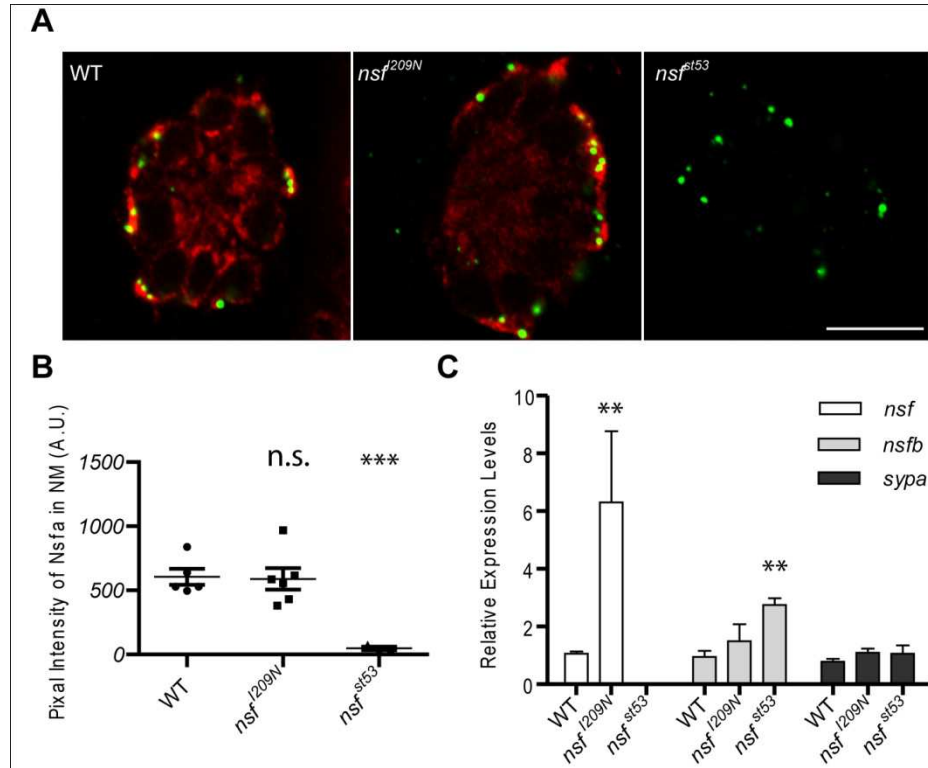


Figure 28. Increased *nsf* transcripts but not proteins in *nsf*^{I209N} mutants. (A)

Confocal optical sections of L1 neuromast are shown (5 dpf). Ribeye b (green) antibody labelling is used as a marker for presynaptic ribbons of hair cells. Nsf (red) signals are seen in both hair cells and afferent synaptic terminals.

(B) The fluorescent intensity (A.U.) of Nsfa (E) in hair cells was quantified in WT (607±63), *nsf*^{I209N} mutants (590±84), and

nsf^{s153} (48.0±14) mutants. (C) QPCR was used to determine the expression levels of genes in brain cDNA from WT, *nsf*^{I209N}, and *nsf*^{s153} mutant larvae (5 dpf). Gene expression level in wild-type larvae was normalized to 1. Quantification data are shown as mean ± S.E.; P

values are determined by ANOVA tests to compare with WT group. **p<0.01,

***p<0.001. Scale bar = 10µm.

3.7. Enhanced transcription of *nsf* in *nsf*^{I209N} mutants

Because there is a null copy of *nsf* gene in *nsf*^{I209N/st53} mutants, we used *nsf*^{I209N} homozygotes and their WT siblings to check the expression of transcripts and protein of *nsf*. Although *nsf*^{I209N} mutation appears to affect the fidelity of hair-cell synaptic transmission in zebrafish, we do not know how the *nsf*^{I209N} mutation might affect the activity of the protein. To determine if the *nsf*^{I209N} mutation has an effect on the stability of the protein, we examined immunolabeling of Nsf in our mutants. As expected, there was no labeling of Nsf protein in the *nsf*^{st53} mutants. In contrast, the expression of Nsf protein in *nsf*^{I209N} allele in hair cells was not changed compared to WT levels (Figure 28A, B). Additionally, there was no change of subcellular localization of Nsf protein in mutant larvae (Figure 28A). The immunolabeling indicates that the mutant Nsf protein is present, however, it is not clear if the turnover is increased. It is possible that *nsf* transcription may change in response to increased turnover of the mutant protein. Because there is a paralog of *nsf* in zebrafish, *nsfb*, expression of this gene may compensate for Nsf dysfunction in *nsf*^{I209N} mutants (Kurrasch et al., 2009; Mo and Nicolson, 2011). We examined the levels of transcripts of both *nsf* and *nsfb* genes using quantitative PCR. In agreement with results reported by Kurrasch et al., *nsfb*, but not *nsf*, was upregulated in the *nsf*^{st53} mutants (Figure 28C). However, expression of *nsf*, but not *nsfb*, was increased in *nsf*^{I209N} mutants (Figure 28C). Our results suggest that to maintain the protein level of Nsf, more mRNA is transcribed in the *nsf*^{I209N} mutant. It therefore seems likely that the I209N mutation affects the stability of the mutated protein.

4. Discussion

In this article, we report a new *nsf* mutant allele in zebrafish: *nsf*^{I209N}. The *nsf*^{I209N} mutant was initially identified as a circler mutant with vestibular but not auditory defects. In our behavioral analysis, we found that *nsf*^{I209N/st53} mutants have both hearing and balance deficits. Electrophysiological recording from the soma pLLG neurons also found that action potentials were slightly delayed in *nsf*^{I209N/st53} mutants. Potentially, protein trafficking of components required for accurate synaptic transmission could account for the shift in the phase locking with the stimulus. However, the morphology of hair-cells synapses, and the lateral line nerves including in myelin sheath was largely unchanged in *nsf*^{I209N/st53} mutants. One exception was a slight reduction in CSP, a protein that has an opposing function to NSF in regulating SNARE complexes. We also observed increased *nsf* transcripts, but not Nsf protein levels in *nsf*^{I209N} mutant hair cells, suggesting instability of the mutant form of the Nsf protein and possible effects on its enzymatic activity in the mutants.

In agreement with previous findings (Nouvian et al., 2011), most of the neuronal SNAREs, the targets of NSF, were also not found in hair-cell ribbon-synapses of zebrafish. Nevertheless, we identified two v-SNAREs, VAMP-2 and -8, in zebrafish hair cells. Our results suggest that zebrafish hair cells require a set of unconventional SNAREs to mediate synaptic transmission.

4.1. Mutation I209N in zebrafish Nsf protein

How does the I209N mutation affect the ability of Nsf to catalyze disassembly of SNARE complexes? Acting as a homohexameric ATPase, the NSF protein contains 3 domains (N, D1, and D2). The I209N mutation is present within a linker region near the beginning of the D1 domain, which is the ATPase domain that catalyzes the dissociation of SNAREs. Although crystal structures of the N and D2 domains have been solved for over a decade (Lenzen et al., 1998; Yu et al., 1998, 1999; Babor and Fass, 1999; May et al., 1999), the structure of D1 domain and full length NSF has yet to be determined. Analysis of NSF (Hanson et al., 1997; Furst et al., 2003) and NSF-SNAP-SNARE complex (Hohl et al., 1998; Furst et al., 2003; Chang et al., 2012; Moeller et al., 2012) using electron microscopy have provided the structural layout of different domains of NSF protein. The crystal structure of the N domain, however, cannot fit into the EM structure, which is probably due to its structural flexibility. The flexibility could be important to create an interface for the N domain to bind with its substrates. According to the latest EM structure, the 209 Isoleucine is within an N-D1 linker region with high flexibility (Chang et al., 2012). The catalytic activity of NSF relies on the flexible N-D1 linker that mediates the movement of the N domain towards the D2 region (see Figure 11). Several studies have reported the same large conformational change of the N domain upon hydrolysis of ATP (Hanson et al., 1997; Chang et al., 2012; Moeller et al., 2012). There are at least two possible ways an asparagine mutation in the N-D1 linker can affect NSF function. As asparagine is highly acidic, compared to the isoleucine, it may interfere with the hydrophobic environment the isoleucine residue may face. This could impact the enzymatic activity of NSF. Alternatively, asparagines are more flexible than isoleucines,

which may decrease the stability of the NSF protein as a whole. Indeed, we did find the *nsf* mRNA, but not Nsf protein, is upregulated in *nsf*^{I209N} mutants (Figure 28). This result suggests that Nsf^{I209N} is less stable than the WT protein. Whether the I209N mutation results in protein instability or a reduction in the conformation changes upon catalysis of ATP requires more biochemical analysis of the mutant protein.

Although we do not observe obvious changes in hair-cell morphology, a loss of Nsf activity may affect both development and function of hair cells in zebrafish larvae in many ways as almost all vesicle fusions in eukaryotic cells are dependent on NSF activity (Haas, 1998; Südhof and Rizo, 2011). Although no NSF mutants in mouse have been reported, both NSF1 and NSF2 in *Drosophila* can affect neuronal development (Sanyal and Krishnan, 2001; Laviolette et al., 2005; Stewart et al., 2005). Nsf proteins in zebrafish have been reported to have neuroprotective role (Mo and Nicolson, 2011), to be required for secretion of neuroendocrines (Kurrasch et al., 2009), and to affect development of myelin sheaths (Woods et al., 2006). However, no function of NSF in hair cells has been reported. The present study reveals a subtle impairment of the timing of evoked afferent nerve activity and a small but significant reduction in CSP protein expression in hair cells. Although the reduction of CSP expression may be an indication of immaturity or dysfunction of hair cells, it is more likely a functional compensation of reduced NSF activity. NSF is known to catalyze dissociation of SNAREs post-vesicle-fusion, while CSP is found to promote assembly of SNAREs and vesicle fusion (Sharma et al., 2011, 2012; Rozas et al., 2012). Accumulation of SNARE complexes have been found in fly NSF mutants (Littleton et al., 2001), suggesting a similar consequence of *nsf* mutation in zebrafish. Expression of CSP proteins could be suppressed upon

accumulation of SNARE complexes. Moreover, reduction of CSP proteins has been found in cases in which exocytosis is impaired (Ohyama et al., 2007; Stowers and Isacoff, 2007). Our findings suggest that delayed action potentials are due to a reduced NSF function and not developmental defects. Whether the reduction in phase-locking is strictly due to reduced activity of Nsf in hair cells or whether the firing properties of the afferent neurons are also altered in *nsf*^{d209N} mutants remains to be determined.

4.2. NSF and SNAREs in hair-cell ribbon synapses

The actual substrates of NSF in hair-cells synapses are largely unknown. Using immunostaining, we have identified expression of Nsf, VAMP-2, and VAMP-8 in zebrafish hair cells (Figure 27). Our results largely agree with recent findings that conventional neuronal SNAREs including SNAP-25, Syntaxin-1, and VAMP-1 are not present in mouse IHCs (Nouvian et al., 2011), but differ from other reports from chicken, rat, and guinea pig, in which it was found that all neuronal SNAREs are expressed in hair cells (Safieddine and Wenthold, 1999; Eybalin et al., 2002; Uthaiyah and Hudspeth, 2010). These conflicting findings may be due to two reasons. Firstly, improvement of fixation or antibody affinities may be needed to visualize SNAREs in ribbon synapses, as the ribbon structure or other unconventional protein structures in hair cells may mask epitopes in an unknown way. Some differences of antibody labeling have been explored using different methods (Nouvian et al., 2011), but none of them explain the variability of observations. Secondly, unspecific signals may be misleading. In the rat and guinea pig studies, no hair-cell markers were used to counter stain with SNARE antibodies to confirm their colocalization (Eybalin et al., 2002). Non-hair cell controls were also not included used to

visualize SNARE antibodies in chicken (Uthaiyah and Hudspeth, 2010). More data is needed to support either statement.

Nevertheless, our data do suggest that NSF is required for accurate synaptic transmission in hair cells. Although it is not clear which SNARE machinery is required, VAMP7 and VAMP8 are interesting candidates for mediating synaptic transmission in hair cells. The tetanus toxin-insensitive VAMP7 was recently found to identify a subgroup of synaptic vesicles that are spontaneously released in cultured hippocampal neurons (Hua et al., 2011). VAMP8 is specifically expressed in a number of tissues including nose, otic vesicle, lateral line and pronephric ducts in zebrafish (Thisse et al., 2004). Both VAMP-7 and -8 interact with SNAP23 and Syntaxin-4 to trigger exocytosis in human mast cells (Sander et al., 2008). To understand why non-neuronal SNAREs are employed at ribbon synapses in hair cells, and how these SNAREs contribute to the properties of synaptic transmission would be a very interesting follow-up of our current research.

Chapter 4. Nsf in preventing Degeneration of Hair- Cell Synapses

Reprinted from Mo W, Nicolson T. Both pre- and postsynaptic activity of Nsf prevents degeneration of hair-cell synapses. PLoS One. 2011;6(11):e27146. Epub 2011 Nov 3. Copyright: © 2011 Mo, Nicolson.

1. Summary

Vesicle fusion is required for the maintenance of synapses in the nervous system by mediating events such as synaptic transmission, release of neurotrophic factors, and trafficking of membrane receptors. N-ethylmaleimide-sensitive factor (NSF) is indispensable for dissociation of the SNARE-complex following vesicle fusion. Although NSF function has been characterized extensively *in vitro*, the *in vivo* role of NSF in synaptogenesis is relatively unexplored. Zebrafish possess two *nsf* genes, *nsf* and *nsfb*. Here, we examine the role of either Nsf or Nsfb function in the pre- and postsynaptic cells of the zebrafish lateral line organ and demonstrate that Nsf, but not Nsfb, is required for maintenance of afferent synapses on hair cells. In addition to peripheral defects in *nsf* mutants, neurodegeneration of glutamatergic synapses in the central nervous system also occurs in the absence of Nsf function. Expression of an *nsf* transgene in the null background indicates that stabilization of synapses requires Nsf function in both hair cells and afferent neurons. To identify potential targets of Nsf-mediated fusion, we examined the expression of genes implicated in stabilizing synapses and found that transcripts for multiple genes including *bdnf* were significantly reduced in *nsf* mutants. With regard to trafficking of Bdnf, we observe a striking accumulation of Bdnf in the neurites of Nsf mutant afferent neurons. In addition, injection of recombinant BDNF protein partially rescues the degeneration of afferent synapses in *nsf* mutants. These results establish a role for Nsf in synaptic maintenance, in part via secretion of trophic signaling factors. In terms of innervation of hair cells, Nsf function is required in both hair cells and afferent neurons for stability of afferent synapses.

2. Materials and methods

Zebrafish strains and husbandry. Adult zebrafish strains were maintained as previously described (Westerfield, 1995). All lines used in this study were maintained in a Tübingen or Top Long Fin background. *TgBAC(neurod:EGFP)n11* transgenic fish were previously described (Obholzer et al., 2008); the *nsf^{st53}* (Woods et al., 2006) and *nsfb^{hi2869Tg}* allele (Amsterdam and Hopkins, 2004) were obtained from the Zebrafish International Resource Center.

Transgenic fish. Stable transgenic lines were generated as described previously (Kwan et al., 2007). The promoter sequence of *myo6b* gene (-6myo6b), described previously (Obholzer et al., 2008), was cloned into a 5-prime entry (p5E) vector in the Tol2 kit vector #381 p5E-MCS (Kwan et al., 2007). To clone the promoter sequence of *neurod* gene, the following primers were used to amplify and insert an approximate 5kb fragment (-5neurod) into the same p5E vector: Forward primer with Fse I site: GGC CGG CCC GGC ATC AAA CCG CCT CGA GAG, Reverse primer with Asc I site: GGC GCG CCG TCG GAA CTC TGC AAA GCG ATA AAG C.

Phylogenetic analysis. Protein sequences of Nsf from different species were obtained from UCSC genome browser (<http://genome.ucsc.edu/>). They are yeast NSF (YBR080C), nematode NSF (NP_00107660), fly dNSF1 (CG1618-RA) and dNSF2 (CG33101-RA), zebrafish Nsf (NP_001037793) and Nsfb (NP_001019625), mouse NSF (NP_032766), and human NSF (NP_006169). A phylogenetic tree was generated by ClustalW2, statistically evaluated by Bootstrap for 1000 times.

Immunofluorescent staining. Whole-mount immunostaining was performed according to a previous report with minor changes (Sheets et al., 2011). Briefly, fish larvae were fixed at 4°C for 4 hours with 4% paraformaldehyde, 4% sucrose, and 0.01% Tween-20 in PBS solution. After rinsing twice with 0.25% Tween-20, and 1% DMSO in PBS (PBSDT), fixed embryos were permeabilized by exposure to 100% acetone at -20°C and then washed with H₂O and PBSDT. Embryos were blocked with 6% goat serum, 3% bovine serum albumin in PBSDT for 1 hour, and then followed by incubation with primary antibody at 4°C overnight. After rinsing with PBSDT for 2 hours, samples were stained with a secondary antibody at 4°C overnight or 5 hours at room temperature. Primary antibodies used in this study are listed in Table 1. Alexa Fluor-conjugated secondary antibodies (Invitrogen) were used at 1:1500.

Confocal microscopy and quantification. Specimens were mounted in Elvanol mounting media and dried overnight. Confocal imaging and data analysis procedure was described previously (Sheets et al., 2011) with the following changes. Z-stack images were acquired using a Zeiss LSM 700 confocal microscope with either 10X or 60X oil lens using Zen software and the pinhole was set to 1 auto unit. Filters were set at default settings for Alex 488, 568 or 647 fluorescent signals. Z-stack images were transformed into Tiff images with Image J (NIH, Bethesda, MD, USA) before being analyzed by Metamorph (Molecular Devices, Sunnyvale, CA, USA). Using the maximal projection of each image, individual neuromasts were selected manually and the background, defined as the average intensity of the whole image, was deducted before using the integrated morphometry analysis function for quantification of the fluorescent intensity of antibody labeling or the number of punctae. Individual neuromasts were selected based on the

fluorescent signals of Ribeye b staining, which specifically labels the presynaptic ribbon synapses in hair cells. A punctum was defined as containing ≥ 20 pixels with three-fold intensity above background. To quantify BDNF, Pan-Cadherins, Acetylated Tubulin and MBP staining in LLN, the LLN was selected manually on a maximum projection image based on the fluorescent signal of the Acetylated Tubulin antibody. Only positively labeled regions were used for calculating the average fluorescent signals in Figure 36. For all other figures, the total intensity of antibody labeling is shown. A region before the first melanophore was selected for all images of LLNs. All quantities in figures are presented as mean \pm standard error. 2-tailed unpaired student t test was used to compare two groups of data.

Quantification of apoptosis and cell numbers. A confocal Z-stack with 10 slices was taken from selected regions. For analysis of apoptosis, one digital section image with the most apoptotic cells was picked from each Z-stack. Apoptotic and normal cells were counted in every image. To count cell numbers in each image, the digital section with the most cell numbers was chosen from each Z-stack scanning. Cells were counted based on the GFP fluorescence from *TgBAC(neurod:EGFP)n11* transgenic fish and/or DAPI staining in each image. Numbers were then analyzed using Microsoft Excel (Microsoft, WA) and graphs were made using Prism (GraphPad Software, CA).

RT-PCR and qPCR. 5 days post fertilization (dpf) zebrafish larvae or adult fish were anaesthetized in MESAB/Tricaine solution, and then tissues from adult fish or larvae were dissected and immediately put into RNAlater (Applied Biosystems/Ambion). Total RNA was extracted from wild-type or *nsf* mutants using the RNeasy mini kit (Qiagen).

5µg RNA was then reverse transcribed using the EcoDry premixes (Clontech, # 639541). For qPCR purpose, 0.2µl cDNA in 10µl SYBR green mixture in 384-well plates was used for each qPCR reaction on an Applied Biosystems 7900 HT real-time PCR machine. The RNA level for each gene was first calculated from a cDNA standard curve and then normalized to *actin* RNA. To perform RT-PCR, 0.2µl cDNA was used in a 20µl PCR reaction.

Table 1 List of antibodies for immunostaining

Antibody	Dilution	Suppliers	References
NSF	1:50	Cell Signaling #3924	
Ribeye b	1:4000	Generated by Openbiosystems	(Sheets et al., 2011)
Zn12	1:500	ZIRC, Zn-12	(Becker et al., 2001)
MAGUK	1:500	Neuromab, #73-029	(Sheets et al., 2011)
Vglut3	1:1000	Generated by Proteintech	(Obholzer et al., 2008)
Vglut1	1:1000	Generated by Proteintech	(Bae et al., 2009)
Casp3	1:250	Cell signaling #9661	(Eimon et al., 2006)
BDNF	1:100	Santa Cruz, sc-65513	(Germanà et al., 2010)
Cadherins	1:500	Sigma, C3678	(Shin et al., 2008)
MBP	1:50	Generated by Talbot lab	(Woods et al., 2006)
Acetylated-Tubulin	1:1500	Sigma, T6793	(Becker et al., 2001)
GFP	1:500	Aves lab, #GFP-1020	(Chung et al., 2008)

3. Results

3.1. Innervation in zebrafish *nsf* and *nsfb* mutants

The zebrafish genome contains two copies of *nsf*, *nsf* (also called *nsfa*) and *nsfb*. Nsf and Nsfb proteins share 83% identity and 91% similarity to each other. In the phylogenetic tree, zebrafish Nsf is more similar to mammalian NSF s than Nsfb (Figure 29A). To determine the spatial expression of the two *nsf* orthologs in zebrafish, we examined the expression of *nsf* and *nsfb* transcripts in different tissues. An RT-PCR experiment was used to detect both *nsf* and *nsfb* mRNA in adult tissues. *nsf* mRNA was detected in mainly neuronal tissues, but not in non-neuronal tissues (Figure 29B). In contrast, *nsfb* was expressed in both neuronal and non-neuronal tissues (Figure 29B). To ascertain whether both genes were expressed in hair cells, we isolated single neuromasts from 5 dpf zebrafish larvae and performed RT-PCR (Obholzer et al., 2008). We detected the presence of both *nsf* and *nsfb* transcripts in neuromasts (Figure 29C).

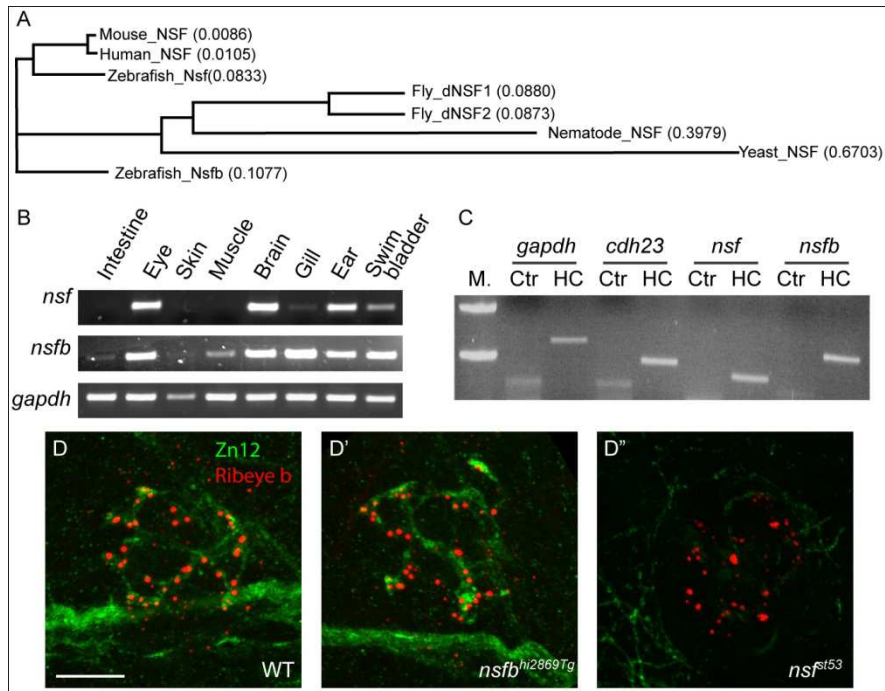


Figure 29. Expression of *nsf* and *nsfb* in zebrafish, and defective innervation of hair cells in *nsf* mutants. (A) Protein sequences of NSF from yeast, nematode, fly, zebrafish, mouse and human were aligned using ClustalW to generate a phylogenetic tree. The total amino acid substitutions of a specific protein are proportional to the length of each branch. The substitute rates of single amino acids were numbered in brackets after each protein. (B) Detection of *nsf* and *nsfb* transcripts in adult zebrafish tissues by RT-PCR. (C) RT-PCR of neuromasts isolated from 5 dpf larvae. *cdh23* was used as a neuromast-specific positive control. M.= Marker/DNA ladder, Ctr = Control with no reverse transcriptase, HC = Hair cell. (D) Larvae (4 dpf) labeled with nerve fiber-specific Zn12 (green), and anti-Ribeye b antibodies (red). The merged images showed the innervation of the first lateral line neuromast (L1) by posterior lateral line neurons. Scale bar, 10 μ m. The position of the specimen is dorsal up and anterior to the left, and each image is a projection of 10 optical sections (1 μ m each). Scale bar is 10 μ m.

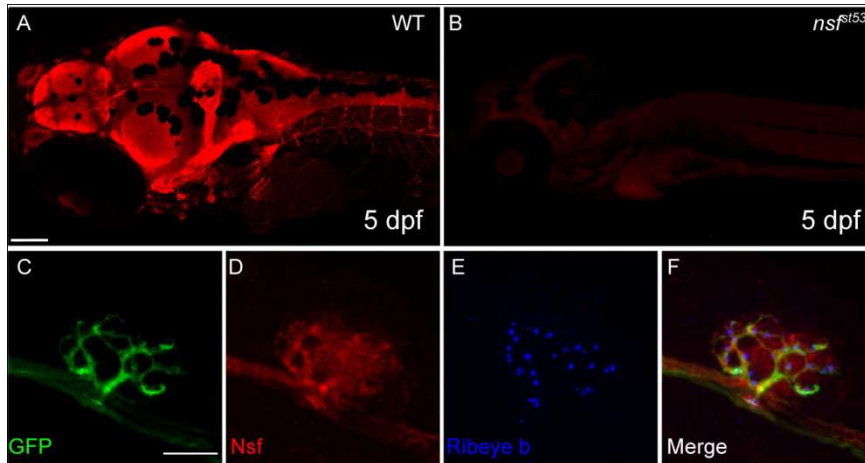


Figure 30. Expression of Nsf in the CNS and lateral line organ (5 dpf). (A) An antibody against human NSF protein labels the larval nervous system (5 dpf). (B) Labeling is absent in *nsf^{st53}* mutants. Images are projections of 5 optical sections of 10 μ m thickness. Scale bar, 100 μ m. (C-F) Confocal projections (10 X 1 μ m sections) of anti-NSF (red) and Ribeye b (Blue) in *TgBAC(neurod:EGFP)nll* transgenic fish. Nsf is found in the afferent nerve (marked by GFP) and in Ribeye b-positive hair cells. Scale bar, 10 μ m.

Because both *nsf* genes are expressed in neuromasts, we examined the contribution of both genes to ribbon-synapse formation in hair cells. We obtained *nsf^{st53}* and *nsfb^{hi2869Tg}* mutant lines: the *nsf^{st53}* mutation results in a truncated protein before the second ATPase domain (Woods et al., 2006), whereas the *nsfb^{hi2869Tg}* mutation results in a truncation of *nsfb* gene after the 18th exon, also before the second ATPase domain (Amsterdam and Hopkins, 2004). The *nsf* and *nsfb* genes are on chromosome 3 and 12, respectively. Both mutants are paralyzed at 4 dpf. Whereas *nsf^{st53}* mutants survive until 7 to 8 dpf, most

nsfb^{hi2869Tg} mutants die at 5 dpf. Therefore, we examined hair-cell innervation at 4 dpf, the latest stage possible for *nsfb*^{hi2869Tg} mutants. In wild-type larvae, afferent nerve fibers form an elaborate pattern or web beneath neuromast hair cells (Becker et al., 2001; Sheets et al., 2011). Typically, this highly branched structure is formed by two ganglion neurons, which make extensive contacts with the basal surfaces of the hair cells. The web of nerve fibers is more apparent when imaged using a top down view of the neuromast (Figure 29D and Figure 30C). Although the nerve fibers do not form distinctive boutons, the location of active zones can be visualized with antibodies against a ribbon-specific component, Ribeye b (Figure 29D and 30E) (Sheets et al., 2011). We compared innervation of neuromast hair cells in *nsf*^{st53} and *nsfb*^{hi2869Tg} mutants at 4 dpf, before extensive degeneration was visible in *nsfb*^{hi2869Tg} mutants (Figure 29D'-D''). Although the overall number of neuromasts was reduced in *nsfb*^{hi2869Tg} mutants, when hair cells were present, we observed innervation by the afferent nerve (n= 20 neuromasts, 5 larvae from 2 independent experiments) (Figure 29D'). Surprisingly, lateral line nerve fibers were mostly absent in *nsf*^{st53} mutants at the same developmental stage (Figure 29D''). Together, these results suggest that Nsf, but not Nsfb, is required for stable afferent innervation of hair cells. Consequently, in the following experiments, we exclusively focused on the role of Nsf in the innervation of lateral-line hair cells.

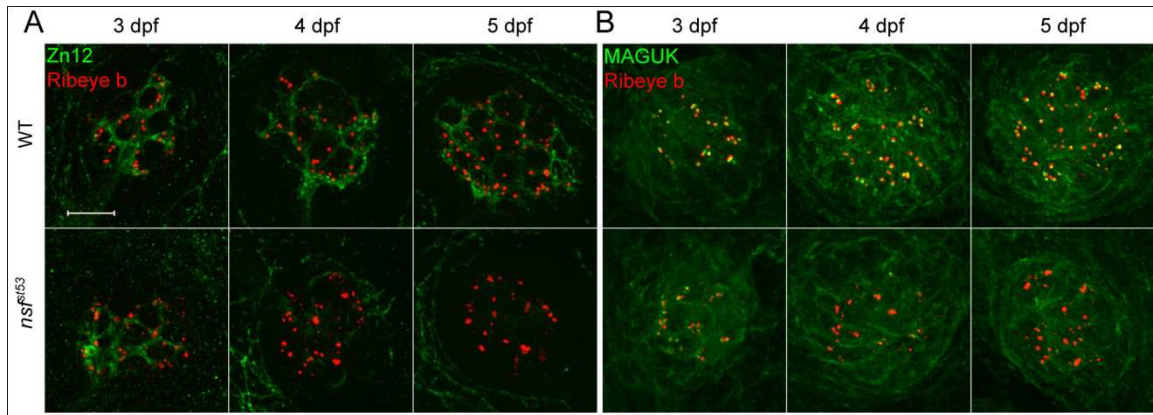


Figure 31. Degeneration of hair-cell synapses in *nsf^{st53}* mutants during development.

(A) Antibodies against Zn12 (green) and Ribeye b (red) were used to label afferent fibers and hair-cell ribbons, respectively, in wild-type (WT) and *nsf^{st53}* mutant larvae at 3, 4 and 5 dpf. (B) Anti-Ribeye b (red) and MAGUK (green) labels the pre- and postsynaptic compartments respectively in neuromasts of wild-type and *nsf^{st53}* mutants (3 to 5 dpf).

Scale bar: 10µm; z-projection of 10 confocal planes (1µm each).

3.2. Degeneration of hair-cell afferent synapses in *nsf* mutants

To study the defects in afferent innervation in *nsf^{st53}* mutants, we determined whether Nsf is expressed in both lateral line hair cells and afferent neurons. Using immunohistochemistry, we detected Nsf protein predominantly in the nervous system of 5 dpf larvae (Figure 30A), but not in *nsf^{st53}* mutants, which have a stop codon positioned before the epitope of the NSF antibody (Figure 30B). To determine whether Nsf is present in afferent neurons, we used *TgBAC(neurod:EGFP)nll* fish to mark afferent neurons and observed Nsf protein in GFP-positive lateral line nerves (Figure 30C-D). Co-labeling with Ribeye b antibody revealed that Nsf is also present in hair cells, consistent

with our RT-PCR analysis (Figure 30E-F). Nsf was also detected in the cell bodies of the posterior lateral line ganglion (pLLG) and hair cells in the inner ear (data not shown). Taken together, these data suggest that Nsf function may be required in both pre- and post-synaptic cells for innervation.

To determine if the lack of afferent innervation in *nsf^{st53}* mutant hair cells is due to a failure to initiate synaptogenesis, or to maintain synaptic contacts, we examined afferent innervation of *nsf^{st53}* mutant hair cells at different developmental stages using Zn12 as a marker. We found that afferent innervation of lateral line neuromasts was relatively normal at 3 dpf (Figure 31A, 34D). However, while the basket-like network of neurites was elaborated in wild-type embryos over days 4 and 5, *nsf^{st53}* mutants exhibited a loss of hair-cell innervation (Figure 31A, 34D). The retraction of neurites was further confirmed by acetylated Tubulin antibody (data not shown). Consistent with these results, immunolabel of the postsynaptic marker Membrane-Associated Guanylate Kinases (MAGUK) was also reduced at later stages in *nsf^{st53}* mutants (Figure 31B). These data suggest that Nsf function is not required to initiate hair-cell synaptogenesis in the lateral line organ, but instead is required for the maintenance of afferent innervation of hair cells.

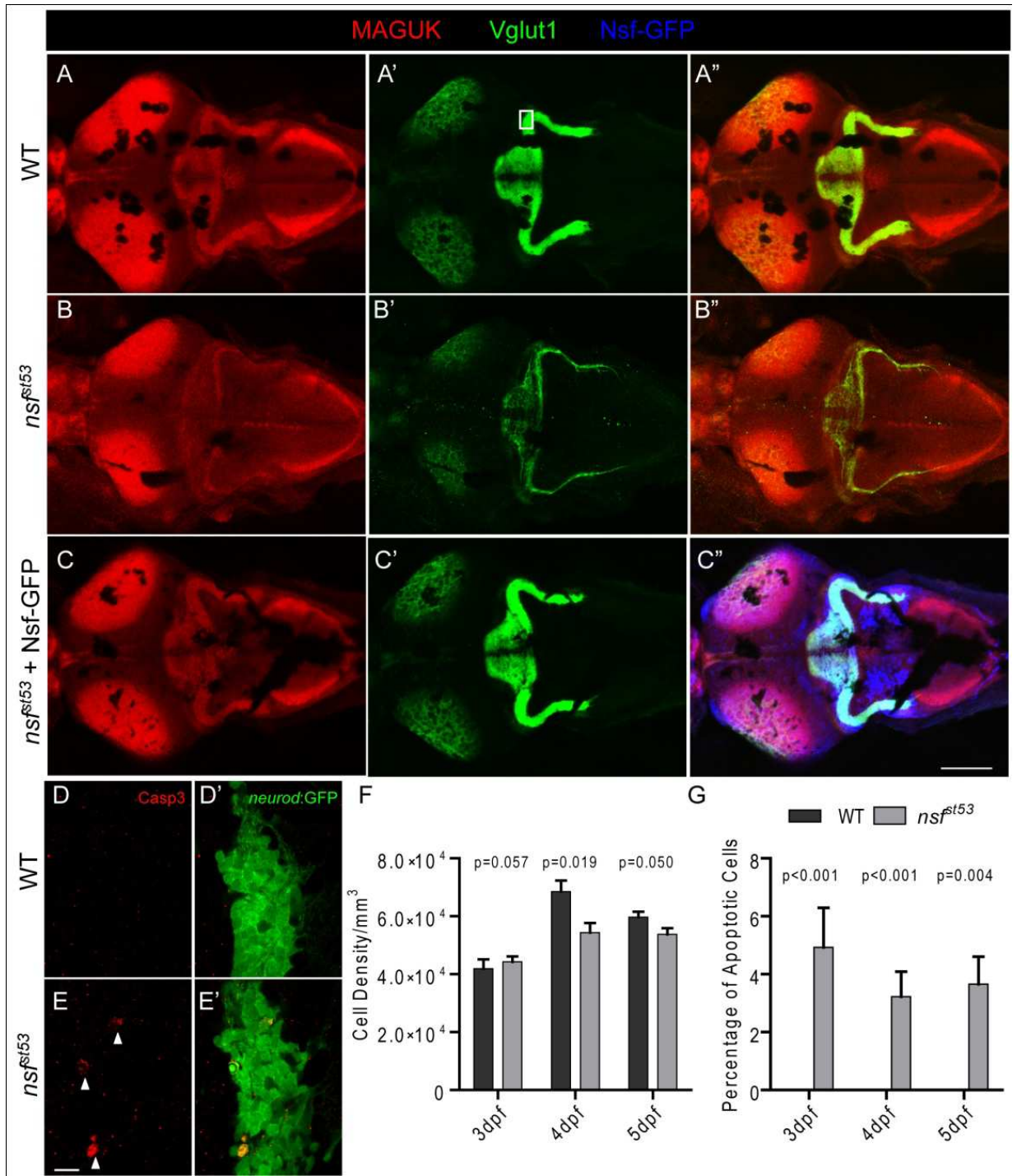


Figure 32. Reduction of glutamatergic synapses in the CNS of *nsf^{st53}* mutants (5 dpf).

Representative z-projections of the optic tectum and cerebellar region from a top view are shown. Wild-type (A), *nsf^{st53}* mutant (B), and *nsf^{st53}* mutant in *Tg(-5neurod:nsf-GFP)vo1* background (C), which expresses Nsf-GFP (Blue) were labeled with Vglut1 (glutamatergic presynapses) and MAGUK antibodies. Scale bar: 100 μ m; z-projection of 15 confocal planes (10 μ m each). (D-E'), Magnified views from the boxed region in panel (A'). Activated Caspase 3 (Casp3) antibody was used to label apoptotic cells (arrow heads) in the cerebellar region, and GFP signals from *TgBAC(neurod:EGFP)n11* fish were used to identify neurons, likely the Purkinje cells, in the cerebellum. (F) Cell density (3 dpf, 41875.0 \pm 3287.4, n=4; 4 dpf, 68500.0 \pm 3840.6, n=5; 5 dpf, 59687.5 \pm 1856.3, n=8 in wild-type and 3 dpf, 44285.7 \pm 1867.2, n=7; 4 dpf, 54375.0 \pm 3264.7, n=8; 5 dpf, 53750.0 \pm 2116.4, n=6 in *nsf^{st53}*) and (G) the rate of apoptosis in the cerebellum of wild-type (0% for 3 dpf to 5 dpf, n=8) and *nsf^{st53}* mutants (3 dpf, 4.3 \pm 1.3%; 4 dpf, 3.2 \pm 0.9%; 5 dpf, 3.1 \pm 1.0%, n=8). P values compare *nsf^{st53}* mutants to their wild-type siblings at the same developmental stage.

3.3. Neurodegeneration in the CNS of *nsf* mutants

Because hair-cell ribbon synapses are highly specialized (Matthews and Fuchs, 2010), we investigated whether Nsf activity is also required for the formation of conventional glutamatergic synapses. We labeled excitatory synapses with antibodies against Vesicular glutamate transporter 1 (Vglut1) and MAGUK, the pre- and postsynaptic markers of glutamatergic synapses in the CNS (Figure 32A-A’). In overviews of the larval brain, the labeling of Vglut1 and MAGUK was greatly reduced in *nsf*⁶¹⁵³ mutant larvae at 5 dpf (Figure 32B-B’), indicative of a reduction, and possibly degeneration of glutamatergic synapses in CNS. In a magnified view of the boxed region in Figure 32A’, Vglut1-labeled presynaptic terminals and postsynaptic densities stained by MAGUK antibody were mainly juxtaposed in both wild-type and mutant larvae (Figure 33). However, the Vglut1 and MAGUK label in this region of the cerebellum was highly variable even in wild-type larvae, preventing reliable quantification of the density or number of the synapses.

To determine if we could rescue the degenerative phenotype in the CNS, we stably expressed Nsf-GFP in the CNS using a minimal *neurod* promoter, which drives expression in cranial nerves and other regions of the brain. We observed robust rescue of the reduction of both Vglut1 and MAGUK in *nsf*⁶¹⁵³ mutants in a *Tg(-5neurod:nsf-GFP)vo1* background. A representative image of the rescue is shown in Figure 32C-C’ (n=10, from 3 independent experiments). These experiments suggest that expression of Nsf is sufficient to stabilize innervation within the brain, and that the C-terminally tagged version of Nsf is functional.

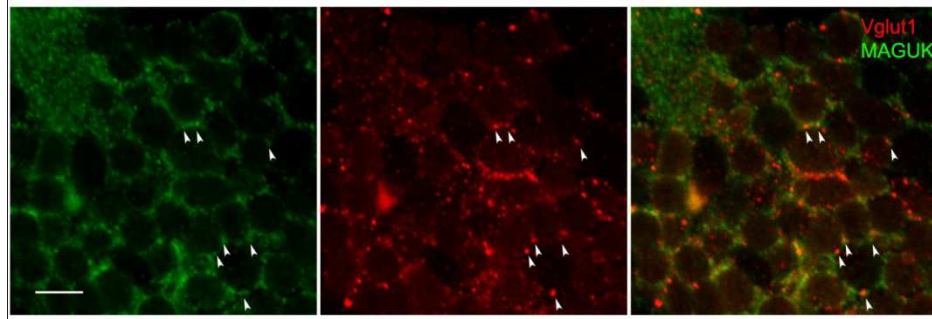


Figure 33. Glutamatergic synapses in the cerebellum. Magnified images of the boxed region in Figure 4A' showed fluorescent signals from Vglut1 (red) and MAGUK (green) antibodies in Purkinje cells of the cerebellar region. Although MAGUK antibody labels both the cell body and postsynaptic density in these neurons, it is possible to observe juxtaposition of MAGUK-positive densities next to Vglut1-labeled presynaptic terminals (arrow heads). Scale bar is 10 μ m.

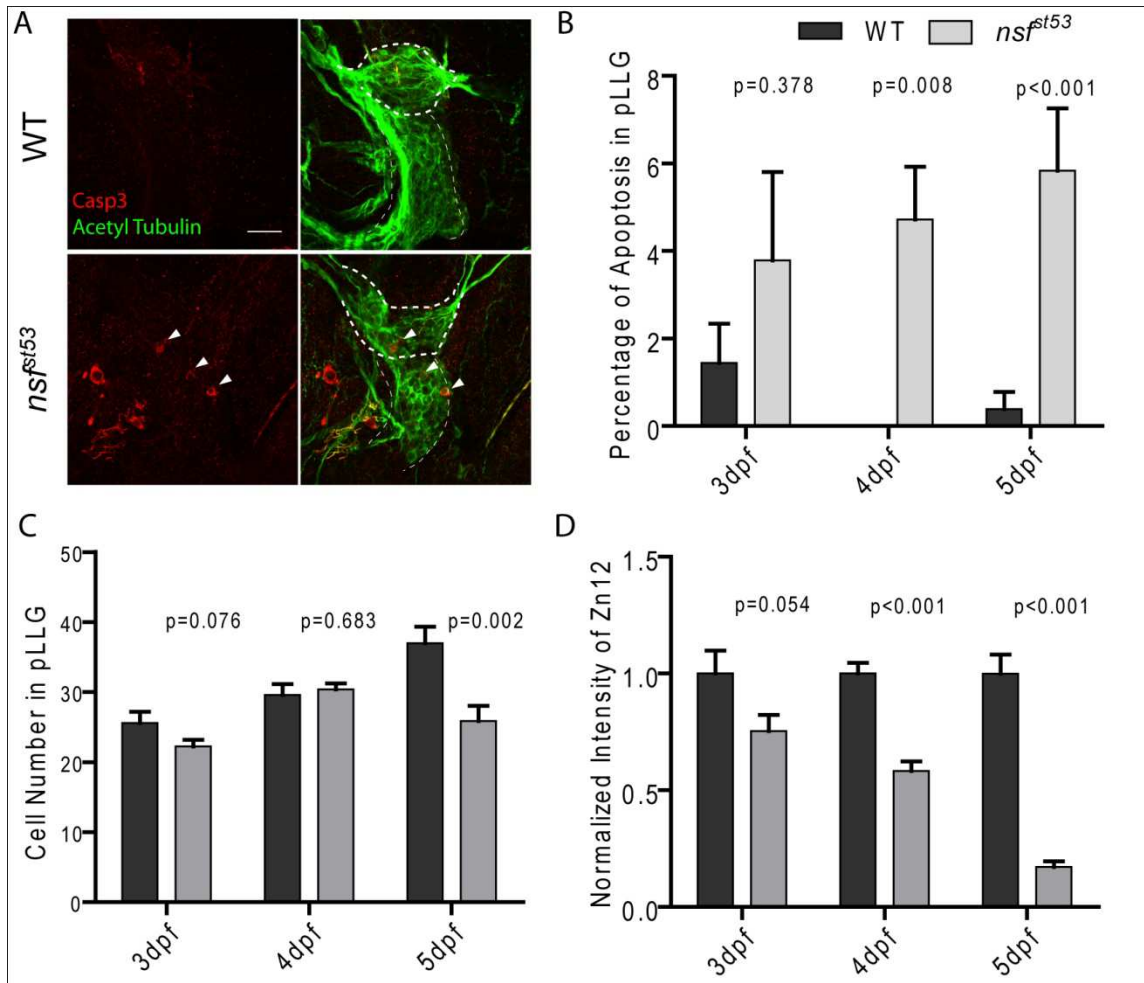


Figure 34. Apoptosis in *nsf^{st53}* mutants (5 dpf). Representative z-projections of the pLLG (thick dashes) and vagal ganglion (thin dashes) are shown in (A). In WT and *nsf^{st53}* mutants, apoptotic cells (arrow heads) were labeled by Casp3 antibody (red), and neurons were labeled by acetylated Tubulin antibody (green). Scale bar: 20 μ m. Images shown in all panels are projections of 6 z-stacks (1.5 μ m each). (B) The percentage of apoptotic cells in the pLLG of both wild-type and *nsf^{st53}* mutant larvae (in wild-type the percentage apoptosis are 1.4 ± 0.9 , n=5, 0.0 ± 0.0 , n=8 and 0.4 ± 0.4 , n=8 from 3 dpf to 5 dpf respectively; 4.8 ± 2.0 , n=7, 4.7 ± 1.2 , n=7, and 5.8 ± 1.4 , n=7 in *nsf^{st53}* mutants). (C) Cell numbers of the pLLG in wild-type increased from 25.6 ± 1.6 , n=5 at 3 dpf to 29.6 ± 1.5 , n=5 at 4 dpf and reached 37.0 ± 2.3 , n=8 at 5 dpf, while the numbers changed from 22.3 ± 0.9 , n=8 to 30.4 ± 0.8 , n=8 and then to 25.9 ± 2.2 , n=7 in *nsf^{st53}* mutants. (D) The ratio of the intensity of Zn12 labeling (Figure 3A) of *nsf^{st53}* to wild-type labeling declined from 3 dpf to 5 dpf (76.2 ± 9.5 , n=6, 58.2 ± 4.1 , n=5, and 17.2 ± 2.4 , n=7).

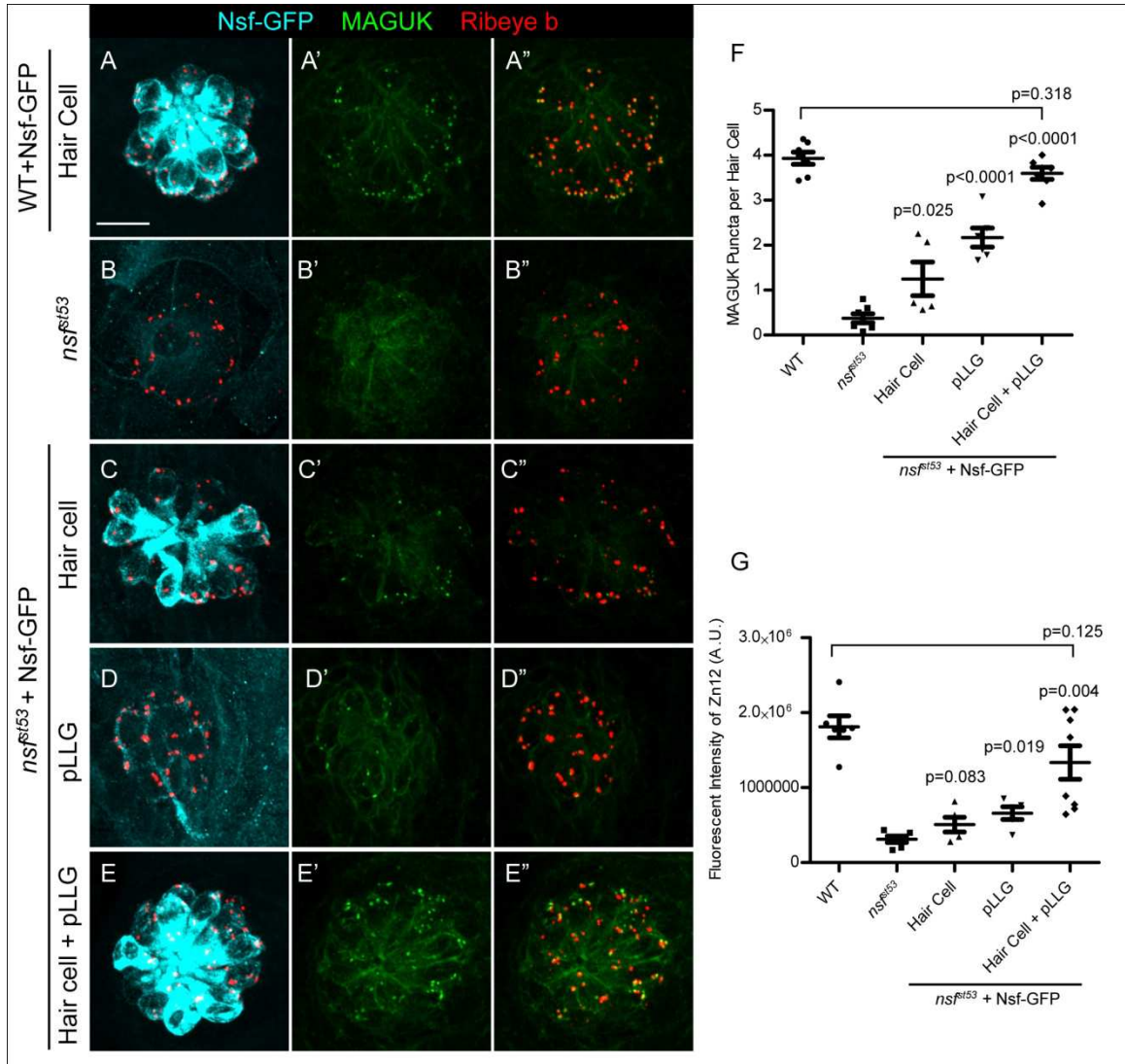


Figure 35. Nsf function is required in both pre- and postsynaptic cells to stabilize afferent innervation of hair cells. (A-E'') Representative z-projections of a single neuromast from a top-down view (5 dpf). Wild-type (A), *nsf^{st53}* mutants (B), and *nsf^{st53}* mutants with Nsf-GFP expressed in hair cells (C), pLLG (D), or in both hair cells and pLLG (E) were labeled by antibodies against GFP (pseudo-colored light blue), MAGUK (green), and Ribeye b (red). Scale bar: 10 μ m. (F) The average number of MAGUK puncta per hair cell in wild-type (3.8 ± 0.1 , n=7), *nsf^{st53}* mutants (0.4 ± 0.1 , n=7), and *nsf^{st53}* mutants with hair-cell Nsf-GFP (1.2 ± 0.4 , n=5), pLLG Nsf-GFP (2.2 ± 0.2 , n=6), or both hair-cells and pLLG Nsf-GFP (3.6 ± 0.1 , n=7). (G) Zebrafish larvae were stained with Zn12 and Ribeye b antibody. The fluorescent intensity (A.U.) of Zn12 was quantified in wild-type ($1.813e6 \pm 147069$, n=6), *nsf^{st53}* mutants (311769 ± 43541 , n=6), and *nsf^{st53}* mutants with Nsf-GFP rescued in hair cells (507787 ± 97798 , n=5), pLLG (659674 ± 85851 , n=5), or both hair cells and pLLG ($1.335e6 \pm 223319$, n=8). The p-values were generated comparing the data from the *nsf^{st53}* mutant to each transgenic mutant line.

3.4. Apoptosis in *nsf* mutants

To determine whether the retraction of the afferent nerve was due to cell death, we used an antibody against cleaved Caspase-3 to detect apoptotic neurons in 5 dpf larvae (Anichtchik et al., 2008). The overall morphology of the ganglion was normal in mutants, however, we observed a slight increase in activated Caspase-3 labeling in the pLLG of *nsf^{st53}* mutants (Figure 34A-B). Labeling of activated Caspase-3 was not detectable in hair cells. Although the retraction of neurites in the *nsf^{st53}* mutant occurred at every synapse at 5 dpf, apoptosis was detected in only a few cells within the pLLG at this stage. To determine if apoptosis caused the retraction of afferent nerves, we counted the number of neurons in the pLLG at different developmental stages, as well as quantifying the degeneration of afferent nerve fibers. We observed around 5% general apoptosis occurring between 3 dpf and 5 dpf in *nsf* null mutants (Figure 34B), with the number of cells in the pLLG in mutants being reduced by 30% at 5 dpf compared to their wild-type siblings (Figure 34C). During the same time interval, the reduction of innervation was much greater. From 3 dpf to 5 dpf, the afferent innervation of hair cells was reduced by more than 80% (Figure 34D). Because most pLLG neurons innervate a single neuromast (López-Schier et al., 2004; Obholzer et al., 2008), it is unlikely that the cell death of pLLG neurons accounts for the total loss of innervation.

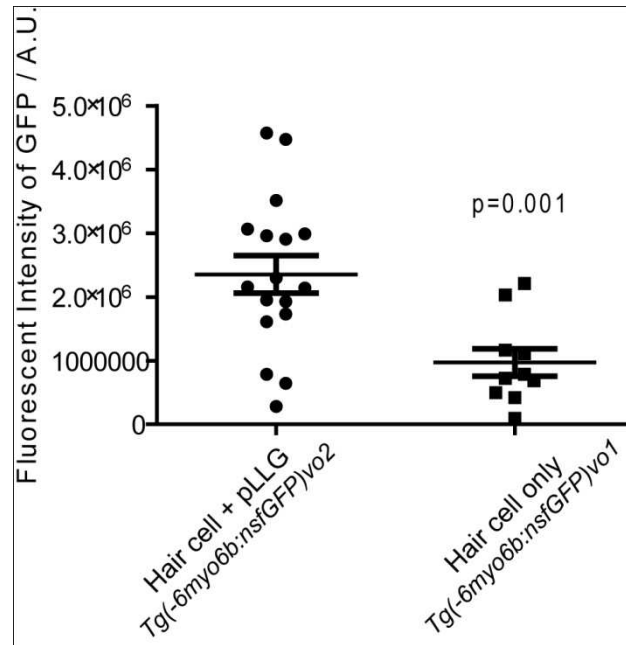


Figure 36. Quantification of GFP fluorescence in *Tg(-6myo6b:nsf-GFP)vo1* and *Tg(-6myo6b:nsf-GFP)vo2* lines. Anti-GFP antibody was used to stain Nsf-GFP fusion proteins in *Tg(-6myo6b:nsf-GFP)/nsf^{st53}* mutants. The fluorescent intensity in the neuromasts of *Tg(-6myo6b:nsf-GFP)vo2* ($2.353e6 \pm 293299$, $n=17$) and *Tg(-6myo6b:nsf-GFP)vo1* (971656 ± 215772 , $n=10$) lines are significantly different ($p=0.001$).

As seen in the pLLG, we also observe increased Caspase-3 labeling in the CNS, a sign of apoptosis in these cells (Figure 32D-E'). We also counted the number of apoptotic cells in the boxed region of Figure 32A'. Similar to the pLLG, the rate of apoptosis was low in the CNS and the cell density did not change drastically in the mutants (Figure 32F and 32G). Our data suggests that the decrease of Vglut1 and MAGUK labeling at 5 dpf is

unlikely due to the loss of neurons, but rather that glutamatergic synapses degenerate in the *nsf*^{st53} mutant.

3.5. Pre- and postsynaptic function of Nsf

Although the neurodegenerative phenotype of *nsf*^{st53} mutants can be rescued by expression of Nsf-GFP in the CNS (Figure 32A-C”), it was not clear whether presynaptic Nsf originating from hair-cells would be sufficient to stabilize ribbon synapses. We sought to answer this question by targeting expression of Nsf-GFP to either hair cells, or afferent neurons of the pLLG. In addition to the minimal *neurod* promoter, we used another minimal 6kb promoter from the *myo6b* gene, which specifically expresses in hair cell (Obholzer et al., 2008). We utilized the *Tg(-5neurod:nsf-GFP)vo1* for expression in the afferent neurons of the pLLG and generated a second line, *Tg(-6myo6b:nsf-GFP)*, to drive expression of Nsf-GFP in hair cells. We characterized the expression of Nsf-GFP in our stable transgenic lines using antibodies against both NSF and GFP (data not shown), and found three transgenic lines with distinct expression patterns: *Tg(-6myo6b:nsf-GFP)vo1* expressed Nsf-GFP only in hair cells; *Tg(-6myo6b:nsf-GFP)vo2* expressed Nsf-GFP in both hair cells and afferent neurons; and *Tg(-5neurod:nsf-GFP)vo1* used for the CNS experiments expressed Nsf-GFP in pLLG neurons, but not hair cells. Innervation of hair cells in mutants was analyzed in the three different transgenic backgrounds and compared to both wild-type and *nsf*^{st53} mutant fish without Nsf-GFP (Figure 35). To evaluate and compare hair-cell innervation, we imaged the same neuromast (L1) in each specimen (Raible and Kruse, 2000). Expression of Nsf-GFP in either hair cells or afferent neurons in *nsf*^{st53} mutants resulted in an increased number of MAGUK punctae (Figure

35C-D”, 35F). Although the number of MAGUK punctae was significantly increased in rescued mutants, the rescue was only partial in comparison to wild-type controls (Figure 35A-A”, 35F). Full rescue was only observed if Nsf-GFP was expressed in both pre- and postsynaptic compartments in the *Tg(-6myo6b:nsf-GFP)vo2* line (Figure 35E-E”, 35F). Quantification of the fluorescent signal obtained with the afferent fiber antibody Zn12 was consistent with the above results in each condition (Figure 35G).

The expression of the transgene in *Tg(-6myo6b:nsf-GFP)vo2* fish was higher than *Tg(-6myo6b:nsf-GFP)vo1*, but this may be partially due to the expression of Nsf-GFP in afferent nerve fibers, which cannot be separated from hair-cell GFP signals (Figure 36). To confirm that full rescue of hair-cell innervation was dependent on expression by both cell types rather than level of expression, we crossed *Tg(-6myo6b:nsf-GFP)vo1* and *Tg(-5neurod:nsf-GFP)vo1* into the *nsf⁶¹⁵³* background. Double transgenic expression of Nsf-GFP yielded better rescue than either transgenic in mutant background alone, as quantified by Zn12 antibody labeling of afferent nerves (Figure 37). These results demonstrate that Nsf function is required in both hair cells and pLLG afferent neurons to stabilize synaptic contacts.

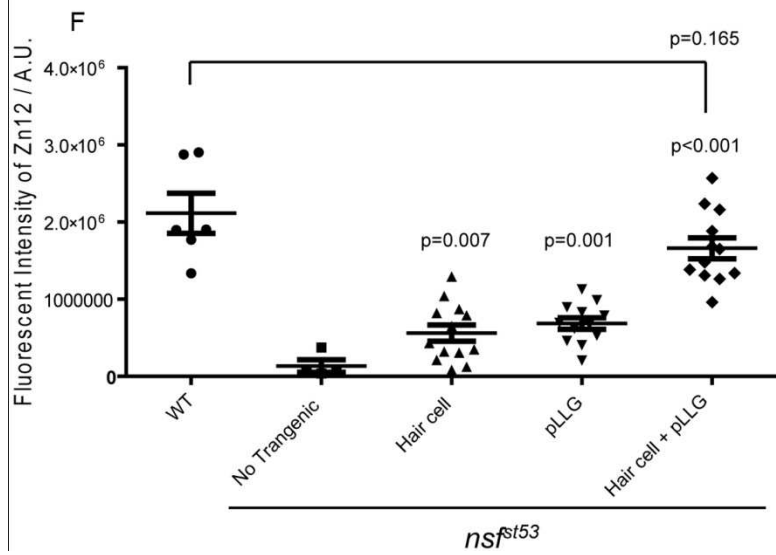
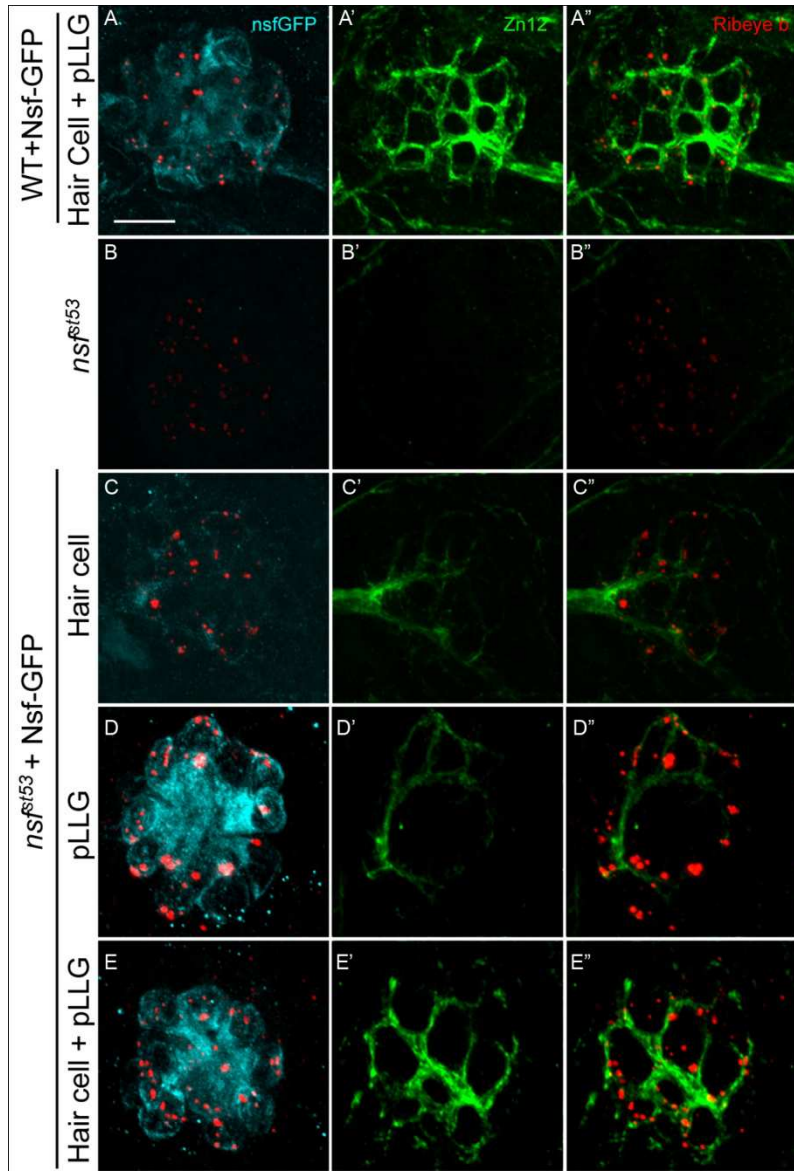


Figure 37. Rescue of afferent innervation by double transgenic expression of Nsf-GFP in *nsf^{st53}* mutants. (A-E”) Top-down views of the first lateral line neuromast (5 dpf) from wild-type (A), *nsf^{st53}* mutants (B), and *nsf^{st53}* mutants with Nsf-GFP expressed in hair cells (C), pLLG (D), or in both hair cells and pLLG (E). Shown is immunolabeling with antibodies against GFP (light blue), Zn12 (green), and Ribeye b (red). Scale bar: 10 μ m. (F) The total intensity of Zn12 antibody labeling per neuromast was quantified in wild-type ($2.113e6 \pm 259343$, n=6), *nsf^{st53}* mutants (133379 ± 80303 , n=4), and *nsf^{st53}* mutants with Nsf-GFP rescued in hair cells (559662 ± 104829 , n=13), pLLG (684537 ± 75475 , n=12), or both hair cells and pLLG ($1.659e6 \pm 136058$, n=12). The p-values were generated comparing the data from the *nsf^{st53}* mutant to each transgenic mutant line.

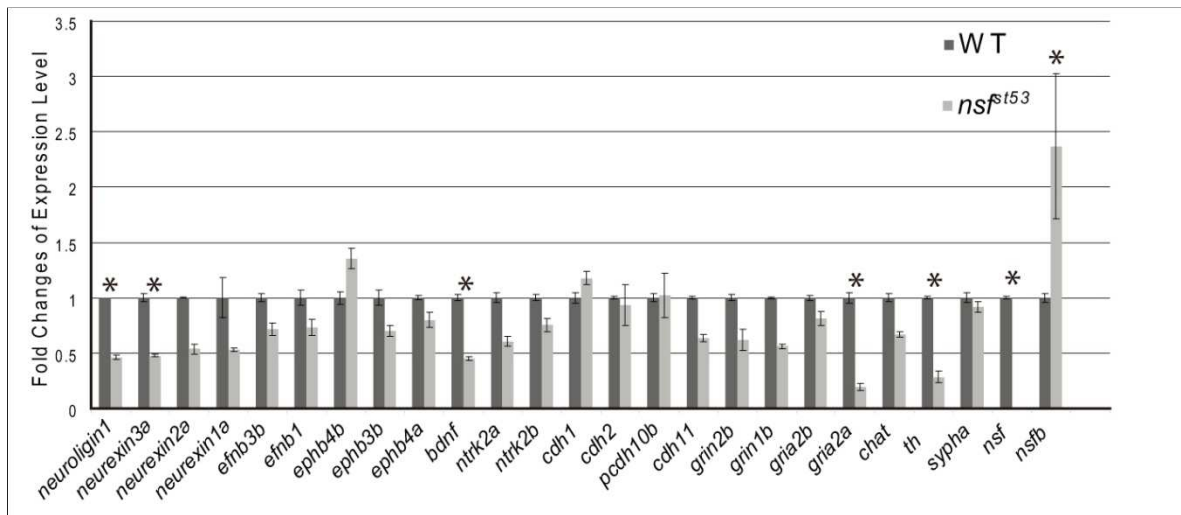


Figure 38. Expression of genes important for synaptic stability is reduced in *nsf*^{st53} mutants. QPCR was used to determine the expression levels of genes in brain cDNA from both wild-type and *nsf*^{st53} mutant larvae (5 dpf). Gene expression level in wild-type larvae was normalized to 1. Genes indicated with “*” showed 2-fold changes or more with $p < 0.001$.

3.6. Loss of Nsf affects BDNF function

Many components that promote synaptic stabilization can potentially be mediated by NSF-dependent membrane trafficking (Zhao et al., 2007; Lin and Koleske, 2010). A previous study examining neuropeptide release found an increase of protein level, but a decrease of mRNA level of several neuropeptides in zebrafish *nsf* mutants (Kurrasch et al., 2009). Decreased transcript levels are likely due to transcriptional repression of genes

encoding proteins that accumulate within the cell body and fail to be secreted. To determine if this were the case for signaling components in hair-cell synapses, we performed real-time quantitative PCR (qPCR) with larval brain tissue to examine the transcript levels for genes that may be important for synaptic stabilization. Among the 22 genes that we analyzed, 5 of them showed a significant repression of more than 2 fold in brain cDNA from *nsf^{st53}* mutant larvae. These genes include *neuroligin 1*, *neurexin 3a*, *bdnf*, *gria2a* and *th* (Figure 38). Expression of *ephrin* and *ephrin receptors*, *cadherins* and *synaptophysin* were unchanged or had less than 2-fold changes (Figure 38). The data obtained from qPCR analysis suggest that signaling pathways involving neurexin-neuroligin, BDNF-TrkB, and neurotransmission are altered by Nsf dysfunction, but Eph receptors, Ephrin ligands, and Cadherins are not affected. In addition, a striking reduction was seen in AMPA receptor transcripts (*gria2a*). Interestingly, mutant *nsf^{st53}* transcripts were degraded, whereas wild-type *nsfb* transcripts were increased, perhaps in compensation for the loss of *nsf* (Figure 38).

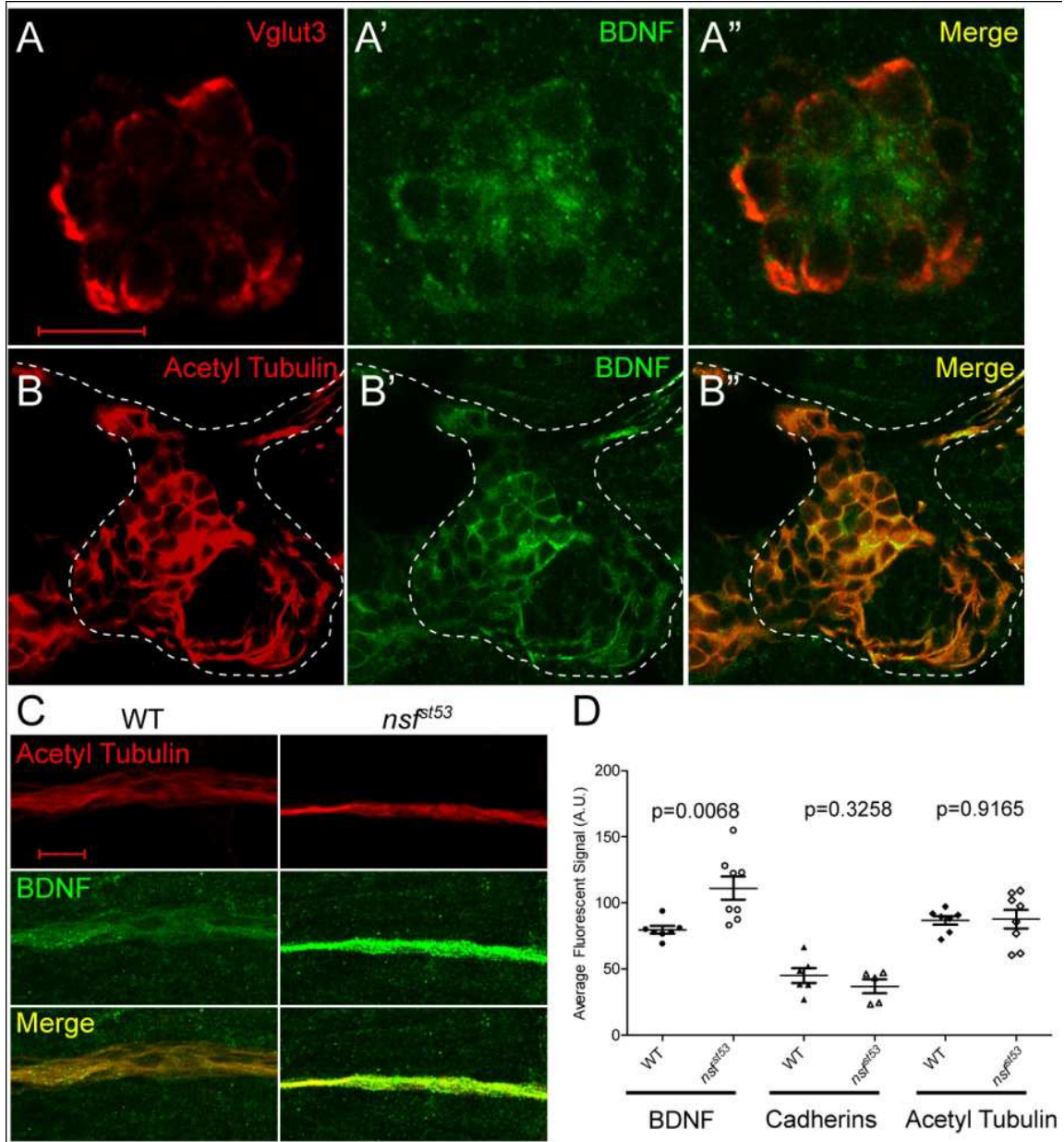


Figure 39. Expression of BDNF in wild-type hair cells and the pLLG, and accumulation of BDNF protein in the lateral line nerve of *nsf^{st53}* mutants. (A) A single optical section of a neuromast from a wild-type zebrafish larva (5 dpf) immunolabeled for Vglut3 (A, red), BDNF (A', green), and merged in (A''). (B) A single optical section of a wild-type pLLG, immunolabeled for acetylated Tubulin (B, red), BDNF (B', green), and merged in (B''). The cell bodies of the pLLG are outlined by dash lines. (C) Representative z-projections of 6 sections (1 μ m each) of acetylated Tubulin (red) and BDNF (green) immunolabeled lateral line nerves in wild-type and *nsf^{st53}* mutant larvae. (D) The average pixel intensity (A.U.) of BDNF (WT, n=7; *nsf^{st53}*, n=8), PAN-Cadherin (WT, n=8; *nsf^{st53}*, n=5), and acetylated Tubulin labeling (WT, n=7; *nsf^{st53}*, n=8) in wild-type control and *nsf^{st53}* mutants. Scale bar is 10 μ m across all panels.

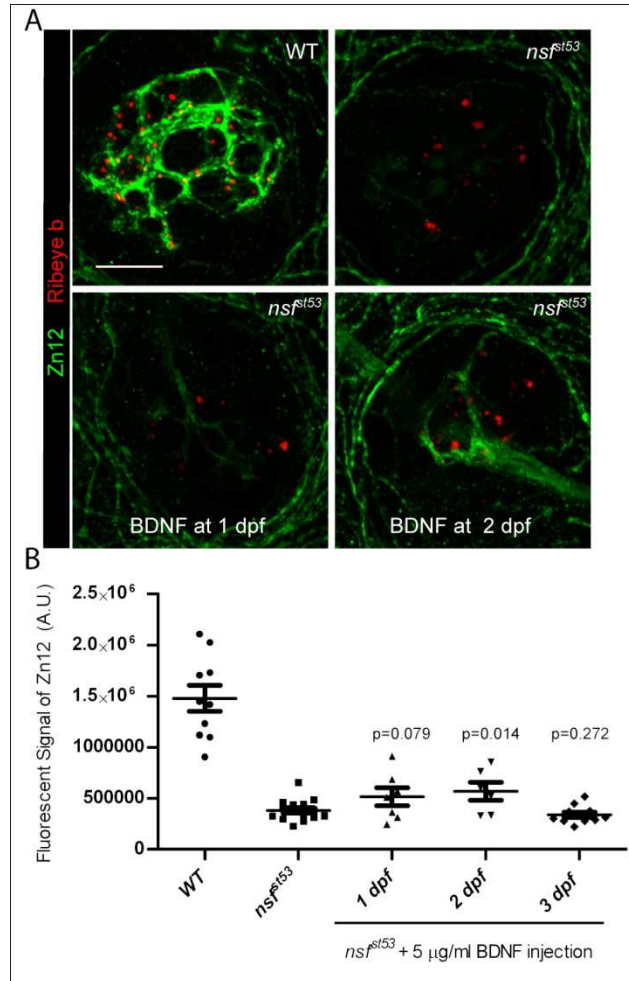


Figure 40. Partial rescue of synaptic contacts in *nsf^{ts153}* mutants by BDNF injection at 2dpf. (A) Representative z-projections of single neuromasts (4 dpf) immunolabeled for Zn12 (green) and Ribeye b (red) in wild-type, *nsf^{ts153}* mutants, and *nsf^{ts153}* mutants injected with 5μg/ml BDNF at 1dpf and 2dpf. 10 optical sections, 1μm each. Scale bar: 10μm. (B) Quantification of total pixel intensity (A.U.) of Zn12 labeling in wild-type ($1.478e6 \pm 128180$, n=10), *nsf^{ts153}* mutants (382343 ± 26874 , n=15), and mutants with BDNF injections at 1dpf (513236 ± 87981 , n=7), 2dpf (568136 ± 88664 , n=6), 3dpf (339253 ± 25527 , n=11). Statistical tests were between uninjected control and BDNF injected mutants.

Of the pathways affected, the BDNF pathway is particularly intriguing. Our data suggest that Nsf function is required in both pre- and postsynaptic cells, and BDNF has been shown to be released from both sides of the synaptic cleft (Kuczewski et al., 2009). *bdnf* mRNA and protein have been previously detected in hair cells in zebrafish (Thisse et al., 2004; Germanà et al., 2010), but BDNF expression in the lateral line ganglion has not been reported. Using an antibody to detect BDNF (Germanà et al., 2010), we found that BDNF colocalized with both a hair-cell marker, Vesicular glutamate transporter 3 (Vglut3), and acetylated Tubulin in the pLLG (Figure 39A-B”). Thus, BDNF is likely to be secreted from both cell types.

If BDNF secretion depends on Nsf activity, we hypothesized that the level of BDNF protein should be elevated in both hair cells and afferent neurons in *nsf^{st53}* mutants. Indeed, BDNF immunolabeling was increased in the cell bodies of afferent neurons (data not shown) and their nerve fibers (Figure 39C), suggesting that BDNF-containing vesicles accumulated within the cytoplasm of *nsf^{st53}* mutant neurites. Unfortunately, we could not measure changes in the BDNF staining of hair cells because the background staining of the skin interfered with quantification.

However, as a control, we also examined the levels of proteins that are predicted to be unaffected in the *nsf^{st53}* mutant based on our qPCR analysis. Consistent with our qPCR results, the fluorescent intensity of two other antibodies against acetylated Tubulin and pan-Cadherins showed no change between *nsf^{st53}* mutants and their wild-type siblings (Figure 39C-D). Thus, transcripts such as *cadherin 1*, *2*, and *11* that were unaffected in the *nsf^{st53}* mutant did not have altered levels of corresponding protein.

Our data suggest that BDNF is acting downstream of Nsf-mediated secretion. In previous studies, injection of recombinant BDNF or incubation of zebrafish larvae in E3 medium containing BDNF protein has been shown to compensate for the loss of endogenous BDNF (Diekmann et al., 2009; Wright and Ribera, 2010). We attempted to rescue the de-innervation of lateral line hair cells in *nsf^{st53}* mutants by injecting recombinant human BDNF protein into the yolk of *nsf^{st53}* mutants at 1 dpf, 2 dpf, and 3 dpf. We then labeled injected fish with Zn12 antibody to visualize afferent fibers (Figure 40A). In *nsf^{st53}* mutants injected with BDNF at 2 dpf, we observed a slight increase of afferent fiber labeling compared to uninjected mutants (Figure 40A-B). Injection of BDNF at earlier or later time points did not significantly increase the fluorescent signal of Zn12 labeling (Figure 40A-B), suggesting that there is a critical time window for BDNF to promote afferent synapse stability. Even within this critical period, restoration of innervation was incomplete in our experiments, suggesting that other factors are required downstream of Nsf to prevent retraction of neurites in *nsf^{st53}* mutants.

4. Discussion

In this study, we examined the pre- and postsynaptic contribution of Nsf in stabilizing zebrafish hair-cell ribbon synapses. Our results indicate that (i) mutation of *nsf*, but not *nsfb*, results in retraction of afferent fibers from hair cells, (ii) both pre- and postsynaptic Nsf activity are essential for maintaining hair-cell synapses, (iii) degeneration of nerve fibers does not result from apoptosis, (iv) mutation of *nsf* alters expression of several genes implicated in synaptic stability, and (v) BDNF accumulates in *nsf^{st53}* mutant afferent fibers, and exogenous BDNF can partially stabilize afferent innervation. Our data

suggest a critical role for Nsf in stabilizing synaptic contacts in both the CNS and peripheral nervous system by mediating the expression and secretion of multiple factors important for synaptic maintenance.

4.1. Differing roles of Nsf and Nsfb in zebrafish

The different expression patterns and mutant phenotypes of the *nsf* and *nsfb* genes suggest that these two genes perform non-overlapping functions. *nsf* is expressed mainly in the nervous system, whereas *nsfb* is ubiquitous. In contrast to the neurodegeneration observed in *nsf*^{st53} mutants, *nsfb*^{hi2869Tg} mutants show an overall progressive degeneration of other tissues at an earlier stage (Amsterdam and Hopkins, 2004). A similar scenario is seen in *Drosophila*, which also expresses two isoforms of dNSF. *dNSF1* is mainly expressed and functions in the nervous system, while *dNSF2* function is required at the first instar larval stage for mesoderm development (Golby et al., 2001; Sanyal and Krishnan, 2001). Perhaps most surprising about the *nsf* mutant phenotype in both flies and zebrafish is that early development is not disrupted. The relatively normal development in single mutants may be due to compensation by the unaffected gene. Indeed, we observe increased levels of *nsfb* mRNA in the *nsf*^{st53} mutants. However, the *nsfb* gene is unable to compensate for the retraction and degeneration of neurites in either the central or peripheral nervous system of *nsf*^{st53} mutants. This suggests that *nsf* plays a specialized role in the maintenance of the synaptic contacts.

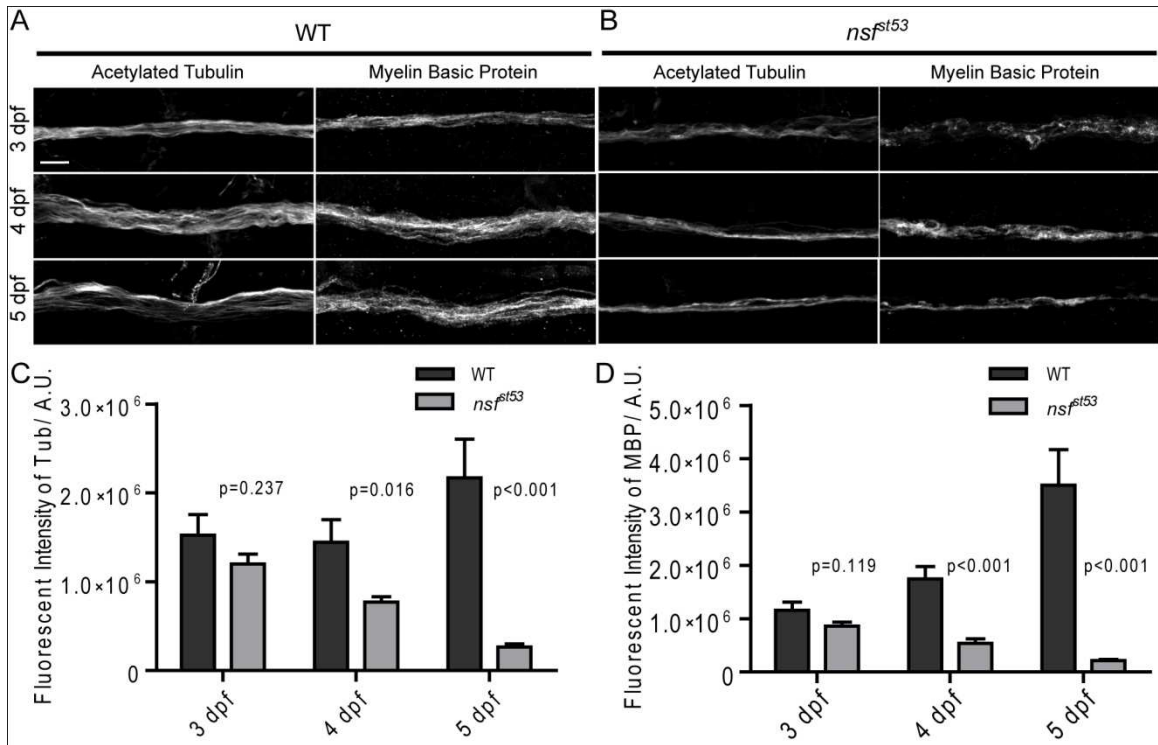


Figure 41. Decreased labeling of acetylated Tubulin and Myelin Basic Protein in *nsf^{st53}* mutants. (A) Antibodies against acetylated Tubulin were used to label lateral line nerves in wild-type and *nsf^{st53}* mutant larvae at 3, 4 and 5 dpf. (B) Anti-Myelin Basic Protein antibody labeled the myelin sheath of the lateral line nerve in both wild-type and *nsf^{st53}* mutants (3 to 5 dpf). (C) The fluorescent intensity of acetylated Tubulin labeling increased over time in wild-type larvae (3 dpf, 1523307±233786; 4dpf, 1445077±252144; 5 dpf, 2170483±434340), but decreased in *nsf^{st53}* mutants (3 dpf, 1201135±110419; 4dpf, 770785±58768; 5 dpf, 264018±35511). (D) The fluorescent labeling of Myelin Basic Protein displayed a dramatic increase in wild-type (3 dpf, 1155025±158382; 4dpf, 1746149±232916; 5 dpf, 3501120±670992), but significantly decreased in *nsf^{st53}* mutants (3 dpf, 860546±74798; 4dpf, 538577±85907; 5 dpf, 212506±24043). Scale bar: 10µm; z-projection of 5 confocal planes (1µm each).

4.2. Nsf and neurodegeneration

Our data indicate that neurodegeneration is a prominent phenotype in both CNS or hair-cell glutamatergic synapses in *nsf^{st53}* mutants. Interestingly, the motility of *nsf^{st53}* mutants is largely normal at 2 dpf compared to their wild-type siblings, but they gradually become paralyzed from 3 dpf to 5 dpf (data not shown). This progressive loss of motility correlates with the timeline of the neurodegenerative phenotypes observed in *nsf^{st53}* mutants (Figure 31). In agreement with our observations, neurodegeneration has also been observed in a number of mouse models with defects in SNARE-complex function (Chandra et al., 2005; Burré et al., 2010; Kunwar et al., 2011; Sharma et al., 2011). The observation of presynaptic disorganization at early stages of neurodegeneration, as well as the crucial function of these proteins in presynaptic vesicle fusion, lends support to the idea that presynaptic dysfunction contributes to neurodegeneration (Burgoyne and Morgan, 2011). Our experiments indicate that maintenance of hair-cell synapses requires Nsf function in both pre- and postsynaptic cells. What could account for this difference in pre- versus postsynaptic roles? It is possible that early presynaptic dysfunction in the mouse CNS does not necessarily exclude a postsynaptic contribution to neurodegeneration. The role of NSF in the regulation of GluR2 externalization at post-synaptic membranes is well established (Nishimune et al., 1998; Osten et al., 1998; Song et al., 1998), and our data clearly demonstrate that *gria2a* AMPA receptor transcripts are decreased in *nsf^{st53}* mutants. Unfortunately, we were unable to immunolabel AMPA receptors in zebrafish larvae. However, our results indicate that postsynaptic BDNF accumulates in the neurites of afferent neurons in *nsf^{st53}* mutants. Moreover, release of mammalian BDNF is thought to occur at both pre- and postsynaptic sites (Kuczewski et al., 2009). Our experiments of

pre- versus postsynaptic expression of *nsf* support the notion that release and membrane trafficking in both cell types is required for maintenance of hair-cell synapses.

4.3. Myelination and neurodegeneration

Nsf has been shown to be indispensable for the development of myelination and nodes of Ranvier in zebrafish larvae (Woods et al., 2006). Here we revealed the role of Nsf in preventing neurodegeneration. Because of the long-known neuroprotective role of glial cells and myelin protein (Wang et al., 2002), the loss of innervation could be due to demyelination in *nsf^{st53}*. Indeed, we observed that Myelin basic protein and acetylated Tubulin were present in the myelin sheath and lateral line nerves (respectively) at 3 dpf, but the levels of both were dramatically reduced from 3 dpf to 5 dpf in *nsf^{st53}* mutants (Figure 41). Since the loss of myelination and innervation occurs coincidentally in *nsf^{st53}* lateral line nerves, it is difficult to determine a causal relationship with respect to degeneration. The production of myelin is in part, however, dependent on neuronal signaling. For example, neuregulins are key signals secreted by neurons for Schwann cell development and myelination (Nave and Salzer, 2006), and our data indicate that zebrafish Nsf is required for release of neurotrophic factors, such as BDNF. It is likely that Nsf promotes myelination through release of gliatrophic factors from lateral line neurons. In contrast to lateral line neurons, the glutamatergic neurons of the CNS that we examined do not have a myelin sheath (Figure 42). The neuroprotective role of Nsf can therefore be independent of myelination.

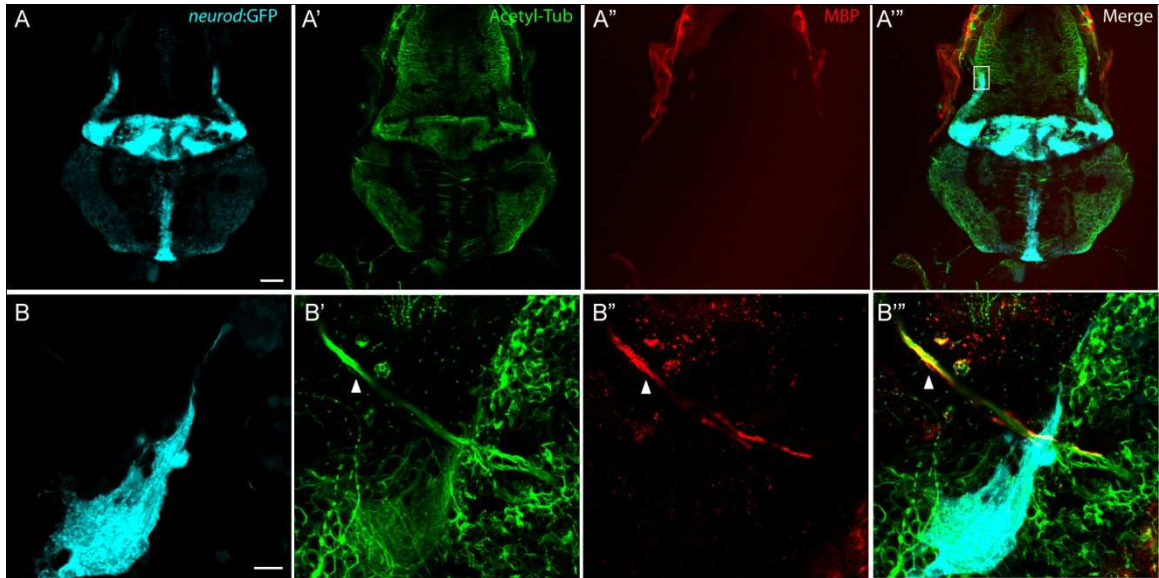


Figure 42. Myelin Basic Protein expresses is present in peripheral nerves, but not in the CNS. (A-A''') A representative top-down projection of a zebrafish brain at 5 dpf labeled by GFP in the *TgBAC(neurod:EGFP)nl1* background (A, light blue), antibodies against acetylated Tubulin (Acetyl Tub, A', green) and Myelin Basic Protein (MBP, A'', red). MBP protein was not detected in the CNS. Scale bar: 100 μ m. (B-B''') Close up of the boxed region in panel (A'''). Although MBP fluorescence was associated with nerve fibers from the anterior lateral line ganglion (arrow head), there was no labeling of MBP in nerve fibers in the cerebellar region (highlighted by GFP expression). Scale bar: 10 μ m.

4.4. Nsf function in hair cells

An interesting finding of this study is that Nsf in hair cells is required for synaptic stability in hair cells. Despite some differences in exocytic machinery at ribbon synapses, many core proteins of the SNARE-complex that interact with NSF have been detected in

ribbon synapses isolated from chicken hair cells and in mouse cochlea hair cells (Safieddine and Wenthold, 1999; Uthaiyah and Hudspeth, 2010). The presence of SNARE proteins is indicative of a role in membrane fusion, however, botulinum neurotoxins that normally cleave SNAP25 and Syntaxins in conventional synapses have no effect on synaptic transmission in mouse inner hair cells (Nouvian et al., 2011). Our results do not address whether zebrafish Nsf is required for synaptic transmission, but rather indicate that in the absence of Nsf activity, afferent neurons fail to maintain stable contacts with hair cells. Based on the reduction in transcripts for synaptic proteins that have been implicated in maintenance, and the internal accumulation of BDNF, Nsf appears to participate in trafficking components required for synaptic stability. Our results indicate that Nsf-mediated activity is required on both sides of the cleft and we speculate that core components of the SNARE-complex are likely to be involved in this process.

4.5. Factors acting downstream of NSF-mediated vesicle fusion

One of the most widely studied signaling molecules released from both pre- and postsynapses is BDNF. Release of BDNF triggers both pre- and postsynaptic signaling events (Li et al., 1998; Hartmann et al., 2001; Regehr et al., 2009), and is important for synaptic maintenance in the brain (Xu et al., 2000; Gorski et al., 2003). Loss of BDNF in zebrafish larvae affects early neuronal development and causes a more severe phenotype than *nsf^{st53}* mutants (Diekmann et al., 2009; Henshall et al., 2009). Blockade of synaptic transmission is also known to reduce neurotrophic factor secretion (Voets et al., 2001), thus it is possible that the neurodegeneration in *nsf^{st53}* mutants is due to lack of trophic support. Indeed, the presence of higher levels of BDNF in *nsf^{st53}* afferent neurons

suggests that trafficking and secretion of BDNF is reduced at the hair-cell synapse. BDNF injection or incubation has been successfully used to rescue neuronal growth in zebrafish larvae (Diekmann et al., 2009; Wright and Ribera, 2010), however, we observed only a partial stabilization of afferent innervation of hair cells in *nsf^{st53}* mutants that received an injection of recombinant BDNF. The partial rescue suggests that BDNF alone is insufficient and may simply delay but not rescue neurodegeneration. Similar results have been observed in mouse *Munc-18-1* mutants; the neurodegeneration phenotype was delayed but not rescued by application of BDNF and insulin (Heeroma et al., 2004). Partial rescue with BDNF can be explained in several ways. First, BDNF can stimulate cell survival (Knüsel et al., 1992; Wu et al., 2010) and injection of BDNF into *nsf^{st53}* mutants may have delayed the retraction of afferent neurites. Second, exogenous BDNF may not be able to reach the synaptic cleft efficiently; hence full rescue of the phenotype is not possible even if BDNF were sufficient to stabilize synaptic contacts. Third, it is possible that the trafficking of TrkB receptors is affected in *nsf^{st53}* mutants. Lastly, BDNF is likely to be one of many factors secreted at hair-cell synapses. Indeed, our expression data indicates that the BDNF pathway is potentially one of multiple signaling or adhesion complexes that may be required for stabilization of synaptic contacts. Further investigation may reveal which of these factors mediates synaptogenesis in hair cells, but regardless of the downstream signaling events, our data suggest that both sides of the hair-cell synaptic cleft require NSF for long-term maintenance of synapses.

Chapter 5. Fishing for the hair-cell mechanotransduction complex

1. Summary

The hair cell transduces mechanic stimuli into electrochemical signals, a role that is central to both auditory and vestibular function. This process is called mechanotransduction or mechanoelectrical transduction (MET). Identifying the molecular components of the MET complex is critical to understand how transduction in hair cells is controlled. However, despite considerable efforts over the past decades, the identity of hair cells' MET channel is still mysterious. To uncover novel molecules involved in MET, and to identify MET channel candidates, we took 2 approaches: (1) a candidate gene approach to examine which TRP channels are expressed in zebrafish neuromast hair-cells; and (2) an unbiased, modified yeast two-hybrid technique to screen for protein interactions with the tip-link protein Pcdh15a.

Transient receptor potential (TRP) channels become interesting candidates for hair-cell MET channels, because (1) TRP channels play important roles in sensing noxious mechanical stimuli, osmotic pressure, touch and hearing in invertebrates (Arnadóttir and Chalfie, 2010); (2) Many TRP channels have similar biophysical features to hair-cell MET channels in that they are nonselective cation channels with high single-channel conductance (Owsianik et al., 2006). To determine which zebrafish TRP genes could be involved in MET, we first examined TRP gene expression in zebrafish lateral line hair

cells and found *trpm7* expressed at high level. However, assays for MET in hair cells where Trpm7 function was perturbed were inconclusive as to whether Trpm7 is a bona fide part of the MET complex. Based on our results, we conclude that although it could still be a part of the MET complex, Trmp7 is not the only component of MET channel in zebrafish hair cells.

In a parallel effort, we identified candidate MET complex proteins using split-ubiquitin based membrane yeast two-hybrid (MYTH)(Stagljar et al., 1998)(Figure 46A). Based on several lines of evidence suggesting that Pcdh15 is the lower tip-link protein responsible for activating the MET channel, we used the zebrafish Pcdh15a as the bait in our experiment. Our screen uncovered 9 candidate interactors of Pcdh15a. One of them is Tmc2a, a molecule has been suggested to be required for mechanotransduction in hair cells. Further researches are needed to elucidate the exact role of Tmc2a in regulating MET currents in hair cells.

2. Materials and methods

Fish strain and growth. Zebrafish were maintained and bred according to standard protocols (Westerfield, 1995). All experimental procedures were conducted according to the policies of Animal Care and Use Committee in Oregon Health & Science University. Wild-type fish were maintained in a hybrid background of WIK and TL. *trpm7*^{j124e1} fish (Elizondo et al., 2005) were obtained from the Zebrafish International Resource Center. Tg(*hsp:DN-trpm7-gfp*) transgenic fish expressing dominant negative Trpm7 tagged with eGFP are gifts from Dr. Robert Cornell (unpublished data).

Heat shock of zebrafish embryos. To heat shock zebrafish embryos, 20 embryos were kept in E3 media in a 1.5 ml centrifuge tube at 4°C for 15 min, 37°C for 1.5 hours, and 4°C for 15 min. After heat shock, embryos were transferred into a Petri dish and incubated at 30°C. Tg(*hsp:DN-trpm7-gfp*) transgenic larvae and their WT siblings were heat-shocked twice at 19 and 36 hpf. Heat shock of larvae older than 24 hpf does not induce DN-T7-GFP fluorescence effectively. Double heat shock induced GFP fluorescence peaking at around 30 hpf and stayed fluorescent until about 64 hpf.

FM4-64 measurement. FM4-64 and FM1-43 was applied to 3 and 5 dpf zebrafish larvae as described (Seiler and Nicolson, 1999) with minor changes. Single zebrafish larva were put into E3 medium with tricaine methanesulfonate for 1 minute to anesthetize, followed by 1 minute labeling in E3 containing FM1-43. The larva was then washed twice in E3 with tricaine methanesulfonate. A 60× water lens is used to take pictures of FM1-43 or FM4-64 labeled neuromasts on Zeiss Axiovert ImagerM.1 microscope with an LSM700 confocal scanhead. Confocal sections of the basolateral part of each neuromast are used for quantitative analysis. To quantify fluorescent intensities, the average fluorescence of the whole picture is subtracted as background. The total fluorescent signals of a neuromast are calculated using Metamorph (Molecular Devices).

RT-PCR from extracted neuromast preparation. The neuromast RT-PCR protocol is modified from (Trapani et al., 2009). 20µl ddH₂O with 1µL RNasin or RNaseOUT RNase inhibitor was added into a PCR tube. Cells from neuromasts were sucked using a glass pipette and put into the PCR tube in step 1 (total volume should be less than 25µl; otherwise less water would be used in step 1). Cells were lysed by pipetting up and down.

The cell mixture was then transferred to an EcoDry RT-PCR tube (Cat No. 639531, Clontech). RT-PCR reaction was performed according to the manufacture's instruction. 4-5µl RT-PCR products were then used for each PCR reaction (Choice Taq Blue Mastermix, Denville). PCR products were detected on 2% agarose gel using electrophoresis. Primers for amplifying TRP channel genes were designed based on known sequences in database (Table 2). All primers used for neuromast RT-PCR were pretested using total cDNA from whole larvae.

Construction of the Ear cDNA library. Immediately after juvenile zebrafish (25dpf -50 dpf) were killed in E3 medium with tricaine methanesulfonate, ears were dissected out using forceps. About 1500 ears were collected for building the library. A 1.5µg total ear cDNA was collected using RNeasy midi kit (Qiagen) and sent to Dualsystems Biotech AG for cDNA library construction. cDNA library was constructed using pPR3-N vector, which has a NubG fragment tagged to the N terminus of every insert cDNA (Ear-pPR3-NubG-x library). The NubG-x library contains a total of 1×10^7 clones, with an average insert size of 1.7kb.

Yeast strain and transformation. The *Saccharomyces cerevisiae* NMY51 strain (*MATa his3Δ200 trp1-901 leu2-3, 112 ade2 LYS2::(lexAop)₄-HIS3 ura3::(lexAop)₈-lacZ ade2::(lexAop)₈-ADE2 GAL4*) was purchased from Dualsystems Biotech AG. Growing and Transformation of NMY51 strain was done according to protocols from Dualsystems Biotech with minor changes. For transformation, yeast cells were cultured overnight at 30°C with shaking. 20 ml yeast culture was then pelleted at 700g centrifugation and resuspended in 1 ml sterile water. Then 100 µl yeast suspension was added into 300 µl

PEG/LiOAc/ssDNA/plasmid master mixture then vortexed for 1 min. The final mixture with yeast cells was heat-shocked for 45 min at 42°C. After heatshock, yeast cells were collected by 700g centrifugation, and dissolved with 0.9% NaCl before they were spread on selective plates. After transformation, yeast cells were incubated at 30°C for 2-3 days.

Molecular biology for Yeast-two hybrid. The following PCR primers were used to insert Pcdh15a full length into pBT3-SUC vector using Sfi1 restriction sites. Pcdh15a Forward: (ATT AAC AAG GCC ATT ACG GCC aac act gaa gac tgg cac tat gag), Pcdh15a-CD1 reverse: (AAC TGA TTG GCC GAG GCG GCC CCt aca tcg ttc ttg ttg tca tat tta ac), Pcdh15a-CD3 reverse (AAC TGA TTG GCC GAG GCG GCC ccg agt ttt gtc att ggt atg t). It should be able to fuse with the Cub-LexA-VP16 cassette. Primers on pBT3-SUC vector (forward primer: 5'-gga atc cct ggt ggt cca tac and backward primer: 5'-gcg tcc caa aac ctt ctc aag) are used for PCR from yeast colonies.

Yeast-two hybrid screen. Membrane protein yeast two hybrid screens were followed the manufacturer's manual with necessary changes (DUALmembrane kit, Biotech, Switzerland). NMY51 yeast colonies containing the bait vectors were grown in 20 ml SD-Leu selective media overnight. The yeast culture was then re-inoculated into 100 ml SD-Leu to grow for another overnight incubation before transformation. 30 OD₅₄₆ units yeast cells were collected at 700 g spin for 5 minutes. Yeast cells were grown in 200 ml YPAD media until OD₅₄₆=0.6. Then standard transformation protocol was used to transform 20 µg cDNA library plasmids. Ten microliter of co-transformed yeast cells with serial dilutions were then plated on SD-LeuTrp (SD-LW) plates to calculate transformation efficiency. The majority of the transformants were plated on SD-

LeuTrpHisAde (SD-LWHA) + 4 mM 3-AT selective plates for screening. After 2-3 days, colonies would appear on SD-LW plates. It took another 1-3 days for yeast colonies to be seen on the quadruple selective plates. Hundred colonies were replicated on new selective plates for retest. After retest, lacZ positive clones on new selective plates were picked for colony PCR amplification and sequencing. Candidate clones were selected based on sequencing results. Vectors from these clones were then recovered from yeast and amplified in *E. coli* XL-10 gold strain. Recovered prey vectors with unique gene products inserted were co-transformed with bait vectors into NMY51 yeast to confirm their interactions.

3. Screen TRP channel candidates for mechanotransduction

3.1. Expression of TRP channels in zebrafish hair cells

Over the past a few decades, studies have determined the importance of TRP channels in hearing transduction of *Drosophila* and zebrafish, especially TRPN1/NompC (Walker et al., 2000; Kim et al., 2003; Sidi et al., 2003; Gong et al., 2004; Göpfert et al., 2006; Effertz et al., 2012). However, lack of a clear TRPN1 homolog in mammals suggests that it is not a part of the elusive MET channel (reviewed by Vollrath et al., 2007). Still, it is possible that other TRP channels are part of the hair-cell MET complex. We explored this possibility by first determining which TRP channels are expressed in zebrafish hair cells.

Table 2 Expression of TRP channels in neuromasts

Gene	Expression in neuromasts	Primer sequences
<i>trpc1</i>	No	Forward: ATCTGTTCCCACACCTCCAC Reverse: TCCATGCTCTGCATCTTCTG
<i>trpc2</i>	No	Forward: ACCGCATTCCCTACAGACAG Reverse: ACTTTGCTGAGCTCCGTGAT
<i>trpc3</i>	No	Forward: TTGCCGGCTAATGAGAGTTT Reverse: GCTTTCCTCAACCGTGGTAA
<i>trpc4a</i>	Yes	Forward: GCTCGTCACGAATTCACAGA Reverse: CGAGCAAATTTCCACTCGAT
<i>trpc6</i>	No	Forward: TCTTTGGGACGAACTGTGAA Reverse: TGACCTCAGAAAGGCCAAAT
<i>trpc7</i>	No	Forward: TGGTTCTGCTCAACATGCTC Reverse: TTGATGCGGATGATCAGGTA
<i>trpp2</i>	No	Forward: TTTGGGACAGAGGTGGAAAC Reverse: TCATTGATGATGGCCAGAAA
<i>trpn1</i>	Yes	Forward: AGATGTGCTCGTCGGAGTCT Reverse: CTGCGCTGAGACAGAACTG
<i>trpm1</i>	Yes	Forward: GCCCGCAACATCTTCTACAT Reverse: TTGGCCACCAACAAGTAACA
<i>trpm3</i>	Yes	Forward: AGAGCAGTGCATGGAGGAGT Reverse: CTCTCTAGGGCCACAGCAAT
<i>trpm5</i>	No	Forward: ACTTTGCTGAGGATGGTTGG Reverse: CTTTTGGTGCCTCTCTGTCA
<i>trpm7</i>	Yes	Forward: CCTTCAGCCACTGGACGTAT Reverse: GATGTTTGGCACGGAAGTTT
<i>trpv1</i>	No	Forward: CAGGGGAAGAGAAGGACCTC Reverse: AGGGTCTTGTGTGCATTTCC
<i>trpv4</i>	No	Forward: TCAAATCTGGGCATCATCA Reverse: GGCTCCATCTCTACGGTGTG
<i>trpv6</i>	No	Forward: TTGAACGAAAGTTGCCACAG Reverse: TATGTCATTGCGATCCTCCA
<i>trpa1a</i>	Yes	Forward: CGCCTGCTTAAAGAGGATTG Reverse: ATTCCCTCCGAAAAACCATC

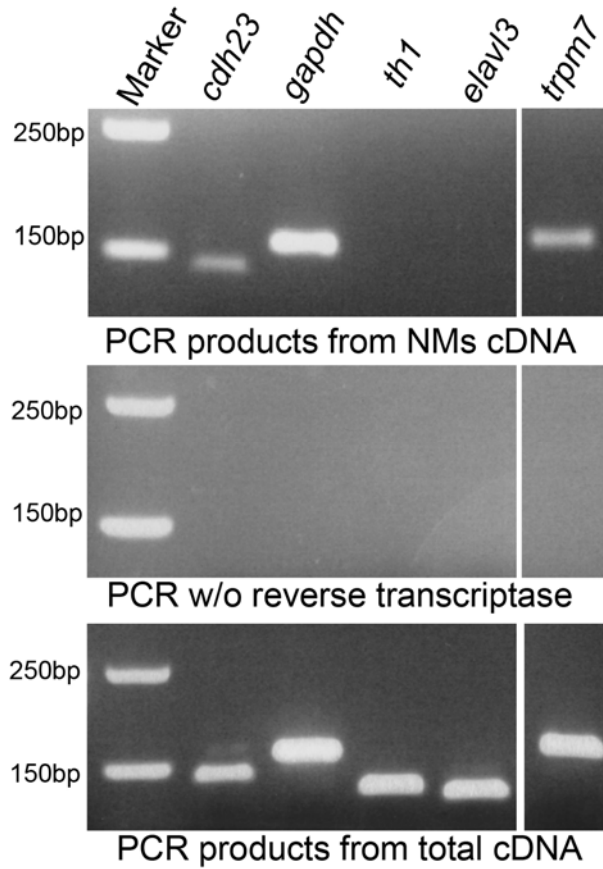


Figure 43. Expression of *trpm7* in zebrafish neuromasts. Detection of *cdh23*, *gapdh*, *th1*, *elavl3*, and *trpm7* transcripts in 5dpf zebrafish neuromasts and total cDNA by RT-PCR. *cdh23* was a positive control as a neuromast-specific gene, *th1* and *elavl3* was used as neuronal markers. NM=neuromast.

To assay for TRP gene expression in hair cells, we performed RT-PCR from isolated lateral line neuromasts (Figure 2A). Neuromast hair cells can be easily isolated together with their supporting cells using a glass pipette (Trapani et al., 2009). However, it is possible that this preparation includes the afferent and efferent synapses, in which ion

channels may be highly expressed. To rule out contamination of our neuromast preparation, we first checked expression *th1* and *elavl3*, two genes that expressed in efferent and afferent neurons respectively (unpublished observation). Expression of hair-cell marker *cdh23* was found in our neuromast extraction, but no expression of *th1* and *elavl3* was seen (Figure 43), indicating that transcripts in afferent or efferent synapses would not affect our RT-PCR results. Using the same experimental condition, we screened for 16 TRP channels (other primers for annotated TRP channels failed to amplify transcripts from zebrafish total cDNA) and successfully amplified 6 TRP channel genes from the neuromast extraction, of which *trpm7* has the highest expression level (Table 2, Figure 43).

3.2. Trpm7 in zebrafish hair cells

We are especially interested in the function of *trpm7* gene in hair cells, because TRPM7 was recently found to interact with PCDH15, both *in vitro* and in mouse cochlea (unpublished observation from Peter Gillespie lab). Thus, TRPM7 is likely to be part of the mammalian MET complex. To determine if *Trpm7* plays a role in zebrafish hair cell mechanotransduction, we assayed for MET function in *trpm7* mutants using FM dye uptake. FM1-43 is a vital dye that is permeable through the MET channel (Meyers et al., 2003). It has been used to assess the function of MET channels in lateral line hair cells extensively (Sidi et al., 2003, 2004; Seiler et al., 2004; Hailey et al., 2012). FM4-64 has similar structure to FM1-43, but it has long-wavelength red fluorescence that can be used to co-label with GFP. Similar to FM1-43, FM4-46 cannot label hair cells with impaired mechanotransduction (Data not shown). Interestingly, we found that MET was not

impaired in *trpm7*^{*j124e1*} mutants that have a truncation of the C-terminal intracellular domain (Elizondo et al., 2005). The fluorescent signal intensities of both FM4-64 (Figure 44) and FM1-43 (data not shown) did not differ between *trpm7* mutants and their wild type siblings at both 48, 60, and 96 (data not shown) hpf. Our results suggest that *trpm7* is not required for zebrafish hair cells to take up FM1-43 and FM4-64 dye through their MET channel.

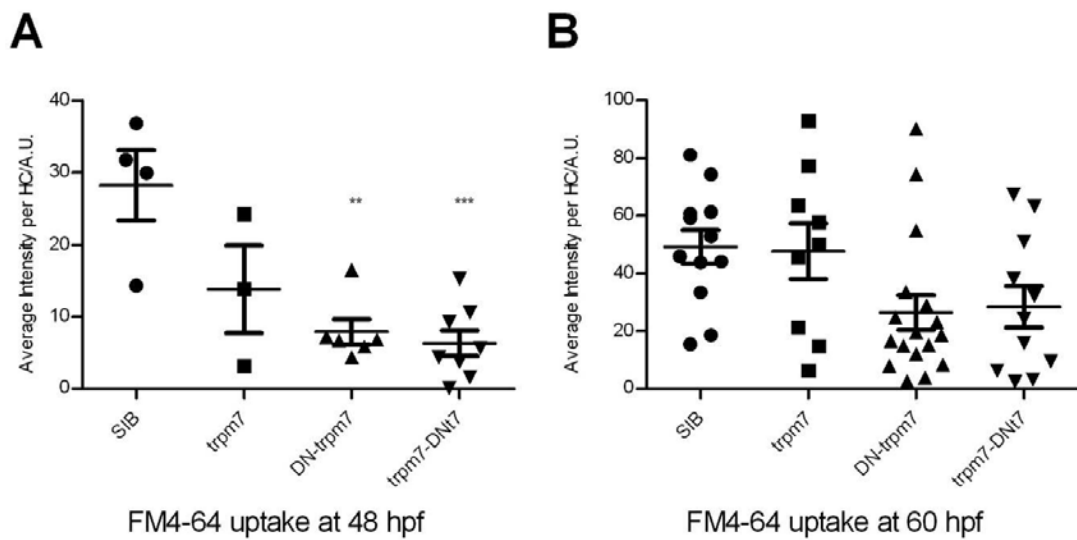


Figure 44. FM4-64 uptake in *trpm7* mutants. FM4-64 fluorescent intensities were measured in neuromast hair cells after 1 min treatment. Zebrafish larvae at 48 hpf (A) and 60 hpf (B) were used for experiment. SIB=wild-type siblings, *trpm7*=*trpm7*^{*j124e1*} mutants, DN-*trpm7*=Tg(*hsp:DN-trpm7-gfp*), *trpm7*-DNt7= *trpm7*^{*j124e1*}/ Tg(*hsp:DN-trpm7-gfp*). Quantification data are shown as mean ± S.E.; P values are determined by ANOVA tests to compare with SIB group. **p<0.01, ***p<0.001.

Another way to interfere with Trpm7 function is to overexpress dominant negative forms of Trpm7 (DN-T7) (Krapivinsky et al., 2006). Transgenic expression of zebrafish GFP tagged DN-T7 using an inducible *heat-shock* promoter ($Tg(hsp:DN-trpm7-gfp)$) phenocopies the melanocyte defects seen in $trpm7^{j124e1}$ mutants (unpublished observation from Robert Cornell lab). This approach has the benefit of not only affecting Trpm7 function, but also other channels that function in the same complex, perhaps uncovering genetic redundancies in the MET complex. Therefore, we crossed $Tg(hsp:DN-trpm7-gfp)$ with $trpm7^{j124e1}$ mutants and induced expression of DN-T7-GFP by heat-shocking $Tg(hsp:DN-trpm7-gfp)$ larvae. Because the fluorescent spectrum of GFP overlaps with FM1-43, we used FM4-64 to measure MET function in $Tg(hsp:DN-trpm7-gfp)$ larvae at 48 and 60 hpf. Expression of DN-T7-GFP in wild-type siblings and $trpm7^{j124e1}$ mutants significantly lowered the FM4-64 labeling at 48 hpf (Figure 44A). However, this difference was no longer statistically significant at 60 hpf (Figure 44B). There are at least two reasons why this is the case. First, fewer hair cells are present in the $Tg(hsp:DN-trpm7-gfp)$ and $trpm7^{j124e1}$ mutants (data not shown), which may be a developmental delay in $trpm7$ mutants. Although we have normalized the fluorescent intensity to the number of hair cells, it remains possible that younger hair cells are less labeled by FM dyes. Second, expression level of DN-T7-GFP was low after 48 hpf; and additional heat-shock did not increase GFP fluorescence (Data not shown). It is possible that the residual expression of DN-T7-GFP was not enough to block Trpm7 function at 60 hpf. Since we did not observe robust GFP signal in any of our heat shock experiments, it is possible that this particular transgenic line is not an effective tool to analyze TRP channel function in

zebrafish hair cells. Taken together, our experiments show *trpm7* expressing in neuromasts, but *trpm7*^{*j124e1*} mutation does not affect hair-cell mechanotransduction.

4. Yeast two-hybrid screen of interactors of Pcdh15a

4.1. Expression of *pcdh15a* splice variants in zebrafish

Hair-cell MET channels are thought to localize at the lower tip-link site that directly or indirectly connect to the cytoplasmic domain of PCDH15 (Beurg et al., 2009)(Figure 5). In mice, 3 different isoforms (CD1, CD2, and CD3) of the cytoplasmic domains of PCDH15 are expressed at hair bundles (Ahmed et al., 2006). With duplicated genes, zebrafish have *pcdh15a* expressed in hair cells and *pcdh15b* in retina (Seiler et al., 2005). However, the cytoplasmic domain isoforms for zebrafish *pcdh15a* have not been characterized. As a first step towards screening for proteins that interact with the cytoplasmic domain of *pcdh15a*, we characterized *pcdh15a* isoforms in hair cells using primers in the transmembrane domain for 5' and 3'RACE reactions. Many extracellular splice variants were identified by 5'RACE (data not shown); and two major intracellular isoforms, *pcdh15a-CD1* and *pcdh15a-CD3*, were uncovered by 3'RACE (Figure 45). We find neither the transcript nor the conserved genomic sequence of CD2 isoform in zebrafish. To characterize expression of CD1 and CD3 domain in hair cells, primers flanking the transmembrane domain and the last exon of each variant were used to amplify transcripts from our extracted neuromast preparation. Both CD1 and CD3 transcripts were amplified from neuromast cDNA, indicating their expression in hair cells. Sequencing of PCR bands resulted three additional splice variants in both CD1 and CD3

isoforms (Figure 45). Full length ORFs representing the longest transcripts of *pcdh15a-CD1* and *pcdh15a-CD3* were subsequently cloned.

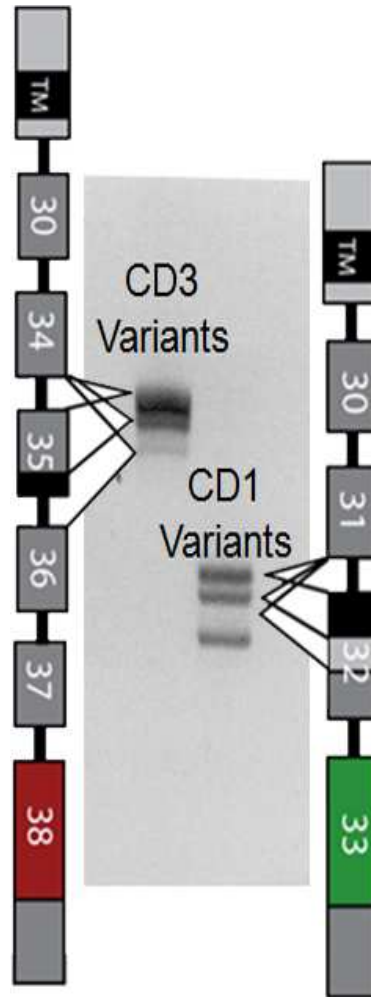


Figure 45. Structure and expression of intracellular domains of Pcdh15a. The diagram shows different splicing patterns for two isoforms of *pcdh15a* gene, as determined by RT-PCR from zebrafish neuromast RNA. The intracellular gene structures of *pcdh15a-CD1* (green), and *pcdh15a-CD3* (red) isoforms are shown. Three additional splice variants were detected for each isoform in 5dpf zebrafish neuromasts. The corresponding splicing sites of three bands on an agarose gel are depicted.

4.2. Generation of Pcdh15a bait

We cloned the full length of both *pcdh15a-CD1* and *pcdh15a-CD3* into the bait vector pBT3-SUC for split-ubiquitin membrane yeast two-hybrid (MYTH) screen (Figure 46A). The MYTH technique is potentially suitable to identify protein interactors of Pcdh15a because (1) the interaction between PCDH15 and the MET complex may be directly or indirectly depend on membrane structure; (2) PCDH15 may interact with membrane proteins; (3) PCDH15 proteins may fold incorrectly without membrane involvement. The finished pBT3-SUC-Pcdh15a vector contained a signal peptide at N-terminus and a Cub-LexA-VP16 tag at the C-terminus, as shown in Figure 47A.

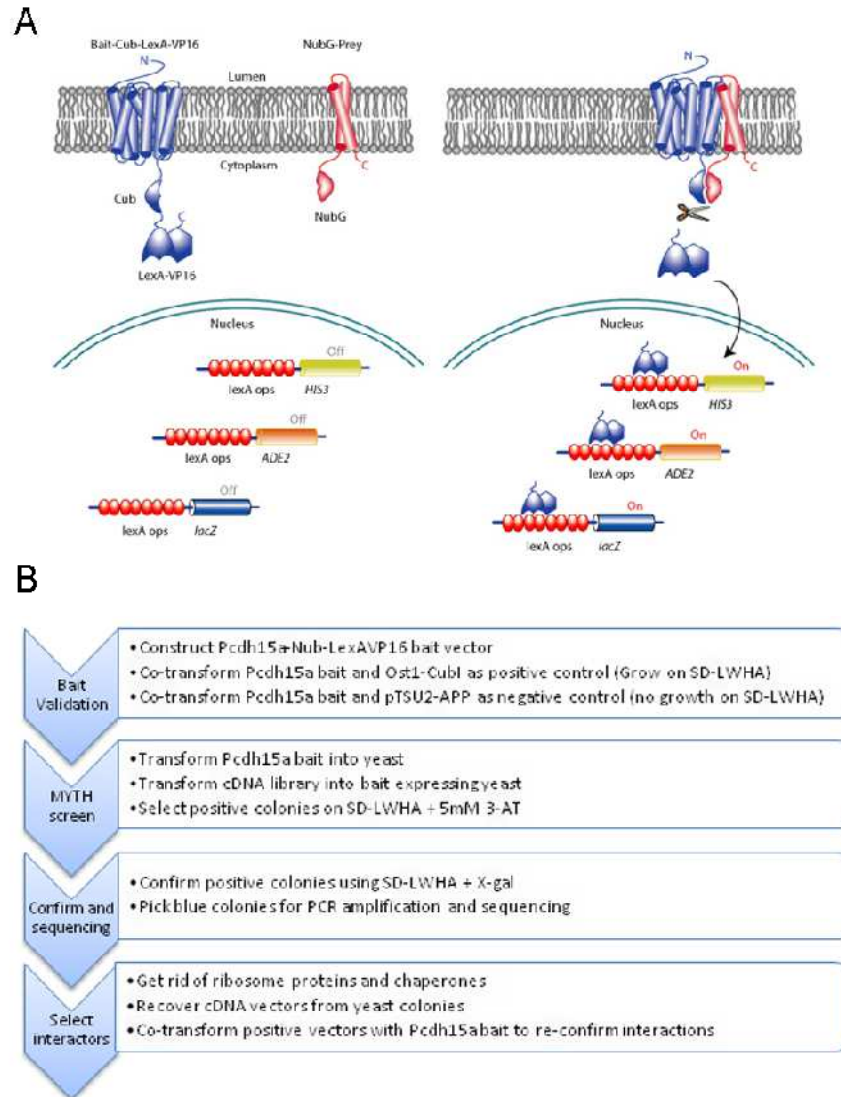


Figure 46. The principle and flow chart of membrane yeast two-hybrid screen (MYTH). (A) Schematic diagram of MYTH. Cub is the C-terminal of ubiquitin. LexA-VP16 is an artificial transcription factor. When the NubG (mutated N-terminal of ubiquitin) tagged prey protein can interact with the bait protein, the Cub and NubG reconstructs the ubiquitin, which is subsequently cleaved to release LexA-VP16. LexA-VP16 can then enter into nuclei to activate transcription of reporter genes, in this case, HIS3, ADE2 and LacZ. (B) The flow chart used to screen Pcdh15a interactors.

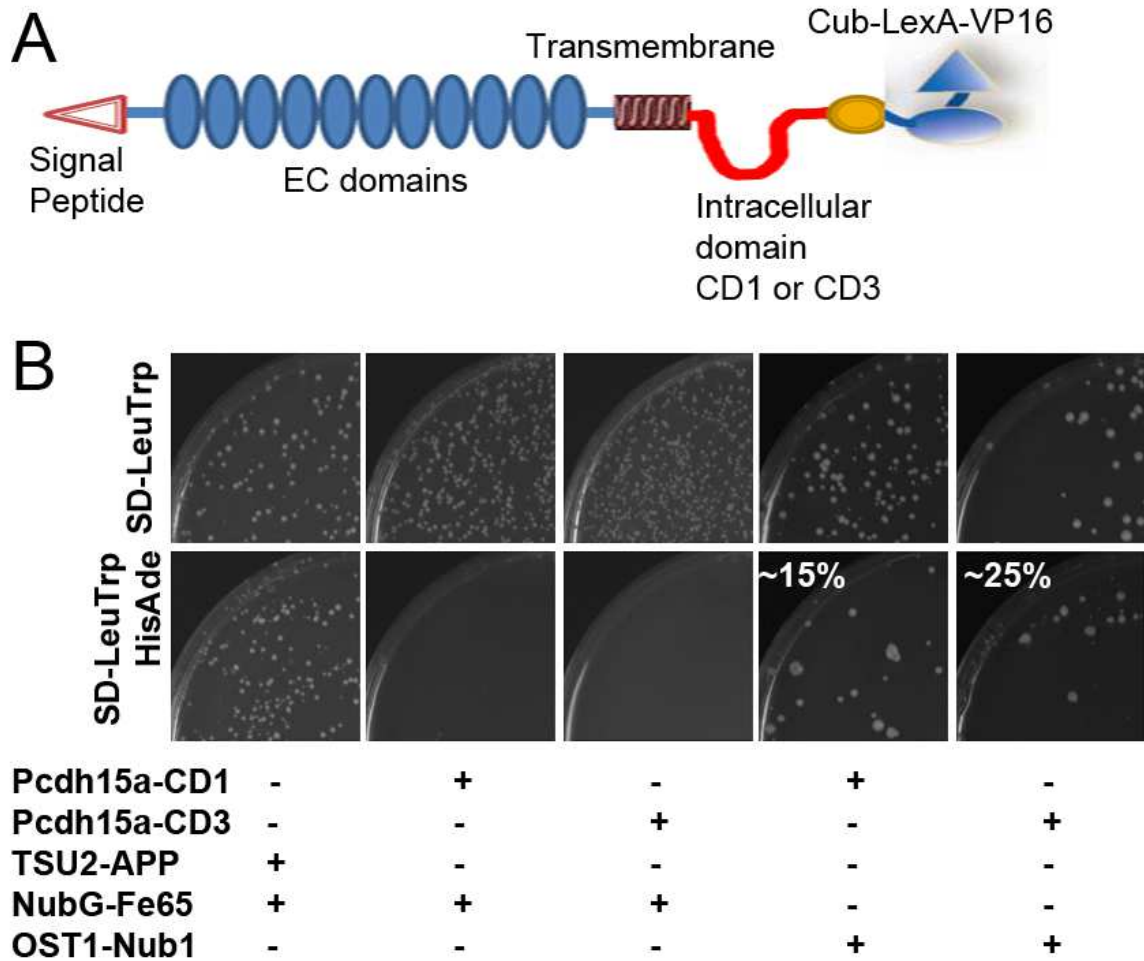


Figure 47. Validate expression of tagged Pcdh15a in yeast. (A). A cartoon to show the structure of Pcdh15a bait. (B) The membrane-based yeast two-hybrid analysis of different vectors. TSU2 and Fe65 are known to interact with each other. Co-transformation of TSU2-APP and NunG-Fe65 was a positive control to show their growth on both media. Since NubG-Fe65 does not interact with Pcdh15a, yeast co-transformed with these vectors only grew on double selection medium (SD-LeuTrp), but not on quadruple selection medium (SD-LeuTrpHisAde). Co-transformation of OST1-Nub1 with Pcdh15a-CD1 had about 15% colonies grown on quadruple medium, and with Pcdh15a-CD3 had 25% colonies grown on quadruple medium.

As outlined in Figure 46B, our first priority is to ensure that the Pcdh15a bait can interact with prey proteins in yeast. We co-transformed NMY51 yeast strain with Pcdh15a-bait and a positive control prey pOST1-NubI (Dualsystems Biotech). OST1 encodes the alpha subunit of the yeast oligosaccharyltransferase complex in the ER lumen. Theoretically, it does not partner with Pcdh15a. The OST1-NubI fusion protein has an N-terminal of Ubiquitin (NubI) domain that can interact with Cub (C-terminal of ubiquitin) of the Cub-LexA-VP16 tag attached to the Pcdh15a protein. Co-transformation of pOST1-Nub1 and pBT3-SUC-Pcdh15a can thus make a complete ubiquitin by combining the split NubI and Cub. Reconstructed ubiquitin can then be cut to release LexA-VP16, which will result in activation of the receptor genes including *his3*, *ade2*, and *lacZ*. This allows growth of NMY51 yeast on quadruple selective plate (SD-LWHA). As shown in Figure 47B, both Pcdh15a-CD1 and Pcdh15a-CD3 in pBT3-SUC granted growth of NMY51 on SD-LWHA when they were cotransformed with pOST1-NubI. Although Pcdh15a-CD1 bait gave less growth on quadruple selective plates than Pcdh15a-CD3 bait, both are in an acceptable range according to the technique manual from Dualsystems Biotech. If a control vector expressing NubG-Fe65, which contains a mutated NubG that cannot interact with Cub, was cotransformed with pBT3-SUC-Pcdh15a, NMY51 could only grow on double selective plate (SD-LW), but not on SD-LWHA (Figure 47B). When NubG-Fe65 was co-expressed with TSU2-APP (TSU2-Cub-LexA-VP16 fusion protein) in NMY51 yeast, the interaction of Fe65 with TSU2 brings NubG close enough to Cub, which can be cut as an ubiquitin. This interaction makes NubG-Fe65 and TSU2-APP double transformed yeast to grow on SD-LWHA plate (Figure 47B). Together, our data suggest that Pcdh15a bait was synthesized in yeast with its Cub-LexA-VP16 tag; and it did not interact with NubG-

Fe65 unspecifically, which allowed us to screen for protein-protein interactions for the cytoplasmic domain of Pcdh15a.

4.3. Split-Ubiquitin Membrane Yeast Two-Hybrid using Pcdh15a

We performed split-ubiquitin membrane yeast two-hybrid (MYTH) screen using a DUALmembrane starter kit from Dualsystems Biotech as shown in Figure 46B. An Ear-pPR3-NubG-x library library was built by Dualsystems Biotech using total RNA from zebrafish inner ear. For MYTH screen, about 20 µg of cDNA library was transformed into NMY51 yeast containing Pcdh15a-CD1 and Pcdh15-CD3 bait with a transformation efficiency of $\sim 5 \times 10^5$ and 3×10^5 cfu/µg respectively. Positive yeast colonies were selected using SD-LWHA plates containing 4mM 3-AT, a competitive inhibitor of HIS3 to minimize background growth. All positive colonies were retested on selective plates for β-galactosidase activity screen. More than 400 colonies from Pcdh15a-CD1 bait and 300 colonies from Pcdh15a-CD3 bait were picked from the 2nd round screen for PCR amplification of cDNA inserts. All PCR products were sequenced to identify corresponding genes. A total of 37 colonies were chosen as promising candidates and amplified in *E. coli* for retest. 9 of them were confirmed as real interactors (Table 3). Some of the retested cDNA clones are shown in Figure 48.

Positive prey proteins have various cellular functions (Table 3). The *prkar2aa* gene encodes the type II regulatory domain of protein kinase A, which has been found to regulate motility of cilia (Jivan et al., 2009). Its paralog, the type I regulatory subunit, has been found to interact with MYO7A, a PCDH15 binding protein (Küssel-Andermann et al., 2000). *tmem35* is expressed throughout the zebrafish embryo including the embryonic

inner ear (Coimbra et al., 2002; Thisse et al., 2004). Cldnb is a tight junction protein highly expressed in the lateral line system of zebrafish (Gallardo et al., 2010). Tmed9, a putative transmembrane protein, is also found in the zebrafish inner ear, although no functional study has been reported (Thisse et al., 2004). LPPR1 is a phosphatase-like protein expressed in the nervous system without known function (Savaskan et al., 2004). Beta-thymosin is an actin-binding protein that regulates actin filament dynamics (Husson et al., 2010). Although no report of its function in hair cells, beta-thymosin could be an important regulator of the actin-rich stereocilia. Sdcbp/syntenin is potentially an interesting interactor of Pcdh15a because it binds with syndecan protein to regulate mechanotransduction signaling in fibroblasts (Bellin et al., 2009). Sec61g is part of the translocon complex that responsible for membrane protein translation (Shao and Hegde, 2011), which may be irrelevant to PCDH15 function in hair bundles. Tmc2a is perhaps the most interesting protein on the list, which will be further addressed in section 4.4. In conclusion, the MYTH is a good screening technique for interactors with Pcdh15a and we have generated a list of interesting interaction proteins to be further characterized in the future.

Table 3 Potential prey proteins

	Bait	Prey	Description
Strong	Pcdh15a-CD3	Prkar2aa	protein kinase, cAMP-dependent, regulatory, type II, alpha A
Strong	Pcdh15a-CD3	Tmem35	transmembrane protein 35
Strong	Pcdh15a-CD1	Cldnb	claudin b
Strong	Pcdh15a-CD1	Tmed9	transmembrane emp24 protein transport domain containing 9
Weak	Pcdh15a-CD1	LPPR1	lipid phosphate phosphatase-related protein type 1
Weak	Pcdh15a-CD1	Sdcbp	syndecan binding protein (syntenin) 2
Weak	Pcdh15a-CD1	Tmc2a	transmembrane channel-like 2a
Weak	Pcdh15a-CD1	Tmsb	thymosin, beta
Weak	Pcdh15a-CD1	Sec61g	Sec61 gamma subunit

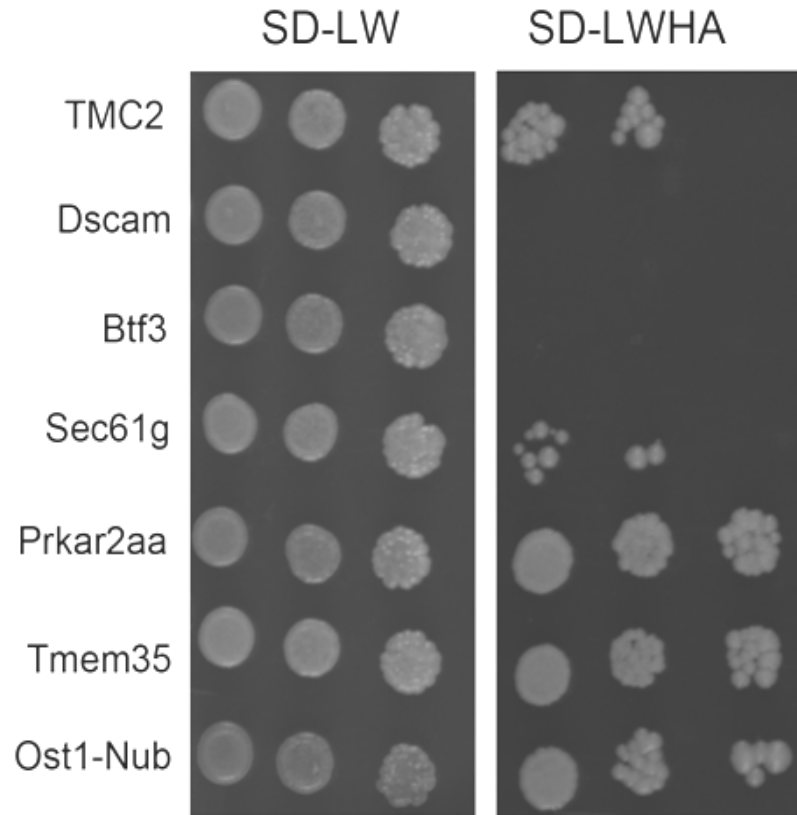


Figure 48. Confirmation of interaction proteins of Pcdh15a. Growth of yeast cells with 3×5 folds serial dilutions. Genes inserted in prey vectors are listed on the left. Only those proteins that interact with Pcdh15a can grow on the quadruple selection plate on the right.

4.4. Expression of *tmc* genes in zebrafish

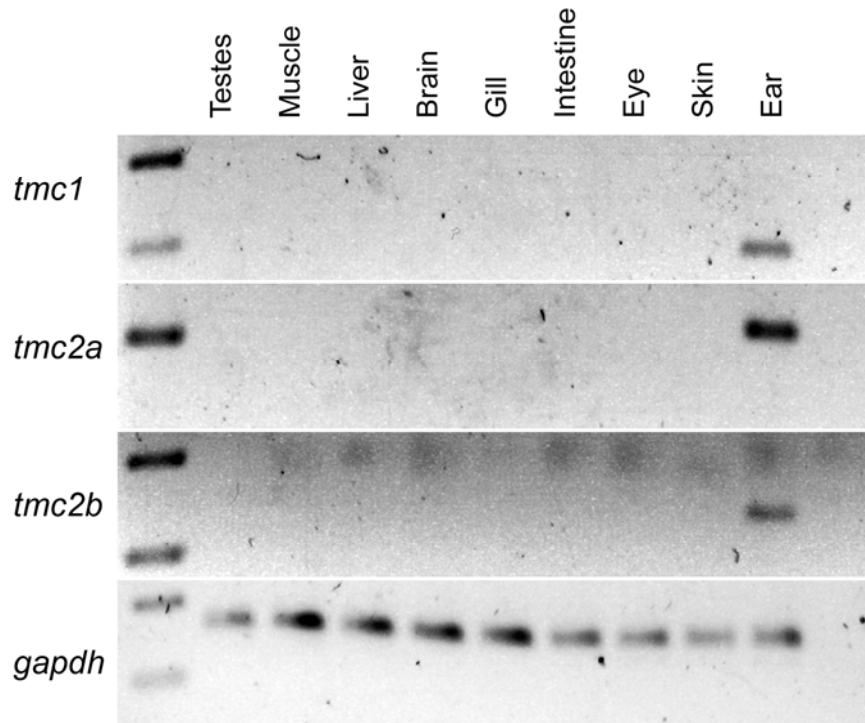


Figure 49. Expression of *tmc* genes in zebrafish adult tissues. Expression of *tmc1*, *tmc2a*, and *tmc2b* was checked in 9 different tissues in adult zebrafish by RT-PCR. *gapdh* was used as a control.

The MYTH screen using Pcdh15a as bait has identified Tmc2a, a channel-like protein whose cellular function is currently unclear. Both TMC1 and TMC2 are found in mouse hair cells and are required for normal mechanotransduction through an unknown mechanism (Kawashima et al., 2011). However, given the putative interaction with Pcdh15, their clear role in MET and their channel-like structure, the Tmc proteins must be considered as MET channel candidates. Therefore, we determined the expression of

zebrafish *tmc* genes, *tmc1*, *tmc2a*, and *tmc2b*, in different tissues by RT-PCR. All three genes are highly expressed in the adult inner ear (Figure 48). Expression of all three genes in other tissues can only be detected with 5 additional PCR cycles (a total of 35 cycles, data not shown). Our results confirmed the ear-enriched expression of *tmc1*, *tmc2a*, and *tmc2b*. It is likely that the interaction between Tmc2a and Pcdh15a-CD1 is physiologically important.

5. Discussion

In this study, we have used two approaches to identify candidates for MET channels in hair cells. First, by checking the expression of TRP channels in zebrafish neuromasts, we have identified 6 TRP channels potentially expressed in hair cells. *trpm7* was the highest expressed TRP channel genes in neuromasts. However, mechanotransduction was not affected in either *trpm7*^{*j124e1*} mutants, nor in transgenic fish expressing dominant negative Trpm7-GFP at 60 hpf. Our results suggest that Trpm7 is not the major contributor of the MET channel complex. However, our experiments cannot rule out the possibility that Trpm7, or other TRP channels, are involved in MET. In addition, we used membrane yeast two-hybrid screen to identify interaction proteins of Pcdh15a. Using an Ear-pPR3-NubG-x library, we discovered 9 putative interactors of Pcdh15a. Among them, Tmc2a is the most likely to be directly involved with MET. We then checked the expression of *tmc2a* and two of its homologous genes, *tmc1* and *tmc2b*, in adult zebrafish tissues. Three genes were found to have enriched expression in the inner ear. Since *tmc1* and *tmc2* are required for mechanotransduction in mouse hair cells, their function in zebrafish hair cells is worthy to explore in the future.

5.1. TRP channels as candidates for MET channel

Mutations in the TRPN1 channel (also known as *nompC*), two TRPV genes—*Inactive (iav)* and *Nanchung (nan)*, and two TRPA channels—*painless(pain)* and *pyrexia(pyx)* have been shown to impair hearing and/or vestibular function in *Drosophila* (Walker et al., 2000; Kim et al., 2003; Gong et al., 2004; Sun et al., 2009; Effertz et al., 2012). More detailed experiments have suggested that *nompC* is directly involved in transduction channel gating (Effertz et al., 2011, 2012), while TRPV channels are likely essential for mechanic feedbacks (Göpfert et al., 2006). *nompC* is also required for mechanotransduction in zebrafish hair cells (Sidi et al., 2003), but it is not localized to the tip link where MET happens (Shin et al., 2005) and not found in mammalian genomes. Hence, *nompC* unlikely contribute to MET in mammalian hearing.

Mammalian homologs of *Drosophila* TRPA and TRPV genes are also found in hair cells. Screen of TRP channels genes expressed in mouse inner ear identified TRPA1 (Corey et al., 2004), but it appears to be receptor for thermal and chemical stimuli rather than hearing (Kwan et al., 2006; Macpherson et al., 2007; Prober et al., 2008; Cordero-Morales et al., 2011). TRPV4 channel is found to regulate ionic homeostasis in cochlear duct, but not required for normal MET currents (Tabuchi et al., 2005). We also identified transcripts of *trpa1a* but not *trpv* genes in zebrafish neuromasts (Table 2).

Recent studies have recognized partial hearing loss and reduced MET currents in TRPC3/TRPC6 double-knockout mice (Quick et al., 2012), but it is likely through regulation of intracellular Ca^{2+} but not mechanotransduction itself (Raybould et al., 2007)

In my experiment, *trpc4a* transcripts but not *trpc3* and *trpc6* was found in neuromasts (Table 2). It is likely that their expression level is too low to be detected by our method.

TRPP channels are another group of interesting candidates, because TRPP -1 and -2 are found to be mechanoreceptors in kidney cells (Nauli et al., 2003). Analysis of TRPP channels have revealed similar biophysical properties to the hair-cell MET channels (reviewed by Fettiplace, 2009). In my experiment, primers for *trpp1* did not work well in total cDNA, while the transcript of *trpp2* was not amplified from neuromast cDNA (Table 2). However, expression of TRPP -1, -2, -2L1 and -REJ has been found in the mouse organ of Corti (Cuajungco et al., 2007). Although TRPP1 protein is localized to the stereocilia, TRPP1 mutation leads to minor structural defects of hair bundle, but does not affect MET currents (Steigelman et al., 2011). However, it is possible that TRPP1 mutation can be compensate by other TRPP channels in hair cells. It is also interesting to know the function of TRP channels in the hair bundle even if they are not the MET channels.

We found expression of zebrafish *trpm7* in lateral line hair cells (Figure 43). Meanwhile, the Gillespie lab has found TRPM7 interacting with PCDH15 both *in vitro* and *in vivo* (unpublished observations). However, we did not observe dramatic change of MET channel function in either *trpm^{7j124e1}* mutants or Tg(*hsp:DN-trpm7-gfp*) transgenic fish (Figure 44). The channel properties of TRPM7 itself are also different than what has been measured for the mammalian hair cell MET channels. For example, the TRPM7 channel has a single-channel conductance ranging from 40–105 pS, but the MET channel has much higher conductance at 150-300 pS. However, it is possible that TRPM7 can form

heterooligomers with other TRPM channels such as TRPM6 (Middelbeek et al., 2010) *in vivo*, which may change the channel conductance and also possibly complement MET function in *trmp7* mutants. It remains an open question as to whether TRPM channels (or other TRP channels) directly contribute to mechanotransduction in hair cells.

So far, TRPP and TRPM channels remain possible candidates for the mechanosensory receptors for human hearing and balance.

5.2. TMC channels as candidates for mechanoreceptors of hearing

The transmembrane channel-like protein (TMC) is a family of 8 proteins (TMC1 to TMC8) shares homologous TMC domains (Kurima et al., 2003). The topology analysis of TMC1 suggests that it is a channel or transporter with six transmembrane domains with N- and C-terminal outward the cytoplasm. The transmembrane organization of TMC1 resembles some of the TRP and Kv channels (Labay et al., 2010). However, no channel or transporter activity has been shown from several electrophysiological recordings (Vreugde et al., 2002; Marcotti et al., 2006; Labay et al., 2010). It is possible that other subunits or partners are required to open the TMC channels.

Mutations in the human TMC1 gene are associated with both dominant (DFNA36) and recessive (DFNB7/B11) hearing loss (Kurima et al., 2002). Five different mutations in TMC1 have also been found to affect hearing in mice (Vreugde et al., 2002; Manji et al., 2012). TMC2 is a closely homologous protein of TMC1. Expression analyses of murine TMC1 and TMC2 has found both of them in hair cells (Kurima et al., 2002; Vreugde et

al., 2002). Other TMC genes are also expressed in the cochlea but they may not be specific to hair cells (Mutai et al., 2005).

Transduction currents in TMC1 mutant hair cells were originally found to be normal, suggesting that TMC1 was not directly involved in MET (Marcotti et al., 2006). However, recent work suggests that MET currents are only slightly affected in TMC1 mutants due to genetic redundancy with the closely related TMC2 gene. The MET currents in hair cells are totally abolished only when both TMC1 and TMC2 are mutated (Kawashima et al., 2011). These data suggest that TMC protein function is absolutely required for MET, and that there is genetic redundancy between TMC1 and TMC2 in this regard.

Our MYTH protein interaction screen for Pcdh15a interactors revealed *Tmc2a*, a zebrafish homolog of mouse TMC2. Two *tmc2* genes and *tmc1* in zebrafish are specifically expressed in adult inner ear, supporting the idea that they perform an important function in hair cells. It is tempting to hypothesize that the interaction with Pcdh15a could be important for TMC function in hair-cell mechanotransduction. The most intriguing model is that TMC1 and TMC2 is the pore forming subunits of the MET channel complex. In fact, both TMC1 and TMC2 have dimerization domains at their N- and C-terminus that can possibly contribute to dimer or tetramer channels. Different composition of MET channels in different hair cells could be source of heterogeneity of channel conductance (Fettiplace, 2009). Several dominant mutations found in mouse and human (Kurima et al., 2002; Vreugde et al., 2002; Kitajiri et al., 2007; Yang et al., 2010) also support the idea of TMC1 and TMC2 being heterologous channel subunits. To act in a dominant negative fashion, these mutations are likely affecting the interaction of

different subunits or the opening pore of the channel. Exploring the biochemical properties of these mutations might give us clues of how TMCs contribute to mechanotransduction in hair cells.

Chapter 6. Summary and Conclusions

Hair cells use specialized structures, hair bundles, to transfer mechanical stimuli such as sound into electric signals, and another specialized structure called ribbon synapse to transmit signals to the brain. It is hard to experimentally study the structure and function of hair cells, because they are limited in number and scattered all over the inner ear, which is embedded in the skull. Genetic studies of human deafness genes have revealed molecules that are important for the structure and function of hair cells. Among them, PCDH15 and CDH23 are key components of the tip link in the hair bundle and crucial for MET process. At hair-cell ribbon synapses, a few unique proteins such as Ribeye, Vglut3, Cav1.3 and Otoferlin have been characterized.

As a powerful vertebrate genetic model, zebrafish has been used to study embryonic development and human diseases. Our lab pioneers in using zebrafish as a genetic model to study hair-cell function. My dissertation has advanced our current knowledge by (1) providing the first-ever behavioral analysis to assess vestibular function in zebrafish mutants; (2) presenting compelling evidence that Nsf is required for the function and maintenance of hair-cell ribbon synapses; and (3) characterization of a few candidates that biochemically interact with Pcdh15 and are thus potentially important for mechanotransduction in hair cells.

6.1. Behavioral analysis of zebrafish larvae

Zebrafish has been introduced as an excellent genetic model to study the development and function of hair cells. Methods to quantify the function of hearing and balance in

zebrafish mutants are critical in understanding the defects. In Chapter 2, we have described a behavioral assessment of vestibular function in zebrafish larvae for the first time. Eye movements that are induced by vestibular stimulation (e.g. the vestibuloocular reflex, VOR) have been systematically analyzed. We have also determined that zebrafish larvae display robust eye movements only when stimulated with rotations around an earth horizontal axis. Zebrafish mutants with balance defects have reduced or abolished VOR responses. With respect to developmental onset, we are able to detect VOR responses in WT larvae by 72 hpf. Our data also suggest that the utricular/anterior otolith is indispensable for VOR in larval zebrafish. Follow-up studies from Bianco and colleagues have confirmed most of our findings (Bianco et al., 2012).

Our studies of the VOR provide an important tool for quantitative analysis of vestibular function in zebrafish larvae. We have successfully used this method to measure vestibular function in several zebrafish mutants (Obholzer et al., 2008; Trapani et al., 2009; Sheets et al., 2011). The deficits in vestibular function in these mutants assessed by behavioral analysis largely agree with the findings observed in electrophysiological experiments.

One future direction of these studies is to investigate how the VOR response is used to stabilize gaze in zebrafish larvae. An improved device has been developed by Bianco and coworkers to measure the gain of VOR responses (Bianco et al., 2012). They have also shown that the tangential nucleus controls the VOR response in zebrafish larvae. It is still unknown whether the tangential nucleus incorporates sensory information from different sensory systems. Further studies will be needed to resolve the neuronal circuitry of VOR

responses and how the VOR circuit collaborates with visual inputs to stabilize gaze in zebrafish larvae.

6.2. Nsf function in hair cells

In several large-scale genetic screens, over one hundred alleles have been found to affect the auditory and vestibular system in zebrafish larvae. Many of these mutants affect hair-cell mechanotransduction or synaptic transmission. In Chapter 3, we have characterized the *milky way* allele identified from genetic screens as a balance defect mutant.

Via positional cloning, we identified a point mutation in *milky way* mutants: *nsf*^{J209N}.

Using behavioral analysis, we have determined that the *nsf*^{J209N} mutation leads to both hearing and balance defects in zebrafish. Electrophysiological recording from the soma of pLLG neurons has also found that action potentials are slightly delayed in the mutants.

Using several antibodies against protein markers of lateral line nerve and hair-cell synaptic vesicles, we have determined that the morphology of hair-cell synapses, and the lateral line nerves, including the myelin sheath, is largely unchanged by the point mutation. CSP protein, which has an opposite function of Nsf, was observed to be slightly reduced at hair-cell ribbon synapses. Since the function of Nsf is to dissociate SNARE proteins, we have used antibodies against neuronal SNAREs in zebrafish larvae and found VAMP-2 and -8 are expressed in hair cells, while VAMP-1, Syntaxin-2 and SNAP25 are expressed in the nerves innervating hair cells. Collectively, our studies of the *Nsf*^{J209N} mutation indicate that Nsf has an important function in regulating synaptic transmission in hair cells.

Further analysis of *nsf* null mutant, *nsf^{st53}*, in Chapter 4 revealed an important function of Nsf in maintaining hair-cell synapses. We examined the afferent innervations of hair cells in *nsf* and *nsfb* mutants and found that only mutation of *nsf*, but not *nsfb*, causes degeneration of afferent nerve fibers. Using tissue specific expression of Nsf-GFP fusion protein, we determined that both pre- and postsynaptic Nsf proteins are essential for maintenance of hair-cell synapses. The neurodegeneration phenotype is not secondary to apoptosis, but likely directly caused by the loss of Nsf. Using RT-PCR, we have characterized expression of several genes that have been implicated in synaptic stability. Among the genes that are down regulated in *st53* mutants, BDNF proteins were found to accumulate in *nsf^{st53}* mutant afferent fibers. Because failure to release BDNF can be a cause of neurodegeneration, we supplied exogenous BDNF to *st53* mutants, and found partial rescue of afferent innervation in *nsf* null mutants.

Our data from both *nsf^{Δ209N}* and *nsf^{st53}* mutations suggest a critical role for Nsf in hair cells. Our results agree with previous findings that Nsf is part of the protein complex at hair-cell ribbon synapses (Uthaiyah and Hudspeth, 2010). Because several synaptic markers in hair cells have been found to be abnormal in *nsf* null mutants (Chapter 3 and 4), it is likely that Nsf is essential for normal development of hair cells. Transient blockage of Nsf function in hair cells will confirm whether it catalyzes synaptic transmission at hair-cell synapses.

Our results support the idea that Nsf catalyzes unconventional SNARE complexes in hair cells. In a search for targeting proteins of Nsf in hair cells, we also found expression of two SNARE proteins, VAMP-2 and -8, in zebrafish hair cells. Results from different

studies were controversial regarding the expression of SNARE proteins in hair cells (Table 4). Since the SNARE complex is the key regulator of synaptic transmission in most neurons, it will be interesting to know if Nsf catalyzes other unconventional SNARE proteins at hair-cell ribbon synapses. Because many SNARE proteins share homologous sequences with neuronal SNAREs, cross reactivity of antibodies may lead to false positive labeling of SNAREs in hair cells. It will be necessary to validate antibodies that are used to against SNARE proteins in future studies.

Table 4 Expression of neuronal SNAREs in hair cells

Animal	Syntaxin1	SNAP25	VAMP1	VAMP2	Ref.
Guinea Pig	Yes	Yes	Yes	Yes	(Safieddine and Wenthold, 1999)
Chicken	Yes	Yes	No	Yes	(Uthaiiah and Hudspeth, 2010)
Mouse	No	No	No	No	(Nouvian et al., 2011)
Zebrafish	No	No	No	Yes	Chapter 3

6.3. Mechanotransduction in hair cells

Genetic screens in zebrafish have identified a few components that are required for mechanotransduction, including Pcdh15a and Cdh23. The mammalian PCDH15 protein is thought to interact with the MET complex. To extend our knowledge of the MET complex, we have presented two approaches to identify candidates for MET channels in

hair cells in this dissertation. We have characterized two potential interactors of Pcdh15a protein, *Trpm7* and *Tmc2a*.

Our results suggest that *Trpm7* is not the major contributor of the MET channel complex. Although *trpm7* is the highest expressed TRP channel genes in neuromasts, mechanotransduction was not affected in either *trpm7^{j124e1}* mutants, nor in transgenic fish expressing dominant negative *Trpm7*-GFP at 60 hpf. However, our experiments cannot rule out the possibility that *Trpm7*, or other TRP channels, are involved in MET process, because there may be other channels compensating the function of TRPM7 in *trpm7^{j124e1}* mutants. Since TRPM7 and TRPM6 forms a heterotetramer in mammalian cells, it will be interesting to see if TRPM6 can compensate TRPM7 function in hair cells. Another future direction is to find the role of *Trpm7* channels in hair cells. Our data also suggest a developmental delay of *trpm7* defective hair cells. Given the important role of *Trmp7* in regulating magnesium homeostasis, finding out whether *Trpm7* is important for maturation of hair cells would potentially reveal an important role of magnesium in hair-cell development.

In addition, we have identified *Tmc2a* as an interaction partner of *Pcdh15a* using a membrane-based yeast two-hybrid screen. In the same screen, we have also discovered 9 putative interactors of *Pcdh15a*. Among them, *Tmc2a* is the most likely to be directly involved with mechanotransduction. Using RT-PCR, we have discovered the specific expression of *tmc2a* and two of its homologous genes, *tmc1* and *tmc2b*, in the zebrafish inner ear. Since *tmc1* and *tmc2* are required for mechanotransduction in mouse hair cells, their function in zebrafish hair cells is worthwhile to explore in the future. The important

question is whether they act directly as MET channels. Experimental evidence has to confirm that (1) they are channels that can be opened by mechanical force; (2) they are localized to where cations enter hair cells when MET channels are open; (3) they have the same biophysical properties as MET channels.

In summary, my dissertation successfully established a novel method of measuring vestibular function in zebrafish larvae, which has been proven to be a useful behavioral analysis tool. In characterizing zebrafish mutants, *nsf*^{209N} and *nsf*^{st53}, we have shown the importance of Nsf in hair cells. The final part of my dissertation opens a window to study potential proteins that are important for mechanotransduction in hair cells. These studies expand our knowledge of hair-cell function and our usage of zebrafish as a model organism to study hair-cell functions.

Appendices

1. Gravity changes in VOR measurement

During our experiments, three different forces were acting on the otoliths: (i) gravity; (ii) centripetal force; and (iii) tangential force. Because the forces were proportional to the mass of the otolith, the acceleration, rather than force, is used in the analysis below. In the following sections, we consider the acceleration of a single otolith.

Gravity change

As shown in Figure A1, the anterior macula is at an angle of 23° from the fish body axis. To simplify the analysis, we assume that only the gravity component in the direction parallel to the plane of the anterior macula g_{Eff} (effective gravity) stimulates the vestibular sensory cell. The gravity does not change during the rotation, but g_{Eff} changes with the rotational angle:

$$g_{Eff} = g \cdot \cos(\theta) \quad (A1)$$

where θ is the angle of the anterior macula to the vertical axis (gravity). As shown in Figure A1, in a rotation cycle, the fish body changes from -45° to 45° and θ changes from 68° to -22° . The peak-to-peak change of g_{Eff} is $g \cdot \cos(0^\circ) - g \cdot \cos(-68^\circ) = 0.625g = 6.13(\text{m/s}^2)$.

(This analysis assumes the anterior macula is perpendicular to the rotation plan, which is also the coronal plane of the fish. In zebrafish, the angle between the anterior macula and

the coronal plan is about 76° . Therefore, the maximum change of g_{Eff} is actually

$$6.13 \cdot \sin(76^\circ) = 5.95 \text{ m/s}^2$$

This analysis of G_{eff} for the macula on the other side could be calculated by applying a mirror image analysis. But how information from the both maculae is integrated in fish brain is a complex question won't be a focus in this paper.

Centripetal Acceleration

Here we estimate the centripetal force on the otolith. The fish was mounted at a radial distance 3.2 cm from the rotational axis. The centripetal acceleration can be calculated by $a_c = \omega^2 \cdot r$, where ω is the angular velocity and r is the radius of the rotation. In the experiment, the fish was moved in a sinusoidal manner. Its position can be described as

$$\varphi = \varphi_0 \cdot \cos(\Omega t) \quad (\text{A2})$$

where $\varphi_0 = \frac{\pi}{4}$ is the maximum rotational angle; $\Omega = \frac{2\pi}{T} = \frac{\pi}{2}$ is the angular frequency (in radians/s), $T = 4$ second is the rotational period. Therefore, the angular velocity

$$\omega = \frac{d\varphi}{dt} = -\varphi_0 \cdot \Omega \cdot \sin(\Omega t) \quad (\text{A3})$$

The maximum angular velocity is $\omega_m = \varphi_0 \cdot \Omega = \frac{\pi}{4} \cdot \frac{\pi}{2} = \frac{\pi^2}{8}$, and the maximum

centripetal acceleration is $a_{cm} = \omega_m^2 \cdot r = \left(\frac{\pi^2}{8}\right)^2 \cdot 0.032 = 0.049 \text{ (m/s}^2\text{)}$. This value is

less than 1/120 of the change due to tilt with respect to gravity. Therefore, we concluded that the gravity change during the experiment is the major stimulus to the vestibular sensory cell and the effect of the centripetal force is negligible.

Tangential Acceleration

Besides the centripetal acceleration, changes of velocity during rotations apply tangential acceleration to the otolith. The tangential acceleration has a direction along the tangent of the sinusoidal movements and it can be calculated by $a_T = \frac{d\omega}{dt} \cdot r$. With ω calculated from A3, then the tangential acceleration

$$a_T = \frac{d\omega}{dt} \cdot r = -\varphi_0 \cdot \Omega^2 \cdot \cos(\Omega t) \cdot r$$

Therefore, the maximum tangential acceleration is

$$a_T = -\varphi_0 \cdot \Omega^2 \cdot \cos(\Omega t) \cdot r = \frac{\pi}{4} \cdot \left(\frac{\pi}{2}\right)^2 \cdot 0.032 = 0.062(\text{m/s}^2)$$

This maximum tangential acceleration is about 1/100 of the change due to tilt with respect to gravity. Therefore, we concluded that the gravity change during the experiment is the major stimulus to the vestibular sensory cell and the effect of the centripetal force is negligible.

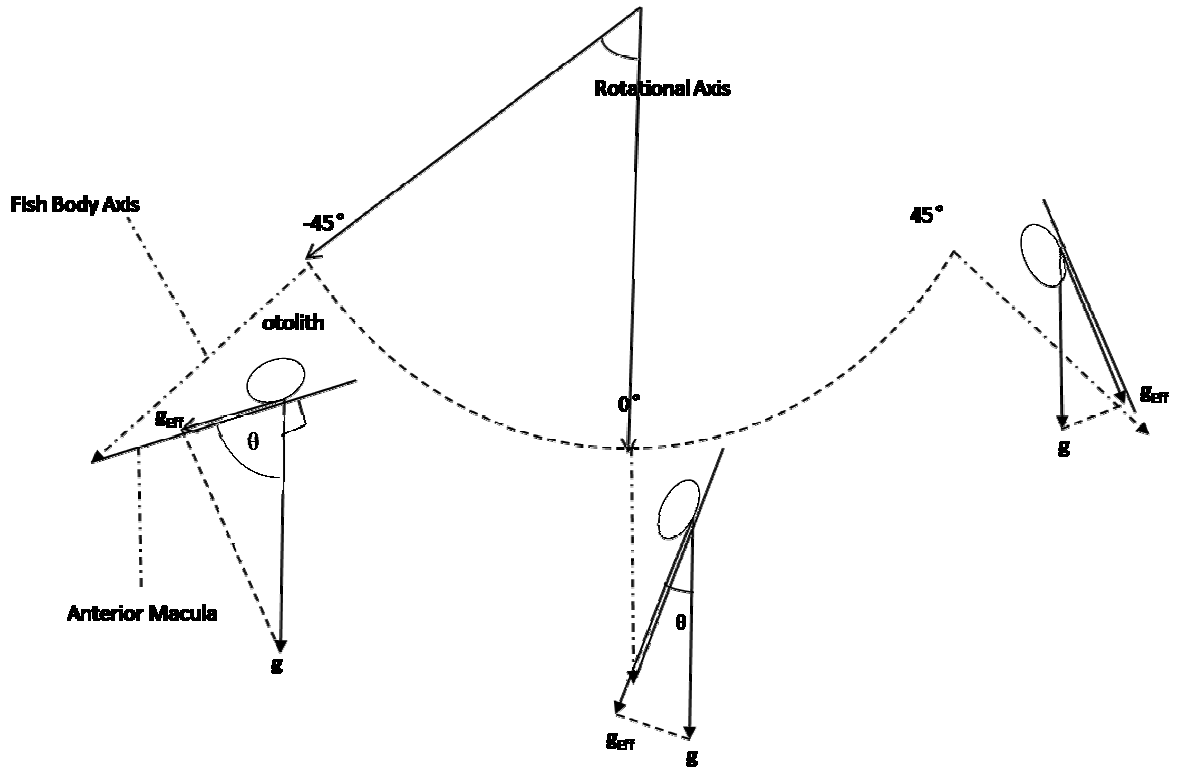


Figure 50. Schematic of g_{Eff} change during a rotation cycle. The relative angular position between the fish body, the anterior macula and gravity is shown in three positions during a rotation cycle. The gravity has a component g_{Eff} in the direction parallel to the plane of the anterior macula. The value of this component is determined by position of the otolith with respect to gravity and the position or angle to the anterior macula θ . Therefore, g_{Eff} varies with different rotational position as shown.

2. Detailed protocol of VOR measurement

2.1. Data acquisition

1. Separate siblings and mutants into different petridishes
2. Pre-heat 2% low-melting-point agarose at 40°C
3. Isolate a larva in a drop of E3
4. Put the larva with minimal E3 (1-2µl) onto a round coverslip
5. Add a drop of 2% Low-melt Agarose to mount fish in it. It's best to mount the fish heading to the edge.
6. Cool the coverslip on a metal rack until the agarose is solidified. Using a forceps to cut away agarose from around the head. It is important to free both eyes of the larva but remain both pectoral fins in the agarose.
7. Add less than 1 µL of E3/H₂O into the agarose whole to immerse the head.
8. Put the cover slip onto the specimen platform. A drop of water on the platform or back of the cover slip is required to increase surface tension by capillary action.
9. On computer, open two software programs: Scope Photo and Motion Planner
10. Turn on the light source at the back of the specimen platform/on the gear box of the motor.
11. In Scope Photo, click the camera to start and select DIC 130 for current setting.
12. To rotate the platform, use Motion Planner to create a new terminal and type "sinewave" or "sinewa." This will start the rotating.
13. For VOR recording, a black box or blanket is used to keep fish larva in the dark.

14. To record a video, Capture>Start Capture Video. Files are usually stored in folder “D:\VOR Raw Data”; please create a folder for your own. Existing files are named as “allele_sib/mut_age_VOR/OKR#”, example: am046_sib_5dpf_VOR3.
15. After recording, type “!k” in Motion Planner to stop the program.
16. The video capture is a minute.
17. In Motion Planner, Stop the rocking motion by typing “!k”

2.2. Using Matlab to analyze videos

1. Copy your raw video into a new folder, usually it will be “D:\VOR processing”; be sure to have your own folder created in the common folder. In “D:\VOR processing”, all files are used for processing and shall be copied into your own folder before analysis.
2. After you put video files and Matlab program files in the same folder.
In Matlab software program, open following files from your new folder:
 - a. Batchreadwmv_saveROIandGreyROI.m
 - b. BatchProcess.m
 - c. PlotbatchResultsAlignedexcel0515.m
3. Run (a) program first. In the window popped out, Matlab will ask you to define an eye region for calculation. Click the upper left and lower right to select a square box to define your desired region.
4. After processing, you will get a new folder for each video.

5. In each new folder, there is a file named “(your video name)GrayROI”. Copy all files with the same name pattern to the main folder that have all Matlab program files.
Then run (b) program for 2nd processing step.
6. By running (b) program, you will get result files named “(your video name)GrayROIresults”. There is a chance that (b) program stop for some reasons. In that case, go to Matlab to find which GrayROI file causes the problem and delete it (and possibly any GrayROIs that have been analyzed) from the folder. Run (b) again. Repeat this, if (b) stops, until all files are analyzed.
7. Run program (c) to plot all results into excel files. In each excel file you will get two sheets: time and FFT. In each sheet, there are six columns that contains following information: Left Area; Right Area; Left Ratio; Right Ratio; Left Phase (angle); Right Phase (angle).
8. In “time” sheet, those are raw data that have numbers for each frame of your video. E.g. the area of the left eye in the 2nd frame would be plotted at A2.
9. In “FFT” sheet, the power spectrum of each column in “time” sheet is calculated using Fast Fourier Transform.
10. You will still have to figure out what the “good” data is by looking at raw data and their amplitudes after FFT.

3. Whole mount immunohistochemical detection of proteins in embryonic zebrafish

MATERIALS

1X phosphate buffered saline (PBS): 0.8% NaCl, 0.02% KCl, 0.02 M PO₄, pH 7.3

Antibodies, primary and secondary

Blocking solution (FSGGB) (2% normal goat serum, 2% fish gelatin, 1% BSA, and 1% DMSO in PBS)

16% paraformaldehyde (PFA) in 1X PBS

PBSDTT: 1% DMSO, 0.1% Triton X-100 and 0.2% Tween20 in 1X PBS

Sucrose (8%), dissolved in 1X PBS

1. Collect and fix whole zebrafish embryos in microcentrifuge tubes containing 16% PFA:8% Sucrose:PBSDTT=1:2:1
2. Incubate the samples in 4% PFA 4 hours or overnight at 4°C with rocking.
3. Remove the 4% PFA. Rinse the specimens three times in 1X PBSDTT for 5 minutes each.
4. Optional: Permeabilization ddH₂O 5min@RT, prechilled Acetone 6min@-20°C, ddH₂O 5min@RT
5. Blocking in FSGGB overnight @ RT or 4°C
6. Dilute primary antibody in FSGGB and incubate overnight@4°C with rocking
7. Carefully discard the supernatant
8. Wash with PBSDTT for 2 hours with 6 changes
9. Add secondary antibody in FSGGB:PBS=1:3, 4°C overnight or 3-5 hours@RT

10. Wash with PBSDDT for 2 hours with 6 changes
11. Replace PBSDDT with PBS, put fish embryos on to slides
12. Rearrange embryos to the same direction on the slide
13. Drain as much PBS from the slides as possible
14. Add several small drops of Elvanol mounting medium directly onto embryos
15. Carefully place a coverslip onto each slide, avoiding bubbles
16. Squeeze embryos with a forceps
17. Allow Elvanol to harden for at least 3 hours at room temperature in the dark before imaging.

Slides may be placed for up to several weeks at 4°C until ready to image.
18. Image the slides on a confocal or fluorescent microscope.

References

Ackermann, G.E., and Paw, B.H. (2003). Zebrafish: a genetic model for vertebrate organogenesis and human disorders. *Frontiers in Bioscience : a Journal and Virtual Library* 8, d1227–53.

Adato, A., Michel, V., Kikkawa, Y., Reiners, J., Alagramam, K.N., Weil, D., Yonekawa, H., Wolfrum, U., El-Amraoui, A., and Petit, C. (2005). Interactions in the network of Usher syndrome type 1 proteins. *Human Molecular Genetics* 14, 347–356.

Ahmed, Z.M., Goodyear, R., Riazuddin, S., Lagziel, A., Legan, P.K., Behra, M., Burgess, S.M., Lilley, K.S., Wilcox, E.R., Riazuddin, S., et al. (2006). The tip-link antigen, a protein associated with the transduction complex of sensory hair cells, is protocadherin-15. *The Journal of Neuroscience : the Official Journal of the Society for Neuroscience* 26, 7022–7034.

Akil, O., and Lustig, L.R. (2012). Severe vestibular dysfunction and altered vestibular innervation in mice lacking prosaposin. *Neuroscience Research* 72, 296–305.

Alagramam, K.N., Goodyear, R.J., Geng, R., Furness, D.N., van Aken, A.F.J., Marcotti, W., Kros, C.J., and Richardson, G.P. (2011). Mutations in protocadherin 15 and cadherin 23 affect tip links and mechanotransduction in mammalian sensory hair cells. *PLoS One* 6, e19183.

Alagramam, K.N., Murcia, C.L., Kwon, H.Y., Pawlowski, K.S., Wright, C.G., and Woychik, R.P. (2001). The mouse Ames waltzer hearing-loss mutant is caused by mutation of *Pcdh15*, a novel protocadherin gene. *Nature Genetics* 27, 99–102.

Alpadi, K., Magupalli, V.G., Käppel, S., Köblitz, L., Schwarz, K., Seigel, G.M., Sung, C.-H., and Schmitz, F. (2008). RIBEYE recruits Munc119, a mammalian ortholog of the *Caenorhabditis elegans* protein *unc119*, to synaptic ribbons of photoreceptor synapses. *The Journal of Biological Chemistry* 283, 26461–26467.

Amsterdam, A., and Hopkins, N. (2004). Retroviral-mediated insertional mutagenesis in zebrafish. *Methods in Cell Biology* 77, 3–20.

Angelaki, D., Shaikh, A., Green, A., and Dickman, J. (2004). Neurons compute internal models of the physical laws of motion. *Nature*.

Angelaki, D.E., McHenry, M.Q., Newlands, S.D., and Dickman, J.D. (1999). Functional organization of primate translational vestibulo-ocular reflexes and effects of unilateral labyrinthectomy. *Annals of the New York Academy of Sciences* 871, 136–147.

Anichtchik, O., Diekmann, H., Fleming, A., Roach, A., Goldsmith, P., and Rubinsztein, D.C. (2008). Loss of PINK1 function affects development and results in neurodegeneration in zebrafish. *The Journal of Neuroscience : the Official Journal of the Society for Neuroscience* 28, 8199–8207.

Arnadóttir, J., and Chalfie, M. (2010). Eukaryotic mechanosensitive channels. *Annual Review of Biophysics* 39, 111–137.

Assad, J.A., Hacohen, N., and Corey, D.P. (1989). Voltage dependence of adaptation and active bundle movement in bullfrog saccular hair cells. *Proceedings of the National Academy of Sciences of the United States of America* 86, 2918–2922.

Assad, J.A., Shepherd, G.M., and Corey, D.P. (1991). Tip-link integrity and mechanical transduction in vertebrate hair cells. *Neuron* 7, 985–994.

Babor, S.M., and Fass, D. (1999). Crystal structure of the Sec18p N-terminal domain. *Proceedings of the National Academy of Sciences of the United States of America* 96, 14759–14764.

Bae, Y.-K., Kani, S., Shimizu, T., Tanabe, K., Nojima, H., Kimura, Y., Higashijima, S., and Hibi, M. (2009). Anatomy of zebrafish cerebellum and screen for mutations affecting its development. *Developmental Biology* 330, 406–426.

Bahloul, A., Michel, V., Hardelin, J.-P., Nouaille, S., Hoos, S., Houdusse, A., England, P., and Petit, C. (2010). Cadherin-23, myosin VIIa and harmonin, encoded by Usher syndrome type I genes, form a ternary complex and interact with membrane phospholipids. *Human Molecular Genetics* 19, 3557–3565.

Bang, P.I., Yelick, P.C., Malicki, J.J., and Sewell, W.F. (2002). High-throughput behavioral screening method for detecting auditory response defects in zebrafish. *Journal of Neuroscience Methods* 118, 177–187.

Beck, J.C., Gilland, E., Tank, D.W., and Baker, R. (2004). Quantifying the ontogeny of optokinetic and vestibuloocular behaviors in zebrafish, medaka, and goldfish. *Journal of Neurophysiology* 92, 3546–3561.

Becker, T., Becker, C.G., Schachner, M., and Bernhardt, R.R. (2001). Antibody to the HNK-1 glycoepitope affects fasciculation and axonal pathfinding in the developing posterior lateral line nerve of embryonic zebrafish. *Mechanisms of Development* 109, 37–49.

Bellin, R.M., Kubicek, J.D., Frigault, M.J., Kamien, A.J., Steward, R.L., Barnes, H.M., Digiacomo, M.B., Duncan, L.J., Edgerly, C.K., Morse, E.M., et al. (2009). Defining the role of syndecan-4 in mechanotransduction using surface-modification approaches.

Proceedings of the National Academy of Sciences of the United States of America *106*, 22102–22107.

van de Berg, W.D.J., Hepp, D.H., Dijkstra, A.A., Rozemuller, J.A.M., Berendse, H.W., and Foncke, E. (2012). Patterns of α -synuclein pathology in incidental cases and clinical subtypes of Parkinson's disease. *Parkinsonism & Related Disorders* *18 Suppl 1*, S28–30.

Beurg, M., Evans, M.G., Hackney, C.M., and Fettiplace, R. (2006). A large-conductance calcium-selective mechanotransducer channel in mammalian cochlear hair cells. *The Journal of Neuroscience : the Official Journal of the Society for Neuroscience* *26*, 10992–11000.

Beurg, M., Fettiplace, R., Nam, J.-H., and Ricci, A.J. (2009). Localization of inner hair cell mechanotransducer channels using high-speed calcium imaging. *Nature Neuroscience* *12*, 553–558.

Beurg, M., Michalski, N., Safieddine, S., Bouleau, Y., Schneggenburger, R., Chapman, E.R., Petit, C., and Dulon, D. (2010). Control of exocytosis by synaptotagmins and otoferlin in auditory hair cells. *The Journal of Neuroscience : the Official Journal of the Society for Neuroscience* *30*, 13281–13290.

Bianco, I.H., Ma, L.-H., Schoppik, D., Robson, D.N., Orger, M.B., Beck, J.C., Li, J.M., Schier, A.F., Engert, F., and Baker, R. (2012). The tangential nucleus controls a gravito-inertial vestibulo-ocular reflex. *Current Biology : CB* *22*, 1285–1295.

Bleckmann, H., and Zelick, R. (2009). Lateral line system of fish. *Integrative Zoology* *4*, 13–25.

Bock, J.B., Matern, H.T., Peden, A.A., and Scheller, R.H. (2001). A genomic perspective on membrane compartment organization. *Nature* *409*, 839–841.

Boëda, B., El-Amraoui, A., Bahloul, A., Goodyear, R., Daviet, L., Blanchard, S., Perfettini, I., Fath, K.R., Shorte, S., Reiners, J., et al. (2002). Myosin VIIa, harmonin and cadherin 23, three Usher I gene products that cooperate to shape the sensory hair cell bundle. *The EMBO Journal* *21*, 6689–6699.

Brandt, A., Khimich, D., and Moser, T. (2005). Few CaV1.3 channels regulate the exocytosis of a synaptic vesicle at the hair cell ribbon synapse. *The Journal of Neuroscience : the Official Journal of the Society for Neuroscience* *25*, 11577–11585.

Brandt, A., Striessnig, J., and Moser, T. (2003). CaV1.3 channels are essential for development and presynaptic activity of cochlear inner hair cells. *The Journal of Neuroscience : the Official Journal of the Society for Neuroscience* *23*, 10832–10840.

Brenner, S. (1974). The genetics of *Caenorhabditis elegans*. *Genetics* *77*, 71–94.

- Brockerhoff, S., Hurley, J., Janssen-Bienhold, U., Neuhauss, S., Driever, W., and Dowling, J. (1995). A Behavioral Screen for Isolating Zebrafish Mutants with Visual System Defects. *Proceedings of the National Academy of Sciences* 92, 10545–10549.
- Brodsky, M., Donahue, S., and Vaphiades, M. (2006). Skew deviation revisited. *Survey of Ophthalmology*.
- Brösamle, C., and Halpern, M.E. (2002). Characterization of myelination in the developing zebrafish. *Glia* 39, 47–57.
- Buck, L.M.J., Winter, M.J., Redfern, W.S., and Whitfield, T.T. (2012). Ototoxin-induced cellular damage in neuromasts disrupts lateral line function in larval zebrafish. *Hearing Research* 284, 67–81.
- Burgoyne, R.D., and Morgan, A. (2011). Chaperoning the SNAREs: a role in preventing neurodegeneration? *Nature Cell Biology* 13, 8–9.
- Burré, J., Sharma, M., Tsetsenis, T., Buchman, V., Etherton, M.R., and Südhof, T.C. (2010). Alpha-synuclein promotes SNARE-complex assembly in vivo and in vitro. *Science (New York, N.Y.)* 329, 1663–1667.
- Caberlotto, E., Michel, V., Foucher, I., Bahloul, A., Goodyear, R.J., Pepermans, E., Michalski, N., Perfettini, I., Alegria-Prévot, O., Chardenoux, S., et al. (2011). Usher type 1G protein sans is a critical component of the tip-link complex, a structure controlling actin polymerization in stereocilia. *Proceedings of the National Academy of Sciences of the United States of America* 108, 5825–5830.
- Cervi, A.L., Poling, K.R., and Higgs, D.M. (2012). Behavioral measure of frequency detection and discrimination in the zebrafish, *Danio rerio*. *Zebrafish* 9, 1–7.
- Chalfie, M. (2009). Neurosensory mechanotransduction. *Nature Reviews. Molecular Cell Biology* 10, 44–52.
- Chandra, S., Gallardo, G., Fernández-Chacón, R., Schlüter, O.M., and Südhof, T.C. (2005). Alpha-synuclein cooperates with CSPalpha in preventing neurodegeneration. *Cell* 123, 383–396.
- Chang, L.-F., Chen, S., Liu, C.-C., Pan, X., Jiang, J., Bai, X.-C., Xie, X., Wang, H.-W., and Sui, S.-F. (2012). Structural characterization of full-length NSF and 20S particles. *Nature Structural & Molecular Biology* 19, 268–275.
- Chapman, E.R. (2008). How does synaptotagmin trigger neurotransmitter release? *Annual Review of Biochemistry* 77, 615–641.

Chartier-Harlin, M.-C., Kachergus, J., Roumier, C., Mouroux, V., Douay, X., Lincoln, S., Levecque, C., Larvor, L., Andrieux, J., Hulihan, M., et al. (2004). Alpha-synuclein locus duplication as a cause of familial Parkinson's disease. *Lancet* *364*, 1167–1169.

Chung, W.-S., Shin, C.H., and Stainier, D.Y.R. (2008). Bmp2 signaling regulates the hepatic versus pancreatic fate decision. *Developmental Cell* *15*, 738–748.

Coimbra, R.S., Weil, D., Brottier, P., Blanchard, S., Levi, M., Hardelin, J.-P., Weissenbach, J., and Petit, C. (2002). A subtracted cDNA library from the zebrafish (*Danio rerio*) embryonic inner ear. *Genome Research* *12*, 1007–1011.

Cong, M., Perry, S.J., Hu, L.A., Hanson, P.I., Claing, A., and Lefkowitz, R.J. (2001). Binding of the beta2 adrenergic receptor to N-ethylmaleimide-sensitive factor regulates receptor recycling. *The Journal of Biological Chemistry* *276*, 45145–45152.

Cooper, B., Hemmerlein, M., Ammermüller, J., Imig, C., Reim, K., Lipstein, N., Kalla, S., Kawabe, H., Brose, N., Brandstätter, J.H., et al. (2012). Munc13-independent vesicle priming at mouse photoreceptor ribbon synapses. *The Journal of Neuroscience : the Official Journal of the Society for Neuroscience* *32*, 8040–8052.

Cordero-Morales, J.F., Gracheva, E.O., and Julius, D. (2011). Cytoplasmic ankyrin repeats of transient receptor potential A1 (TRPA1) dictate sensitivity to thermal and chemical stimuli. *Proceedings of the National Academy of Sciences of the United States of America* *108*, E1184–91.

Corey, D.P., García-Añoveros, J., Holt, J.R., Kwan, K.Y., Lin, S.-Y., Vollrath, M.A., Amalfitano, A., Cheung, E.L.-M., Derfler, B.H., Duggan, A., et al. (2004). TRPA1 is a candidate for the mechanosensitive transduction channel of vertebrate hair cells. *Nature* *432*, 723–730.

Crawford, A.C., Evans, M.G., and Fettiplace, R. (1989). Activation and adaptation of transducer currents in turtle hair cells. *The Journal of Physiology* *419*, 405–434.

Cuajungco, M.P., Grimm, C., and Heller, S. (2007). TRP channels as candidates for hearing and balance abnormalities in vertebrates. *Biochimica Et Biophysica Acta* *1772*, 1022–1027.

Curtis, L., Datta, P., Liu, X., Bogdanova, N., Heidelberger, R., and Janz, R. (2010). Syntaxin 3B is essential for the exocytosis of synaptic vesicles in ribbon synapses of the retina. *Neuroscience* *166*, 832–841.

Curtis, L.B., Doneske, B., Liu, X., Thaller, C., McNew, J.A., and Janz, R. (2008). Syntaxin 3b is a t-SNARE specific for ribbon synapses of the retina. *The Journal of Comparative Neurology* *510*, 550–559.

Delprat, B., Michel, V., Goodyear, R., Yamasaki, Y., Michalski, N., El-Amraoui, A., Perfettini, I., Legrain, P., Richardson, G., Hardelin, J.-P., et al. (2005). Myosin XVa and whirlin, two deafness gene products required for hair bundle growth, are located at the stereocilia tips and interact directly. *Human Molecular Genetics* *14*, 401–410.

tom Dieck, S., Altmann, W.D., Kessels, M.M., Qualmann, B., Regus, H., Brauner, D., Fejtová, A., Bracko, O., Gundelfinger, E.D., and Brandstätter, J.H. (2005). Molecular dissection of the photoreceptor ribbon synapse: physical interaction of Bassoon and RIBEYE is essential for the assembly of the ribbon complex. *The Journal of Cell Biology* *168*, 825–836.

Diekmann, H., Anichtchik, O., Fleming, A., Futter, M., Goldsmith, P., Roach, A., and Rubinsztein, D.C. (2009). Decreased BDNF levels are a major contributor to the embryonic phenotype of huntingtin knockdown zebrafish. *The Journal of Neuroscience : the Official Journal of the Society for Neuroscience* *29*, 1343–1349.

Dulon, D., Safieddine, S., Jones, S.M., and Petit, C. (2009). Otoferlin is critical for a highly sensitive and linear calcium-dependent exocytosis at vestibular hair cell ribbon synapses. *The Journal of Neuroscience : the Official Journal of the Society for Neuroscience* *29*, 10474–10487.

Easter, S.S., and Nicola, G.N. (1997). The development of eye movements in the zebrafish (*Danio rerio*). *Developmental Psychobiology* *31*, 267–276.

Eberl, D.F., Duyk, G.M., and Perrimon, N. (1997). A genetic screen for mutations that disrupt an auditory response in *Drosophila melanogaster*. *Proceedings of the National Academy of Sciences of the United States of America* *94*, 14837–14842.

Effertz, T., Nadrowski, B., Piepenbrock, D., Albert, J.T., and Göpfert, M.C. (2012). Direct gating and mechanical integrity of *Drosophila* auditory transducers require TRPN1. *Nature Neuroscience* *15*, 1198–1200.

Effertz, T., Wiek, R., and Göpfert, M.C. (2011). NompC TRP channel is essential for *Drosophila* sound receptor function. *Current Biology : CB* *21*, 592–597.

Eimon, P.M., Kratz, E., Varfolomeev, E., Hymowitz, S.G., Stern, H., Zha, J., and Ashkenazi, A. (2006). Delineation of the cell-extrinsic apoptosis pathway in the zebrafish. *Cell Death and Differentiation* *13*, 1619–1630.

Einhorn, Z., Trapani, J.G., Liu, Q., and Nicolson, T. (2012). Rabconnectin3 α promotes stable activity of the H⁺ pump on synaptic vesicles in hair cells. *The Journal of Neuroscience : the Official Journal of the Society for Neuroscience* *32*, 11144–11156.

- Elizondo, M.R., Arduini, B.L., Paulsen, J., MacDonald, E.L., Sabel, J.L., Henion, P.D., Cornell, R.A., and Parichy, D.M. (2005). Defective skeletogenesis with kidney stone formation in dwarf zebrafish mutant for *trpm7*. *Current Biology : CB* 15, 667–671.
- Elledge, H.M., Kazmierczak, P., Clark, P., Joseph, J.S., Kolatkar, A., Kuhn, P., and Müller, U. (2010). Structure of the N terminus of cadherin 23 reveals a new adhesion mechanism for a subset of cadherin superfamily members. *Proceedings of the National Academy of Sciences of the United States of America* 107, 10708–10712.
- Epps, H.V., Hayashi, M., and Lucast, L. (2004). The zebrafish *nrc* mutant reveals a role for the polyphosphoinositide phosphatase *Journal of*
- Ernest, S., Rauch, G.J., Haffter, P., Geisler, R., Petit, C., and Nicolson, T. (2000). *Mariner* is defective in myosin VIIA: a zebrafish model for human hereditary deafness. *Human Molecular Genetics* 9, 2189–2196.
- Eybalin, M., Renard, N., Aure, F., and Safieddine, S. (2002). Cysteine-string protein in inner hair cells of the organ of Corti: synaptic expression and upregulation at the onset of hearing. *European Journal of Neuroscience* 15, 1409–1420.
- Fan, C.-Y., Cowden, J., Simmons, S.O., Padilla, S., and Ramabhadran, R. Gene expression changes in developing zebrafish as potential markers for rapid developmental neurotoxicity screening. *Neurotoxicology and Teratology* 32, 91–98.
- Fasshauer, D., Sutton, R.B., Brunger, A.T., and Jahn, R. (1998). Conserved structural features of the synaptic fusion complex: SNARE proteins reclassified as Q- and R-SNAREs. *Proceedings of the National Academy of Sciences of the United States of America* 95, 15781–15786.
- Fernández-Chacón, R., Wölfel, M., Nishimune, H., Tabares, L., Schmitz, F., Castellano-Muñoz, M., Rosenmund, C., Montesinos, M.L., Sanes, J.R., Schneggenburger, R., et al. (2004). The synaptic vesicle protein CSP alpha prevents presynaptic degeneration. *Neuron* 42, 237–251.
- Fettiplace, R. (2009). Defining features of the hair cell mechano-electrical transducer channel. *Pflügers Archiv : European Journal of Physiology* 458, 1115–1123.
- Fremeau, R.T., Kam, K., Qureshi, T., Johnson, J., Copenhagen, D.R., Storm-Mathisen, J., Chaudhry, F.A., Nicoll, R.A., and Edwards, R.H. (2004). Vesicular glutamate transporters 1 and 2 target to functionally distinct synaptic release sites. *Science (New York, N.Y.)* 304, 1815–1819.
- Froehlicher, M., Liedtke, A., Groh, K.J., Neuhauss, S.C.F., Segner, H., and Eggen, R.I.L. (2009). Zebrafish (*Danio rerio*) neuromast: promising biological endpoint linking

developmental and toxicological studies. *Aquatic Toxicology* (Amsterdam, Netherlands) *95*, 307–319.

Furst, J., Sutton, R.B., Chen, J., Brunger, A.T., and Grigorieff, N. (2003). Electron cryomicroscopy structure of N-ethyl maleimide sensitive factor at 11 Å resolution. *The EMBO Journal* *22*, 4365–4374.

Gallardo, V.E., Liang, J., Behra, M., Elkahloun, A., Villablanca, E.J., Russo, V., Allende, M.L., and Burgess, S.M. (2010). Molecular dissection of the migrating posterior lateral line primordium during early development in zebrafish. *BMC Developmental Biology* *10*, 120.

García-Junco-Clemente, P., Cantero, G., Gómez-Sánchez, L., Linares-Clemente, P., Martínez-López, J.A., Luján, R., and Fernández-Chacón, R. (2010). Cysteine string protein- α prevents activity-dependent degeneration in GABAergic synapses. *The Journal of Neuroscience : the Official Journal of the Society for Neuroscience* *30*, 7377–7391.

Gasser, T. (2001). Genetics of Parkinson's disease. *Journal of Neurology* *248*, 833–840.

Germanà, A., Sánchez-Ramos, C., Guerrero, M.C., Calavia, M.G., Navarro, M., Zichichi, R., García-Suárez, O., Pérez-Piñera, P., and Vega, J.A. (2010). Expression and cell localization of brain-derived neurotrophic factor and TrkB during zebrafish retinal development. *Journal of Anatomy* *217*, 214–222.

von Gersdorff, H. (2001). Synaptic ribbons: versatile signal transducers. *Neuron* *29*, 7–10.

Ghysen, A., and Dambly-Chaudière, C. (2007). The lateral line microcosmos. *Genes & Development* *21*, 2118–2130.

Gleason, M.R., Nagiel, A., Jamet, S., Vologodskaya, M., López-Schier, H., and Hudspeth, A.J. (2009). The transmembrane inner ear (Tmie) protein is essential for normal hearing and balance in the zebrafish. *Proceedings of the National Academy of Sciences of the United States of America* *106*, 21347–21352.

Glover, G., Mueller, K.P., Söllner, C., Neuhauss, S.C.F., and Nicolson, T. (2012). The Usher gene cadherin 23 is expressed in the zebrafish brain and a subset of retinal amacrine cells. *Molecular Vision* *18*, 2309–2322.

Golby, J.A., Tolar, L.A., and Pallanck, L. (2001). Partitioning of N-ethylmaleimide-sensitive fusion (NSF) protein function in *Drosophila melanogaster*: dNSF1 is required in the nervous system, and dNSF2 is required in mesoderm. *Genetics* *158*, 265–278.

Gong, Z., Son, W., Chung, Y.D., Kim, J., Shin, D.W., McClung, C.A., Lee, Y., Lee, H.W., Chang, D.-J., Kaang, B.-K., et al. (2004). Two interdependent TRPV channel

subunits, inactive and Nanchung, mediate hearing in *Drosophila*. *The Journal of Neuroscience : the Official Journal of the Society for Neuroscience* 24, 9059–9066.

Gonzalez, R., Woods, R., and Eddins, S. (2004). Digital image processing using MATLAB.

Goodrich, L.V. (2005). Hear, hear for the zebrafish. *Neuron* 45, 3–5.

Gorski, J.A., Zeiler, S.R., Tamowski, S., and Jones, K.R. (2003). Brain-derived neurotrophic factor is required for the maintenance of cortical dendrites. *The Journal of Neuroscience : the Official Journal of the Society for Neuroscience* 23, 6856–6865.

Goto, H., Terunuma, M., Kanematsu, T., Misumi, Y., Moss, S.J., and Hirata, M. (2005). Direct interaction of N-ethylmaleimide-sensitive factor with GABA(A) receptor beta subunits. *Molecular and Cellular Neurosciences* 30, 197–206.

Granato, M., van Eeden, F.J., Schach, U., Trowe, T., Brand, M., Furutani-Seiki, M., Haffter, P., Hammerschmidt, M., Heisenberg, C.P., Jiang, Y.J., et al. (1996). Genes controlling and mediating locomotion behavior of the zebrafish embryo and larva. *Development (Cambridge, England)* 123, 399–413.

Gras, C., Herzog, E., Bellenchi, G.C., Bernard, V., Ravassard, P., Pohl, M., Gasnier, B., Giros, B., and El Mestikawy, S. (2002). A third vesicular glutamate transporter expressed by cholinergic and serotonergic neurons. *The Journal of Neuroscience : the Official Journal of the Society for Neuroscience* 22, 5442–5451.

Grati, M., and Kachar, B. (2011). Myosin VIIa and sans localization at stereocilia upper tip-link density implicates these Usher syndrome proteins in mechanotransduction. *Proceedings of the National Academy of Sciences of the United States of America* 108, 11476–11481.

Greten-Harrison, B., Polydoro, M., Morimoto-Tomita, M., Diao, L., Williams, A.M., Nie, E.H., Makani, S., Tian, N., Castillo, P.E., Buchman, V.L., et al. (2010). $\alpha\beta\gamma$ -Synuclein triple knockout mice reveal age-dependent neuronal dysfunction. *Proceedings of the National Academy of Sciences of the United States of America* 107, 19573–19578.

Grillet, N., Xiong, W., Reynolds, A., Kazmierczak, P., Sato, T., Lillo, C., Dumont, R.A., Hintermann, E., Sczaniecka, A., Schwander, M., et al. (2009). Harmonin mutations cause mechanotransduction defects in cochlear hair cells. *Neuron* 62, 375–387.

Göpfert, M.C., Albert, J.T., Nadrowski, B., and Kamikouchi, A. (2006). Specification of auditory sensitivity by *Drosophila* TRP channels. *Nature Neuroscience* 9, 999–1000.

Haas, A. (1998). NSF--fusion and beyond. *Trends in Cell Biology* 8, 471–473.

Haberman, A., Williamson, W.R., Epstein, D., Wang, D., Rina, S., Meinertzhagen, I.A., and Hiesinger, P.R. (2012). The synaptic vesicle SNARE neuronal Synaptobrevin promotes endolysosomal degradation and prevents neurodegeneration. *The Journal of Cell Biology* 196, 261–276.

Haffter, P., and Nüsslein-Volhard, C. (1996). Large scale genetics in a small vertebrate, the zebrafish. *The International Journal of Developmental Biology* 40, 221–227.

Hailey, D.W., Roberts, B., Owens, K.N., Stewart, A.K., Linbo, T., Pujol, R., Alper, S.L., Rubel, E.W., and Raible, D.W. (2012). Loss of Slc4a1b Chloride/Bicarbonate Exchanger Function Protects Mechanosensory Hair Cells from Aminoglycoside Damage in the Zebrafish Mutant persephone. *PLoS Genetics* 8, e1002971.

Hanson, P.I., Roth, R., Morisaki, H., Jahn, R., and Heuser, J.E. (1997). Structure and conformational changes in NSF and its membrane receptor complexes visualized by quick-freeze/deep-etch electron microscopy. *Cell* 90, 523–535.

Hartmann, M., Heumann, R., and Lessmann, V. (2001). Synaptic secretion of BDNF after high-frequency stimulation of glutamatergic synapses. *The EMBO Journal* 20, 5887–5897.

Haswell, E.S., Phillips, R., and Rees, D.C. (2011). Mechanosensitive channels: what can they do and how do they do it? *Structure (London, England : 1993)* 19, 1356–1369.

Heeroma, J.H., Roelandse, M., Wierda, K., van Aerde, K.I., Toonen, R.F.G., Hensbroek, R.A., Brussaard, A., Matus, A., and Verhage, M. (2004). Trophic support delays but does not prevent cell-intrinsic degeneration of neurons deficient for munc18-1. *The European Journal of Neuroscience* 20, 623–634.

Heffner, H., and Heffner, R. (2003). Audition. In *Handbook of Research Methods in Experimental Psychology*, (Boston: Blackwell), pp. 340–413.

Held, N., Smits, B.M.G., Gockeln, R., Schubert, S., Nave, H., Northrup, E., Cuppen, E., Hedrich, H.J., and Wedekind, D. (2011). A mutation in Myo15 leads to Usher-like symptoms in LEW/Ztm-ci2 rats. *PLoS One* 6, e15669.

Henshall, T.L., Tucker, B., Lumsden, A.L., Nornes, S., Lardelli, M.T., and Richards, R.I. (2009). Selective neuronal requirement for huntingtin in the developing zebrafish. *Human Molecular Genetics* 18, 4830–4842.

Heydorn, A., Søndergaard, B.P., Hadrup, N., Holst, B., Haft, C.R., and Schwartz, T.W. (2004). Distinct in vitro interaction pattern of dopamine receptor subtypes with adaptor proteins involved in post-endocytotic receptor targeting. *FEBS Letters* 556, 276–280.

Higgs, D.M., Rollo, A.K., Souza, M.J., and Popper, A.N. (2003). Development of form and function in peripheral auditory structures of the zebrafish (*Danio rerio*). *The Journal of the Acoustical Society of America* *113*, 1145–1154.

Higgs, D.M., Souza, M.J., Wilkins, H.R., Presson, J.C., and Popper, A.N. (2002). Age- and size-related changes in the inner ear and hearing ability of the adult zebrafish (*Danio rerio*). *Journal of the Association for Research in Otolaryngology : JARO* *3*, 174–184.

Hohl, T.M., Parlati, F., Wimmer, C., Rothman, J.E., Söllner, T.H., and Engelhardt, H. (1998). Arrangement of subunits in 20 S particles consisting of NSF, SNAPs, and SNARE complexes. *Molecular Cell* *2*, 539–548.

Holt, J.R., Gillespie, S.K.H., Provance, D.W., Shah, K., Shokat, K.M., Corey, D.P., Mercer, J.A., and Gillespie, P.G. (2002). A chemical-genetic strategy implicates myosin-1c in adaptation by hair cells. *Cell* *108*, 371–381.

Hong, W. (2005). SNAREs and traffic. *Biochimica Et Biophysica Acta* *1744*, 120–144.

Horwitz, G.C., Lelli, A., Géléoc, G.S.G., and Holt, J.R. (2010). HCN channels are not required for mechanotransduction in sensory hair cells of the mouse inner ear. *PloS One* *5*, e8627.

Horwitz, G.C., Risner-Janiczek, J.R., Jones, S.M., and Holt, J.R. (2011). HCN channels expressed in the inner ear are necessary for normal balance function. *The Journal of Neuroscience : the Official Journal of the Society for Neuroscience* *31*, 16814–16825.

Howard, J., and Bechstedt, S. (2004). Hypothesis: a helix of ankyrin repeats of the NOMPC-TRP ion channel is the gating spring of mechanoreceptors. *Current Biology : CB* *14*, R224–6.

Howard, J., and Hudspeth, A.J. (1988). Compliance of the hair bundle associated with gating of mechano-electrical transduction channels in the bullfrog's saccular hair cell. *Neuron* *1*, 189–199.

Hua, Z., Leal-Ortiz, S., Foss, S.M., Waites, C.L., Garner, C.C., Voglmaier, S.M., and Edwards, R.H. (2011). v-SNARE composition distinguishes synaptic vesicle pools. *Neuron* *71*, 474–487.

Huang, S.-P., Brown, B.M., and Craft, C.M. (2010). Visual Arrestin 1 acts as a modulator for N-ethylmaleimide-sensitive factor in the photoreceptor synapse. *The Journal of Neuroscience : the Official Journal of the Society for Neuroscience* *30*, 9381–9391.

Husson, C., Cantrelle, F.-X., Roblin, P., Didry, D., Le, K.H.D., Perez, J., Guittet, E., Van Heijenoort, C., Renault, L., and Carlier, M.-F. (2010). Multifunctionality of the beta-

thymosin/WH2 module: G-actin sequestration, actin filament growth, nucleation, and severing. *Annals of the New York Academy of Sciences* 1194, 44–52.

Huynh, H., Bottini, N., Williams, S., Cherepanov, V., Musumeci, L., Saito, K., Bruckner, S., Vachon, E., Wang, X., Kruger, J., et al. (2004). Control of vesicle fusion by a tyrosine phosphatase. *Nature Cell Biology* 6, 831–839.

Issa, F.A., Mazzochi, C., Mock, A.F., and Papazian, D.M. (2011). Spinocerebellar ataxia type 13 mutant potassium channel alters neuronal excitability and causes locomotor deficits in zebrafish. *The Journal of Neuroscience : the Official Journal of the Society for Neuroscience* 31, 6831–6841.

Jahn, R., and Scheller, R.H. (2006). SNAREs--engines for membrane fusion. *Nature Reviews. Molecular Cell Biology* 7, 631–643.

Jaramillo, F., and Hudspeth, A.J. (1993). Displacement-clamp measurement of the forces exerted by gating springs in the hair bundle. *Proceedings of the National Academy of Sciences of the United States of America* 90, 1330–1334.

Jeans, A.F., Oliver, P.L., Johnson, R., Capogna, M., Vikman, J., Molnár, Z., Babbs, A., Partridge, C.J., Salehi, A., Bengtsson, M., et al. (2007). A dominant mutation in Snap25 causes impaired vesicle trafficking, sensorimotor gating, and ataxia in the blind-drunk mouse. *Proceedings of the National Academy of Sciences of the United States of America* 104, 2431–2436.

Jivan, A., Earnest, S., Juang, Y.-C., and Cobb, M.H. (2009). Radial spoke protein 3 is a mammalian protein kinase A-anchoring protein that binds ERK1/2. *The Journal of Biological Chemistry* 284, 29437–29445.

Johnson, S.L., Franz, C., Kuhn, S., Furness, D.N., Rüttiger, L., Münkner, S., Rivolta, M.N., Seward, E.P., Herschman, H.R., Engel, J., et al. (2010). Synaptotagmin IV determines the linear Ca²⁺ dependence of vesicle fusion at auditory ribbon synapses. *Nature Neuroscience* 13, 45–52.

Juusola, M., French, A.S., Uusitalo, R.O., and Weckström, M. (1996). Information processing by graded-potential transmission through tonically active synapses. *Trends in Neurosciences* 19, 292–297.

Kantardzhieva, A., Peppi, M., Lane, W.S., and Sewell, W.F. (2012). Protein composition of immunoprecipitated synaptic ribbons. *Journal of Proteome Research* 11, 1163–1174.

Katbamna, B., Langerveld, A.J., and Ide, C.F. (2006). Aroclor 1254 impairs the hearing ability of *Xenopus laevis*. *Journal of Comparative Physiology. A, Neuroethology, Sensory, Neural, and Behavioral Physiology* 192, 971–983.

Katsumata, O., Ohara, N., Tamaki, H., Niimura, T., Naganuma, H., Watanabe, M., and Sakagami, H. (2009). IQ-ArfGEF/BRAG1 is associated with synaptic ribbons in the mouse retina. *The European Journal of Neuroscience* *30*, 1509–1516.

Kawashima, Y., Géléoc, G.S.G., Kurima, K., Labay, V., Lelli, A., Asai, Y., Makishima, T., Wu, D.K., Della Santina, C.C., Holt, J.R., et al. (2011). Mechanotransduction in mouse inner ear hair cells requires transmembrane channel-like genes. *The Journal of Clinical Investigation* *121*, 4796–4809.

Kazmierczak, P., and Müller, U. (2012). Sensing sound: molecules that orchestrate mechanotransduction by hair cells. *Trends in Neurosciences* *35*, 220–229.

Kazmierczak, P., Sakaguchi, H., Tokita, J., Wilson-Kubalek, E.M., Milligan, R.A., Müller, U., and Kachar, B. (2007). Cadherin 23 and protocadherin 15 interact to form tip-link filaments in sensory hair cells. *Nature* *449*, 87–91.

Kernan, M., Cowan, D., and Zuker, C. (1994). Genetic dissection of mechanosensory transduction: mechanoreception-defective mutations of *Drosophila*. *Neuron* *12*, 1195–1206.

Khimich, D., Nouvian, R., Pujol, R., Tom Dieck, S., Egner, A., Gundelfinger, E.D., and Moser, T. (2005). Hair cell synaptic ribbons are essential for synchronous auditory signalling. *Nature* *434*, 889–894.

Kim, J., Chung, Y.D., Park, D.-Y., Choi, S., Shin, D.W., Soh, H., Lee, H.W., Son, W., Yim, J., Park, C.-S., et al. (2003). A TRPV family ion channel required for hearing in *Drosophila*. *Nature* *424*, 81–84.

Kimmel, C.B. (1989). Genetics and early development of zebrafish. *Trends in Genetics : TIG* *5*, 283–288.

Kitajiri, S., Makishima, T., Friedman, T.B., and Griffith, A.J. (2007). A novel mutation at the DFNA36 hearing loss locus reveals a critical function and potential genotype-phenotype correlation for amino acid-572 of TMC1. *Clinical Genetics* *71*, 148–152.

Knox, G.W., Isaacs, J., Woodard, D., Johnson, L., and Jordan, D. (1993). Short latency vestibular evoked potentials. *Otolaryngology--head and Neck Surgery : Official Journal of American Academy of Otolaryngology-Head and Neck Surgery* *108*, 265–269.

Knüsel, B., Beck, K.D., Winslow, J.W., Rosenthal, A., Burton, L.E., Widmer, H.R., Nikolics, K., and Hefti, F. (1992). Brain-derived neurotrophic factor administration protects basal forebrain cholinergic but not nigral dopaminergic neurons from degenerative changes after axotomy in the adult rat brain. *The Journal of Neuroscience : the Official Journal of the Society for Neuroscience* *12*, 4391–4402.

- Korn, H., and Faber, D.S. (2005). The Mauthner cell half a century later: a neurobiological model for decision-making? *Neuron* 47, 13–28.
- Krapivinsky, G., Mochida, S., Krapivinsky, L., Cibulsky, S.M., and Clapham, D.E. (2006). The TRPM7 ion channel functions in cholinergic synaptic vesicles and affects transmitter release. *Neuron* 52, 485–496.
- von Kriegstein, K., and Schmitz, F. (2003). The expression pattern and assembly profile of synaptic membrane proteins in ribbon synapses of the developing mouse retina. *Cell and Tissue Research* 311, 159–173.
- Kros, C.J., Marcotti, W., van Netten, S.M., Self, T.J., Libby, R.T., Brown, S.D.M., Richardson, G.P., and Steel, K.P. (2002). Reduced climbing and increased slipping adaptation in cochlear hair cells of mice with *Myo7a* mutations. *Nature Neuroscience* 5, 41–47.
- Kuczewski, N., Porcher, C., Lessmann, V., Medina, I., and Gaiarsa, J.-L. (2009). Activity-dependent dendritic release of BDNF and biological consequences. *Molecular Neurobiology* 39, 37–49.
- Kunwar, A., Tripathy, S.K., Xu, J., Mattson, M.K., Anand, P., Sigua, R., Vershinin, M., McKenney, R.J., Yu, C.C., Mogilner, A., et al. (2011). Mechanical stochastic tug-of-war models cannot explain bidirectional lipid-droplet transport. *Proceedings of the National Academy of Sciences of the United States of America* 108, 18960–18965.
- Kurima, K., Peters, L.M., Yang, Y., Riazuddin, S., Ahmed, Z.M., Naz, S., Arnaud, D., Drury, S., Mo, J., Makishima, T., et al. (2002). Dominant and recessive deafness caused by mutations of a novel gene, *TMC1*, required for cochlear hair-cell function. *Nature Genetics* 30, 277–284.
- Kurima, K., Yang, Y., Sorber, K., and Griffith, A.J. (2003). Characterization of the transmembrane channel-like (TMC) gene family: functional clues from hearing loss and epidermodysplasia verruciformis. *Genomics* 82, 300–308.
- Kurrasch, D.M., Nevin, L.M., Wong, J.S., Baier, H., and Ingraham, H.A. (2009). Neuroendocrine transcriptional programs adapt dynamically to the supply and demand for neuropeptides as revealed in NSF mutant zebrafish. *Neural Development* 4, 22.
- Kwan, K.M., Fujimoto, E., Grabher, C., Mangum, B.D., Hardy, M.E., Campbell, D.S., Parant, J.M., Yost, H.J., Kanki, J.P., and Chien, C.-B. (2007). The Tol2kit: a multisite gateway-based construction kit for Tol2 transposon transgenesis constructs. *Developmental Dynamics : an Official Publication of the American Association of Anatomists* 236, 3088–3099.

Kwan, K.Y., Allchorne, A.J., Vollrath, M.A., Christensen, A.P., Zhang, D.-S., Woolf, C.J., and Corey, D.P. (2006). TRPA1 contributes to cold, mechanical, and chemical nociception but is not essential for hair-cell transduction. *Neuron* 50, 277–289.

Küssel-Andermann, P., El-Amraoui, A., Safieddine, S., Hardelin, J.P., Nouaille, S., Camonis, J., and Petit, C. (2000). Unconventional myosin VIIA is a novel A-kinase-anchoring protein. *The Journal of Biological Chemistry* 275, 29654–29659.

Labay, V., Weichert, R.M., Makishima, T., and Griffith, A.J. (2010). Topology of transmembrane channel-like gene 1 protein. *Biochemistry* 49, 8592–8598.

Lagziel, A., Ahmed, Z.M., Schultz, J.M., Morell, R.J., Belyantseva, I.A., and Friedman, T.B. (2005). Spatiotemporal pattern and isoforms of cadherin 23 in wild type and waltzer mice during inner ear hair cell development. *Developmental Biology* 280, 295–306.

Lagziel, A., Overlack, N., Bernstein, S.L., Morell, R.J., Wolfrum, U., and Friedman, T.B. (2009). Expression of cadherin 23 isoforms is not conserved: implications for a mouse model of Usher syndrome type 1D. *Molecular Vision* 15, 1843–1857.

Lambert, F.M., Beck, J.C., Baker, R., and Straka, H. (2008). Semicircular canal size determines the developmental onset of angular vestibuloocular reflexes in larval *Xenopus*. *The Journal of Neuroscience : the Official Journal of the Society for Neuroscience* 28, 8086–8095.

Laviolette, M.J., Nunes, P., Peyre, J.-B., Aigaki, T., and Stewart, B.A. (2005). A genetic screen for suppressors of *Drosophila* NSF2 neuromuscular junction overgrowth. *Genetics* 170, 779–792.

Layton, M.G., Robertson, D., Everett, A.W., Mulders, W.H.A.M., and Yates, G.K. (2005). Cellular localization of voltage-gated calcium channels and synaptic vesicle-associated proteins in the guinea pig cochlea. *Journal of Molecular Neuroscience : MN* 27, 225–244.

Lenzen, C.U., Steinmann, D., Whiteheart, S.W., and Weis, W.I. (1998). Crystal structure of the hexamerization domain of N-ethylmaleimide-sensitive fusion protein. *Cell* 94, 525–536.

Lenzi, D., Runyeon, J.W., Crum, J., Ellisman, M.H., and Roberts, W.M. (1999). Synaptic vesicle populations in saccular hair cells reconstructed by electron tomography. *The Journal of Neuroscience : the Official Journal of the Society for Neuroscience* 19, 119–132.

Li, Y.X., Xu, Y., Ju, D., Lester, H.A., Davidson, N., and Schuman, E.M. (1998). Expression of a dominant negative TrkB receptor, T1, reveals a requirement for presynaptic signaling in BDNF-induced synaptic potentiation in cultured hippocampal

neurons. *Proceedings of the National Academy of Sciences of the United States of America* 95, 10884–10889.

Lieberman, L.D., Wang, H., and Liberman, M.C. (2011). Opposing gradients of ribbon size and AMPA receptor expression underlie sensitivity differences among cochlear-nerve/hair-cell synapses. *The Journal of Neuroscience : the Official Journal of the Society for Neuroscience* 31, 801–808.

Lieberman, M.C., Dodds, L.W., and Pierce, S. (1990). Afferent and efferent innervation of the cat cochlea: quantitative analysis with light and electron microscopy. *The Journal of Comparative Neurology* 301, 443–460.

Lin, Y.-C., and Koleske, A.J. (2010). Mechanisms of synapse and dendrite maintenance and their disruption in psychiatric and neurodegenerative disorders. *Annual Review of Neuroscience* 33, 349–378.

Littleton, J.T., Barnard, R.J., Titus, S.A., Slind, J., Chapman, E.R., and Ganetzky, B. (2001). SNARE-complex disassembly by NSF follows synaptic-vesicle fusion. *Proceedings of the National Academy of Sciences of the United States of America* 98, 12233–12238.

Lv, C., Gould, T.J., Bewersdorf, J., and Zenisek, D. (2012). High-resolution optical imaging of zebrafish larval ribbon synapse protein RIBEYE, RIM2, and CaV 1.4 by stimulation emission depletion microscopy. *Microscopy and Microanalysis : the Official Journal of Microscopy Society of America, Microbeam Analysis Society, Microscopical Society of Canada* 18, 745–752.

Lyons, D.A., Pogoda, H.-M., Voas, M.G., Woods, I.G., Diamond, B., Nix, R., Arana, N., Jacobs, J., and Talbot, W.S. (2005). *erbb3* and *erbb2* are essential for schwann cell migration and myelination in zebrafish. *Current Biology : CB* 15, 513–524.

López-Schier, H., Starr, C.J., Kappler, J.A., Kollmar, R., and Hudspeth, A.J. (2004). Directional cell migration establishes the axes of planar polarity in the posterior lateral-line organ of the zebrafish. *Developmental Cell* 7, 401–412.

Löscher, W. (2010). Abnormal circling behavior in rat mutants and its relevance to model specific brain dysfunctions. *Neuroscience and Biobehavioral Reviews* 34, 31–49.

Macpherson, L.J., Xiao, B., Kwan, K.Y., Petrus, M.J., Dubin, A.E., Hwang, S., Cravatt, B., Corey, D.P., and Patapoutian, A. (2007). An ion channel essential for sensing chemical damage. *The Journal of Neuroscience : the Official Journal of the Society for Neuroscience* 27, 11412–11415.

Magupalli, V.G., Schwarz, K., Alpadi, K., Natarajan, S., Seigel, G.M., and Schmitz, F. (2008). Multiple RIBEYE-RIBEYE interactions create a dynamic scaffold for the

formation of synaptic ribbons. *The Journal of Neuroscience : the Official Journal of the Society for Neuroscience* 28, 7954–7967.

Mandell, J.W., Townes-Anderson, E., Czernik, A.J., Cameron, R., Greengard, P., and De Camilli, P. (1990). Synapsins in the vertebrate retina: absence from ribbon synapses and heterogeneous distribution among conventional synapses. *Neuron* 5, 19–33.

Manji, S.S.M., Miller, K.A., Williams, L.H., and Dahl, H.-H.M. (2012). Identification of three novel hearing loss mouse strains with mutations in the *Tmc1* gene. *The American Journal of Pathology* 180, 1560–1569.

Marcotti, W., Erven, A., Johnson, S.L., Steel, K.P., and Kros, C.J. (2006). *Tmc1* is necessary for normal functional maturation and survival of inner and outer hair cells in the mouse cochlea. *The Journal of Physiology* 574, 677–698.

Matsushita, K., Morrell, C.N., Cambien, B., Yang, S.X., Yamakuchi, M., Bao, C., Hara, M.R., Quick, R.A., Cao, W., O'Rourke, B., et al. (2003). Nitric oxide regulates exocytosis by S-nitrosylation of N-ethylmaleimide-sensitive factor. *Cell* 115, 139–150.

Matsushita, K., Morrell, C.N., Mason, R.J.A., Yamakuchi, M., Khanday, F.A., Irani, K., and Lowenstein, C.J. (2005). Hydrogen peroxide regulation of endothelial exocytosis by inhibition of N-ethylmaleimide sensitive factor. *The Journal of Cell Biology* 170, 73–79.

Matteoli, M., Verderio, C., Rossetto, O., Iezzi, N., Coco, S., Schiavo, G., and Montecucco, C. (1996). Synaptic vesicle endocytosis mediates the entry of tetanus neurotoxin into hippocampal neurons. *Proceedings of the National Academy of Sciences of the United States of America* 93, 13310–13315.

Matthews, G., and Fuchs, P. (2010). The diverse roles of ribbon synapses in sensory neurotransmission. *Nature Reviews. Neuroscience* 11, 812–822.

Matveeva, E.A., Whiteheart, S.W., Vanaman, T.C., and Slevin, J.T. (2001). Phosphorylation of the N-ethylmaleimide-sensitive factor is associated with depolarization-dependent neurotransmitter release from synaptosomes. *The Journal of Biological Chemistry* 276, 12174–12181.

May, A.P., Misura, K.M., Whiteheart, S.W., and Weis, W.I. (1999). Crystal structure of the amino-terminal domain of N-ethylmaleimide-sensitive fusion protein. *Nature Cell Biology* 1, 175–182.

Mburu, P., Kikkawa, Y., Townsend, S., Romero, R., Yonekawa, H., and Brown, S.D.M. (2006). Whirlin complexes with p55 at the stereocilia tip during hair cell development. *Proceedings of the National Academy of Sciences of the United States of America* 103, 10973–10978.

McDonald, P.H., Cote, N.L., Lin, F.T., Premont, R.T., Pitcher, J.A., and Lefkowitz, R.J. (1999). Identification of NSF as a beta-arrestin1-binding protein. Implications for beta2-adrenergic receptor regulation. *The Journal of Biological Chemistry* 274, 10677–10680.

McRory, J.E., Rehak, R., Simms, B., Doering, C.J., Chen, L., Hermosilla, T., Duke, C., Dyck, R., and Zamponi, G.W. (2008). Syntaxin 1A is required for normal in utero development. *Biochemical and Biophysical Research Communications* 375, 372–377.

Meyers, J.R., MacDonald, R.B., Duggan, A., Lenzi, D., Standaert, D.G., Corwin, J.T., and Corey, D.P. (2003). Lighting up the senses: FM1-43 loading of sensory cells through nonselective ion channels. *The Journal of Neuroscience : the Official Journal of the Society for Neuroscience* 23, 4054–4065.

Michalski, N., Michel, V., Caberlotto, E., Lefèvre, G.M., van Aken, A.F.J., Tinevez, J.-Y., Bizard, E., Houbron, C., Weil, D., Hardelin, J.-P., et al. (2009). Harmonin-b, an actin-binding scaffold protein, is involved in the adaptation of mechano-electrical transduction by sensory hair cells. *Pflügers Archiv : European Journal of Physiology* 459, 115–130.

Michel, V., Goodyear, R.J., Weil, D., Marcotti, W., Perfettini, I., Wolfrum, U., Kros, C.J., Richardson, G.P., and Petit, C. (2005). Cadherin 23 is a component of the transient lateral links in the developing hair bundles of cochlear sensory cells. *Developmental Biology* 280, 281–294.

Michna, M., Knirsch, M., Hoda, J.-C., Muenkner, S., Langer, P., Platzer, J., Striessnig, J., and Engel, J. (2003). Cav1.3 (alpha1D) Ca²⁺ currents in neonatal outer hair cells of mice. *The Journal of Physiology* 553, 747–758.

Middelbeek, J., Clark, K., Venselaar, H., Huynen, M.A., and van Leeuwen, F.N. (2010). The alpha-kinase family: an exceptional branch on the protein kinase tree. *Cellular and Molecular Life Sciences : CMLS* 67, 875–890.

Mo, W., Chen, F., Nechiporuk, A., and Nicolson, T. (2010a). Movie 1. Representative eye movements of a 5 dpf wild-type larva rotated around an earth horizontal axis under infrared illumination.

Mo, W., Chen, F., Nechiporuk, A., and Nicolson, T. (2010b). Movie 2. Eye movements of a homozygous *cdh231619ag* larva in dark (upper panel) and bright conditions (lower panel) at 5 dpf.

Mo, W., Chen, F., Nechiporuk, A., and Nicolson, T. (2010c). Quantification of vestibular-induced eye movements in zebrafish larvae. *BMC Neuroscience* 11, 110.

Mo, W., and Nicolson, T. (2011). Both pre- and postsynaptic activity of Nsf prevents degeneration of hair-cell synapses. *PloS One* 6, e27146.

Moeller, A., Zhao, C., Fried, M.G., Wilson-Kubalek, E.M., Carragher, B., and Whiteheart, S.W. (2012). Nucleotide-dependent conformational changes in the N-Ethylmaleimide Sensitive Factor (NSF) and their potential role in SNARE complex disassembly. *Journal of Structural Biology* 177, 335–343.

Molnár, Z., López-Bendito, G., Small, J., Partridge, L.D., Blakemore, C., and Wilson, M.C. (2002). Normal development of embryonic thalamocortical connectivity in the absence of evoked synaptic activity. *The Journal of Neuroscience : the Official Journal of the Society for Neuroscience* 22, 10313–10323.

Moorman, S.J., Cordova, R., and Davies, S.A. (2002). A critical period for functional vestibular development in zebrafish. *Developmental Dynamics : an Official Publication of the American Association of Anatomists* 223, 285–291.

Morgans, C.W., Brandstätter, J.H., Kellerman, J., Betz, H., and Wässle, H. (1996). A SNARE complex containing syntaxin 3 is present in ribbon synapses of the retina. *The Journal of Neuroscience : the Official Journal of the Society for Neuroscience* 16, 6713–6721.

Mutai, H., Mann, S., and Heller, S. (2005). Identification of chicken transmembrane channel-like (TMC) genes: expression analysis in the cochlea. *Neuroscience* 132, 1115–1122.

Narayan, S.S., Temchin, A.N., Recio, A., and Ruggero, M.A. (1998). Frequency tuning of basilar membrane and auditory nerve fibers in the same cochleae. *Science (New York, N.Y.)* 282, 1882–1884.

Nauli, S.M., Alenghat, F.J., Luo, Y., Williams, E., Vassilev, P., Li, X., Elia, A.E.H., Lu, W., Brown, E.M., Quinn, S.J., et al. (2003). Polycystins 1 and 2 mediate mechanosensation in the primary cilium of kidney cells. *Nature Genetics* 33, 129–137.

Nave, K.-A., and Salzer, J.L. (2006). Axonal regulation of myelination by neuregulin 1. *Current Opinion in Neurobiology* 16, 492–500.

Nemzou N, R.M., Bulankina, A.V., Khimich, D., Giese, A., and Moser, T. (2006). Synaptic organization in cochlear inner hair cells deficient for the CaV1.3 (alpha1D) subunit of L-type Ca²⁺ channels. *Neuroscience* 141, 1849–1860.

Nicolson, T. (2005). The genetics of hearing and balance in zebrafish. *Annual Review of Genetics* 39, 9–22.

Nicolson, T., Rüsçh, A., Friedrich, R.W., Granato, M., Ruppertsberg, J.P., and Nüsslein-Volhard, C. (1998). Genetic analysis of vertebrate sensory hair cell mechanosensation: the zebrafish circler mutants. *Neuron* 20, 271–283.

- Niessen, C.M., Leckband, D., and Yap, A.S. (2011). Tissue organization by cadherin adhesion molecules: dynamic molecular and cellular mechanisms of morphogenetic regulation. *Physiological Reviews* 91, 691–731.
- Nishimune, A., Isaac, J.T., Molnar, E., Noel, J., Nash, S.R., Tagaya, M., Collingridge, G.L., Nakanishi, S., and Henley, J.M. (1998). NSF Binding to GluR2 Regulates Synaptic Transmission. *Neuron* 21, 87–97.
- Nosková, L., Stránecký, V., Hartmannová, H., Přistoupilová, A., Barešová, V., Ivánek, R., Hůlková, H., Jahnová, H., van der Zee, J., Staropoli, J.F., et al. (2011). Mutations in DNAJC5, encoding cysteine-string protein alpha, cause autosomal-dominant adult-onset neuronal ceroid lipofuscinosis. *American Journal of Human Genetics* 89, 241–252.
- Nouvian, R., Beutner, D., Parsons, T.D., and Moser, T. (2006). Structure and function of the hair cell ribbon synapse. *The Journal of Membrane Biology* 209, 153–165.
- Nouvian, R., Neef, J., Bulankina, A.V., Reisinger, E., Pangršič, T., Frank, T., Sikorra, S., Brose, N., Binz, T., and Moser, T. (2011). Exocytosis at the hair cell ribbon synapse apparently operates without neuronal SNARE proteins. *Nature Neuroscience* 14, 411–413.
- Nusslein-Volhard, C., and Dham, R. (2002). *Zebrafish: A Practical Approach* (Oxford: Oxford University Press).
- Nystuen, A.M., Schwendinger, J.K., Sachs, A.J., Yang, A.W., and Haider, N.B. (2007). A null mutation in VAMP1/synaptobrevin is associated with neurological defects and prewean mortality in the lethal-wasting mouse mutant. *Neurogenetics* 8, 1–10.
- Nüsslein-Volhard, C., and Wieschaus, E. (1980). Mutations affecting segment number and polarity in *Drosophila*. *Nature* 287, 795–801.
- Obholzer, N., Wolfson, S., Trapani, J.G., Mo, W., Nechiporuk, A., Busch-Nentwich, E., Seiler, C., Sidi, S., Sollner, C., Duncan, R.N., et al. (2008). Vesicular glutamate transporter 3 is required for synaptic transmission in zebrafish hair cells. *The Journal of Neuroscience : the Official Journal of the Society for Neuroscience* 28, 2110–2118.
- Ohyama, T., Verstreken, P., Ly, C.V., Rosenmund, T., Rajan, A., Tien, A.-C., Haueter, C., Schulze, K.L., and Bellen, H.J. (2007). Huntingtin-interacting protein 14, a palmitoyl transferase required for exocytosis and targeting of CSP to synaptic vesicles. *The Journal of Cell Biology* 179, 1481–1496.
- Osten, P., Srivastava, S., Inman, G., Vilim, F., Khatri, L., Lee, L., States, B., Einheber, S., Milner, T., Hanson, P., et al. (1998). The AMPA Receptor GluR2 C Terminus Can Mediate a Reversible, ATP-Dependent Interaction with NSF and α - and β -SNAPs. *Neuron* 21, 99–110.

- Owsianik, G., Talavera, K., Voets, T., and Nilius, B. (2006). Permeation and selectivity of TRP channels. *Annual Review of Physiology* 68, 685–717.
- Di Palma, F., Holme, R.H., Bryda, E.C., Belyantseva, I.A., Pellegrino, R., Kachar, B., Steel, K.P., and Noben-Trauth, K. (2001). Mutations in *Cdh23*, encoding a new type of cadherin, cause stereocilia disorganization in waltzer, the mouse model for Usher syndrome type 1D. *Nature Genetics* 27, 103–107.
- Pan, L., Yan, J., Wu, L., and Zhang, M. (2009). Assembling stable hair cell tip link complex via multidentate interactions between harmonin and cadherin 23. *Proceedings of the National Academy of Sciences of the United States of America* 106, 5575–5580.
- Peng, A.W., Salles, F.T., Pan, B., and Ricci, A.J. (2011). Integrating the biophysical and molecular mechanisms of auditory hair cell mechanotransduction. *Nature Communications* 2, 523.
- Phillips, K.R., Tong, S., Goodyear, R., Richardson, G.P., and Cyr, J.L. (2006). Stereociliary myosin-1c receptors are sensitive to calcium chelation and absent from cadherin 23 mutant mice. *The Journal of Neuroscience : the Official Journal of the Society for Neuroscience* 26, 10777–10788.
- Pickles, J.O., Comis, S.D., and Osborne, M.P. (1984). Cross-links between stereocilia in the guinea pig organ of Corti, and their possible relation to sensory transduction. *Hearing Research* 15, 103–112.
- Pontier, S.M., Lahaie, N., Ginham, R., St-Gelais, F., Bonin, H., Bell, D.J., Flynn, H., Trudeau, L.-E., McIlhinney, J., White, J.H., et al. (2006). Coordinated action of NSF and PKC regulates GABAB receptor signaling efficacy. *The EMBO Journal* 25, 2698–2709.
- Popper, A.N., and Fay, R.R. (1993). Sound detection and processing by fish: critical review and major research questions. *Brain, Behavior and Evolution* 41, 14–38.
- Powers, R.J., Roy, S., Atilgan, E., Brownell, W.E., Sun, S.X., Gillespie, P.G., and Spector, A.A. (2012). Stereocilia membrane deformation: implications for the gating spring and mechanotransduction channel. *Biophysical Journal* 102, 201–210.
- Preyer, S., Hemmert, W., Zenner, H.P., and Gummer, A.W. (1995). Abolition of the receptor potential response of isolated mammalian outer hair cells by hair-bundle treatment with elastase: a test of the tip-link hypothesis. *Hearing Research* 89, 187–193.
- Prober, D.A., Zimmerman, S., Myers, B.R., McDermott, B.M., Kim, S.-H., Caron, S., Rihel, J., Solnica-Krezel, L., Julius, D., Hudspeth, A.J., et al. (2008). Zebrafish TRPA1 channels are required for chemosensation but not for thermosensation or mechanosensory hair cell function. *The Journal of Neuroscience : the Official Journal of the Society for Neuroscience* 28, 10102–10110.

Quick, K., Zhao, J., Eijkelkamp, N., Linley, J.E., Rugiero, F., Cox, J.J., Raouf, R., Gringhuis, M., Sexton, J.E., Abramowitz, J., et al. (2012). TRPC3 and TRPC6 are essential for normal mechanotransduction in subsets of sensory neurons and cochlear hair cells. *Open Biology* 2, 120068.

Raible, D.W., and Kruse, G.J. (2000). Organization of the lateral line system in embryonic zebrafish. *The Journal of Comparative Neurology* 421, 189–198.

Ramakrishnan, N.A., Drescher, M.J., Barretto, R.L., Beisel, K.W., Hatfield, J.S., and Drescher, D.G. (2009). Calcium-dependent binding of HCN1 channel protein to hair cell stereociliary tip link protein protocadherin 15 CD3. *The Journal of Biological Chemistry* 284, 3227–3238.

Ramakrishnan, N.A., Drescher, M.J., and Drescher, D.G. (2012a). The SNARE complex in neuronal and sensory cells. *Molecular and Cellular Neurosciences* 50, 58–69.

Ramakrishnan, N.A., Drescher, M.J., Khan, K.M., Hatfield, J.S., and Drescher, D.G. (2012b). HCN1 and HCN2 are expressed in cochlear hair cells: HCN1 can form a ternary complex with protocadherin 15 CD3 and F-actin-binding filamin A or can interact with HCN2. *The Journal of Biological Chemistry*.

Rasband, M.N., Trimmer, J.S., Peles, E., Levinson, S.R., and Shrager, P. (1999). K⁺ channel distribution and clustering in developing and hypomyelinated axons of the optic nerve. *Journal of Neurocytology* 28, 319–331.

Raybould, N.P., Jagger, D.J., Kanjhan, R., Greenwood, D., Laslo, P., Hoya, N., Soeller, C., Cannell, M.B., and Housley, G.D. (2007). TRPC-like conductance mediates restoration of intracellular Ca²⁺ in cochlear outer hair cells in the guinea pig and rat. *The Journal of Physiology* 579, 101–113.

Regehr, W.G., Carey, M.R., and Best, A.R. (2009). Activity-dependent regulation of synapses by retrograde messengers. *Neuron* 63, 154–170.

Reim, K., Wegmeyer, H., Brandstätter, J.H., Xue, M., Rosenmund, C., Dresbach, T., Hofmann, K., and Brose, N. (2005). Structurally and functionally unique complexins at retinal ribbon synapses. *The Journal of Cell Biology* 169, 669–680.

Reiners, J., Märker, T., Jürgens, K., Reidel, B., and Wolfrum, U. (2005a). Photoreceptor expression of the Usher syndrome type 1 protein protocadherin 15 (USH1F) and its interaction with the scaffold protein harmonin (USH1C). *Molecular Vision* 11, 347–355.

Reiners, J., Reidel, B., El-Amraoui, A., Boëda, B., Huber, I., Petit, C., and Wolfrum, U. (2003). Differential distribution of harmonin isoforms and their possible role in Usher-1 protein complexes in mammalian photoreceptor cells. *Investigative Ophthalmology & Visual Science* 44, 5006–5015.

Reiners, J., van Wijk, E., Märker, T., Zimmermann, U., Jürgens, K., te Brinke, H., Overlack, N., Roepman, R., Knipper, M., Kremer, H., et al. (2005b). Scaffold protein harmonin (USH1C) provides molecular links between Usher syndrome type 1 and type 2. *Human Molecular Genetics* *14*, 3933–3943.

Reisinger, E., Bresee, C., Neef, J., Nair, R., Reuter, K., Bulankina, A., Nouvian, R., Koch, M., Bückers, J., Kastrup, L., et al. (2011). Probing the functional equivalence of otoferlin and synaptotagmin 1 in exocytosis. *The Journal of Neuroscience : the Official Journal of the Society for Neuroscience* *31*, 4886–4895.

Ricci, A.J., Crawford, A.C., and Fettiplace, R. (2002). Mechanisms of active hair bundle motion in auditory hair cells. *The Journal of Neuroscience : the Official Journal of the Society for Neuroscience* *22*, 44–52.

Ricci, A.J., Crawford, A.C., and Fettiplace, R. (2003). Tonotopic variation in the conductance of the hair cell mechanotransducer channel. *Neuron* *40*, 983–990.

Richardson, G.P., de Monvel, J.B., and Petit, C. (2011). How the genetics of deafness illuminates auditory physiology. *Annual Review of Physiology* *73*, 311–334.

Riley, B.B., and Moorman, S.J. (2000). Development of utricular otoliths, but not saccular otoliths, is necessary for vestibular function and survival in zebrafish. *Journal of Neurobiology* *43*, 329–337.

Riley, B.B., and Phillips, B.T. (2003). Ringing in the new ear: resolution of cell interactions in otic development. *Developmental Biology* *261*, 289–312.

Roberts, W.M., Jacobs, R.A., and Hudspeth, A.J. (1990). Colocalization of ion channels involved in frequency selectivity and synaptic transmission at presynaptic active zones of hair cells. *The Journal of Neuroscience : the Official Journal of the Society for Neuroscience* *10*, 3664–3684.

Rodriguez-Contreras, A., and Yamoah, E.N. (2001). Direct measurement of single-channel Ca(2+) currents in bullfrog hair cells reveals two distinct channel subtypes. *The Journal of Physiology* *534*, 669–689.

Rohregger, M., and Dieringer, N. (2002). Principles of linear and angular vestibuloocular reflex organization in the frog. *Journal of Neurophysiology*.

Roux, I., Safieddine, S., Nouvian, R., Grati, M., Simmler, M.-C., Bahloul, A., Perfettini, I., Le Gall, M., Rostaing, P., Hamard, G., et al. (2006). Otoferlin, defective in a human deafness form, is essential for exocytosis at the auditory ribbon synapse. *Cell* *127*, 277–289.

- Rozas, J.L., Gómez-Sánchez, L., Mircheski, J., Linares-Clemente, P., Nieto-González, J.L., Vázquez, M.E., Luján, R., and Fernández-Chacón, R. (2012). Motoneurons require cysteine string protein- α to maintain the readily releasable vesicular pool and synaptic vesicle recycling. *Neuron* 74, 151–165.
- Ruel, J., Emery, S., Nouvian, R., Bersot, T., Amilhon, B., Van Rybroek, J.M., Rebillard, G., Lenoir, M., Eybalin, M., Delprat, B., et al. (2008). Impairment of SLC17A8 encoding vesicular glutamate transporter-3, VGLUT3, underlies nonsyndromic deafness DFNA25 and inner hair cell dysfunction in null mice. *American Journal of Human Genetics* 83, 278–292.
- Rzadzinska, A.K., Derr, A., Kachar, B., and Noben-Trauth, K. (2005). Sustained cadherin 23 expression in young and adult cochlea of normal and hearing-impaired mice. *Hearing Research* 208, 114–121.
- Rzadzinska, A.K., and Steel, K.P. (2009). Presence of interstereocilial links in waltzer mutants suggests Cdh23 is not essential for tip link formation. *Neuroscience* 158, 365–368.
- Safieddine, S., El-Amraoui, A., and Petit, C. (2012). The auditory hair cell ribbon synapse: from assembly to function. *Annual Review of Neuroscience* 35, 509–528.
- Safieddine, S., and Wenthold, R.J. (1999). SNARE complex at the ribbon synapses of cochlear hair cells: analysis of synaptic vesicle- and synaptic membrane-associated proteins. *European Journal of Neuroscience* 11, 803–812.
- Sander, L.E., Frank, S.P.C., Bolat, S., Blank, U., Galli, T., Bigalke, H., Bischoff, S.C., and Lorentz, A. (2008). Vesicle associated membrane protein (VAMP)-7 and VAMP-8, but not VAMP-2 or VAMP-3, are required for activation-induced degranulation of mature human mast cells. *European Journal of Immunology* 38, 855–863.
- Sanyal, S., and Krishnan, K.S. (2001). Lethal comatose mutation in *Drosophila* reveals possible role for NSF in neurogenesis. *Neuroreport* 12, 1363–1366.
- Savaskan, N.E., Bräuer, A.U., and Nitsch, R. (2004). Molecular cloning and expression regulation of PRG-3, a new member of the plasticity-related gene family. *The European Journal of Neuroscience* 19, 212–220.
- Schikorski, T., and Stevens, C.F. (1997). Quantitative ultrastructural analysis of hippocampal excitatory synapses. *The Journal of Neuroscience : the Official Journal of the Society for Neuroscience* 17, 5858–5867.
- Schmitz, F. (2009). The making of synaptic ribbons: how they are built and what they do. *The Neuroscientist : a Review Journal Bringing Neurobiology, Neurology and Psychiatry* 15, 611–624.

- Schmitz, F., Königstorfer, A., and Südhof, T.C. (2000). RIBEYE, a component of synaptic ribbons: a protein's journey through evolution provides insight into synaptic ribbon function. *Neuron* 28, 857–872.
- Schmitz, F., Tabares, L., Khimich, D., Strenzke, N., de la Villa-Polo, P., Castellano-Muñoz, M., Bulankina, A., Moser, T., Fernández-Chacón, R., and Südhof, T.C. (2006). CSPalpha-deficiency causes massive and rapid photoreceptor degeneration. *Proceedings of the National Academy of Sciences of the United States of America* 103, 2926–2931.
- Schnee, M.E., Lawton, D.M., Furness, D.N., Benke, T.A., and Ricci, A.J. (2005). Auditory hair cell-afferent fiber synapses are specialized to operate at their best frequencies. *Neuron* 47, 243–254.
- Schoch, S., Deák, F., Königstorfer, A., Mozhayeva, M., Sara, Y., Südhof, T.C., and Kavalali, E.T. (2001). SNARE function analyzed in synaptobrevin/VAMP knockout mice. *Science* 294, 1117–1122.
- Schultz, J.M., Bhatti, R., Madeo, A.C., Turriff, A., Muskett, J.A., Zalewski, C.K., King, K.A., Ahmed, Z.M., Riazuddin, S., Ahmad, N., et al. (2011). Allelic hierarchy of CDH23 mutations causing non-syndromic deafness DFNB12 or Usher syndrome USH1D in compound heterozygotes. *Journal of Medical Genetics* 48, 767–775.
- Schwarz, K., Natarajan, S., Kassas, N., Vitale, N., and Schmitz, F. (2011). The synaptic ribbon is a site of phosphatidic acid generation in ribbon synapses. *The Journal of Neuroscience : the Official Journal of the Society for Neuroscience* 31, 15996–16011.
- Seal, R.P., Akil, O., Yi, E., Weber, C.M., Grant, L., Yoo, J., Clause, A., Kandler, K., Noebels, J.L., Glowatzki, E., et al. (2008). Sensorineural deafness and seizures in mice lacking vesicular glutamate transporter 3. *Neuron* 57, 263–275.
- Seiler, C., Ben-David, O., Sidi, S., Hendrich, O., Rusch, A., Burnside, B., Avraham, K.B., and Nicolson, T. (2004). Myosin VI is required for structural integrity of the apical surface of sensory hair cells in zebrafish. *Developmental Biology* 272, 328–338.
- Seiler, C., Finger-Baier, K.C., Rinner, O., Makhankov, Y.V., Schwarz, H., Neuhaus, S.C.F., and Nicolson, T. (2005). Duplicated genes with split functions: independent roles of protocadherin15 orthologues in zebrafish hearing and vision. *Development (Cambridge, England)* 132, 615–623.
- Seiler, C., and Nicolson, T. (1999). Defective calmodulin-dependent rapid apical endocytosis in zebrafish sensory hair cell mutants. *Journal of Neurobiology* 41, 424–434.
- Self, T., Mahony, M., Fleming, J., Walsh, J., Brown, S.D., and Steel, K.P. (1998). Shaker-1 mutations reveal roles for myosin VIIA in both development and function of cochlear hair cells. *Development (Cambridge, England)* 125, 557–566.

Sendin, G., Bulankina, A.V., Riedel, D., and Moser, T. (2007). Maturation of ribbon synapses in hair cells is driven by thyroid hormone. *The Journal of Neuroscience : the Official Journal of the Society for Neuroscience* 27, 3163–3173.

Senften, M., Schwander, M., Kazmierczak, P., Lillo, C., Shin, J.-B., Hasson, T., Géléoc, G.S.G., Gillespie, P.G., Williams, D., Holt, J.R., et al. (2006). Physical and functional interaction between protocadherin 15 and myosin VIIa in mechanosensory hair cells. *The Journal of Neuroscience : the Official Journal of the Society for Neuroscience* 26, 2060–2071.

Sengupta, S., George, M., Miller, K.K., Naik, K., Chou, J., Cheatham, M.A., Dallos, P., Naramura, M., Band, H., and Zheng, J. (2009). EHD4 and CDH23 are interacting partners in cochlear hair cells. *The Journal of Biological Chemistry* 284, 20121–20129.

Shao, S., and Hegde, R.S. (2011). Membrane protein insertion at the endoplasmic reticulum. *Annual Review of Cell and Developmental Biology* 27, 25–56.

Sharma, M., Burré, J., Bronk, P., Zhang, Y., Xu, W., and Südhof, T.C. (2012). CSP α knockout causes neurodegeneration by impairing SNAP-25 function. *The EMBO Journal* 31, 829–841.

Sharma, M., Burré, J., and Südhof, T.C. (2011). CSP α promotes SNARE-complex assembly by chaperoning SNAP-25 during synaptic activity. *Nature Cell Biology* 13, 30–39.

Sheets, L., Trapani, J.G., Mo, W., Obholzer, N., and Nicolson, T. (2011). Ribeye is required for presynaptic Ca(V)1.3a channel localization and afferent innervation of sensory hair cells. *Development (Cambridge, England)* 138, 1309–1319.

Sherry, D.M., Mitchell, R., Standifer, K.M., and du Plessis, B. (2006). Distribution of plasma membrane-associated syntaxins 1 through 4 indicates distinct trafficking functions in the synaptic layers of the mouse retina. *BMC Neuroscience* 7, 54.

Shin, C.H., Chung, W.-S., Hong, S.-K., Ober, E.A., Verkade, H., Field, H.A., Huisken, J., and Stainier, D.Y.R. (2008). Multiple roles for Med12 in vertebrate endoderm development. *Developmental Biology* 317, 467–479.

Shin, J.-B., Adams, D., Paukert, M., Siba, M., Sidi, S., Levin, M., Gillespie, P.G., and Gründer, S. (2005). *Xenopus* TRPN1 (NOMPC) localizes to microtubule-based cilia in epithelial cells, including inner-ear hair cells. *Proceedings of the National Academy of Sciences of the United States of America* 102, 12572–12577.

Shotwell, S.L., Jacobs, R., and Hudspeth, A.J. (1981). Directional sensitivity of individual vertebrate hair cells to controlled deflection of their hair bundles. *Annals of the New York Academy of Sciences* 374, 1–10.

- Sidi, S., Busch-Nentwich, E., Friedrich, R., Schoenberger, U., and Nicolson, T. (2004). *gemin1* encodes a zebrafish L-type calcium channel that localizes at sensory hair cell ribbon synapses. *The Journal of Neuroscience : the Official Journal of the Society for Neuroscience* 24, 4213–4223.
- Sidi, S., Friedrich, R.W., and Nicolson, T. (2003). NompC TRP channel required for vertebrate sensory hair cell mechanotransduction. *Science (New York, N.Y.)* 301, 96–99.
- Siemens, J., Kazmierczak, P., Reynolds, A., Sticker, M., Littlewood-Evans, A., and Müller, U. (2002). The Usher syndrome proteins cadherin 23 and harmonin form a complex by means of PDZ-domain interactions. *Proceedings of the National Academy of Sciences of the United States of America* 99, 14946–14951.
- Siemens, J., Lillo, C., Dumont, R.A., Reynolds, A., Williams, D.S., Gillespie, P.G., and Müller, U. (2004). Cadherin 23 is a component of the tip link in hair-cell stereocilia. *Nature* 428, 950–955.
- Singleton, A.B., Farrer, M., Johnson, J., Singleton, A., Hague, S., Kachergus, J., Hulihan, M., Peuralinna, T., Dutra, A., Nussbaum, R., et al. (2003). alpha-Synuclein locus triplication causes Parkinson's disease. *Science (New York, N.Y.)* 302, 841.
- Sisneros, J.A. (2007). Saccular potentials of the vocal plainfin midshipman fish, *Porichthys notatus*. *Journal of Comparative Physiology. A, Neuroethology, Sensory, Neural, and Behavioral Physiology* 193, 413–424.
- Slepecky, N.B., Galsky, M.D., Swartzentruber-Martin, H., and Savage, J. (2000). Study of afferent nerve terminals and fibers in the gerbil cochlea: distribution by size. *Hearing Research* 144, 124–134.
- Sobkowicz, H.M., Rose, J.E., Scott, G.E., and Slapnick, S.M. (1982). Ribbon synapses in the developing intact and cultured organ of Corti in the mouse. *The Journal of Neuroscience : the Official Journal of the Society for Neuroscience* 2, 942–957.
- Song, I., Kamboj, S., Xia, J., Dong, H., Liao, D., and Huganir, R.L. (1998). Interaction of the N-ethylmaleimide-sensitive factor with AMPA receptors. *Neuron* 21, 393–400.
- Sotomayor, M., Weihofen, W.A., Gaudet, R., and Corey, D.P. (2010). Structural determinants of cadherin-23 function in hearing and deafness. *Neuron* 66, 85–100.
- Sotomayor, M., Weihofen, W.A., Gaudet, R., and Corey, D.P. (2012). Structure of a force-conveying cadherin bond essential for inner-ear mechanotransduction. *Nature* 492, 128–132.
- Spillantini, M.G., Schmidt, M.L., Lee, V.M., Trojanowski, J.Q., Jakes, R., and Goedert, M. (1997). Alpha-synuclein in Lewy bodies. *Nature* 388, 839–840.

Stagljar, I., Korostensky, C., Johnsson, N., and te Heesen, S. (1998). A genetic system based on split-ubiquitin for the analysis of interactions between membrane proteins in vivo. *Proceedings of the National Academy of Sciences of the United States of America* 95, 5187–5192.

Starr, C.J., Kappler, J.A., Chan, D.K., Kollmar, R., and Hudspeth, A.J. (2004). Mutation of the zebrafish choroideremia gene encoding Rab escort protein 1 devastates hair cells. *Proceedings of the National Academy of Sciences of the United States of America* 101, 2572–2577.

Stauffer, E.A., Scarborough, J.D., Hirono, M., Miller, E.D., Shah, K., Mercer, J.A., Holt, J.R., and Gillespie, P.G. (2005). Fast adaptation in vestibular hair cells requires myosin-1c activity. *Neuron* 47, 541–553.

Steigelman, K.A., Lelli, A., Wu, X., Gao, J., Lin, S., Piontek, K., Wodarczyk, C., Boletta, A., Kim, H., Qian, F., et al. (2011). Polycystin-1 is required for stereocilia structure but not for mechanotransduction in inner ear hair cells. *The Journal of Neuroscience : the Official Journal of the Society for Neuroscience* 31, 12241–12250.

Stepanyan, R., and Frolenkov, G.I. (2009). Fast adaptation and Ca²⁺ sensitivity of the mechanotransducer require myosin-XVa in inner but not outer cochlear hair cells. *The Journal of Neuroscience : the Official Journal of the Society for Neuroscience* 29, 4023–4034.

Stewart, B.A., Pearce, J., Bajec, M., and Khorana, R. (2005). Disruption of synaptic development and ultrastructure by *Drosophila* NSF2 alleles. *The Journal of Comparative Neurology* 488, 101–111.

Stowers, R.S., and Isacoff, E.Y. (2007). *Drosophila* huntingtin-interacting protein 14 is a presynaptic protein required for photoreceptor synaptic transmission and expression of the palmitoylated proteins synaptosome-associated protein 25 and cysteine string protein. *The Journal of Neuroscience : the Official Journal of the Society for Neuroscience* 27, 12874–12883.

Suli, A., Watson, G.M., Rubel, E.W., and Raible, D.W. (2012). Rheotaxis in larval zebrafish is mediated by lateral line mechanosensory hair cells. *PloS One* 7, e29727.

Sun, Y., Liu, L., Ben-Shahar, Y., Jacobs, J.S., Eberl, D.F., and Welsh, M.J. (2009). TRPA channels distinguish gravity sensing from hearing in Johnston's organ. *Proceedings of the National Academy of Sciences of the United States of America* 106, 13606–13611.

Söllner, C., Rauch, G.-J., Siemens, J., Geisler, R., Schuster, S.C., Müller, U., and Nicolson, T. (2004). Mutations in cadherin 23 affect tip links in zebrafish sensory hair cells. *Nature* 428, 955–959.

- Südhof, T.C. (2012). Calcium control of neurotransmitter release. *Cold Spring Harbor Perspectives in Biology* 4, a011353.
- Südhof, T.C., and Rizo, J. (2011). Synaptic vesicle exocytosis. *Cold Spring Harbor Perspectives in Biology* 3,.
- Tabuchi, K., Suzuki, M., Mizuno, A., and Hara, A. (2005). Hearing impairment in TRPV4 knockout mice. *Neuroscience Letters* 382, 304–308.
- Tanimoto, M., Ota, Y., and Horikawa, K. (2009). ... of Inner Ear after Formation of Functional Afferent Pathway in Zebrafish. *Journal of Neuroscience*.
- Thisse, B., Heyer, V., Lux, A., Alunni, V., Degrave, A., Seiliez, I., Kirchner, J., Parkhill, J.-P., and Thisse, C. (2004). Spatial and temporal expression of the zebrafish genome by large-scale in situ hybridization screening. *Methods in Cell Biology* 77, 505–519.
- Trapani, J.G., and Nicolson, T. (2010). Physiological recordings from zebrafish lateral-line hair cells and afferent neurons. *Methods in Cell Biology* 100, 219–231.
- Trapani, J.G., and Nicolson, T. (2011). Mechanism of spontaneous activity in afferent neurons of the zebrafish lateral-line organ. *The Journal of Neuroscience : the Official Journal of the Society for Neuroscience* 31, 1614–1623.
- Trapani, J.G., Obholzer, N., Mo, W., Brockerhoff, S.E., and Nicolson, T. (2009). Synaptotagmin1 is required for temporal fidelity of synaptic transmission in hair cells. *PLoS Genetics* 5, e1000480.
- Tucker, T., and Fettiplace, R. (1995). Confocal imaging of calcium microdomains and calcium extrusion in turtle hair cells. *Neuron* 15, 1323–1335.
- Uthaiyah, R.C., and Hudspeth, A.J. (2010). Molecular anatomy of the hair cell's ribbon synapse. *The Journal of Neuroscience : the Official Journal of the Society for Neuroscience* 30, 12387–12399.
- Venkatesan, J.K., Natarajan, S., Schwarz, K., Mayer, S.I., Alpadi, K., Magupalli, V.G., Sung, C.-H., and Schmitz, F. (2010). Nicotinamide adenine dinucleotide-dependent binding of the neuronal Ca²⁺ sensor protein GCAP2 to photoreceptor synaptic ribbons. *The Journal of Neuroscience : the Official Journal of the Society for Neuroscience* 30, 6559–6576.
- Verderio, C., Coco, S., Bacci, A., Rossetto, O., De Camilli, P., Montecucco, C., and Matteoli, M. (1999). Tetanus toxin blocks the exocytosis of synaptic vesicles clustered at synapses but not of synaptic vesicles in isolated axons. *The Journal of Neuroscience : the Official Journal of the Society for Neuroscience* 19, 6723–6732.

Voas, M.G., Lyons, D.A., Naylor, S.G., Arana, N., Rasband, M.N., and Talbot, W.S. (2007). α II-spectrin is essential for assembly of the nodes of Ranvier in myelinated axons. *Current Biology* : CB 17, 562–568.

Voets, T., Toonen, R.F., Brian, E.C., de Wit, H., Moser, T., Rettig, J., Südhof, T.C., Neher, E., and Verhage, M. (2001). Munc18-1 promotes large dense-core vesicle docking. *Neuron* 31, 581–591.

Vollrath, M.A., Kwan, K.Y., and Corey, D.P. (2007). The micromachinery of mechanotransduction in hair cells. *Annual Review of Neuroscience* 30, 339–365.

Vreugde, S., Erven, A., Kros, C.J., Marcotti, W., Fuchs, H., Kurima, K., Wilcox, E.R., Friedman, T.B., Griffith, A.J., Balling, R., et al. (2002). Beethoven, a mouse model for dominant, progressive hearing loss DFNA36. *Nature Genetics* 30, 257–258.

Waguespack, J., Salles, F.T., Kachar, B., and Ricci, A.J. (2007). Stepwise morphological and functional maturation of mechanotransduction in rat outer hair cells. *The Journal of Neuroscience : the Official Journal of the Society for Neuroscience* 27, 13890–13902.

Walker, R.G., Willingham, A.T., and Zuker, C.S. (2000). A *Drosophila* mechanosensory transduction channel. *Science (New York, N.Y.)* 287, 2229–2234.

Wan, L., Almers, W., and Chen, W. (2005). Two ribeye genes in teleosts: the role of Ribeye in ribbon formation and bipolar cell development. *The Journal of Neuroscience : the Official Journal of the Society for Neuroscience* 25, 941–949.

Wang, Y., Chang, C.F., Morales, M., Chiang, Y.H., and Hoffer, J. (2002). Protective effects of glial cell line-derived neurotrophic factor in ischemic brain injury. *Annals of the New York Academy of Sciences* 962, 423–437.

Washbourne, P., Thompson, P.M., Carta, M., Costa, E.T., Mathews, J.R., Lopez-Benditó, G., Molnár, Z., Becher, M.W., Valenzuela, C.F., Partridge, L.D., et al. (2002). Genetic ablation of the t-SNARE SNAP-25 distinguishes mechanisms of neuroexocytosis. *Nature Neuroscience* 5, 19–26.

Webb, S.W., Grillet, N., Andrade, L.R., Xiong, W., Swarthout, L., Della Santina, C.C., Kachar, B., and Müller, U. (2011). Regulation of PCDH15 function in mechanosensory hair cells by alternative splicing of the cytoplasmic domain. *Development (Cambridge, England)* 138, 1607–1617.

Weimer, R.M., Richmond, J.E., Davis, W.S., Hadwiger, G., Nonet, M.L., and Jorgensen, E.M. (2003). Defects in synaptic vesicle docking in unc-18 mutants. *Nature Neuroscience* 6, 1023–1030.

Westerfield, M. (1995). *The zebrafish book: a guide for the laboratory use of zebrafish (Danio ...*

Whitfield, T.T. (2002). Zebrafish as a model for hearing and deafness. *Journal of Neurobiology* 53, 157–171.

Whitfield, T.T., Granato, M., van Eeden, F.J., Schach, U., Brand, M., Furutani-Seiki, M., Haffter, P., Hammerschmidt, M., Heisenberg, C.P., Jiang, Y.J., et al. (1996). Mutations affecting development of the zebrafish inner ear and lateral line. *Development (Cambridge, England)* 123, 241–254.

Willott, J.F. (2006). Overview of methods for assessing the mouse auditory system. *Current Protocols in Neuroscience / Editorial Board, Jacqueline N. Crawley ... [et Al.] Chapter 8, Unit8.21A.*

Wilson, D.W., Whiteheart, S.W., Wiedmann, M., Brunner, M., and Rothman, J.E. (1992). A multisubunit particle implicated in membrane fusion. *The Journal of Cell Biology* 117, 531–538.

Wilson, D.W., Wilcox, C.A., Flynn, G.C., Chen, E., Kuang, W.J., Henzel, W.J., Block, M.R., Ullrich, A., and Rothman, J.E. (1989). A fusion protein required for vesicle-mediated transport in both mammalian cells and yeast. *Nature* 339, 355–359.

Woods, I.G., Lyons, D.A., Voas, M.G., Pogoda, H.-M., and Talbot, W.S. (2006). nsf is essential for organization of myelinated axons in zebrafish. *Current Biology : CB* 16, 636–648.

Wright, M.A., and Ribera, A.B. (2010). Brain-derived neurotrophic factor mediates non-cell-autonomous regulation of sensory neuron position and identity. *The Journal of Neuroscience : the Official Journal of the Society for Neuroscience* 30, 14513–14521.

Wu, C.-L., Hwang, C.-S., Chen, S.-D., Yin, J.-H., and Yang, D.-I. (2010). Neuroprotective mechanisms of brain-derived neurotrophic factor against 3-nitropropionic acid toxicity: therapeutic implications for Huntington's disease. *Annals of the New York Academy of Sciences* 1201, 8–12.

Wu, L., Pan, L., Zhang, C., and Zhang, M. (2012). Large Protein Assemblies Formed by Multivalent Interactions between Cadherin23 and Harmonin Suggest a Stable Anchorage Structure at the Tip Link of Stereocilia. *The Journal of Biological Chemistry* 287, 33460–33471.

Wuyts, F.L., Furman, J., Vanspauwen, R., and Van de Heyning, P. (2007). Vestibular function testing. *Current Opinion in Neurology* 20, 19–24.

Xu, B., Gottschalk, W., Chow, A., Wilson, R.I., Schnell, E., Zang, K., Wang, D., Nicoll, R.A., Lu, B., and Reichardt, L.F. (2000). The role of brain-derived neurotrophic factor receptors in the mature hippocampus: modulation of long-term potentiation through a presynaptic mechanism involving TrkB. *The Journal of Neuroscience : the Official Journal of the Society for Neuroscience* 20, 6888–6897.

Xu, Z., Oshima, K., and Heller, S. (2010). PIST regulates the intracellular trafficking and plasma membrane expression of cadherin 23. *BMC Cell Biology* 11, 80.

Xu, Z., Peng, A.W., Oshima, K., and Heller, S. (2008). MAGI-1, a candidate stereociliary scaffolding protein, associates with the tip-link component cadherin 23. *The Journal of Neuroscience : the Official Journal of the Society for Neuroscience* 28, 11269–11276.

Yan, J., Pan, L., Chen, X., Wu, L., and Zhang, M. (2010). The structure of the harmonin/sans complex reveals an unexpected interaction mode of the two Usher syndrome proteins. *Proceedings of the National Academy of Sciences of the United States of America* 107, 4040–4045.

Yang, T., Kahrizi, K., Bazazzadeghan, N., Meyer, N., Najmabadi, H., and Smith, R.J.H. (2010). A novel mutation adjacent to the Bth mouse mutation in the TMC1 gene makes this mouse an excellent model of human deafness at the DFNA36 locus. *Clinical Genetics* 77, 395–398.

Yonezawa, S., Hanai, A., Mutoh, N., Moriyama, A., and Kageyama, T. (2008). Redox-dependent structural ambivalence of the cytoplasmic domain in the inner ear-specific cadherin 23 isoform. *Biochemical and Biophysical Research Communications* 366, 92–97.

Yu, R.C., Hanson, P.I., Jahn, R., and Brünger, A.T. (1998). Structure of the ATP-dependent oligomerization domain of N-ethylmaleimide sensitive factor complexed with ATP. *Nature Structural Biology* 5, 803–811.

Yu, R.C., Jahn, R., and Brunger, A.T. (1999). NSF N-terminal domain crystal structure: models of NSF function. *Molecular Cell* 4, 97–107.

Zallocchi, M., Delimont, D., Meehan, D.T., and Cosgrove, D. (2012a). Regulated Vesicular Trafficking of Specific PCDH15 and VLGR1 Variants in Auditory Hair Cells. *The Journal of Neuroscience : the Official Journal of the Society for Neuroscience* 32, 13841–13859.

Zallocchi, M., Meehan, D.T., Delimont, D., Rutledge, J., Gratton, M.A., Flannery, J., and Cosgrove, D. (2012b). Role for a novel Usher protein complex in hair cell synaptic maturation. *PloS One* 7, e30573.

Zanazzi, G., and Matthews, G. (2009). The molecular architecture of ribbon presynaptic terminals. *Molecular Neurobiology* 39, 130–148.

Zanazzi, G., and Matthews, G. (2010). Enrichment and differential targeting of complexins 3 and 4 in ribbon-containing sensory neurons during zebrafish development. *Neural Development* 5, 24.

Zarelli, V.E.P., Ruete, M.C., Roggero, C.M., Mayorga, L.S., and Tomes, C.N. (2009). PTP1B dephosphorylates N-ethylmaleimide-sensitive factor and elicits SNARE complex disassembly during human sperm exocytosis. *The Journal of Biological Chemistry* 284, 10491–10503.

Zeddies, D.G., and Fay, R.R. (2005). Development of the acoustically evoked behavioral response in zebrafish to pure tones. *The Journal of Experimental Biology* 208, 1363–1372.

Zenisek, D., Horst, N.K., Merrifield, C., Sterling, P., and Matthews, G. (2004). Visualizing synaptic ribbons in the living cell. *The Journal of Neuroscience : the Official Journal of the Society for Neuroscience* 24, 9752–9759.

Zhao, C., Slevin, J.T., and Whiteheart, S.W. (2007). Cellular functions of NSF: not just SNAPs and SNAREs. *FEBS Letters* 581, 2140–2149.

Zhao, C., Smith, E.C., and Whiteheart, S.W. (2012). Requirements for the catalytic cycle of the N-ethylmaleimide-Sensitive Factor (NSF). *Biochimica Et Biophysica Acta* 1823, 159–171.

Zhao, Y., Yamoah, E.N., and Gillespie, P.G. (1996). Regeneration of broken tip links and restoration of mechanical transduction in hair cells. *Proceedings of the National Academy of Sciences of the United States of America* 93, 15469–15474.

Zou, S., Li, L., Pei, L., Vukusic, B., Van Tol, H.H.M., Lee, F.J.S., Wan, Q., and Liu, F. (2005). Protein-protein coupling/uncoupling enables dopamine D2 receptor regulation of AMPA receptor-mediated excitotoxicity. *The Journal of Neuroscience : the Official Journal of the Society for Neuroscience* 25, 4385–4395.

List of Publications

1. **Mo W**, Trapani JG, Sheets L, Nicolson T. Nsf function in hair cell synaptic transmission: lesson from a point mutation in *milky way* mutant, in preparation.
2. **Mo W**, Nicolson T. Both pre- and postsynaptic activities of NSF are required for the stability synapses, PLoS One, 2011;6(11):e27146.
3. Sheets L, Trapani JG, **Mo W**, Obholzer N, Nicolson T. Ribeye is required for presynaptic Ca(V)1.3a channel localization and afferent innervation of sensory hair cells. Development. 2011 Apr;138(7):1309-19.
4. **Mo W**, Chen F, Nechiporuk A, Nicolson T. Quantification of vestibular-induced eye movements in zebrafish larvae. BMC Neurosci. 2010 Sep 3;11:110.
5. Wright MA, **Mo W**, Nicolson T, Ribera AB. In vivo evidence for transdifferentiation of peripheral neurons. Development. 2010 Sep;137(18):3047-56.
6. Trapani JG, Obholzer N, **Mo W**, Brockerhoff SE, Nicolson T. Synaptotagmin1 is required for temporal fidelity of synaptic transmission in hair cells. PLoS Genet. 2009 May;5(5):e1000480.
7. Obholzer N, Wolfson S, Trapani JG, **Mo W**, Nechiporuk A, Busch-Nentwich E, Seiler C, Sidi S, Söllner C, Duncan RN, Boehland A, Nicolson T. Vesicular glutamate transporter 3 is required for synaptic transmission in zebrafish hair cells. Journal of Neuroscience. 2008 Feb 27;28(9):2110-8.